

DOCTOR OF PHILOSOPHY

Investigating the structure-property relationships of a high-temperature epoxy matrix for structural and thermal applications

Swan, Samuel

Award date:
2022

Awarding institution:
Coventry University
Deakin University

[Link to publication](#)

General rights

Copyright and moral rights for the publications made accessible in the public portal are retained by the authors and/or other copyright owners and it is a condition of accessing publications that users recognise and abide by the legal requirements associated with these rights.

- Users may download and print one copy of this thesis for personal non-commercial research or study
- This thesis cannot be reproduced or quoted extensively from without first obtaining permission from the copyright holder(s)
- You may not further distribute the material or use it for any profit-making activity or commercial gain
- You may freely distribute the URL identifying the publication in the public portal

Take down policy

If you believe that this document breaches copyright please contact us providing details, and we will remove access to the work immediately and investigate your claim.

Investigating the structure-property relationships of a high-temperature epoxy matrix for structural and thermal applications

by

Samuel R. Swan
M.S. Mechanical Engineering

Submitted in partial fulfilment of the requirements for the degree of
Doctor of Philosophy

Deakin University & Coventry University

August, 2021

Acknowledgements

It would have been a struggle to make it this far without the support of my parents, family, friends, mentors, and teachers. To Steven J. Wright I owe a debt of gratitude for asking a young high school version of myself what I wanted to do and then how we were going to make it happen. That catalysed this whole engineering and composites thing for the last decade and culminated in me finally doing work for an Americas Cup sailing team. To Dr. Christopher Lee, who told me only five people scored as low as I did on the first calculus exam and only one had gone to pass, thank you for helping me be the second. Without that support I doubt I would have made it to the end of my first semester at UP. Without Dr. Heather Dillon nudging me to just apply to three Masters programs by the end of the week, I wouldn't have ended up on a trajectory that's gotten me to Deakin University. Also, a great deal of thanks goes to Professor Dave Kim for all the support during my Masters and affording me the trust to pursue that research with a great deal of independence. Without Dr. Khalid H. Khan's continued encouragement over the years, I doubt I would have ever applied to any PhD programs and I wouldn't have had the amazing experience in Australia and the UK.

At Deakin, I owe much thanks to my advisors Professor Russell Varley and Dr. Claudia Creighton. At Coventry my thanks go to my advisors, Dr. James Griffin and Dr. Bekim Gashi. They have always received me with professionalism, trust, and given excellent guidance on my research. It goes without saying that I couldn't have done it alone but even more importantly I couldn't have gained the same level of skill and knowledge without them going above and beyond.

Throughout everything, I cannot help but thank my parents for accepting that I was always going to make my own way. It's meant four years (and counting) away from home which hasn't always been easy. But I wouldn't have been as capable doing that if you hadn't raised me to work hard, pursue my goals, and fostered my independence. It has gotten me to the other side of the world and made it so I can find my own way back.

List of Publications

Primary Authorship

1. **S.R. Swan**, T.M. Devenport, S.M. Seraji, J.M. Griffin, B.V. Gashi, C. Creighton, and R.J. Varley, *Study of the acoustic emission response to a core-shell rubber toughened, high-temperature composite*, J. Mat. Sci., vol. 56, Jan. 2021
2. **S.R. Swan**, C. Creighton, B.V. Gashi, J.M. Griffin, and R.J. Varley, *Cure kinetics and network development of a very high T_g naphthalene based epoxy amine network*, Submitted
3. **S.R. Swan**, C. Creighton, B.V. Gashi, J.M. Griffin, and R.J. Varley, *Highly Crosslinked Glycidyl Ether versus Glycidyl Amine Epoxy Networks: Influence of Epoxide Conversion and Monomer Structure*, Submitted

Contributing Authorship

1. F. Vuković, **S. R. Swan**, L. Q. Reyes, R. J. Varley, and T. R. Walsh, *Beyond the ring flip: A molecular signature of the glass–rubber transition in tetrafunctional epoxy resins*, Polymer., vol. 206, p. 122893, Oct. 2020
2. D. Kim, **S.R. Swan** et al., *A study on the machinability of advanced arc PVD AlCrN-coated tungsten carbide tools in drilling of CFRP/titanium alloy stacks*, Carbon Lett., vol. 1, p. 3, 2020
3. H. Gan, S. M. Seraji, J. Zhang, **S. R. Swan**, S. Issazadeh, and R. J. Varley, *Synthesis of a phosphorus-silicone modifier imparting excellent flame retardancy and improved mechanical properties to a rapid cure epoxy*, React. Funct. Polym., vol. 157, 2020
4. L. Q. Reyes, **S. R. Swan**, H. Gan, S. M. Seraji, J. Zhang, and R. J. Varley, *The role of β relaxations in controlling compressive properties in hyperbranched polymer-modified epoxy networks*, Polym. J., 2020
5. J. M. Misasi, B.N. Dao, C. Dell'Olio, **S.R. Swan**, S. Issazadeh, J.S. Wiggins and R.J. Varley, *Polyaryletherketone (PAEK) thermoplastic composites via in-situ ring opening polymerisation*, Compos. Sci. Technol., vol. 201, 2021

Presentations

S.R. Swan, C. Creighton, B.V. Gashi, J.M. Griffin, and R.J. Varley, *Technical Presentation*, Asian-Australian Conference on Composite Materials, 2018

*The defining responsibility of the artist is to go beyond the edge of human experience
and send back reports*

Webb Chiles

ABSTRACT

This project explores the network formation and structure-property relations of some high temperature epoxy resins cured with aromatic diamines. A highly aromatic dimeric naphthalene epoxy resin monomer, bis(2,7 glycidyl ether naphthalenediol) methane (NNE), is cured with 4,4'-diaminodiphenyl sulfone (DDS) to produce a network that exhibits rapid gelation, vitrification, and an ultimate glass transition temperature approaching 350°C. An array of thermal, spectral, rheological, and thermo-mechanical analysis techniques are used to comparatively assess the formation of the NNE-DDS network to a commercial high- T_g epoxy resin comprised of 4,4'-tetraglycidyl diaminodiphenyl methane (TGDDM) and DDS. The difference between the glycidyl ether (NNE) resin and glycidyl amine (TGDDM) resin through cure was explored. It was determined that the NNE resin showed primarily epoxy-amine addition and no signs of etherification or side reactions which was, in contrast to TGDDM, attributed to the absence of tertiary amine within the epoxy backbone. The time-temperature-transformation (TTT) diagrams of the resins are constructed to explain the processing and formation of the glass transition temperature and show competition between devitrification (T_g) and the ultimate glass transition temperature of NNE.

The structure-property relations of the NNE and TGDDM networks are explored via thermal analysis and mechanical testing of the cured resins and their carbon fibre composites. It is shown that the structure of the NNE monomer and limited mobility produces a network with high free volume and poor equilibrium packing density. The rapid vitrification at low degree of conversion prevents a high degree of cure and the network becomes topologically constrained. That in turn results in higher moisture ingress, lower strength and modulus, but achieves better thermal stability than TGDDM at temperatures above 200°C. Further ageing of the resins and composites at 250°C for 504hr indicate some benefit for high temperature, short duration thermal performance of NNE compared to TGDDM. That is attributed to the limited mobility of the matrix after cure and the effects of the tertiary amine contained in TGDDM providing more pathways to degradation.

The NNE resin, whilst possessing superior thermal performance, is difficult to process and exhibits poor mechanical performance compared to TGDDM. An approach to modify the network for improved strength and stiffness combined with reduced viscosity was taken at the molecular level. A monofunctional reactive epoxy diluent, partially reacted substructures (PRS), a molecular fortifier (MFN), and pure naphthalene were synthesised and cured with

NNE in percentages ranging from 5-20 mol% or wt%. This survey showed an antiplasticising effect where strength reduced, and modulus increased significantly. Further, the monofunctional epoxy and naphthalene, when added at 10 mol % and 10 wt%, respectively, reduced the melt viscosity and increased the processing window to values in the range of conventional resin transfer moulding parameters. Carbon fibre composites of the modified resins at 10% loading showed the neat resin properties transferred to improvements in the composite flexural modulus with minimal impact on strength and interlaminar shear.

Finally, the toughening of a multi-functional epoxy resin was achieved by use of core-shell rubber (CSR) particle toughening. The improvement to room temperature fracture toughness of nearly 40% of the neat resin at 20 wt% particle addition was then used to create a carbon fibre composite. The composite mode I fracture toughness was evaluated by means of in situ acoustic emission (AE) spectroscopy and scanning electron microscopy (SEM) imaging of the fracture surface. A nearly two-fold increase in G_{IC} was shown. AE spectroscopy indicated that toughening by CSR contributed to high frequencies of interply-, fibre bridging-, and fibre-dominated failure events than the unmodified composite where the frequencies of events showed lower energy matrix-dominated failure.

This project investigates the capabilities of a high temperature naphthalene-based epoxy-amine resin formulations and routes to achieve simultaneous improvements to thermal resistance and stability, mechanical performance, and fracture toughness for structural composite applications.

Table of Contents

Abstract	1
<i>1 Introduction</i>	<i>10</i>
1.1 Industry Applications of Polymer Composites	10
1.2 Glass Transition Temperatures and Thermal Stability of Polymers	11
1.3 Polymer Matrix Selection for Composites and Mechanical Performance of High-Temperature Resins and Matrices	13
1.4 Research Aim and Objectives	16
1.5 Outline of Works in this Thesis	18
<i>2 Literature Review</i>	<i>21</i>
2.1 High Temperature Polymers	21
2.2 Epoxy Resins	23
2.3 High-Temperature Epoxies and Significance of Glycidyl Ethers and Glycidyl Amines in Network Formation	25
2.4 Role of Network Structure on Processability, Thermal Stability, and Mechanical Properties	27
2.5 Modified Epoxy Resins and Translation to the Composite	30
2.6 Polymer Composites	36
2.7 Modifications to Polymer Composites	40
2.8 Thermal Performance and Stability of Polymer Composites	42
2.9 Summary of the Literature	44
<i>3 Experimental Methods and Materials</i>	<i>45</i>
3.1 Introduction	45
3.2 Materials	45
3.3 Neat Resin Cure Kinetics	47
3.4 Rheology	49
3.5 Near Infrared Spectroscopy	51
3.6 Mechanical Properties and Fracture Toughness	54
<i>4 Network Development of the Tetrafunctional Epoxy Resins</i>	<i>57</i>
4.1 Introduction	57
4.2 Materials	60
4.3 Results and Discussion	61
4.4 Summary	85
<i>5 Properties of the Bulk Resins and Thermal Ageing of the Carbon-Fibre Composites</i>	<i>86</i>
5.1 Introduction	86
5.2 Materials	88
5.3 Results and Discussion – Neat Resin Properties	90
5.4 Results and Discussions – Thermal Ageing of the Composite	107
5.5 Summary of Work	116
<i>6 Molecular Additives as Modifiers of the Tetrafunctional Epoxy-Amine Resin System</i>	<i>118</i>
6.1 Introduction	118
6.2 Materials and Experimental Details	122
6.3 Results and Discussions	125
6.4 Summary	142
<i>7 Toughening of a Highly Crosslinked Epoxy Matrix via Core Shell Rubbers</i>	<i>147</i>
7.1 Introduction	147
7.2 Experimental	148
7.3 Results and Discussions	150
7.4 SEM Investigation of Failure Mechanisms	160

7.5	CONCLUSIONS	162
8	<i>Conclusions and Future Work</i>	163
8.1	Summary and Future Works	165
9	<i>References</i>	166
	Appendix A – NETWORK DEVELOPMENT OF THE TETRAFUNCTIONAL EPOXY RESINS	198
	Appendix B – PROPERTIES OF THE BULK RESINS AND THERMAL AGEING OF THE CARBON-FIBRE COMPOSITES	200
	Appendix C – MOLECULAR ADDITIVES AS MODIFIERS OF THE TETRAFUNCTIONAL EPOXY-AMINE RESIN SYSTEM	205

Table of Figures

Figure 1-1	- Chemical structure of the dimeric naphthalene epoxy monomer, NNE	17
Figure 2-1	- Example of (a) oxirane ring, (b) aromatic monofunctional o-cresyl glycidyl ether and (c) aliphatic monofunctional n-butyl glycidyl ether	23
Figure 2-2	- Examples of (a) primary amine addition, (b) secondary amine addition, and (c) etherification reaction	24
Figure 2-3	- Example structure of the TGDDM epoxy monomer	26
Figure 2-4	- Diagram and SEM images of phase separated, co-continuous, and phase inverted epoxy/TP systems [100]	31
Figure 2-5	- SEM image of core shell rubber particles dispersed in a matrix system with diagram of CSR structure [106]	32
Figure 2-6	- Fundamental model of cure-induced antiplasticisation for a thermosetting network [120]	34
Figure 2-7	- Trend in aircraft efficiency based on the effect of the introduction of technological advances (borrowed from [146])	39
Figure 2-8	- Comparison of initiation and propagation fracture energy of the CFRP to the neat resin fracture energy [160]	41
Figure 2-9	- Relation between weight loss and ageing on the T_g of a composite [171]	43
Figure 3-1	- Chemical structures of (a) NNE, (b) TGDDM, and (c) 44DDS monomers	45
Figure 3-2	- Diagram of the SENB specimen and loading configuration	55
Figure 4-1	- Example of a cyclic defect (left) and cyclic member (right) formed during reaction of glycidyl ammine with a primary amine	59
Figure 4-2	- HPLC gradient elutions of the epoxy monomers, NNE and TGDDM at nominally 100 μ mol	62
Figure 4-3	- Dynamic DSC traces for the NNE resin at increasing heating rates	63
Figure 4-4	- Arrhenius plot of the activation energies from dynamic DSC for the three resins	64
Figure 4-5	- Isothermal DSC traces of the three resins at 150 $^{\circ}$ C	65
Figure 4-6	- Dynamic re-heating of the three resins after isothermal cure at 150 $^{\circ}$ C	66
Figure 4-7	- Plots of (a) NNE conversion at different isothermal temperatures, and (b) the three resins cured at 150 $^{\circ}$ C	67
Figure 4-8	- Kinetic rate constant (a) k_1 and (b) k_2 of the three resins	67
Figure 4-9	- NIR spectra of the NNE resin from the uncured and cured states after 150 $^{\circ}$ C isothermal cure and a 220 $^{\circ}$ C post-cure	70

Figure 4-10 – Plots of (a) Fractional conversion from NIR for the epoxy and primary amine functional groups and (b) changes to SA and OH peaks for 150°C isothermal cure	71
Figure 4-11 - Ratio of the SA and OH areas relative to epoxy conversion	72
Figure 4-12 - Change to the secondary amine and hydroxyl area ratio relative to the conversion after cure and post-cure	73
Figure 4-13 - Dynamic rheological traces of (a) NNE, (b) NTG, and (c) TGDDM resins	75
Figure 4-14 - Isothermal rheological traces of the three resins at 130°C showing (a) G' (dashed) and G'' (solid) crossover at gelation and (b) complex viscosity with respect to isothermal time	76
Figure 4-15 - Traces of the storage modulus and tan(δ) of the three resins isothermally cured at 160°C	77
Figure 4-16 - Traces of the tan(δ) spectra for NNE relative to the isothermal cure temperature	78
Figure 4-17 - Comparison of the DSC conversion at times for gelation and vitrification determined from DMTA	79
Figure 4-18 - Traces of the tan(δ) peak under dynamic heating after the isothermal cure for NNE (inset plots T _g s of the three resins)	80
Figure 4-19 - Traces of the tan(δ) for the three resins at post-cure	82
Figure 4-20 - TTT diagrams of the NNE resin (solid) and TGDDM resin (open). Squares represent gelation, circles vitrification, triangles the sub-T _g peaks from DMTA rescans, and inverted triangles are the T _{g□} values with horizontal lines demarking the limit of the material prior to some thermal degradation. A TTT diagram of the NTG blend is provided in Appendix A	84
Figure 5-1 - Differential scanning calorimetry traces of the cured resins at (a) increasing cure condition of NNE and (b) between the three different epoxy formulations	90
Figure 5-2 - Fractional conversion of the three resins as determined by DSC	91
Figure 5-3 - Near-infrared spectroscopy of the NNE resin after cure and post-cure (a) and of the NNE, NTG, and TGDDM resins from cure at 180°C to post-cure	92
Figure 5-4 - Fractional conversion of epoxy as determined by near-infrared spectroscopy	93
Figure 5-5 - DMTA traces for storage modulus and tan(δ) of the different cure conditions	94
Figure 5-6 - DMTA traces for storage modulus and tan(δ) of the different resin formulations	95
Figure 5-7 - Traces of the tan(δ) spectra under sub ambient DMTA for (a) NNE at increasing cure and (b) the three resins	96
Figure 5-8 – (a) TMA traces of NNE (220°C), NTG (220°C), and TGDDM (200°C) post-cure conditions and (b) thermal coefficient of expansion relative to cure temperature and resin system	98
Figure 5-9 - Plot of the mass loss (solid) and derivative of mass loss (dashed) for the three resin systems heated at 10°C/min	99
Figure 5-10 - Plot of (a) Arrhenius-like degradation model and (b) activation energies relative to retained mass (at 2.5°C/min heating rate) of the three resins	100
Figure 5-11 - Isothermal TGA traces for the three resins at 250°C and a comparison of mass loss for 225-300°C isothermal heating runs	102
Figure 5-12 - Moisture ingress of (a) the NNE resin relative to conversion and (b) between the three resin formulations	103

Figure 5-13 - DMTA traces relative to extent of cure for NNE of (a) storage modulus and (b) the $\tan(\delta)$ behaviour after moisture-ingress	104
Figure 5-14 - DMTA traces of NNE, NTG, and TGDDM of (a) storage modulus, and (b) the $\tan(\delta)$ behaviour after moisture ingress	104
Figure 5-15 - NIR of OH peak for (a) NNE relative to extent of cure and (b) between the three resin formulations	105
Figure 5-16 - Mechanical properties showing the flexural (a) strain at failure, b) ultimate strength, c) modulus and d) fracture toughness from SENB testing	107
Figure 5-17 - Mass loss of the composite (left) and of the neat resins (right) under thermal ageing	108
Figure 5-18 - The (a) full mid-infrared spectra and (b) narrow range spectra for the NNE resin progressively aged	110
Figure 5-19 - The (a) full mid-infrared spectra and (b) narrow range spectra for the NTG resin progressively aged	110
Figure 5-20 -The (a) full mid-infrared spectra and (b) narrow range spectra for the TGDDM resin progressively aged	111
Figure 5-21 - Near infrared spectra of (a) NNE, (b) NTG, and (c) the TGDDM resins progressively aged	113
Figure 5-22 - DMTA traces of storage modulus (left) and $\tan(\delta)$ spectra (right) for the aged NNE composite	114
Figure 5-23 - Change in glass transition of the three composites with respect to ageing duration	115
Figure 5-24 - Mechanical properties of the aged composites with respect to duration of exposure	116
Figure 6-1 – Diagram representation depicting the reactive (CGE), reactive and hydrogen-bonded (33CGE and 44CGE), hydrogen-bonded (MFN), and non-reactive (NAPH) modification approaches within the cured epoxy network	122
Figure 6-2 - Structures of (a) 4,4'-diaminodiphenylsulfone reacted with (b) 0.5 molar ratio of o-cresyl glycidyl ether to form (c) the partially reacted substructure where a free primary amine group remains to further react with the bulk epoxy network	124
Figure 6-3 - Constituents of (a) 2,7'-dihydroxynaphthalene and (b) o-cresyl glycidyl ether reacted in the presence of a tertiary amine to (c) induce ring-opening polymerisation of the oxirane ring and hydrogen bonding with the hydroxyl of 27DHN and form the molecular fortifier	124
Figure 6-4 - Dynamic DSC thermograms of the resins at 10 % modifier addition	126
Figure 6-5 - Near infrared spectra of the unmodified and modified resins at 10% loading	128
Figure 6-6 - Dynamic rheological trace of the NNE resin and modified NCGE, NAPH, and MFN resins at 10% concentration showing (a) the change to complex viscosity, and (b) the gelation point crossover of G' and G''	129
Figure 6-7 - DMA ramp traces of storage modulus and $\tan(\delta)$ for the modified resins at 10% modifier addition	131
Figure 6-8 - Comparison of peak temperatures from $\tan(\delta)$ spectra respective to % modifier addition	132
Figure 6-9 – Sub-ambient DMA traces of storage modulus and $\tan(\delta)$ for the modified resins at 10% modifier addition	133

Figure 6-10 - Dynamic TGA (10°C/min heating rate) comparison at 10% modifier addition showing wt % (left axis) and derivative of mass loss (right axis)	134
Figure 6-11 - Moisture ingress of the unmodified NNE and the 10% modified CGE, NAPH, and MFN formulations	136
Figure 6-12 - Flexural modulus with respect to % modifier addition	138
Figure 6-13 - Flexural strength relative to % modifier addition	138
Figure 6-14 - Effect of % modifier addition on fracture toughness of the resins	139
Figure 6-15 - Mechanical properties of the composites in flexural 3-point bending showing (a) strain-to-failure, (b) flexural strength at failure, and (c) the flexural modulus of the composites	141
Figure 6-16 – Interlaminar shear strength of the 10% modifier addition composites	142
Figure 7-1 - Diagram of AE sensors onto DCB specimens for fracture toughness characterization	150
Figure 7-2 - DSC thermograms of uncured resins for (a) the unmodified 0 wt% CSR and (b) the 20 wt% CSR formulations	151
Figure 7-3 - Dynamic rheological traces of the unmodified and 20 wt% CSR resins	152
Figure 7-4 - NIR of (a) fully cured TGDDM-DDS from 0-20 wt% CSR loading and (b-c) the unmodified and 20 wt% for epoxide, hydroxyl, and primary/secondary amine peaks	153
Figure 7-5 - Scans from dynamic mechanical analysis showing (a) storage modulus and (b) tan(δ) relative to ramp temperature	154
Figure 7-6 - Summary of flexural strength, modulus, and SENB fracture toughness for 0-20 wt% CSR modified neat resins	156
Figure 7-7 – Summary load profile (black), counts (red), and hits versus relative test time for (a-b), TGDDM-DDS Sample 1 and (c-d) TGDDM-DDS 20 wt% CSR Sample 5	157
Figure 7-8 - Summary of mean and peak frequencies relative to test time for (a-b), TGDDM-DDS Sample 1 and (c-d) TGDDM-DDS 20 wt% CSR Sample 5	158
Figure 7-9 – Count of (a) mean frequencies and (b) peak frequency events per band for unmodified and 20 wt% CSR samples averaged across all AE tests	159
Figure 7-10 - Fracture toughness R-curves of (a) unmodified and (b) 20 wt% CSR laminates	160
Figure 7-11 - SEM fractograms of the (a) unmodified and (b) 20 wt% CSR toughened composites taken from a segment of the laminate at the 25mm region of the crack length	161
Figure 7-12 - SEM fractograms of the (a) unmodified and (b-d) 20 wt% CSR modified neat resins at different magnifications	161

Table of Tables

Table 2-1 - Summary of investigations exploring CSR toughening, the type of epoxy investigated, T_g of the resulting matrix, and fracture toughness/energy	33
Table 3-1 - Main epoxy and amine hardeners used in this study	45
Table 3-2 - Typical absorbance bands for epoxy-amine systems	52
Table 4-1 - Summary of materials used in the study	60
Table 4-2 - Epoxy and amine equivalent weight of the monomers	61
Table 4-3 - Enthalpies of reaction, peak exotherms, and activation energies from the dynamic DSC study	64

Table 4-4 – Fractional conversion, glass transition temperature, kinetics rate constants, and the critical conversion determined from isothermal DSC.....	69
Table 4-5 - Summary of epoxy conversion time and fractional conversion from NIR	73
Table 4-6 - Summary of the isothermal gelation times and storage modulus at gelation.....	76
Table 4-7 – Gelation times, vitrification times, and glass transition temperatures.....	83
Table 5-1 - Summary of materials used in the study	88
Table 5-2 – Cure schedule of the neat resins studied in this chapter.....	90
Table 5-3 - DMTA values for the glass transition onset from E' and peak of tan(δ).....	95
Table 5-4 - Sub-ambient DMTA values for peak temperature and partial areas of the tan(δ) traces	97
Table 5-5 - Values of degradation temperature, char yield, and activation energies from dynamic TGA.....	100
Table 5-6 - Density, moisture ingress at equilibrium, and diffusion coefficients of the resins	103
Table 5-7 - Peak and band assignments for mid- and near-IR analysis.....	108
Table 6-1 - Summary of materials used in this chapter	123
Table 6-2 - Values of peak exothermic temperature, average enthalpy, and activation energies for dynamic DSC	127
Table 6-3 - Dynamic rheological behaviour of the modified resins	130
Table 6-4 - Results of dynamic TGA analysis for degradation onsets and char yield.....	135
Table 6-5 - Physical density and equilibrium moisture uptake for the NNE, CGE, NAPH, and MFN resins.....	136
Table 7-1 - Summary of peak temperature, enthalpies, and activation energies for neat resins studied by differential scanning calorimetry.....	151
Table 7-2 - Dynamic rheology of the compositions from 0-20 wt%	152
Table 7-3 - Summary of glass transition, degradation temperatures, and char yield for the neat resins	155
Table 7-4 – Fracture toughness and cumulative AE energy	160

Abbreviations

NIR	Near Infrared Spectroscopy
DSC	Differential Scanning Calorimetry
DMTA/DMA	Dynamic Mechanical Thermal Analysis
TMA	Thermomechanical Analysis
TGA	Thermogravimetric Analysis
3PB	Three Point Bending
SENB	Single Edge Notch 3-point Bending
DCB	Dual Cantilever Beam
NNE	bis(2,7 glycidyl ether naphthalenediol) methane
TGDDM	tetraglycidyl-diaminodiphenyl methane
44DDS/DDS	4,4'-diaminodiphenylsulfone
33DDS	3,3'-diaminodiphenylsulfone
T _{gel}	Temperature at gelation
T _{vit}	Temperature at vitrification
T _g	Glass Transition Temperature
T _g	Ultimate Glass Transition Temperature
T _d	Degradation Temperature
T _p	Peak Exothermic Temperature
TTT	Time Temperature Transformation
SEM	Scanning Electron Microscopy
CTE	Coefficient of Thermal Expansion
AE	Acoustic Emission Spectroscopy
E _a	Activation Energy Barrier
K _{1C}	Plane Strain Fracture Toughness (kJ- ²)
G _{1C}	Strain Energy Release Rate (Fracture Energy, kJ/m ²)
FRP	Fibre reinforced plastic
CFRP	Carbon fibre reinforced plastic

1 INTRODUCTION

Polymers for fibre reinforced composites are a branch of materials that must have compatibility with reinforcement and properties that can withstand the design loads and environmental factors during a structures' lifecycle. At a basic level, strength, stiffness, and toughness are essential to most structural composite applications. Increasingly, with the expansion of markets where composites are performance or cost-competitive with traditional engineered materials, the requirements of modern polymer composites can include stability at temperature extremes and in caustic environments. For the manufacturers of these structures, the processing characteristics present another area of concern both in terms of economic viability and build quality.

In this chapter, a brief overview of the current state of polymer composites in industry is presented alongside background of the fundamentals behind some common thermosetting polymer materials used for composites and other research that is relevant to the work in this thesis. Specifically, this work aims to investigate some high temperature epoxy resins as matrix systems for composites where structural and thermal performance are important functional criteria. Involved are studies of the network development of the epoxy-amine system, evaluation and origin of key thermal, material, and mechanical properties, the translation of resin properties to the matrix of a carbon fibre composite, and routes to modify and enhance such properties. The ultimate goal is to understand the structure-property relations of a key set of high-temperature epoxy networks and demonstrate their viability as matrix systems for advanced composites. That includes general information about thermoplastic and thermoset resins that are relevant to composites and how the chemical structure of epoxy resins can affect properties and performance as well as how those may be altered or modified. Finally, an overview of the work and an outline of the remaining thesis is provided.

1.1 INDUSTRY APPLICATIONS OF POLYMER COMPOSITES

Polymer composites, especially carbon fibre reinforced plastics (CFRP), are now a recognized material system outside of engineering and technology disciplines. Cars such as the Lamborghini *Sesto Elemento*, which of course pay homage to the sixth element of the periodic table, have made it into mainstream television, magazines, and as pin-up posters on bedroom walls. Even more ubiquitous is the fast scale-up of composite technology in the aerospace industry. The Airbus A350-900XWB is to contain nearly 52% composites by weight [1].

Composites are recognizable in aerospace, wind energy, recreational, industrial, and automotive applications [2]–[5]. Recent estimates suggest that the amount of plastics and polymer composites integrated into aircraft will increase by 5% through 2021 [6]. A structural composite is comprised of at least one reinforcing material, generally long-form fibres, and a matrix that binds to and maintains dimensional stability of the reinforcement. The range of fibres can include various types of glass, basalt, boron, carbon, and a number of proprietary aramid fibres of which Kevlar™ is the most common. The advantage of composites lies in the ability to adapt fibre and matrix to suit a number of key performance criteria for a structure whether it be impact resistance, strength, stiffness, and resistance to thermal and environmental degradation.

Composite matrix materials can range from ceramics, metals, alloys, and polymers. However, polymer matrix composites dominate the global markets with thermosetting polymers accounting for approximately 70% of the structural composite market and of those, more than half are epoxy-based [7]. Increasingly, a desire for repairable low-cost composites has driven advanced thermoplastic matrices although there are still numerous constraints with the properties and production of composites for many typical applications. In general, epoxy-based thermosetting resins produce a combination of strength, stiffness, and environmental performance suitable for most applications by conventional manufacturing techniques.

A variety of alternatives to epoxies exist and are usually employed to target lower cost production (polyester, vinylesters, polyurethanes) or performance at high temperatures (bismaleimides, phenolic novolacs, cyanate esters, benzoxazines) but tend to have higher raw material cost and usually difficult to process. An overview of these high-temperature resins is covered later in this work. In essence, epoxies are preferred and attractive because they perform favourably across a range of metrics. It is the high-temperature space where epoxies are out-performed hence why it is of interest to develop increasingly higher-temperature epoxy resin systems to continue to meet the demands of an expanding composites market.

1.2 GLASS TRANSITION TEMPERATURES AND THERMAL STABILITY OF POLYMERS

Polymers are generally characterised by a few distinct changes in state with respect to temperature. These can include the melting temperature (T_m or T_{melt}), crystallisation temperature (T_c or $T_{crystal}$), peak exothermic temperature (T_p or T_{exo}), the glass transition

temperature (T_g), and a degradation temperature (T_d or T_{deg}). The latter three temperatures are most relevant to thermosetting polymers and are discussed in more detail within this work. Significant to the discussion of high temperature performance is the role of the glass transition temperature of a polymer and the composite as it relates to thermal stability. In addition to their melt temperature, thermoplastics can exhibit a glass transition temperature while thermosets, primarily amorphous glasses or semi-crystalline in nature, go through a transitional range of temperatures where the network transforms from a hard solid to a soft, compliant material similar to a rubber [8]. As a polymer is heated the molecular mobility at the chemical network level increases at a differential rate until the temperature applied exceeds the glass transition temperature, resulting in large-scale changes to the mechanical properties of the bulk polymer [9]. This glass to rubber transition generally results in a rubber plateau where, irrespective of increased temperature the elastic modulus of the material is constant. In practical terms the glass to rubber transition represents an onset over a range of temperatures where there is non-linearity from equilibrium for the stiffness of the resin or composite. Therefore, the T_g is useful in defining the upper limit of a service temperature ($T_{service}$) which is an engineering term used to define a maximum operating temperature that is outlined by the service requirements.

The degradation temperature can represent purely thermal, thermal-oxidative (in the presence of oxygen), and hygrothermal temperatures (in a moisture-rich environment) at which bonds within the chemical network begin to cleave and network properties significantly deteriorate. In this work, it is primarily thermal and thermal-oxidative degradation that is considered. Much like the glass transition temperature, the value of the T_d is not a phase change but occurs over a range of temperatures. It is further complicated by the temperature dependent activation of the different bonds that form the chemical network. The presence of weak C-H bonds will degrade faster than those with higher bond energies such as the C-F bonds in polytetrafluoroethylene (PTFE) [10] of which commercial TeflonTM is an excellent example, particularly in the form of non-stick coatings gracing kitchen cupboards the world over. Further, with thermo-oxidative degradation, the pathway for oxidation is partly driven by the thermo-mechanical expansion and contraction with exposure to heat. That is a mechanism by which micro-scale cracks can form and create a pathway for the initiation of oxidation, diffusion-controlled process that is accelerated by higher exposed surface areas. It has been shown that thermo-oxidative ageing of the composite can be improved by minimising thermal mismatch between the reinforcing fibre and the resin so that when the resin expands with

heating, fewer pathways are formed by which the diffusion-controlled oxidative reaction can be accelerated [11], [12]. Lifetime modelling based on thermal analysis of some common epoxy resins with significantly different glass transitions have predicted a useful service temperature for 10,000 hours that differ by a mere 2°C for times in the thousands of hours [13].

Therefore, in the context of this work it is important to note the difference between the glass transition temperature and thermal stability. Neither of these temperatures are distinct phase changes and must be considered in context with the application. The resin thermal performance in a composite form and in most applications the thermal stability will be mutually exclusive of the glass transition temperature.

1.3 POLYMER MATRIX SELECTION FOR COMPOSITES AND MECHANICAL PERFORMANCE OF HIGH-TEMPERATURE RESINS AND MATRICES

For applications that demand thermal stability at elevated temperatures, resins such as DGEBA-based epoxies are not always suitable and different types of polymeric networks are utilised. These include phenolic novolac, addition cured polyimides that are most commonly copolymerised bismaleimides (BMI) and the commercial PMR-15 polyimide, cyanate esters (CE), some highly aromatic thermoplastics such as polyetheretherketone (PEEK), and multi-functional epoxy resins [14]. Thermoplastic matrix composites are a growing area due to the potential for shorter processing times, ability to be repaired and recycled, and in some instances the thermal stability. With regard to thermal stability, a few thermoplastics are widely known for high T_g and mechanical performance suitable for aerospace applications. Polyimides are sometimes noted as the upper-limit for service temperature of polymer composites near 350°C [15]. Achieving a composite with high thermal stability is a very difficult task due to the competing performance criteria needed to manufacture complex and high-tech structures as well as in-service performance criteria. Rocket components on the NASA X-30 experimental vehicle were manufactured using PEEK composites but full-scale manufacturing of CFRP/PEEK was unattainable and the matrix was switched to an epoxy [16]. Others such as polyimides (PEI) have been used for service temperatures above 200°C but again these can lack processability due to high melt temperatures [17]. As such, thermosetting matrices and particularly, high performance and low-cost matrices such as epoxy-based resins remain in demand as high performance matrices.

1.3.1 Basic Concepts in the Chemistry of High Temperature Epoxies

Thermal stability of polymers can generally be attained by a combination of aromatic components in the backbone of the monomer units, strength of the chemical bonds, and high crosslink density between polymer chains. Generally, the degree of crosslinking results in greater energy needed to cleave chemical bonds [17]. Rigid aromatic groups such as phenyl or naphthalene units resist bond rupture and increase thermal stability [18]–[20] but also tend to lead to a higher room temperature glassy modulus which is associated with lower ductility and toughness [21], [22]. Typically, the increase to thermal stability reduces mechanical strength because of the higher crosslink density and constrained mobility of the molecular network.

Of the epoxy-based resins, diglycidyl ether of bisphenol A (DGEBA) is most widely used in commercial formulations and as a standalone resin or for epoxy-based polymer composites. DGEBA epoxy monomers result from the synthesis of epichlorohydrin with an excess of bisphenol A which results in two oxirane rings, one each bound terminally to the hydroxyl groups of the bisphenol backbone. The relative ease of synthesis and the good mechanical and thermal properties make it suitable for many applications. Polyamines, anhydrides, acrylic acids and inorganic catalysts can induce ring-opening via chain or step growth polymerisation and subsequent crosslinking to form a rigid thermoset network [23].

To form a crosslinked network, the ring-opening of the epoxide group must be in the presence of a suitable nucleophile. The oxirane ring of the epoxy is susceptible to nucleophilic attack due to the electrophilic nature of the carbon in the C-O bond. Upon ring-opening of the epoxide, the strain of the oxirane ring is relieved and a new bond is formed. Of primary interest are diamine-cured epoxy resins. The amine nucleophile contains a lone electron pair of the nitrogen atom and can bond to the lone carbon after ring-opening. The active hydrogen of the primary amine reacts with the epoxy group to form secondary amine which can then react with another epoxy group. For diamines, the secondary amine can form a second bond through the ring-opening process which is preceded by formation of a tertiary amine that can catalyse side-reactions and etherification [24] although the amine addition reactions remain the predominant mechanism [25]. Other high performance resins such as commercial BMIs are pentafunctional with the possibility of both chain extension and crosslinking from the three double bonds and etherification via two hydroxyl groups [26]. Phenolic resins are even more complex due to the radical polymerisation into high oligomeric networks [27]. The relative simplicity of the epoxy-

amine reaction means that, in general, there are few side reactions that can take place during the cure and cross-linking stages.

The DGEBA monomer is di-functional because it has two oxirane rings. A multi-functional epoxy is classed as an epoxy containing more than two epoxy functional groups attached to the backbone. Commercial triglycidyl-*p*-aminophenol (TGAP) and tetraglycidyl-diaminodiphenyl methane (TGDDM) are the most common multi-functional epoxy resins, containing three and four functional groups, respectively. The aromatic backbone, higher functionality, and resulting high crosslink density when cured with a suitable aromatic polyamine can result in glass transition temperatures above 250°C. However, the thermal stability can be affected by internal cyclisation and dissociation caused by the glycidyl amine linkage [28]. Again, the higher glass transition temperature can be mutually exclusive of thermal stability.

1.3.2 Modification and Toughening of Polymers and Composites

The formation of crosslinks within a polymer network enhance the stiffness by reducing the molecular mobility which tends to have an adverse impact on strength, strain to failure, and fracture toughness but an increase to strength and modulus. Also, the ability of the monomers to occupy free volume as the network forms can affect stiffness so that even for high functionality, the resulting cured resin modulus can be lower. Therefore, a large body of work revolves around how to enhance the intrinsic properties of thermoset polymer networks and their composites whether for improved mechanical properties or improved toughness, although ideally both.

Some common routes to modify resins can be classified as extrinsic toughening where a material is added at the nanoscale or microscale level and those that are intrinsic where the network is modified. Further, there can be functional and non-functional forms of either. Nano-clays, emulsion-polymerised rubbers, and silica beads are shown to improve the toughness of thermosetting resins and could be considered extrinsic and non-reactive modifiers [29], [30]. More traditionally, to enhance fracture toughness, thermoplastics or rubbers are added in quantities from 5 to as much as 30 wt% where phase-separated morphologies containing large micro-scale domains of tougher thermoplastics help to create energy-absorbing failure mechanisms under fracture [31], [32].

Enhanced modulus can be achieved by modifying the cured network. One such phenomenon that results in increased stiffness and sometimes strength is antiplasticisation. At the network level, monofunctional additives have been shown to enhance stiffness of multifunctional epoxy networks [33]. Molecular additives that suppress segmental motions in the network have also shown to enhance modulus due to limited network mobility [34]. For high temperature resins and composites, a consideration must always be had for how the modifier affects the glass transition temperature and thermal stability.

Other routes that try to balance thermal and mechanical properties include combining multiple polymeric species of differing properties. Interpenetrating networks of two or more chemically-different thermosetting polymers have also shown to influence the properties of the polymer blend and can be tailored to balance the properties of the two for thermal, mechanical, and environmental stability [35]. Unlike the IPN approach, co-polymerisation creates a homogenous network between two or more functionally similar monomers in the polymer formulation. These can also be tailored to change the thermal and mechanical properties from those of the monomeric constituents [36]. In all, however, similarly high temperature resins tend to have similar mechanical properties so the resulting effects may not be amplified in the blend.

In brief, there are many challenges to employing high temperature epoxies for structural and thermal applications. Performance both in terms of thermal resistance and ageing require highly aromatic and rigid network structures which adversely impacts mechanical properties. Modification of the resin needs to balance thermal and mechanical behaviour as well as processability, especially for translation to a reinforced composite. Hence, there is a strong need to explore new epoxy resins and strategies to modify the matrix to meet the demands of high-temperature performance of composite structures.

1.4 RESEARCH AIM AND OBJECTIVES

The commercial TGDDM and resins are characteristic of glycidyl amine and in the case of TGAP, characteristics of both glycidyl amine and glycidyl ether resins. DGEBA is purely a glycidyl ether resin. An epoxy resin of interest to high temperature composites is the tetrafunctional dimeric naphthalene based resin, bis(2,7 glycidyl ether naphthalenediol) methane (NNE). First synthesised by Ogura & Takahashi, the homopolymerized resin is

characterised by a very high T_g of 328°C which is claimed to be the highest of any known epoxy resin [37]. The structure of the epoxy monomer is shown in Figure 1-1.

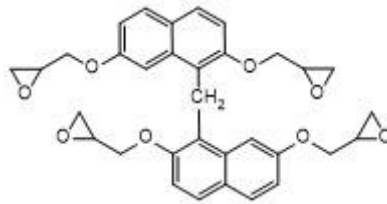


Figure 1-1 - Chemical structure of the dimeric naphthalene epoxy monomer, NNE

Limited research into tetrafunctional epoxy glycidyl ethers either as a neat resin or composite exists making the structure-property relations between glycidyl ether and glycidyl amines a focal point of this work. Further, this resin is in a class of naphthalene-containing epoxies and bismaleimides which have shown benefits in terms of enhanced glass transition and thermal stability [38]–[45]. Therefore, the effect of naphthalene backbones on composite performance and thermal stability is also a primary focus of this work. The objective is to apply a fundamental knowledge of the evolution of cure and the mechanical properties of the neat resin and then systematically modify the resin to produce a balance of thermal, mechanical, and processing characteristics that would be desirable for structural composite applications. These would include:

- ◁ A high thermal stability above 200°C for long durations (<100 hours) and a glass transition temperature above 250°C
- ◁ Lower viscosity for processing by liquid moulding and other out-of-autoclave techniques
- ◁ A strength, stiffness, and fracture toughness comparable to commercial TGDDM
- ◁ Routes to modification and enhancement of properties via particle modification, molecular reinforcement, reactive diluents, and partially reacted substructures

While resins based on TGDDM would appear to meet many of the aforementioned performance parameters, the nature of the glycidyl amine resins presents some challenges to furthering the available matrix systems for high-temperature polymer composites. A thorough

investigation of the tetrafunctional glycidyl ether, NNE, cured with conventional aromatic diamines could present a viable alternative to TGDDM and allow for realised performance benefits in the area of high-temperature composite structures. However, there is a general lack of comparable studies on the structure-property relations for multifunctional glycidyl ether resins and their composites and even less so for high aromatic naphthalene-based epoxies.

1.5 OUTLINE OF WORKS IN THIS THESIS

Chapter 2 presents the relevant literature relating to high performance polymers for composites with special attention to the high-temperature and thermally stable resins used for composite applications. The effect of chemistry and processing on the network formation is reviewed in terms of curing kinetics, chemical bond formation, degradation, and how it relates to the time-temperature-transition signature of epoxy resins. Special emphasis is placed on the structural differences for epoxy glycidyl ethers versus epoxy glycidyl amines and how the past research relates to this work comparing two tetrafunctional epoxies that differ in this way. Further, a review of proven and emerging strategies for the enhancement of the resin properties, primarily for improved mechanical performance and toughness, are presented. Translation of thermal and mechanical properties from the resin to composite are reviewed.

Chapter 3 details the experimental techniques and equipment that are employed to investigate the research goals outlined in the previous chapter. Except where specified, the measurement and analysis techniques common across the proceeding results chapters are presented.

Results of the various investigations outlined in this work are presented across the next range of chapters followed by a summary conclusion. Chapter 4 presents an investigation of the cure kinetics and evolution of the glass transition temperature of the unmodified resins utilised in this work. A combined approach compiles thermal cure kinetics by differential scanning calorimetry (DSC) with near-infrared Fourier Transform spectroscopy (NIR) and dynamic thermal-mechanical analysis (DMTA) at increasing isothermal temperatures. The results of DSC are used to calculate the kinetic rate constants of the three resins and measure the growth of the T_g relative to the isothermal cure temperature. NIR is utilised to capture the change in the reactive groups of the different formulations and quantify the change in epoxy, primary amine, the primary/secondary amine overtone, and the growth of the hydroxyl groups relative to time and isothermal temperature. Significantly, contrasting behaviour between the change in functional groups of the glycidyl ether and glycidyl amine networks are observed after

elevated temperature post-cure. That is determined to relate to potential for etherification between glycidyl ether and glycidyl amine network. The DMTA analysis further expands on the kinetic analysis, showing the growth of the rigid network structure and T_g through changes to the isothermal cure and post-cure temperatures. This chapter culminates in the time-temperature-transition (TTT) phase diagrams for the tetrafunctional glycidyl ether and glycidyl amine resins.

Chapter 5 expands the work of the preceding chapter to investigate the structure-property relation between the glycidyl ether and glycidyl amine resins as well as the influence of the dimeric naphthalene structure of the former. Neat resin properties are studied at varying cure conditions and compared to the pure glycidyl amine and the bi-component blend of the two. Here, the effect of conversion is studied by increasing the cure and post-cure of the NNE network and the effect of crosslink density is studied between NNE, TGDDM, and a bi-component blend of the two. DMTA and thermogravimetric analysis (TGA) of the cured resins as well as density and moisture ingress studies provide insight into the network properties. Carbon fibre reinforced composites of the three resin formulations are manufactured and evaluated in the as-cured state and a thermal ageing study is presented to compare the three resins in terms of their thermal-oxidative performance in the composite at a high isothermal temperature. It is shown that the glycidyl ether nature of the tetrafunctional resin is superior for composite applications due to the limited effect of thermal expansion in the composite accelerating the thermo-oxidative reaction in the early stages of ageing.

Chapter 6 investigates some novel and emerging strategies to modify the resin and composite. Aromatic monofunctional epoxy additives and partially reacted substructures (PRS) assembled from pre-reaction of the diamine with the mono-functional epoxy are synthesised and added to the epoxy resin in stoichiometric quantities. Additionally, non-covalently bound naphthalene and a molecular additive are added to occupy free volume in the network and provide fortification to the network. The effect of these additives is investigated with respect to cure kinetics, rheological behaviour, thermal properties, moisture ingress and mechanical performance for the neat resin. The influence of the additives on the composite is investigated. It is shown that 10-20 mol% of a mono-functional epoxy and 10-20 wt% of naphthalene addition can significantly reduce the melt temperature, viscosity, and processing window of

the neat resin. An increase in modulus is immediately apparent for both resin and composite at 5 wt% for the mono-functional additive, the PRS, and naphthalene.

Chapter 7 presents a resin and composite study into the core-shell rubber (CSR) toughened tetrafunctional epoxy resin and the carbon fibre composite. While CSRs have been utilised for toughening since the late 90s, their efficacy on highly crosslinked brittle materials is not well-presented. In this work, an in-depth investigation of the efficiency between CSR addition to the resin and translation of the composite is presented. Multi-spectral sensing of the composite Mode I fracture toughness response is utilised to determine the difference in acoustic response of the CSR laminate and enhance the understanding of mechanical fracture toughness test data. It is shown that CSR addition dramatically improves the composite fracture toughness of a tetrafunctional epoxy.

Chapter 8 provides a summary of the body of work and outlines aims for future developments within these fields of research.

2 LITERATURE REVIEW

2.1 HIGH TEMPERATURE POLYMERS

While epoxy resins are the most common of thermoset materials in composites there are a number of high-performance, high-temperature polymers that are used for such applications. These include some phenolics, benzoxazines, cyanate esters, and bismaleimides as well as other high-temperature thermoplastics. Also, hybrid resin formulations comprised of the above resins or co-polymerised with epoxies has been extensively studied.

2.1.1 Phenolic Novolac Resins

Phenolic resins are a type of polymer that has excellent thermal and chemical stability. These systems find widespread use in a variety of demanding applications from bushings used in rotary equipment to electronic chip-boards and applications requiring good flame-retardant properties. One common issue with phenolic resins is excessive amount of water vapour that volatilises during cure. In work by Hodzik et al., a comparison of glass-fibre phenolic composites to a polyester-based composite showed the phenolic species gained nearly 2% total mass after aging in a moisture rich environment compared to just 0.3%. Subsequently, the water-aged specimens exhibited much less stable fracture toughness than the polyester composite [46]. Critically, as water vapour precipitates during the cure cycle it may become entrapped between layers of the composite structure and form a void thereby severely limiting the structural integrity. While not a hard rule, most phenolic composites tend to have a low laminate thickness to ensure minimal void content in the final laminate.

2.1.2 Benzoxazine Resins

Benzoxazine-based resins for structural composites applications have only gained the interest of researchers and engineers within the last decade and are not as widely discussed as any of the former matrix systems mentioned. One of the repeated advantages that are reported suggests these types of resins have a low melt viscosity, excellent flame retarding characteristics, thermal stability, and a relatively high T_g above 300°C compared to standard epoxy-based resins [47], [48].

Some recent developments continue to make benzoxazines and poly-benzoxazines attractive. Harehane et al. produces an imidazole-based benzoxazine that cured at a lower temperature than typical systems [49] which is a significant development because of the very high energy cost associated with curing most high- T_g resins. Also, Agag et al. were able to produce a

repeating, linear benzoxazine molecule that had a thermoplastic character however, upon cross-linking to achieve a higher T_g and thermal stability, the resin was noted for being severely embrittled [47]. As with BMIs, phenolics, and cyanate esters, this alternative high-temperature matrix is still disadvantageous as a result of high cure temperatures and embrittlement.

2.1.3 Cyanate Esters

Cyanate esters are a class of polymers that are generally used in applications with demanding hot-wet performance. The isocyanate crosslinks to form cyanurate rings via the process of cyclotrimerization and as a result are one-part systems or one-part catalysed to reduce the long gelation time [50]. The reaction results in a polymer network with high thermal stability, toughness, and low water absorption after cure [14]. T_g can be as high as 290°C [51] and water uptake can be as little as 0.5 wt % [52]. Cyanate esters can be co-polymerised with epoxies to produce interpenetrating networks that can enhance performance compared to the neat epoxy resin, particularly by increasing the glass transition temperature and reducing equilibrium moisture ingress [53]–[55].

2.1.4 Bismaleimides

Bismaleimides are an addition-cured polyimide and are a class of resins that are notable for high T_g and long-term thermal stability. A common bismaleimide 4,4'-bismaleimidophenyl methane (BMIM) co-polymerised with 2,2'-diallyl of bisphenol A (DABA) is penta-functional with the ability to undergo crosslinking with the allyl, maleimide, and etherification [56]. These resins tend to have low viscosity, can be resin-transfer moulded at room temperature, and are cited as a replacement for epoxies due to the excellent thermal (T_g in the range of 300°C) and mechanical properties [20]. The backbone is based on an imide linkage which results in higher crosslink density which makes the cured resin relatively brittle [14]. One development of note for the bismaleimide system is the potential for mending. The Diels-Alder reaction between a diene and a dienophile (imide) is a reversible reaction meaning it can be re-formed with the addition of heat and pressure. Bismaleimides have been central to various investigations into the reversible Diels-Alder reaction for potential to heal damaged polymer composites [57]. As with cyanate esters, bismaleimides may also be co-polymerised with epoxies to improve thermal stability and mechanical properties of the latter [35], [58]–[60].

2.2 EPOXY RESINS

2.2.1 Fundamentals and Basic Structure of Epoxies

The fundamental building block of an epoxy monomer is the terminal epoxide group also referred to as an oxirane ring. The oxirane ring itself can undergo two mechanisms of reaction either direct coupling via homo-polymerisation or between the epoxide and a reactant [61]. The ability to react with a variety of curing agents makes epoxy resins versatile for a number of different applications. Another benefit is the ability to tailor performance by designing the structure of the epoxy monomer. The oxirane ring can be bound terminally to both aromatic and aliphatic units and the functionality (number of oxirane rings terminally bound to the backbone) can be manipulated. The ring itself is highly strained which makes it a very reactive species compared to other building blocks of thermosetting polymers such as the imide formation in bismaleimides [26] and the homopolymerized cure of cyanate esters which require elevated temperatures above 200°C and the use of catalysts [62]. An example of the oxirane ring structure and some aromatic and aliphatic mono-epoxies is shown in Figure 2-1.

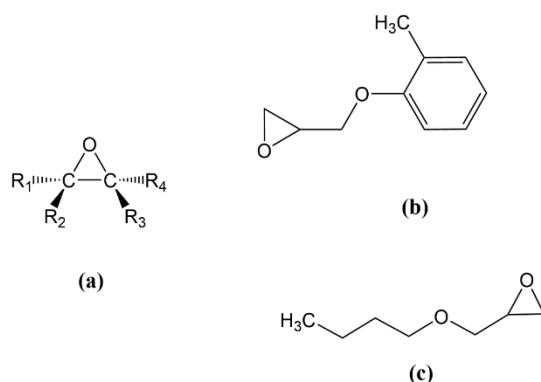


Figure 2-1 - Example of (a) oxirane ring, (b) aromatic monofunctional o-cresyl glycidyl ether and (c) aliphatic monofunctional n-butyl glycidyl ether

In order to produce a cross-linked network, the functionality of epoxide groups terminally bound to the backbone must be equal or greater than two [63]. Additionally, the curing agent, in the case of direct coupling, must follow the same rule. These principals hold true for the case of di-functional epoxies such as diglycidyl ether of bisphenol A (DGEBA) whereas for multi-functional epoxies the crosslinking is determined both from the epoxy and diamine. The reactivity of epoxy resins is relatively high due to the strained nature of the oxirane rings and is particularly reactive with proton donors and the cured network structures can show glass transition temperatures (T_g) in the range of 60-250°C [63] although modern developments in epoxy resin technology and hybridisation have shown T_g s above 250°C are possible [37], [64].

The primary route to achieving high temperature performance, the main interest of this work, is by maximising the epoxide functionality, utilising aromatic structures within the backbone, and using suitable curing agents with similar properties in functionality and aromaticity.

2.2.2 Amine-addition During the Cure of Epoxy Resins

There are two ways by which epoxy resins can form cross-linked networks, namely co-reaction and catalytic homo-polymerisation. The latter is a chain-growth polymerisation process where, upon catalysing the ring-opening of the epoxide group, the free oxygen can form a hydrogen bond with an adjacent epoxide unit and forms a polymeric chain until termination. However, the chain-growth polymerisation can cause early termination of primary chains which can then negatively impact thermal and mechanical properties [23]. The step-growth polymerisation between the functional group of a monomer and that of the co-reactant are considered mutually independent from other reactions also occurring during polymerisation [65] and generally results in a higher cross-link density than chain-growth polymerisation. For epoxies, the example of the step-growth process is the polymerisation of the epoxide functionality via primary and secondary amine addition and then the etherification reaction which is depicted in Figure 2-2. While a significant advantage for epoxy resins are the number of possible curing agents (alcohols, imidazole catalysts, acid anhydrides, and polyamines) the cure with aromatic polyamines is of primary interest for building high temperature, thermally stable resins formulations.

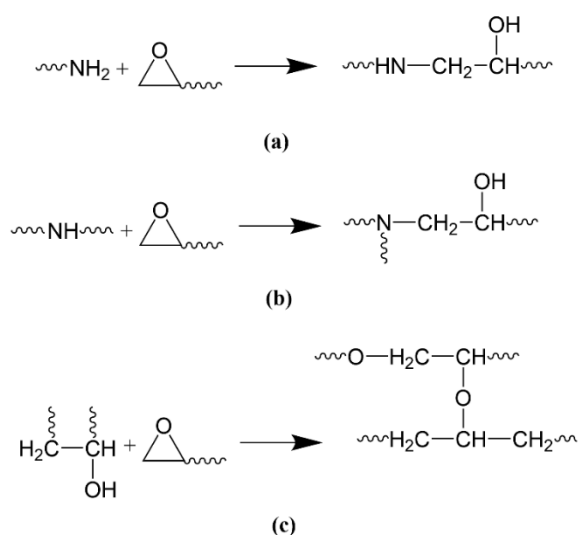


Figure 2-2 - Examples of (a) primary amine addition, (b) secondary amine addition, and (c) etherification reaction

The initial step-wise growth via primary amine addition results in linear chain formation. Following the reaction of epoxide with primary amine, a secondary amino functional group is formed which can then undergo ring-opening polymerisation and reaction with a second epoxide group. After the secondary amine is consumed there forms a tertiary amine. Tertiary amine can catalyse further ring-opening and hydrogen bonding with free hydroxyl produced during the primary and secondary amine reaction. The effect of etherification in the later stages of cure, especially at elevated temperatures, can change the bulk properties of the cured network after primary amine consumption [66], [67]. For an ideal epoxy-amine polymerisation with no side reactions, the consumption of primary amine leads to the formation of a macromolecular structure and typifies the gelation point of the system [68]. Empirical formulas such as the Flory-Stockmeyer theorem express gelation as a function of the epoxide and hardener functionality but the gel point occurs as a result of both primary and secondary amine reactivity [69], [70] and experimentally, conversion of epoxide functional groups tend to deviate by as much as 15-30% from the theoretical predictions [71]. For most resins, particularly those commercially available, impurities and oligomers will affect how the network is formed.

2.3 HIGH-TEMPERATURE EPOXIES AND SIGNIFICANCE OF GLYCIDYL ETHERS AND GLYCIDYL AMINES IN NETWORK FORMATION

As previously noted, the functionality, aromaticity, and co-monomer largely dictate thermal characteristics of the cured epoxy network. While high temperature performance and thermal stability are rightly judged based on the application and service conditions there are some metrics reported that classify a polymeric material as a “high-temperature.” These have included durability above 180°C for long-term thermal exposure (>10,000 hrs) [17] and stability above 200°C for greater than 100 hours and a T_g greater 250°C [72]. However, it is also important to consider the resistance to physical ageing at elevated temperatures and the long-term changes to mechanical properties [14].

The most common epoxy resin for high temperature composites is tetraglycidyl diamine diphenyl methane (TGDDM) which tends to exhibit a glass transition temperature in the range of ~250°C [64], [73]–[76]. The reaction of diamine diphenyl methane (DDM) in an excess of epichlorohydrin followed by the dehydrochlorination of the product with sodium hydroxide to produce the epoxidized monomer [77]. Figure 2-3 shows the chemical structure of TGDDM.

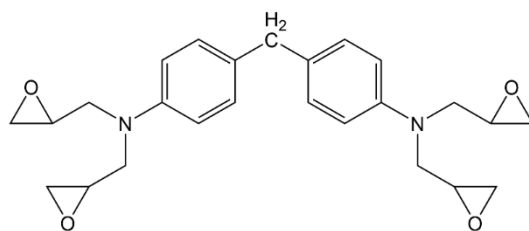


Figure 2-3 - Example structure of the TGDDM epoxy monomer

Here the aromatic phenyl rings in the backbone and the four terminally bound epoxide groups lend to the resins thermal performance at elevated temperatures. However, also present is the tertiary amino where the epoxide groups are bound to the nitrogen atoms on either side of the backbone. The presence of the nitrogen has been of particular concern for reasons to do with reaction mechanisms through the cure cycle and other properties affected in the cross-linked network.

This resin, a glycidyl amine, has been shown to undergo significant etherification and can also form cyclic rings during cure which can adversely affect thermal and mechanical performance. Levchek et al. explored the homopolymerized TGDDM and showed that at temperatures above 150°C, the formation of cycloaliphatic rings catalysed either by the tertiary amine or other impurities, was present and does not contribute to cross-linking and polymerisation [78]. The effect from the formation of internal cyclic structures can adversely affect phase transformations during cure and the resulting thermal and mechanical performance of the resin. Matejka studied diglycidyl amine and diglycidyl ether resins cured with aromatic diamines and showed consistently lower molecular weight of the glycidyl amine resins due to the formation of cyclic structures pendant to the cross-linked network [79]. The results of their kinetic analysis also showed that the overall reaction rate was slowed by the presence of glycidyl amine and cyclisation was accelerated by increasing the cure temperature. That is a significant concern with epoxy resins for high temperature because of the generally high final cure temperatures ($T_{\text{cure}} > 180^{\circ}\text{C}$) typically used with TGDDM-based and other resin formulations.

In contrast to the epoxy-amine reaction induced cyclisation found for glycidyl amines, such behaviour is largely absent for glycidyl ethers. Matejka et al. studied diglycidyl ether of bisphenol A (DGEBA) and TGDDM cured with both aromatic and aliphatic amines [69]. In their survey they noted significant cyclization for the nitrogen-containing epoxies while DGEBA showed no signs of cyclisation. Further, the gelation of DGEBA-based formulations was dependent only on the reactivity of the primary and secondary active hydrogen of the

amino group. Min et al studied DGEBA-based systems modified with the addition of polysulfone thermoplastic and showed no appreciable etherification or side-reactions until the system viscosity began to affect network reactivity and only a small fraction (9%) was consumed by such mechanisms [80]. Clearly then, glycidyl ether resins promise an advantage over glycidyl amine resins to approach defect-free and controlled epoxy-based networks.

More recently, new research into tertiary-amine free epoxy polymers for high temperature ($T_g > 250^\circ\text{C}$) has demonstrated alternatives to TGDDM- and TGAP-based resins. Liu et al formulated a high molecular weight tetrafunctional glycidyl ether and showed similar glass transition temperature and superior mechanical performance for a blended system comprised of DGEBA and DDS versus TGDDM [28]. Further, Xing et al. formulated a similar tetrafunctional glycidyl ether epoxy and demonstrated the viability as a matrix for carbon-fibre reinforced polymer composites at elevated temperatures by improved inter-laminal shear strength (ILSS) versus TGDDM-based composites [81]. Other benefits included reduced moisture uptake, reduced dielectric loss, and improved fracture toughness, strength, and higher temperature of degradation. Zhang et al. synthesised and studied the performance of a novel sulphonated tetrafunctional glycidyl ether resin and showed similar performance improvements for the neat resin and as a composite matrix when stoichiometrically blended into a DGEBA-DDS formulation. Of course, in all cases these tetrafunctional glycidyl ethers are very high molecular weight and the authors all make note of the high viscosity and melt temperature above 90°C , hence the need for dilution into DGEBA. In the course of the research and development in new high temperature resins, processing constraints frequently become a limiting factor. As such, factors such as low viscosity, high melt temperature, and reduced reactivity can restrict the usefulness of new resins for real-world plastic and composite applications, regardless of performance enhancements over conventional high- T_g epoxies such as TGDDM and TGAP.

2.4 ROLE OF NETWORK STRUCTURE ON PROCESSABILITY, THERMAL STABILITY, AND MECHANICAL PROPERTIES

Certain chemical structures have been shown to have a repeated and characteristic effect on the thermal stability of epoxies and other thermosetting materials. In early work on the incorporation of naphthalene units into a bismaleimide-based resin, Wang et al. reported significantly increased molecular weight, T_g , degradation onset, and peak exotherm during cure [20]. In subsequent work the addition of a pendant naphthalene unit decreased the very high

melt point but also decreased thermal stability from near 300 to 260 [43]. The incorporation of naphthalene units into an epoxy monomer generally improves the thermal performance of epoxies compared to phenyl and biphenyl groups of the same functionality [42], [82]. Due to the planar nature of phenyl and naphthalene structures these molecules can be tightly organized which decreases mobility of the polymer network. The naphthalene unit has been reported to exhibit greater hydrophobicity than phenyl-based resins which was attributed to less epoxy ring opening and subsequently less –OH groups present [40]. .

2.4.1 Crosslink Density and the Effect on Chain Segment Mobility

The crosslink density is a value that is determined from all segments and chains that are formed during polymerisation and after the reaction has ceased. The establishment of a crosslinked network structure is fundamental to thermosetting polymers and is a major factor that influences the resulting thermal and mechanical properties, in addition to affecting fracture toughness.

The effects of crosslink density on polymeric materials are generally pronounced and consistent. At low crosslink densities the polymer network is characterised by poor dimensional stability and generally low stiffness [83]. Conversely, as the crosslink density increases, the mobility of these segments becomes restricted and are less free to deform in three dimensional space [84]. The higher crosslink density and limited mobility tends to result in a higher modulus.

Thermal properties are also affected as crosslink density increases. The degree of crosslinking results in greater energy needed to cleave chemical bonds [17]. Rigid phenyl or naphthalene units resist bond rupture and increase thermal stability [18]–[20] but also tend to cause embrittlement and low toughness due to a less flexible network architecture [21], [22]. Increasing thermal stability can result in inverse mechanical performance.

2.4.2 Thermal Degradation and Stability

While aspects related to the glass transition temperature of a polymer can inform thermal performance at temperatures near the T_g , thermal stability deals with the performance over a time-scale that is factors of magnitude longer than the various test methods utilised to study the T_g . Indeed, the degradation mechanisms at temperatures below the T_g of epoxies has been a major area of study since the early years of commercially-useful epoxy resins [85], [86]. Bishop & Smith investigated the thermal degradation of amine and anhydride cured epoxies

by gas chromatography and identified non-chain scission degradation below 500°C and the breakdown of the aliphatic portions of the network in the range of 500-600°C and later the aromatic phenol groups at 700°C [87]. Later work by Grassie et al. improved upon the earlier experimental observations using gas chromatography techniques and, utilising an amine-cured DGEBA resin, identified the evolution of secondary alcohols as low as 240°C and decomposition of the cross-linked networks above 340°C [88]. Levchik et al. studied the homopolymerized TGDDM system and proposed the scission of alkyl-ether and allyl-amine bonds which evolved from 260°C after dehydration of secondary alcohols in the structure [89]. Further work by Levchik et al. in to the amine-cured TGDDM network and measured lower char yield and higher volatiles content as a result of the increase in tertiary amine species and decrease in ether groups that results from the co-polymerisation of TGDDM and DDS [90]. The crosslinks formed upon ring-opening of the epoxide group are aliphatic compounds so while the aromatic backbone and high crosslink density contribute to limited network mobility, thereby enhancing T_g , the long-term thermal stability of the resin is limited by the aliphatic nature of linkages.

Thermal analysis, while frequently employed is limited in the ability to determine a lifetime assessment of thermally-aged resins. By non-isothermal TGA, the onset(s) of degradation and the char yield are easily determined. The final char yield is a result of the dehydration of secondary alcohols in the network followed by polymerisation into new compounds of aliphatic and aromatic hydrocarbons which can repeat many times until a stable char is formed by pyrolysis [89]. Some attempts to utilise thermal analysis for lifetime and service temperature predictions have shown interesting behaviour. Al-Yami et al. investigated a proposed epoxy resin ($T_g = 126.8^\circ\text{C}$) by isothermal TGA from 280-360°C and utilised the isothermal scans to develop a model for the lifetime expectancy at sub- T_g continuous service temperatures [91] For aspects of service temperature, Stutz evaluated DGEBA and TGDDM resins cured with 44DDS and through conventional isothermal TGA at increasing service temperatures below the T_g , noted only a 10°C difference in lifetime of the latter resin, even at $T_{\text{service}} \approx T_g$ of DGEBA-DDS [13]. It was noted that DGEBA showed appreciably higher activation energy of degradation than TGDDM but, regardless, Stutz concluded that only a few bonds needed to be broken for TGDDM to exhibit a rapid decrease in T_g and reach a lifetime service temperature comparable to DGEBA.

2.5 MODIFIED EPOXY RESINS AND TRANSLATION TO THE COMPOSITE

2.5.1 Thermoplastic Toughened Polymers

Thermoplastic (TP) modification of epoxy and other thermosetting polymer matrices is a widely reported toughening strategy. Introduction of a thermoplastic in small quantities can lead to separate phases during the cure of the thermoset. The availability of high-temperature thermoplastics with favourable toughness means certain epoxies can be toughened with minimal impact on thermal stability. These plastics, such as polysulfone and polyetherimide, have been heavily studied on commercial high-temperature epoxy, cyanate ester, and bismaleimide resins [92]–[96].

These separate thermoplastic phases become apparent at the microscopic level, forming independent of the bulk matrix into a variety of morphologies which can increase the fracture energy through shear yielding and crack branching [97]. At small concentrations of thermoplastic doping into an epoxy the morphology tends to be homogenous or contain small phase separated regions of thermoplastics [98]. For larger concentrations the phases of epoxy-rich and thermoplastic-rich material can become co-continuous or phase inverted where the epoxy phase becomes entrapped in thermoplastic-rich phases [99]. At concentrations less than 20% by weight these thermoplastics separate into microscale phases within the cured epoxy network. The thermoplastic-rich regions lack crosslinks which enable greater dissipation of energy which imbues a greater toughness to the material. Figure 2-4 shows the various phase morphologies of TP-modified epoxy networks pictographically alongside physical examples by SEM imaging.

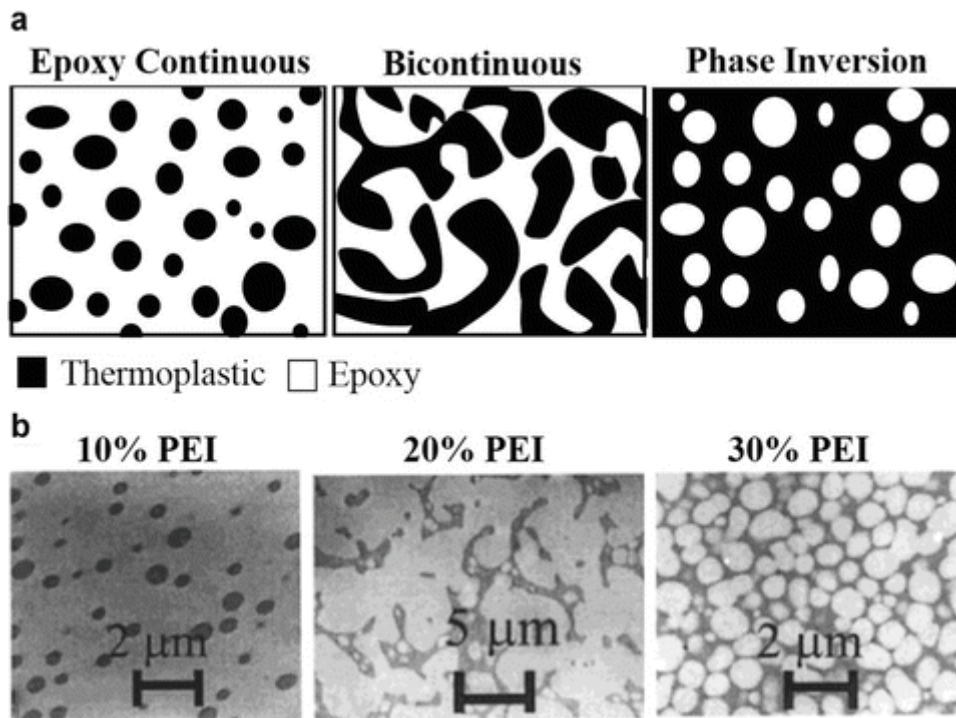


Figure 2-4 - Diagram and SEM images of phase separated , co-continuous, and phase inverted epoxy/TP systems [100]

The introduction of a thermoplastic phase can affect the material properties in a variety of ways. Brooker et al similarly investigated the effect of PES on a DGEBA/TGAP blend cured with MDCEA and shows phase-separated spherical regions of $1\mu\text{m}$ at 15-20% PES while co-continuous and inverted phases occurred at 25 and 30% respectively. The resulting fracture toughness of the phase separated regions was lower than the co-continuous and phase inverted regions and virtually no decrease in T_g occurred as the PES and DGEBA/TGAP blends had near identical T_g [99]. However, for higher functional systems the thermal mismatch between thermosetting polymer and thermoplastic can become deleterious. Kinloch et al investigated the effects of polyethersulfone (PES) addition on highly functional TGAP ($n=3$) and TGDDM ($n=4$) systems cured with 44DDS. These epoxy systems, when mixed with PES contained 0.2-0.4 μm diameter thermoplastic phases which more than doubled the fracture toughness (both K_{1C} and G_{1C}) but decreased both flexural modulus and T_g [101] Similarly, Cheng et al reported that TGDDM/TGAP blends with PES resulted in lower T_g due to lower cross-link density and also negatively impacted the gel time, reducing it from 305 to just 175 minutes [93].

Thermoplastics tend to affect kinetics during the cure of epoxy formulations at large quantities. Giannotti et al reported that epoxy/DDS and epoxy/MCDEA with PES and PEI at 10% resulted in no change to the kinetic rate constants while at 20 wt% the rate constants for both systems

decreased notably as phase-separation began to occur, although effects due to an increase in viscosity from the addition of a high-T_g thermoplastic are also noted [102], [103].

Highly cross-linked materials modified by thermoplastics have been extensively studied in terms of the effect TP addition has on fracture toughness and thermal stability. Suman et al evaluated a dicyanate ester (BADCy) with 5, 10, 15, and 20% PES. They showed that at the lowest concentration, T_g by DMA was virtually unchanged at 289°C while further increases in PES caused two peaks to occur at 201°C (thermoplastic) and 260°C (cyanate ester). Additionally, the impact toughness of glass-fibre laminates (Izod) was decreased at 10% and only marginally increased at 20% concentrations and flexural properties decreased from the unmodified BADCy [94] .

2.5.2 Toughening by Core Shell Rubber Particles

Various researchers have investigated toughening polymers by core shell rubber particles for at least three decades. Core shell rubbers (CSR) are particles on the sub-micro scale (50-200 nm) and are comprised of a soft core material (e.g. butadiene, styrene, silicone gel) encased in a hard copolymer (e.g. polymethylmethacrylate) outer layer. These particles are immiscible in an epoxy solution however have a high degree of dispersion in solution. An example CSR particle manufactured by Kaneka Corporation and an image of it dispersed in an epoxy matrix is shown in Figure 2-5. The diameter of the solid core tends to be much larger than the thickness of the shell. The core material elastic modulus is shown to affect the overall impact on fracture energy [104], [105].

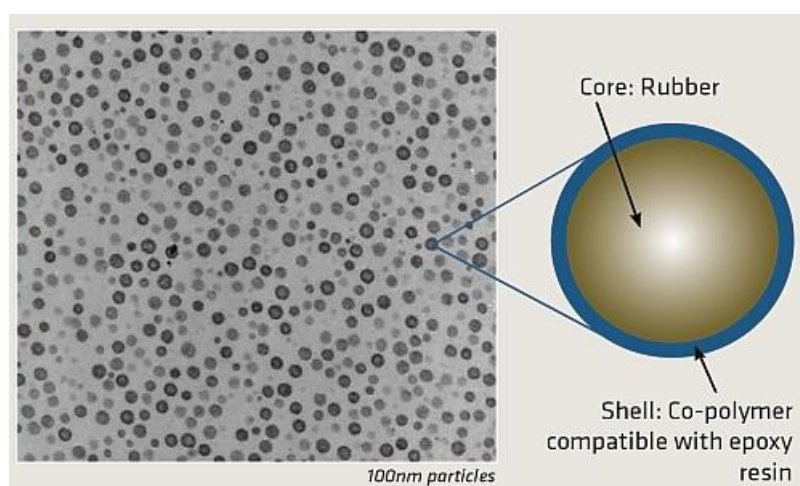


Figure 2-5 - SEM image of core shell rubber particles dispersed in a matrix system with diagram of CSR structure [106]

Some of the earliest work into core shell rubber toughening involved the determination of the toughening mechanisms. The cavitation of the CSR particle accelerates shear yielding [104], [107], [108]. Other research suggests that cavitation is secondary to shear band formation and yielding [109]. In addition to those toughening mechanisms others report crack pinning [110] and crazing [111] as additional mechanisms of toughening by CSR particle addition.

Core shell rubbers (CSR) have been widely studied on di-functional epoxies [30], [104], [105], [109], [112]–[114] and to a much lesser extent for high temperature cyanate ester [115], benzoxazine [116], and a blend of di- and tetrafunctional epoxies[117]. While strength and stiffness generally decrease with increased CSR loading, the glass transition temperature generally remains the same [105], [109], [114]. A summary of the glass transition, epoxy, and improvements to fracture toughness have been collected from the literature and are shown in Table 2-1. Of the studies on CSR-toughened epoxies, none exhibit a glass transition temperature above 200°C.

Table 2-1 - Summary of investigations exploring CSR toughening, the type of epoxy investigated, T_g of the resulting matrix, and fracture toughness/energy

Matrix System	CSR Concentration*	T_g , °C (unmod. / mod.)	K_{Ic} (MPa \sqrt{m})	G_{Ic} (J/m 2)	Notes	Source
DGEBA/DICY	24%	141	0.8 / 1.7	220 / 1130	Decreased E, σ_y	[105]
DGEBA/Phthalic anhydride	3%	163.3 / 171.7	0.53 / .83	-	Decreased $E_{tensile}$ and $E_{flexural}$	[30]
DGEBA/DDM	10%	187.5 / -	-	189 / 562	-	[104]
DGEBA/Albidur HE600	20%	148 / 144	0.70 / 1.46	117 / 947	Decreased E but increased $\sigma_{fracture}$	[109]
DGEBA/DDM	30%	1.20 / 2.64	343 / 2671	122.5 / 128.1	Decreased E, σ_y	[112]
DGEBA/MTHPA	6%	106.5 / 116	-	750 / 1150	No major change in dielectric properties	[113]
DGEBA/TGDDM/DDS Blend	N/A	<190°C	N/A		Increased G_{Ic} of the composite	[118]

*Concentration is reported only at highest fracture toughness reported

2.5.3 Antiplasticisation of Cross-linked Polymer Networks

Anti-plasticisation is a loosely termed behaviour sometimes exhibited by polymeric materials. The nature of anti-plastic behaviour can be induced by many different routes although generally the resulting behaviour is the same. The total strain to failure tends to decrease whilst modulus and sometimes strength increase, resulting in a stress-strain behaviour with little to no plastic yielding [119]. Antiplasticisation can be a phenomenon of the mechanism (i.e. cure schedule) and degree of cure or can be influenced by modifying the resin formulation with additives at the molecular and nano- to micro-scale. Venditti et al. proposed a relation between the higher free volume fraction from more rigid networks and the antiplasticisation phenomenon showing that with increased cure, the unreacted parts of a tetrafunctional epoxy network become constrained within the crosslinked framework thus increasing modulus and reducing the strain-energy dissipating capabilities of the network [120]. Excerpt models of the proposed antiplasticisation effect from increased constraint due to cure are shown in Figure 2-6.

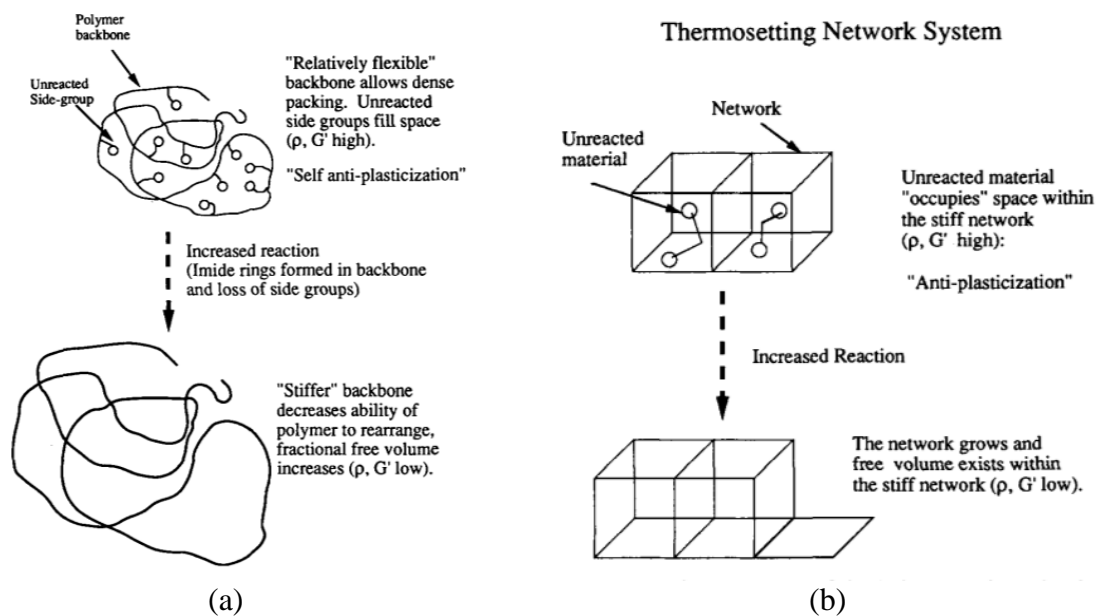


Figure 2-6 - Fundamental model of cure-induced antiplasticisation for a thermosetting network [120]

The mobility of a thermosetting network is complex and defined by the progression from dispersed short-chain molecules through to the formation of a macromolecular structure (i.e. polymeric gel) until vitrification and a “locking in” of the network. The ability of the network to absorb energy then is largely defined by the ability to rearrange the network relative to external force. Hata & Yamauchi investigated the relation between different antiplasticisers of molecular weight between 278-528 g/mol and related the increase to modulus and decrease to

the sub-ambient β -transition to the suppression of free volume effects on the network as the primary mechanism for antiplasticisation [121]. Also of note, there was no change to strain at failure or impact strength for the three antiplasticisers studied but the phenomenon was apparent for all three systems. Further work by Hata & Kumanotani explored even higher molecular weight diluents and showed that at a critical juncture, the epoxy resin modified with the highest MW showed no antiplasticisation again confirming the relation the phenomenon has to the ability to fill the available free volume [122]. Similarly Heux et al. monitored cured epoxy networks by sub-ambient DMTA and nuclear magnetic resonance spectroscopy concluding that the segmental motions across a small number of repeat units was slowed hence the reduction in the β -transition and increase to modulus [123]. Bershstein et al. evaluated the creep strain rate of some antiplasticised systems of varying crosslink density and showed the suppression of hydroxypropylether units near NH functionalities were suppressed by antiplasticisers but had no influence to the ring flip of the epoxy backbone [124].

The culmination of the free-volume filling effect increases modulus but at a consequence to other properties as the T_g becomes a component of the T_g of the diluent or antiplasticiser. Grishchuck et al. utilised co-polymerised benzoxazine (BOX) on an aliphatic and aromatic amine-cured epoxy and reported the co-continuous nano-phases of BOX within the network resulted in lowered T_g , increased modulus, but decreased fracture toughness due to the antiplasticisation [125]. Sauvant & Halary investigated a series of non-reactive molecular additives and showed similar effects to the T_g , modulus and a reduction to moisture uptake but quite different performance in fracture across modifier type and test temperature with some improving fracture toughness and some diminished fracture toughness [126]. They suggested that could be due to the formation of multiple nano-phases during cure and shear yielding but did not extensively investigate the hypothesis.

2.5.4 Reactive and Non-Reactive Diluents

A diluent can be considered any material that, when incorporated into the molten epoxy resin, decreases viscosity. The types of diluents can be categorised as those that can react with the active species within the polymer network to then incorporate into the network and those that do not react. Some common diluents include low viscosity monofunctional epoxies, aliphatic epoxies and amines, and various solvents. Diluents can also aid in the increase or reduction of exotherms, improve chemical resistance, and enhance electrical properties [127]. Diluents can also affect the mechanical properties of the resin or matrix [127], [128].

Reactive diluents for epoxies are mono, bi, and multi-functional epoxies of low molecular weight and viscosity. These monomers tend to contain long and flexible aliphatic segments. When incorporated in stoichiometric quantities to the network of a rigid epoxy they can increase the mobility of the network in response to load. Advantages of reactive diluents can include reduced viscosity, increased toughness, and ancillary benefits to moisture ingress and UV stability. Disadvantages generally include reduced thermal stability due to the aliphatic nature for many of these compounds [33].

Less common are non-reactive diluents and interpenetrating networks to simultaneously reduce viscosity and improve toughness. In either case, the incorporation of a diluent creates systemic changes to the reaction kinetics, processing, and properties of the cured resin. Jena et al demonstrated improved toughness, glass transition temperature, and reduced viscosity with a BMI/DBA modified TGDDM resin [59]. Sinha et al compared a reactive (polyethylene glycol) to non-reactive (toluene) diluents in a DGEBA-TETA system and showed beneficial copolymer formation, increased tensile strength, toughness, and crosslink density for the former, which was maximised at 10 mol%, and generally deleterious performance for the latter [129].

2.6 POLYMER COMPOSITES

2.6.1 Evolution of Composite Materials and Manufacturing

The use of polymer composites dates to the mid-1930s with the simultaneous development of fiberglass and a new class of relatively cheap and easily processable polymers. Games Slayter, a researcher with Owens-Illinois Glass Company, developed the first large-scale method for manufacturing fiberglass filaments [130] which would lead to the creation of Owens-Corning Fiberglass Corporation. In the earlier part of the 1930s, Julian Hill and Wallace Caruthers, two researchers with the DuPont Chemical Company, were developing a series of polyamides and polyester resins that had real potential on an industrial scale [131]–[133]. The advanced in light-weight, high strength fibres and new polymers would shortly lead to the first large-scale composite marine and automotive structures by the 1940s, effectively launching the first composites industries.

It would be the development of high strength, stiff carbon fibres that would launch what is now the near-ubiquitous use of composites in structural applications. Carbonised filaments were developed as early as the 1860s by Sir Joseph Swan and used to demonstrate the viability of electric light [134]. Nearly a century later the technology to develop long-form carbon

filaments of an aspect ratio beneficial for structural applications was realised by a researcher at Union Carbide Corporation, Roger Bacon [135]–[137]. Shortly after, Otani reported on the development of a high strength carbon fibre from polyvinylchloride pitch [138]. While previous research had shown carbon fibre filaments could be manufactured from textile fibres, the results of Otani's work showed the potential for higher strength and stiffness in an economical fashion. Shortly thereafter, researchers from the Royal Aircraft Establishment of the United Kingdom showed the potential for high strength, high stiffness carbon fibre made from textile filaments [139]–[141]. From there, rapid developments in just a few decades would see commercialised carbon fibre applied to airplanes and spacecraft and, with economies of scale, into a multitude of industries from sports and recreational equipment, medical devices, and heavy industry.

In parallel with the rapid developments of new structural fibres and advancements in design capabilities for composites, the role of the polymer matrix quickly evolved. From the 1970s onwards, development in high strength, toughened resins to meet the expanding requirements of composite structures in the aerospace industry led to commercialised multifunctional epoxies, bismaleimides, cyanate esters, and research into the hybridisation of resin formulations.

2.6.2 Applications and Trends in Composites Technology

As the demand for composites grows outward in many directions, certain limitations of these class of material systems have become apparent. An example of that is shown in the adoption of composite bridge and fracture plugs in the natural gas and oil extraction industry. These new plug designs are manufactured from as much as 97% polymer composites and are designed to withstand a temperature of 149°C (300°F) and pressures in the range of 690bar (10,000 psi), all the while reducing drill bore time by nearly 50% over tradition metal and metal-composite plugs [142]. However, hot-wet (hygrothermal) performance has limited the utility of some commercial high-T_g resin systems such as cyanate esters, due to poor performance in a moisture-rich environment.

The focus on degradation for composites has long been on the ingress of moisture and time to saturation that a particular system achieves. However, with the need for elevated service temperature increasingly entering the focus of composites end-users, the development of novel formulations for elevated temperatures in a caustic environment is a relatively new market-

driven demand. The temperatures, pressures, and environmental factors such as working fluids with high salinity can exacerbate degradation of the polymer matrix. Under such conditions, composites may undergo hydrolytic (separation of chemical bonds by addition of moisture) and hygrothermal (change in material properties due to combined thermal and moisture effects) degradation [143]. In such cases, fibreglass, with an osmotic nature, tends to exhibit extended hygrothermal degradation in comparison to carbon composites. The controlling factor then is the matrix.

Polymer composites for extreme temperatures are not solely the focus of heavy industry such as oil & gas applications. Near-engine components in automotive and aerospace structures require a combination of stiffness, lightweight capabilities, and long-term resistance to high temperatures. Researchers with the Fraunhofer Institute developed a new combustion engine and used re-designed valves made of high-temperature phenolic resins and advanced computer simulation to optimize the design and reduce exposure to heat, ultimately achieving a 20% reduction in weight over conventional aluminium components [144]. High-temperature polyimides capable of performance above 300°C resins have also been used to replace traditional metallic components in automotive pistons but ultimately failed to meet the demands of the 425°C operating conditions, even with tailored design for composites and metallic shielding [145].

When considering the aerospace market and near-engine components the demands become increasingly greater. Nickel-based and titanium alloys dominate much of the structure in and around the various components of the gas turbine engines due to the necessity of stable performance around 600°C with minimal long-term creep behaviour [146]. Aluminium alloys are susceptible to long-term creep even at temperatures in the range of most polymer composites making them a target for replacement in areas where the long-term service at elevated temperature is of concern. The effect of such a shift is ongoing in the aircraft industry but is well recognized by the trends in improvements to aircraft structures as shown in Figure 2-7.

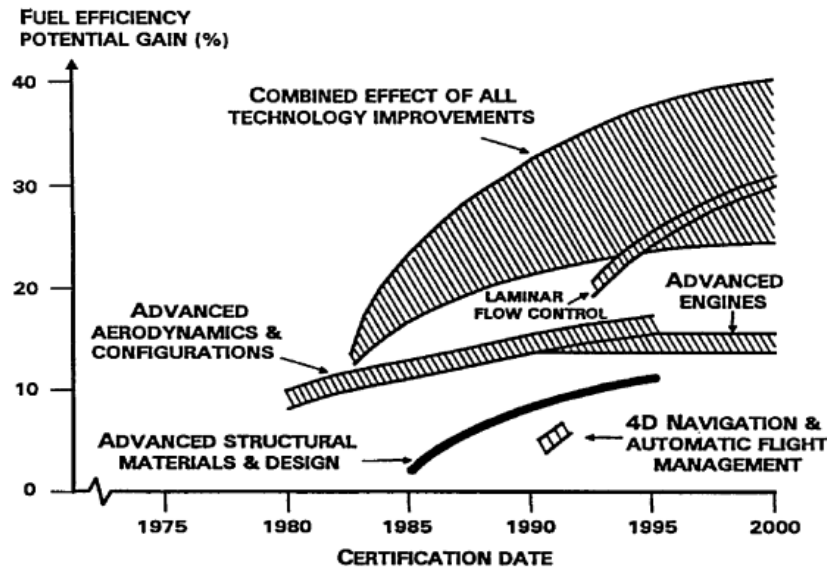


Figure 2-7 - Trend in aircraft efficiency based on the effect of the introduction of technological advances (borrowed from [146])

It is interesting to note that the only areas of major growth have occurred with advances in aerodynamics and the introduction of new materials and design. Engines themselves contribute a major part to efficiency but perhaps less so due to the minimal savings in weight achieved in the structure elsewhere through lightweight composites due to trade-offs such as cost and thermal performance.

Composites may come in many forms from metal-matrix, carbon-carbon, and polymer matrix composites. The majority of composites, approximately 70% by production volume are polymer reinforced, and of those, 71.5% are thermoset matrices [7].

Thermoplastic matrix composites are a growing area of interest due to the potential for rapid manufacture, reparability, and in some instances the thermal stability. With regard to thermal stability, a few TPs are widely known for high T_g and mechanical performance suitable for aerospace applications. Polyimides are sometimes noted as the upper-limit for service temperature of polymer composites near 350°C [15]. Rocket components on the NASA X-30 experimental vehicle were manufactured at the sub-scale using PEEK composites but full-scale manufacturing of CFRP/PEEK was unattainable and the matrix was switched to an epoxy [16]. Others such as polyimides (PEI) have been used for services temperatures above 200 but lack processability due to high melt temperatures [17]. As such, purely thermoplastic composites

are still only a minor part of modern composites since many alternative, highly processable thermosets exist for similar service conditions.

2.7 MODIFICATIONS TO POLYMER COMPOSITES

There are two main routes to modify polymer composites and can be considered intrinsic and extrinsic modifiers. Intrinsic modification would be those where the matrix is modified to enhance some property of the composite. As previously mentioned, these can include thermoplastic tougheners [147], inorganic such as carbon nanotubes [148], nanosilicas and nanoclays [149], and others that are added directly to the matrix. Extrinsic modifiers are added at the composite level and can include films [150] or veils [151], [152] into the interlaminar regions of the composite and reinforcements in the through-thickness direction of a laminate such as z-pins [153]. Composites can also be hybridised to include multiple fibre types which is more of a laminate design scheme than a modification.

Very little reference to antiplasticisers or core shell rubbers used for continuous fibre polymer composites is present in the literature. Frequently, the antiplasticising effects that moisture ingress and ageing have on mechanical properties of polymer composites are reported [154], [155]. One study by Vassileva & Friedrich studied the effects of alumina nanoparticles added to the matrix and studied by DMTA to yield some traces of antiplasticisation but only the context of resins for composites is discussed, not applied [156]. Similarly the work by Subramanian & Sun shows that a hybrid CSR/nanoclay can toughen their DGEBA-based resins but only discusses the possibility to make toughened FRPs from it [157]. In a review of the available literature for CSRs only Riew et al. showed a translation of the resin performance to a composite [158]. That translation of resin properties to the composite is critical for modified matrix systems because the very different stiffness and strain to failure of fibre properties can suppress the effect of modifiers for the neat resin.

The translation of toughness improvements delivered by modification to the neat resin is not always directly proportional to the fibre reinforced composite. Scott & Phillips demonstrated that CTBN-toughened composites showed a markedly reduced fracture energy than the neat resin counterparts which was attributed to the decreased “glue-line” thickness between the composite lamina [159]. Chong & Taylor investigated block co-polymer toughened epoxies and their composites and while the bulk resins showed large improvements to fracture energy, the increase to fracture toughness was not translated to the composites [160]. The fracture energies of the composite and the neat resin are shown in Figure 2-8 below.

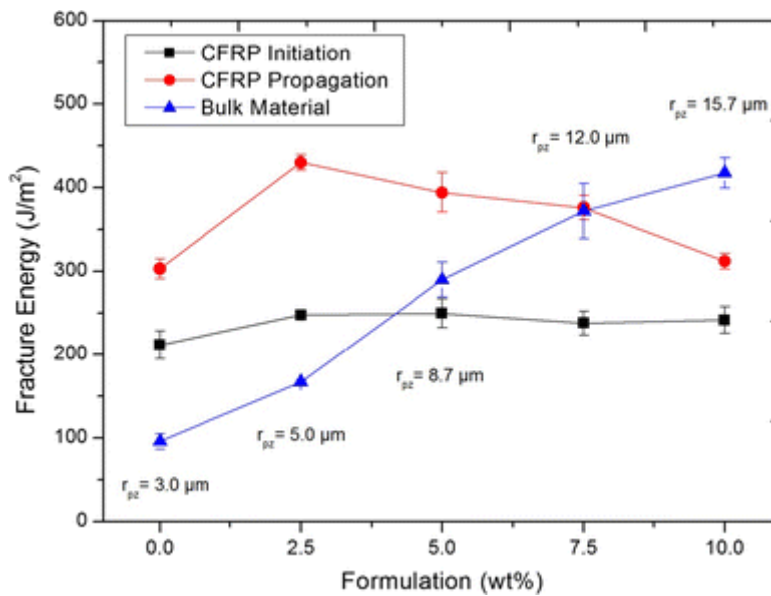


Figure 2-8 - Comparison of initiation and propagation fracture energy of the CFRP to the neat resin fracture energy [160]

The difference in the effect that certain tougheners have on the composite versus the neat resin is considered to be a function of the aspect ratio between the crack tip area in a bulk polymer versus the composite. The plastic zone in the composite is constrained to a small domain in the resin rich regions between lamina. Previous work on epoxy networks has demonstrated the inverse relation between crack growth and the size domain around the crack site [161]–[163]. The theoretical assumption would be that under mode I loading, the fracture energy in the composite would mirror that of the bulk resin. That would be the case if no transverse crack bridging or bifurcations were to occur. That behaviour was noted by Scott & Phillips but the results of fracture energy showed a large deviation between the resin and composite [159].

Conversely, some particle toughening routes show limited effect in resins at the bulk level but improved response in composites. Bradley et al investigated the effect of crosslink density and core shell rubber toughening of three epoxy amine systems with T_g between 189°C (low Mc) and 225°C (high Mc) and concluded that while adding a rubber microphase to low Mc materials could elicit an improvement to toughness, highly crosslinked materials were not toughened by rubber particles [164]. However, work by Riew et al. demonstrated a significant improvement to fracture toughness of a high- T_g epoxy laminate toughened by CSRs [117]. Hsieh et al demonstrated improved toughness to a composite by addition of glass beads that were surface treated to improve bonding with the epoxy matrix and toughness was achieved by deflection

of the crack tip [29]. Therefore, it is important to note that the performance of modifiers on the neat resin can behave independent of the composite.

2.8 THERMAL PERFORMANCE AND STABILITY OF POLYMER COMPOSITES

Thermal stability and resistance to thermal loading (i.e. thermal shock) are mutually exclusive terms with regards to polymer composites due to both physical and chemical changes that can occur on different timescales. For the polymer matrix, exposure to elevated temperatures results in degradation reaction mechanisms such as the formation of alcohols and cleavage of the bonds that comprise the initial cured network structure. The deterioration in mechanical performance with the exposure of temperature extremes has been shown to be driven by the interfacial properties between the fibre and matrix. Tsotsis demonstrated that mass loss and the glass transition temperature are not demonstrative of the reduction in mechanical strength of epoxy composites, that is mass loss always results in a decrease to mechanical properties but not a quantifiable metric [165], [166]. Significantly, the thermal degradation of polymers is usually investigated by mass loss [167], [168] and the products that arise from the degradation of the network. The sub- T_g ageing results in cleavage of bonds, changes to the free volume of the network which can adversely contribute to deterioration in the matrix properties [169]. Rose et al. showed that for TGDDM-DDS, there was no significant change in the chemistry of the degradation products in the inert atmosphere and an oxygen atmosphere up to 340°C, well above the glass transition temperature [170]. The ageing of the composite can proceed by multiple pathways making it a complex phenomenon to investigate.

There are two key aspects that differentiate the effects of thermal ageing on a composite, namely the physical and chemical changes that occur either separate or simultaneously. Weight loss associated with thermal ageing can occur due to the evacuation of volatiles and moisture and thermo-oxidative ageing tends to result in a greater weight loss as shown in Figure 2-9 [171]. After the evolution of volatiles and moisture, a steady-state loss of mass can indicate a thermo-oxidation mechanism which, overtime tends to reach an equilibrium after which subsequent weight loss is associated with new thermo-oxidative processes [172]. Other changes that occur include effects on the T_g , crack density, modulus, fracture toughness, and embrittlement of the matrix as a result of both continued conversion of functional groups and degradation of bonds segments within the network, sometimes concurrently. An increase to the T_g can be associated with network growth (chain extension and crosslinking) while a lower T_g

suggests chain scission and some degradation. Chemical degradation can be complex and result in irreversible changes to the network and subsequently the thermal and mechanical properties.

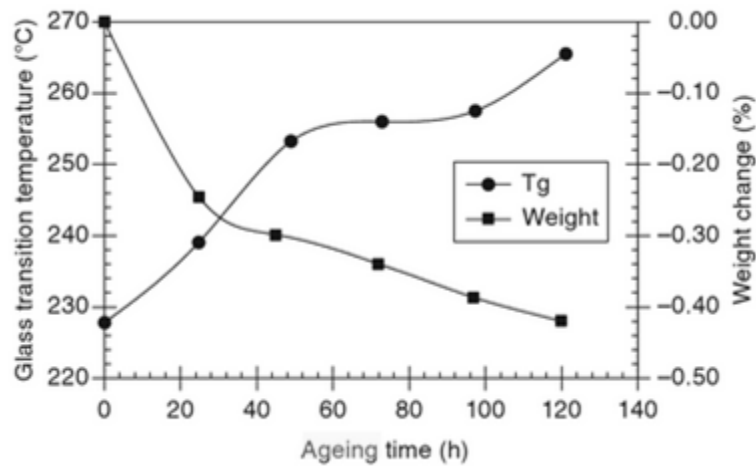


Figure 2-9 – Relation between weight loss and ageing on the T_g of a composite [171]

Thermal-oxidative ageing propagates through a composite from the formation of microstructural cracks primarily at the free edge of the laminate where thermal gradient effects are more pronounced. These defects serve as pathways for air from the environment to penetrate the composite and react with the free polymer surface. It is consistently shown for thermal ageing [173] and thermal shock an cycling [174], [175] result in a deterioration of the interfacial properties between fibre and matrix. Particularly with long-fibre composites, the exposure to heat causes distortion between fibre and matrix due to differing thermal expansion behaviour. Mahato et al. spiked an epoxy/glass fibre composite to 50, 100, 150, and 200°C for durations ranging from 5-40 minutes and showed that shorter exposure decreased tensile strength while the extreme of 40 minutes increased tensile strength [176]. Partly, the improvements after longer exposure times at 100°C and 150°C spike temperatures times were attributed to extended crosslinking of the epoxy matrix. The exception arose for 200°C exposures where, regardless of time, the modulus and strain to failure decreased and was suggested to relate to degradation, embrittlement, and possible micro-cracking of the matrix. Interestingly, there was no clear trend between time, temperature, and the change in modulus and strength at the intermediate steps where a variety of different damage modes were observed. That could suggest a stronger correlation between the initiation and propagation of surface defects than temperature in terms of the effect on the composite.

Stutz described the degradation mechanisms of glycidyl ethers as purely dehydration and cleavage of the hydroxypropyl ether functionality whereas the glycidyl amine undergoes dehydration, cleavage, and dissociation into amine and formaldehyde [13]. It was evident that the degradation of DDS-cured DGEBA and TGDDM, as studied by kinetics, showed similar lifetime service temperatures (115-120°C) regardless of T_g . Delozeanne et al. investigated DDS-cured DGEBA and TGDDM by FTIR and showed different reactive products and deviation of the kinetic models for the degradation of the two epoxies [177]. Purely gravimetric kinetics rely on the assumption of a single mechanism for the degradation of the functional groups, regardless of epoxy, but it was clear that the chemical difference in the two resins had different rates, different products, and therefore, competing chemistries which could impact the thermal stability of the resins regardless of T_g and T_d . While a majority of the previous research into thermal stability of the model high performance aerospace resin, TGDDM, are concerned with sub- T_g temperatures in the range of 120-200°C [170], [177]–[179], a characterisation of the near- T_g performance is not reported.

2.9 SUMMARY OF THE LITERATURE

The current state of the research into high temperature epoxies and their reinforced composites primarily focuses on a small set of commercial epoxies such as TGDDM. While there have been some developments in high-temperature ($T_g < 200^\circ\text{C}$) resins, many trade-offs still exist in terms of thermal stability, mechanical properties, and ease of processing. Some promising improvements to thermal stability are shown with the use of epoxies containing naphthalene backbones which can improve char yield and the glass transition temperature. Of the modification routes, a substantial body of research has investigated thermoplastic and core-shell tougheners and exhibit similar gains to toughness. But the negative impact on T_g of the former and the lack of research on resin systems with T_g greater than 200°C of the latter show a clear need to explore CSR particle toughening strategies on high- T_g , high-crosslink density networks and their composites. An interesting but small body of work on direct antiplasticisation shows promise as a strategy to improve modulus and potentially maintain a high T_g . The translation of increased modulus via antiplasticisation to a composite has not been clearly demonstrated. It is also clear that the glass transition temperature and thermal performance of the resin can be mutually exclusive and therefore it is important to consider both the short- and long-term degradation to properties at elevated temperatures.

3 EXPERIMENTAL METHODS AND MATERIALS

3.1 INTRODUCTION

The standard methodology and materials used in the following studies are outlined in this chapter. Where deviation from the standard methodology outlined in this chapter occurs, it is clearly noted in the subsequent chapters.

3.2 MATERIALS

3.2.1 Epoxy Resins and Amino Hardeners

The main epoxy monomers and hardener utilised in the study are shown in Figure 3-1 and key information are provided in Table 3-1. In the subsequent chapters additional chemicals are noted where used. The epoxy resin to amino hardener stoichiometry, unless otherwise specified was 1:0.95. Commonly, a slight excess of epoxy is included to promote etherification between free hydroxyl and to ensure full consumption of secondary amine [180], [181].

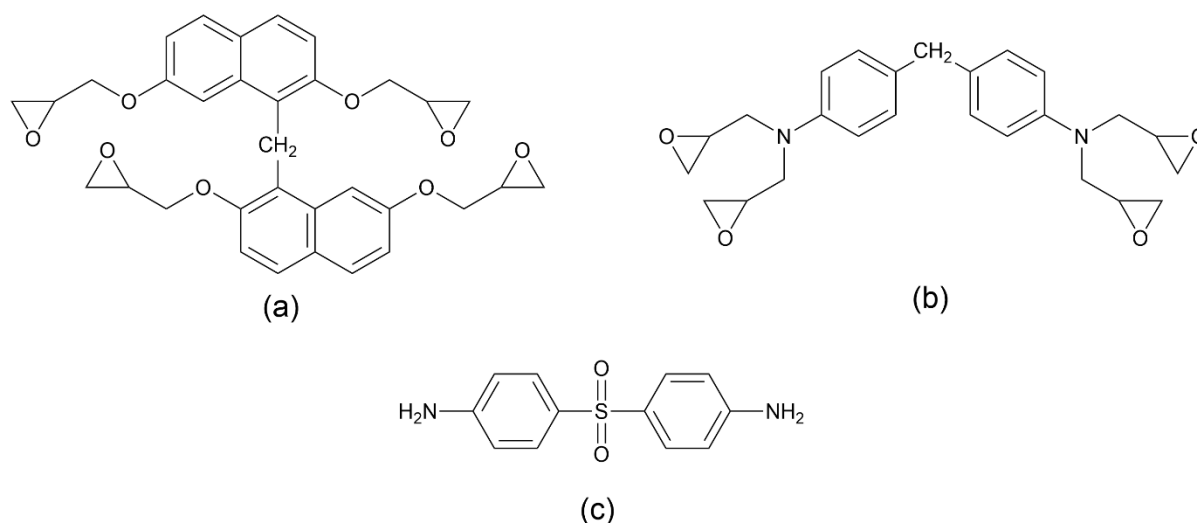


Figure 3-1 - Chemical structures of (a) NNE, (b) TGDDM, and (c) 44DDS monomers

Table 3-1 - Main epoxy and amine hardeners used in this study

Material	Acronym	Chemical Name	EEW (g/mol)	Mfg. Supplier
Epoxy Monomer	NNE	bis(2,7 glycidyl ether naphthalenediol) methane	170	DIC Corp. (JPN)
Epoxy Monomer	TGDDM	Tetraglycidyl diaminodiphenyl methane	124	Huntsman Corp. (USA)
Amine Hardener	44DDS	4,4'-diaminodiphenylsulfone	238.30	TCI Chemical Inc. (JPN)

3.2.2 Pre-Processing of Resin Constituents

All epoxy monomers and silicon moulds used to cast resins were degassed at 65°C in a vacuum oven set to 250mbar for a minimum duration of 24 hours. This is essential to remove excess moisture and potential volatiles that can accumulate in transit from suppliers and whilst in storage. The resins are cast into silicon moulds containing cavities of dimensions suitable for the desired mechanical testing. Prior to formulating resins, silicon moulds were staged in a convection oven. The oven was then heated to 150°C and held at that temperature. This is to prevent adverse thermal shock on the molten resin and also to dry out the moulds of any moisture. Typical cure schedules for resins were 150°C for four hours, 180°C for four hours, and then a free-standing (after demoulding) post-cure 200°C or above for 2 hours.

3.2.3 Formulation of Neat Resins

Resins were prepared utilising a hot oil bath and roto-evaporator equipped to laboratory vacuum supply. The epoxy resins were added to a round-bottom flask and heated to 120°C and degassed for 15-30 minutes until no bubbles were apparent in the molten state. Then the amino hardener was carefully added to the molten epoxy. The epoxy-amine mixture was then transferred back to the roto-evaporator and mixed under heat and vacuum at 130°C for 15 minutes until the DDS was dissolved into epoxy and no bubbles were apparent. Then the mixture was quickly removed from vacuum and transferred to the pre-heated moulds.

3.2.4 Cure of Neat Resins

Cure schedule variations are noted in the subsequent chapters but in general, heating was initiated in a convection oven at 150°C for four hours. Then the temperature was raised to 180°C at 5°C/min heating rate for an additional four hours. Resins were then de-moulded and a free-standing post-cure at 200°C under a heating rate of 3°C/min (for TGDDM-DDS) and 220°C and a heating rate of 3°C/min (for NNE-DDS) was performed.

3.2.5 Characterisation of Monomers by High Performance Liquid Chromatography

Commercial resins generally are not pure but comprised of one or more isomers and some portion of oligomers. In the case of epoxies, that can include monomers that vary in epoxide functionality, lack epoxide groups, contain excess hydroxyl due to ring-opened groups, and other impurities. These defects in turn can affect the catalysis of cure and resulting thermal and mechanical properties. High performance liquid chromatography (HPLC) has been repeatedly used to identify different structures in the uncured resin and determine the averaged molecular weight distribution [77], [182]–[184].

The foundation of HPLC measurements for polymers is to essentially identify traces of these oligomers and isomers by their polarity. A non-polar solution will allow for the rapid transmission of a non-polar molecule to transport through the detector column of an HPLC much faster than more polar species. At the same time, the oligomeric species tend to be high molecular weight and will fall out of solution at a much later time than the main isomers. Therefore, it is essential to allow for sufficient transport of the monomer in order to detect these defects, typically on the order of 30-60 minutes.

An HPLC (Agilent Corp., USA) with a C18 gradient column of 150mm length and diameter was utilised to determine the purity of the various resin monomers investigated. Between 100-250 millimol of epoxy resin was first dissolved into acetonitrile (ACN) which was then diluted to obtain a solution comprised of 70% MilliQ water to 30% ACN. The same gradient of 70% MilliQ water to 30% acetonitrile was used at the initial stage of the gradient elution and slowly increased to 100% ACN over a period of 45 minutes. The flow rate was 1mL/min and the sample volume was 20 uL. A multi-channel UV detector recorded the spectra at wavelengths of 210, 230, 254, 280, and 290 nm. The HPLC results are provided in Appendix A.

3.3 NEAT RESIN CURE KINETICS

The uncured resins are utilised to study the evolution of cure by a variety of techniques ranging from thermal, optical, and rheological methods and techniques.

3.3.1 Differential Scanning Calorimetry

A Netzsch Proteus 205 differential scanning calorimeter (DSC) was utilised for isothermal and dynamic analysis of the uncured and cured resins. DSC measures the difference in heat flow required to raise the temperature of a substance. This can either be measured by the temperature change between the sample and a reference or by controlling the temperature by altering the applied thermal energy, thereby creating a differential in the heat flow measured between the reference and the sample. In this case, the heat flux DSC method is used.

Dynamic DSC involves heating the resin at a constant rate (1-20°C/min) up to a temperature in excess of the peak exothermic temperature of the reaction. A baseline can then be drawn beneath the exothermic peak and the heat flux determined by integration with respect to temperature. The peak temperature of the exotherm and the heat flux can be utilised to determine the energy barrier of activation by performing at least three scans at different ramp

rates. In this work, a minimum of five heating rates are utilised. Both the Kissinger and Flynn-Wall-Ozawa methods are employed to determine activation energy and should be in agreement with one another. The iso-conversional approach to reaction kinetics are based on the assumption that the reaction rate is dependent on temperature and conversion but independent of reaction order. Li et al. studied the kinetics of castor oil pyrolysis by Kissinger and Flynn-Wall-Ozawa (FWO) methods and gave a succinct description of the two methods as applied to degradation kinetics [185]. Under constant heating rates, the kinetic equation is as follows:

$$\frac{da}{dt} = k(T) \times f(\alpha) \rightarrow A\beta \frac{da}{dT} = Ae^{-Ea/RT} \times f(\alpha) \quad \text{Eq. 1}$$

Here, the reaction rate constant is determined by an Arrhenius relationship from the slope of $k(t)$. E_a (J/mol) is the respective activation energy, R (J/mol-K) is the gas constant, and T (K) is the temperature. The heating rate, β (K/t), is constant. The kinetic equation can be integrated to yield:

$$\int_0^a \frac{da}{f(a)} = g(a) = A\beta^{-1} \int_0^T e^{-Ea/RT} dT \quad \text{Eq. 2}$$

For the Kissinger method, the resulting integration can be approximated using the Coates & Redfern [186] approach and is given as:

$$g(a) = \frac{A}{\beta} \times \frac{RT^2}{Ea} e^{-Ea/RT} \quad \text{Eq. 3}$$

Upon some rearrangement of terms and taking the natural logarithm, the equation is simplified to:

$$\ln \frac{\beta}{T^2} = \ln \frac{AEa}{Rg(a)} - \frac{Ea}{RT} \quad \text{Eq. 4}$$

The Flynn-Wall-Ozawa approach is determined by Doyle's approximation and is given as:

$$g(a) = \frac{A}{\beta} 0.00484e^{-1.052Ea/RT} \quad \text{Eq. 5}$$

which can be arranged to arrive at:

$$\ln \beta = \ln \frac{AEa}{Rg(a)} - 5.331 - 1.052 \frac{Ea}{RT} \quad \text{Eq. 6}$$

Isothermal DSC involves heating a resin up rapidly to a specific isothermal temperature and holding it for a sufficient duration of time to establish a zero baseline in the trace of heat flow from which an integration can be carried out with respect to time. Upon cooling to ambient temperature (20-25°C), the cured resin can be dynamically reheated up to a temperature in

excess of the glass transition temperature for the fully cured resin, if known. A residual exotherm in the dynamic scan after isothermal curing indicates the residual enthalpy of the partially reacted resin system. The ratio of the isothermal enthalpy and the residual enthalpy indicates the fractional conversion at that specific isothermal cure temperature. As isothermal curing temperature is increased, the residual exotherm should reduce into the baseline.

The method for performing DSC starts with weighing out an empty aluminium crucible with a pierced lid which serves as the reference crucible. The sensitivity of DSC measurements requires fine control of sample mass. Therefore, an analytical balance capable of measurements to 0.01 mg is utilised. Then, another crucible and pan are weighed, and the balance is zeroed. To the empty crucible, approximately 10 mg of resin is added, compacted to ensure uniform contact with the bottom of the pan, and weighed. The reference and sample crucible lids are crimped, and the tops pierced to allow for the exhaust of volatiles that can evolve whilst the resin is heated. The weights of the reference crucible, sample crucible, and sample mass are recorded and entered into the DSC control software. An auto-sampling robot loads the crucibles into the corresponding reference and sample plates of the DSC heating chamber which is then sealed, and the specific heating profile is performed. Simultaneous conductive heating of the plates and cooling by nitrogen gas controls the sample temperature throughout the heating and cooling cycles.

3.4 RHEOLOGY

Rheology comprises a series of techniques to understand the behaviour of liquid and soft materials where the behaviour is partially or primarily plastic as opposed to elastic. The rheological methods employed with thermosetting polymers include oscillatory rheology of the polymer melt and can also consider dynamic thermomechanical analysis (DMTA) techniques.

3.4.1 Oscillatory Rheometry

The fundamental principal of rheology is that under induced shear stress or shear strain, the response of the material is to deform. A Newtonian fluid is any such material which satisfies a linear shear strain rate versus shear stress. Most polymers are non-Newtonian and exhibit a non-linear deformation with respect to the shear strain rate.

3.4.2 Dynamic Thermomechanical Analysis

Thermosetting and thermoplastic polymers exhibit degrees of elastic and plastic behaviour. For an uncured thermosetting polymer there are three key temperatures at which key events in the

network formation occurs. These include the melt temperature, temperature of gelation, and temperature of vitrification. With respect to time, there are also times to gelation and vitrification which are dependent on the cure temperature. From these points, a master curve can be established which outlines the key phase changes relative to the cure temperature. This is often called the time-temperature-transformation (TTT) diagram.

The DMTA method involves stimulating a polymer at a given oscillating frequency of a mechanical load whilst dynamically or isothermally heated in a chamber. As the oscillating frequency of the mechanical load perturbs the material, a phase lag can occur between the applied load and the elastic response of the material. This phase lag indicates the viscous (plastic) portion of the material.

A Q800 DMTA (TA Instruments, USA) was utilised for all isothermal curing of resins and for sub-ambient and dynamic scans of cured resins. A standard protocol was utilised for each type of measurement and is outlined in detail below. The fixture used for all tests was a dual/single cantilever apparatus with free span length of 35mm in dual cantilever and 17.5mm in single cantilever modes.

Isothermal experiments allow for the determination of gelation, vitrification, and the evolution of glass transition temperature at specific cure temperatures. In this method, strips of unidirectional carbon fibre are doped with uncured resin using a solvent mixture of 50% dichloromethane and 50% acetone to dissolve the epoxy monomer and amino hardener. Then the solvent was evaporated in a convection oven for a minimum one hour at a temperature 75°C and utilising forced extraction. A composite of nominal dimensions of 1-1.5mm thickness, 60mm length, and 10mm width was constructed and wrapped tightly in aluminium foil to prevent bonding to the clamp fixture. The pre-impregnated fibre sample was affixed to the dual cantilever apparatus. The procedure for isothermal curing included a 30 minute dwell at 90°C followed by a ramp to the isothermal temperature (130-180°C) at which the sample was held for 480 minutes. Then the sample was cooled to 50°C and ramped to a temperature above the full T_g at a ramp rate of 5°C/min to determine the glass transition temperature. The gelation and vitrification are evident in the $\tan(\delta)$ as peaks in the initial stages of cure. Upon vitrification, the storage modulus ceases to evolve.

Dynamic heating experiments was performed on single and dual cantilever specimens. Resins were held at an equilibrium temperature of 50°C for 2 minutes after which the specimens were heated at 5°C/min under a displacement amplitude of 10-50µm loading up to a temperature 30-40°C in excess of the expected full T_g. Nominal dimensions were 3mm thickness and 12mm width. The glass transition temperature is apparent when the storage modulus begins to drop from a relatively constant value and a peak emerges in the tan(δ) after the storage modulus onset.

3.5 NEAR INFRARED SPECTROSCOPY

Fourier Transform Infrared Spectroscopy (FT-IR) is a light spectroscopy technique that employs infrared light energy passing through a domain to determine the emissivity or absorbance of the solids, liquids, and gases that occupy the domain. Particularly for polymeric materials, the presence of distinct infrared signatures in the near-IR (NIR) range of 4000-8000cm⁻¹, that correspond well to the presence of chemically uniform species makes it a useful technique for quality inspection and more advanced studies of the polymerisation process. The fundamental principal that determines the absorbed light at any frequency in the IR domain is Beer's law which is given as:

$$A = \log \frac{I_0}{I} \quad \text{Eq. 7}$$

Here, A is the spectral absorbance, I is the light intensity of the source entering the specimen, and I₀ is the light intensity that is measured as passing through the specimen. The absorbance at any wavelength is a function of the corresponding functional group represented. Each of these groups has a molar emissivity and chemical concentration that will affect the measured absorbance. In addition, the physical measure of the length through which the light must travel through (i.e. specimen thickness) will affect absorbance. Therefore, Eq. 1 may be rewritten as:

$$A = \epsilon cl \quad \text{Eq. 8}$$

where ε is the molar emissivity in kg-mol⁻¹ cm⁻¹, c is the molar concentration in mol-kg⁻¹, and l is the path length of the light radiation in cm. Due to variations in thickness, it is usually the case that a standardised peak that is independent of the polymerisation is used to normalise each signal. That enables some further simplification of the above relationship to:

$$A = ac$$

Eq. 9

Absorbance is re-written in terms of a relative molar absorptivity, a , given in $\text{kg}\cdot\text{mol}^{-1}$, and the chemical concentration.

From this relationship, a number of techniques are used to measure the polymerisation of epoxies and similar materials either in terms of time at a temperature suitable for polymerisation or with increasing temperature.

For the case of epoxies cured with amine hardeners, there are a number of distinct and easily resolved peak bands which relate to functional groups. As such, numerous researchers have employed the use of NIR for monitoring the cure formation of epoxy networks [24], [187]–[190]. Some common bands which are typically employed are shown in Table 3-2.

Table 3-2 - Typical absorbance bands for epoxy-amine systems

Absorption Band	Wavenumber (cm^{-1})	Functional Group
Epoxide	4522, 5881, 6070	CH
Primary Amine	5072	NH_2
Primary and Secondary Amine	6577-6692	NH_2 , NHR
Hydroxyl	4903, 6990	OH
Aromatic	4619, 4682, 5992	CH

The epoxy peak at 4522 cm^{-1} is most easily resolved as the peaks at 5881 cm^{-1} and 6070 cm^{-1} overlap with the aromatic peak at 5992 cm^{-1} . The primary amine peak at 5072 is discernible only for low degrees of conversion as primary amine is consumed first. The overlapping signal at $6577\text{-}6692 \text{ cm}^{-1}$ is a combination of primary and secondary amine. Since it can be assumed no secondary amine exists in the uncured state, the primary amine peak at 5072 cm^{-1} is needed to determine the ratio of primary to secondary amine later in the reaction. The aromatic peaks not associated with polymerisation are useful in normalising the respective spectra for quantitative analysis as they should not change as the system polymerises.

Fundamentally, the reaction of epoxy with the functional groups of an amino acid in a semi-sequential order. Firstly, the primary amine reacts to cause the oxirane ring to ring open. The ring-opening polymerisation is succeeded by formation of a hydroxyl unit and the unlocking of a secondary amine for further reaction. Once the primary amine is consumed, these

secondary amines will react with available epoxide species. Following the consumption of secondary amine, both hydroxyl and tertiary amine form.

In the NIR domain, the tertiary amine is undetectable but it is assumed that the difference between available secondary amine and primary amine represent the ideal amount of tertiary amine available. Further, directly determining hydroxyl concentration from any of the resolved peaks in the NIR domain are challenging because the band is representative by free hydroxyl and hydrogen-bonded species. It is also assumed that no net change in hydroxyl concentration occurs even with homo-polymerisation and etherification side-reactions [70].

The conversion of epoxy is simple to determine in the near infrared domain by utilising the well-defined peak at 4522 cm^{-1} . By stoichiometry, the initial epoxide concentration is known. Therefore, the conversion is taken as:

$$\alpha_{EP} = \frac{[EP]_x}{[EP]_0} \quad \text{Eq. 10}$$

where $[EP]_0$ is the initial concentration of epoxide functional groups and $[EP]_x$ is either time-dependent (as with curing isothermally) or temperature dependent. The absorbance of the epoxide band is easily determined after normalisation as the ratio of the scaled absorbance band by the unreacted epoxide concentration derived from stoichiometry of the formulation.

The conversion of primary amine is observed at degrees of cure below the time or temperature necessary to induce gelation. In the same way as with the epoxide molar absorptivity, the primary amine molar absorptivity is determined by scaling the absorbance band and dividing by the stoichiometric concentration of primary amine. Then the conversion of primary amine is determined by:

$$\alpha_{PA} = \frac{[PA]_x}{[PA]_0} \quad \text{Eq. 11}$$

Once again, the $[PA]_0$ is the molar concentration of available primary amine unreacted and $[PA]_x$ is time or temperature dependent concentration determined from the absorbance band.

The cured network properties are, in effect, influenced by the reaction of secondary amine and side reactions such as homopolymerisation and etherification. Determining the values for the

former is complex as the absorbance band is a combination of primary and secondary amine. Researchers have attempted to quantify secondary amine in a number of different ways. Varley et al. proposed utilising the primary amine band at 5072cm^{-1} to resolve the concentration of primary and secondary amine concentrations from the complex band at $6577\text{-}6692\text{ cm}^{-1}$ [191]. The approach is further complicated because tertiary amine formed from the consumption of secondary amines is not visible in the NIR spectra and determination of hydroxyl is complicated by an initial concentration already present in the uncured network. For these reasons it is simpler to consider the change in peak areas of the secondary amine and hydroxyl peaks, particularly with regards to etherification reactions. primary/secondary band.

The etherification reaction is comprised of consumption of an epoxide and a free hydroxyl, and upon bond-formation after the ring-opening of the epoxide, another hydroxyl is formed. Secondary amine is either fully consumed or consumed in a reaction with an epoxide. The normalised spectra then would show a decrease to the peak at 4521cm^{-1} and no net change to the hydroxyl peak at $6800\text{-}7200\text{cm}^{-1}$. In that case, it can be assumed that etherification can be identified by a relationship where the change in the ratio of secondary amine peak area and hydroxyl peak area decreases while epoxide remains unchanged.

3.6 MECHANICAL PROPERTIES AND FRACTURE TOUGHNESS

The mechanical properties which were studied consisted of flexural strength, strain to failure, and bending modulus as well as the notched fracture toughness and the methods of testing were based on the relevant ASTM standards. In addition, composites testing was carried out for flexure and interlaminar shear strength characterisation. All testing was carried out on an Instron 5000 series servo-electromechanical load frame (Illinois Tool Works, Inc., USA).

Flexural properties of the neat resins were studied in accordance with ASTM Standard D790-17. The flat resin strips were of nominal width and thickness of 13×3 mm, respectively. The three-point bend (3PB) flexural test was performed with a nominal span of 48 mm utilising a rolling-pin fixture with 5mm diameter steel rollers.

Singe-edge notch flexural (SENB) testing was performed following ASTM Standard D5045-14. The sample specimens were of nominal cast dimensions of $6\times 13\times 60$ mm and a moulded pre-notch of 6mm depth and 3mm v-grooved opening was a feature of the mould. Prior to loading, a fresh safety razor blade (Wilkinson Sword) was scored along the inside of the slit in

a single motion. Due to the brittle nature of the resins studied, it was not possible to tap in a pre-crack as the favoured method. An optical microscope was utilised to measure the length of the pre-crack. The loading rate of 10mm/min was used for all tests. A diagram of the specimen and loading configuration is shown in Figure 3-2.

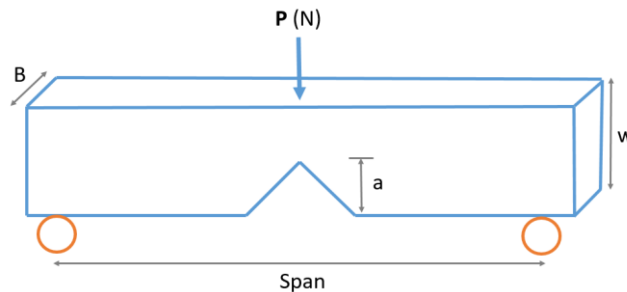


Figure 3-2 - Diagram of the SENB specimen and loading configuration

Fracture toughness is determined by assuming the application of linear elastic fracture mechanics (LEFM) is valid for the material of concern. The value of x , the pre-crack aspect ratio, is determined from the reciprocal of crack length, a , to the specimen width, w , as:

$$x = \frac{a}{w} \quad \text{Eq. 12}$$

In general, $a/w \approx 0.5$ is an ideal specimen ratio for the application of LEFM. This value is then used to determine the crack calibration factor for each specimen.

$$f(x) = 6x^{1/2} \frac{[1.99 - x(1-x)(2.15 - 3.93x + 2.7x^2)]}{(1+2x)(1-x)^{3/2}} \quad \text{Eq. 13}$$

Once the value of $f(x)$ is determined, the fracture toughness is easily determined from the specimen dimensions and the peak load of the load-displacement curve of a fracture test.

$$K_{1C} = \left(\frac{P_{\max}}{BW^{3/2}} \right) f(x) \quad \text{Eq. 14}$$

Of relevance to composite fracture toughness is the resin fracture energy. This is determined from measured values of the elastic tensile modulus, E , and the value of K_{1C} . The fracture energy is in units of J/m^2 and is calculated from the following equation:

$$G_{IC} = \frac{(1-\nu^2)K_{IC}^2}{E} \quad \text{Eq. 15}$$

where E and ν are determined experimentally at the same environmental conditions as the SENB tests.

The composite interlaminar shear strength (ILSS) was determined via the testing procedure of ASTM D2344-16. A minimum of 8 specimens were evaluated with a nominal 2 mm thickness and span of 10mm. All composites were unidirectional laminates and tests were carried out with respect to the 0° fibre orientation oriented in the spanwise direction of the loading fixture.

4 NETWORK DEVELOPMENT OF THE TETRAFUNCTIONAL EPOXY RESINS

4.1 INTRODUCTION

4.1.1 Influence of Monomer Functionality, Chemical Structure, and Cure Temperature on the Glass Transition Temperature

Epoxy-amine resins can be tailored to meet a wide range of performance criteria by relatively simple changes to the formulation of constituents which make up the polymer system. Diglycidyl ether of bisphenol A (DGEBA) epoxy monomers are the building blocks of most commercial epoxy resin systems. Three main components of an epoxy resin system most significantly impact the kinetics of reaction and the final properties of the cured resin. These are generalised as follows:

1. Monomer functionalities
2. Molecular structure of the monomer backbone
3. Substitution pattern of the molecules

A large body of research into epoxy resins means there is ample information with which to hypothesise and even simulate the characteristics of resins to achieve desired performance criteria. For the basis of this research, only epoxide functionality is of concern as the common aerospace diamine hardeners are tetrafunctional (i.e. $n=4$). Commercial monofunctional ($n=1$) up to tetrafunctional ($n=4$) resins exist. As an example, the DGEBA monomer contains two glycidyl rings for a functionality of 2. Epoxy monomers and diamines can contain aliphatic and aromatic constituents with the latter generally exhibiting desirable high temperature characteristics due to the inherent stability of these types of molecular structures. DGEBA contains chain-linked phenyl groups which contribute to a glass transition temperature approaching 200°C when cured with aromatic diamines. Finally, the homogeneity and conformity of the network to extrinsic thermal and mechanical stressors can be affected by the substitution pattern of the functional groups. A prime example is the phenomena observed when epoxy resins are cured with para-para substituted 4,4'-diaminodiphenylsulfone (44DDS) and meta-meta 3,3'-diaminodiphenylsulfone (33DDS). Research has shown that the isomers of DDS result in wide disparities with regards to the thermal, mechanical, and cure kinetics [192], [193].

With regards to thermal stability and for this study the use of the aromatic diamine, 44DDS is used exclusively. In addition, the backbone of epoxy monomers tends to contain aromatic chain-linked structures. The functionality of resins is generally greater than two due to the larger crosslink density afforded by more functional groups [28], [72], [194]. In the current state, triglycidyl-*p*-aminophenol (TGAP, $n=3$) and tetraglycidyl-diaminodiphenyl methane (TGDDM, $n=4$) cured with 44DDS have been shown to exhibit glass transition in the range of 250-300°C, respectively [195]. At the upper end of the spectrum, a novel tetrafunctional dimeric naphthalene-based epoxy monomer (NNE) synthesized by Ogura & Takahashi is shown to exhibit a homopolymerized glass transition temperature of 328°C, which remains the highest epoxy resin T_g reported [37].

The performance of the monomer is linked to the mobility of the cured network, rigidity of the naphthalene units, and tetrafunctional nature. These types of naphthalene-based epoxies are generally targeted towards applications in the electronics markets [196]–[198] and NNE is marketed under the tradename Epiclone HP4710 (DIC Corporation, JPN). Of the previously studied naphthalene-based epoxy resins, they all contain glycidyl ether functional groups and thus provide an opportunity to directly compare their performance against TGDDM, the dominant tetrafunctional epoxy resin available commercially which is based upon glycidyl amine epoxide groups.

The tertiary amines present in TGDDM and TGAP are potential catalysts for chain growth polymerisation and have been shown to be susceptible to internal cyclisation and etherification at later stages of cure and at higher temperatures [199]. Matejka et al. demonstrated the internal cyclisation reaction in nitrogen containing diglycidylamine resins via rapid formation of cyclic products at the beginning of cure [200]. This led to delays in gelation and affected the relative reactivity of the primary to secondary amine groups [64]. Indeed, Attias et al. showed that as much as 65% of the epoxide within a TGDDM amine-cured network can form cyclic structures [201] leaving unreacted amine groups within a heterogeneous network. An example of the chemical reaction that can form a cyclic defect or a normal crosslink ring is provided in Figure 4-1.

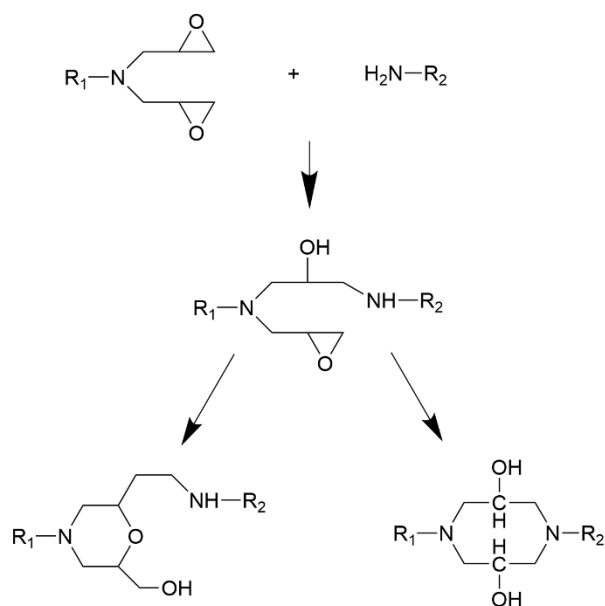


Figure 4-1 - Example of a cyclic defect (left) and cyclic member (right) formed during reaction of glycidyl amine with a primary amine

Residual functionality arising from side reactions produces networks with less than ideal properties and has provided the impetus to search for highly crosslinked tertiary amine free epoxy resins. Liu et al synthesised a nitrogen-free multi-aromatic tetrafunctional epoxy which displayed markedly improved conversion and similar properties to TGDDM which they attributed to lower steric hindrance [28]. Xing et al. also created a tetrafunctional epoxy resin, free of tertiary amine and showed improvements in T_g compared to a DGEBA-based resin at 20 mol% loading, again attributing this to a lack of a cyclisation [81]. Their primary disadvantage related to processing constraints arising from their high viscosity and comparative intractability.

The kinetics and reaction mechanism of epoxy amine cure have been widely studied and is impacted by many factors including temperature, chemical architecture and electronic effects, catalysts and curatives, and environmental conditions to name a few [64], [199], [202]–[205]. Of course, all of these variables are interrelated and compete with each other simultaneously, so it is a challenge to clearly delineate the effect of just one of these variables. Hence, it is fundamental to understand the growth of the network from the unreacted state which is often described as the time-temperature-transformation (TTT) diagrams.

4.1.2 Overview of the Investigation

The characterisation of the constituents of the epoxy-amine formulations prior to and during cure is necessary to determine the processing parameters to manufacture cured resins and

polymer composites. The schedule of cure temperatures must be determined in such a fashion as to grow the polymer network in minimal time but to maximal conversion without under-developed curing or degrading the network. Ultimately, that task requires fundamental understandings of the characteristics of the resin by a variety of methods.

In this section, the epoxy monomers NNE, TGDDM, a bi-component (70:30 molar ratio) blend of the two referred to as NTG, are characterised by acid titration, high-performance liquid chromatography, and near infrared spectroscopy. The monomers are then formulated with 1:0.95 stoichiometric amounts of 44DDS and the cure is studied by dynamic mechanical analysis, near-infrared spectroscopy, rheology, and isothermal dynamic mechanical analysis. Additionally, the late-stage elevated temperature cure, described as post-cure, is studied and the time-temperature-transformation diagram is constructed for the three resins.

4.2 MATERIALS

4.2.1 Materials and Preparation

The epoxy resins and amino hardeners used in this study are shown in Table 4-1. Materials prepared in this study include a 1:0.95 stoichiometric formulation of NNE, a 70:30 molar ratio blend of NNE and TGDDM, and a formulation of TGDDM, all of which are cured with DDS.

Table 4-1 - Summary of materials used in the study

Material	Acronym	Chemical Name	EEW (g-eq.)	Mfg. Supplier
Epoxy Monomer	NNE	bis(2,7 glycidyl ether naphthalenediol) methane	170	DIC Corp. (JPN)
Epoxy Monomer	TGDDM	Tetraglycidyl diaminodiphenyl methane	124	Hunstman Corp. (USA)
Amine Hardener	44DDS	4,4'-diaminodiphenylsulfone	62.08	TCI Chemical Inc. (JPN)

For dynamic thermal mechanical analysis, a strip of 150g/m² unidirectional carbon fibre served as the substrate for the dual cantilever bending clamp. A 10g sample of the epoxy-amine resin mixtures was dissolved in dichloromethane and methyl ethyl ketone as solvents. A series of soaks and drying cycles in a convection oven heated to 65°C were performed until a target saturation of 45 wt% resin in prepregs was achieved and solvents sufficiently evaporated. Four strips of nominal 15 x 60 mm rectangular squares running in the principal fibre orientation

were then formed into a small laminate, wrapped tightly in aluminium foil, and then clamped in the cantilever apparatus of the DMTA. Preparation of the resins and experimental analysis was carried out in accordance with the previously described methodologies in Ch. 3.

4.3 RESULTS AND DISCUSSION

4.3.1 Characterisation of the Epoxy Monomers

Due to the commercial nature of the TGDDM and NNE monomers, an acid titration was performed to determine an experimental value of the EEW in accordance with ASTM standard D1652-11. A total of 0.40 g of the monomer was dissolved in 15mL of dichloromethane (DCM) which was used as a solvent. Then 10mL of tetraethylammonium bromide (TEAB) with anhydrous acetic acid at a concentration of 250 mg/mL was mixed. To the acid solution, 8 drops of crystal violet indicator was added. The solution was then added to the dissolved epoxy solution and mixed using a magnetic stirrer. A buret stand containing 0.1M concentration of perchloric acid was titrated into the mixture dropwise until a stable green colour was obtained. The measured EEW of the epoxy monomers is provided in Table 4-2.

Table 4-2 - Epoxy and amine equivalent weight of the monomers

Monomer	Mfg. EEW (AEHW), g-eq.	Exp. EEW (AEHW), g-eq.
TGDDM	117-134	124.05 ±0.21
NNE	170	170.72 ±0.30
44DDS	62.08	NA

In addition to the epoxy equivalent weight, the monomer purity were investigated by HPLC using a gradient dilution method. Approximately 100 µM of the TGDDM and NNE resins were dissolved in 3mL of acetonitrile (ACN) used as a solvent. Upon dissolution of the monomers in ACN, 7mL of MilliQ® ultrapure water (Merck KGaS, GER) was added. The solutions were then degassed by placing them in an ultrasonic bath at 60°C for 30 minutes. The solution is then forced through a filter using a syringe and deposited into a 2mL vial and loaded into the HPLC autosampler.

In the commercial manufacture of epoxy and other monomers for thermosetting polymers mean there are usually one or two predominant isomers and a series of less resolved oligomers and other impurities. These impurities can greatly affect the kinetics and cured resin properties. HPLC provides an effective way to determine, in a semi-quantitative manner, the level of

impurity. A gradient elution is performed from a low ratio of solvent to water (30:70) over 50 minutes upon which the concentration of solvent is increased gradually to 100% at the final stage. A 15 cm long C18 column equipped with a guard column at the inlet is used to circulate 20 μ L of the solution at flow rates of 1 mL/min and 0.65 mL/min. As the solution passes through the C18 column, the polarity and level of solvent to water cause certain compounds to pass more slowly, effectively separating out the oligomers and impurities as they pass through an ultraviolet light detector. The detector then can pick up the intensity of each compound of which the intensity of the signal is recorded throughout the elution time. A slow flow rate and long elution time is necessary to properly separate out the compounds.

The peak intensities of the monomers are shown in Figure 4-2. A single intense peak exists for NNE and TGDDM at 27 and 29 minutes which represent the idealised structure of the two epoxy monomers. For TGDDM, intense secondary peaks show at 17.3 and 38.4 minutes. As retention time is related to molecular weight, the peak with the lower retention time may represent impurities of lower functionality. The higher peak can relate to high molecular weight species. For NNE, there are a significant number of peaks that arise at lower retention times and above the dominant peak. This suggests a higher degree of impurity compared to TGDDM.

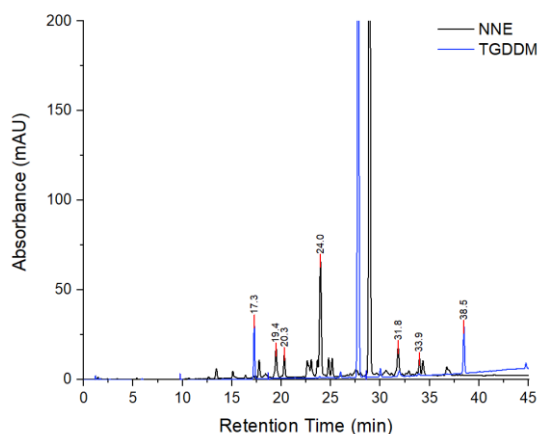


Figure 4-2 - HPLC gradient elutions of the epoxy monomers, NNE and TGDDM at nominally 100 μ mol

4.3.2 Differential Scanning Calorimetry (DSC)

The three resins were studied by dynamic (non-isothermal) and isothermal methods. These were used to calculate activation energies, peak exothermic temperatures, rate constants, thermal cure conversion, the evolution of the glass transition temperature relative to conversion.

4.3.3 Enthalpy of Reactions as Determined by Dynamic DSC

The dynamic measurements involved subjecting a nominal 10mg of uncured resin to five varying heating rates. These were 2.5, 5, 10, 15, and 20 °C/min and the heating cycle extended from 25-325°C. Integrating the area underneath each exothermic peak and averaging amongst the heating rates results in an averaged total enthalpy of reaction. The peak exothermic temperatures are gathered from the dynamic traces to determine a relative activation energy from an Arrhenius plot. A representative series of dynamic scans are shown for NNE in Figure 4-3 and the Arrhenius plot for the three resins is given in Figure 4-4 below. Values of the peak exothermic temperatures, dynamic enthalpies, and calculated activation energies are provided in

Table 4-3.

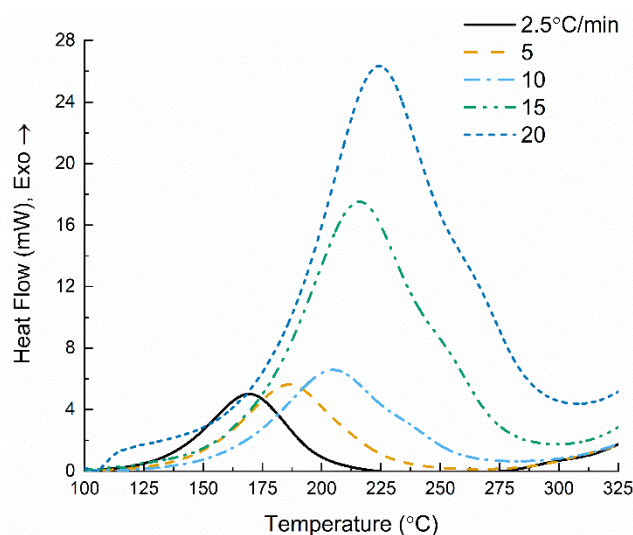


Figure 4-3 - Dynamic DSC traces for the NNE resin at increasing heating rates

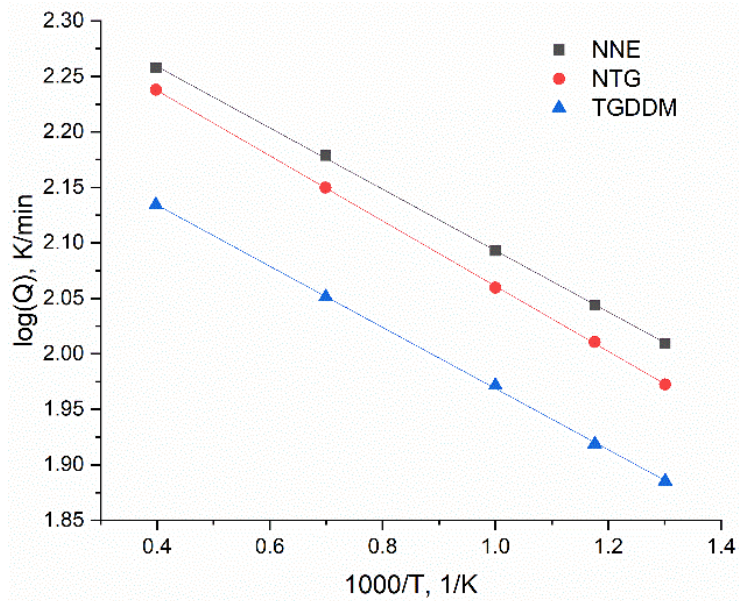


Figure 4-4 - Arrhenius plot of the activation energies from dynamic DSC for the three resins

Table 4-3 - Enthalpies of reaction, peak exotherms, and activation energies from the dynamic DSC study

	NNE		NTG		TGDDM	
Heating Rate (°C/min)	T _p (°C)	8H _{dyn} (J/g)	T _p (°C)	8H _{dyn} (J/g)	T _p (°C)	8H _{dyn} (J/g)
2.5	169.7	283.9	173.7	326.8	195.4	528.4
5	185.8	319.0	192.0	361.9	214.4	580.5
10	204.6	314.7	212.4	343.9	234.0	568.9
15	216.1	308.4	224.2	351.5	248.0	539.9
20	224.5	314.0	233.8	374.6	257.3	518.9
Ave. 8H _{dyn} (J/g)		311.4		335.2		547.3
E _a (kJ/mol)		65.8		62.0		66.0

It is assumed from the kinetic theories of Kissinger and Flynn-Wall-Ozawa that there exists two relationships to the kinetic models, one of which is dependent only on temperature, and the other only on conversion. Further, to satisfy the conditions of the Kissinger method, a relative maximum is reached during the reaction such that the reaction rate, $\frac{dr}{dT}$, is zero [206]. The net effect of these assumptions are that with increased heating rates, the peak exothermic temperature should shift higher and a single peak exotherm should be observed in the DSC trace. That holds true for the three resin systems which is expected due to the same chemical reaction mechanisms in the initial stages of cure.

The activation energies of the three resin systems are similar. This is not unexpected because DSC does not distinguish between the early and late stages of cure. In effect, the activation energies represent an average of the chemically induced reactions up to the diffusion-controlled regime which would predominantly reside in the kinetically-controlled regime [207]. Of interest is the systematic difference between NNE and TGDDM for the averaged δH_{dyn} and the T_p where it is observed that $\text{NNE} < \text{NTG} < \text{TGDDM}$. These trends in the dynamic enthalpy of reaction would indicate a lower fractional conversion after heating [208]. That can be attributed to steric effects within the resin and the higher viscosity of the naphthalene formulations. For the peak exothermic temperature, the lower values of NNE and NTG suggest a more rapid cure.

4.3.4 Extent of Cure and the Autocatalytic Models as Determined by Isothermal DSC

Isothermal DSC was used to further investigate the kinetics of reaction, cure conversion, and evolution of the glass transition across a range of cure temperatures. The resins were rapidly heated at $20^\circ\text{C}/\text{min}$ to an isothermal temperature that ranged from $130\text{--}180^\circ\text{C}$ for an extended period, followed by a cooling to ambient temperature and re-heating the cured resins to an elevated temperature ($300\text{--}350^\circ\text{C}$) at a constant $10^\circ\text{C}/\text{min}$ heating rate. The DSC trace for the isothermal stage of curing at 150°C for the three resins is shown in Figure 4-5 and the dynamic heating cycle in Figure 4-6.

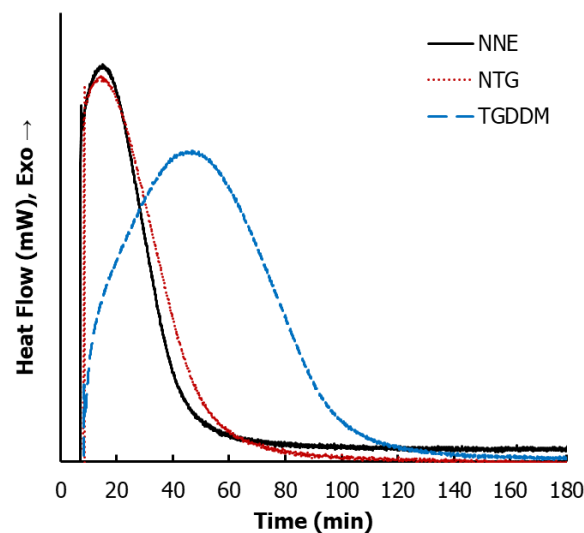


Figure 4-5 - Isothermal DSC traces of the three resins at 150°C

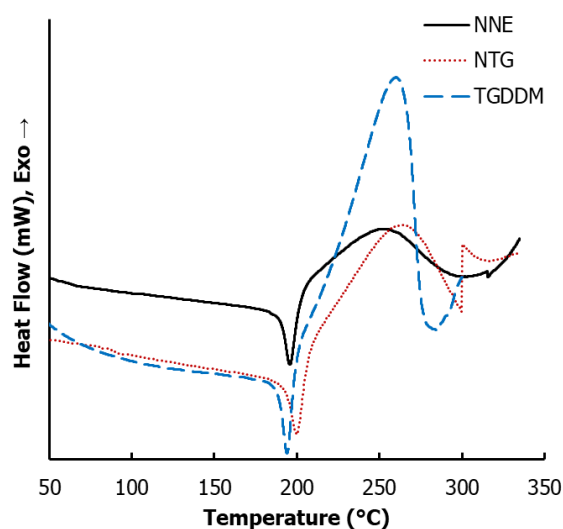


Figure 4-6 - Dynamic re-heating of the three resins after isothermal cure at 150°C

The fractional conversion of NNE at the lower cure temperatures is between 0.58-0.72 and upon heating between 160-180°C, increases sharply to between 0.82-0.86. Interestingly, this behaviour contrasts with the generally constant increase in conversion with temperature for NTG and TGDDM. Further, the conversion at 180°C is significantly higher for TGDDM than the naphthalene resins, 0.91 versus 0.86 and 0.85, respectively. That supports the dynamic DSC study where it was shown that both naphthalene resins exhibited lower peak exothermic temperatures and lower dynamic enthalpies of reaction.

The striking difference shown in the isothermal traces clearly indicate the relatively significant difference in reactivity between NNE and TGDDM. The peak of the exothermic trace differs by nearly 40 minutes. The TGDDM resin is characterised by a broad peak whereas both NNE and NTG are tall and narrow peaks. Upon re-heating the resins, there emerges a slight endothermic peak, taken as the glass transition at the relative fractional conversion achieved under the isothermal condition. After that, an exothermic peak is shown from which the residual enthalpy is calculated for determining the fractional conversion. A plot of the fractional conversion for NNE at the six isothermal temperatures and for the three resins at 150°C is shown in Figure 4-7. The kinetic rate constants k_1 and k_2 are shown in Figure 4-8(a-b) and the raw data from the isothermal study is provided in Table 4-4.

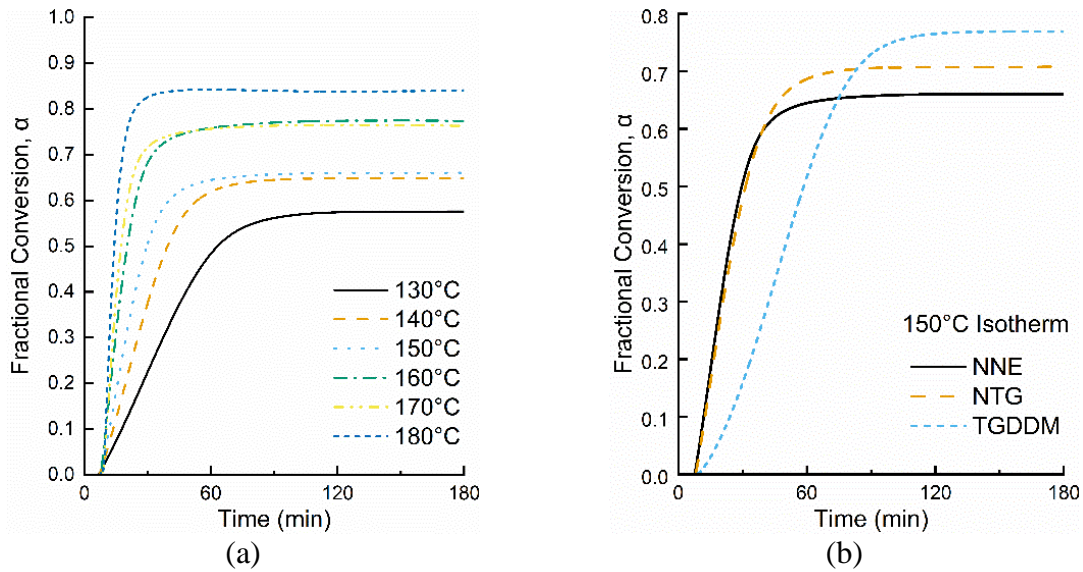


Figure 4-7 - Plots of (a) NNE conversion at different isothermal temperatures, and (b) the three resins cured at 150°C

The kinetic rate constants k_1 and k_2 were determined from between 10-40% conversion which denotes the chemically controlled regime for epoxy-amine cure. The k_1 was found to be markedly higher for the naphthalene resins than TGDDM, even at the lower cure temperatures. The difference in k_2 was insignificant between the three resins except at the lowest cure temperature which probably is influenced by the difference in melt viscosities of the three systems at that temperature. The k_2 parameter shows the influence of catalysis by proton donors and is more significant in the later stages of cure. The lack of a difference between the three resins suggests that process is less important to controlling the overall reaction rate.

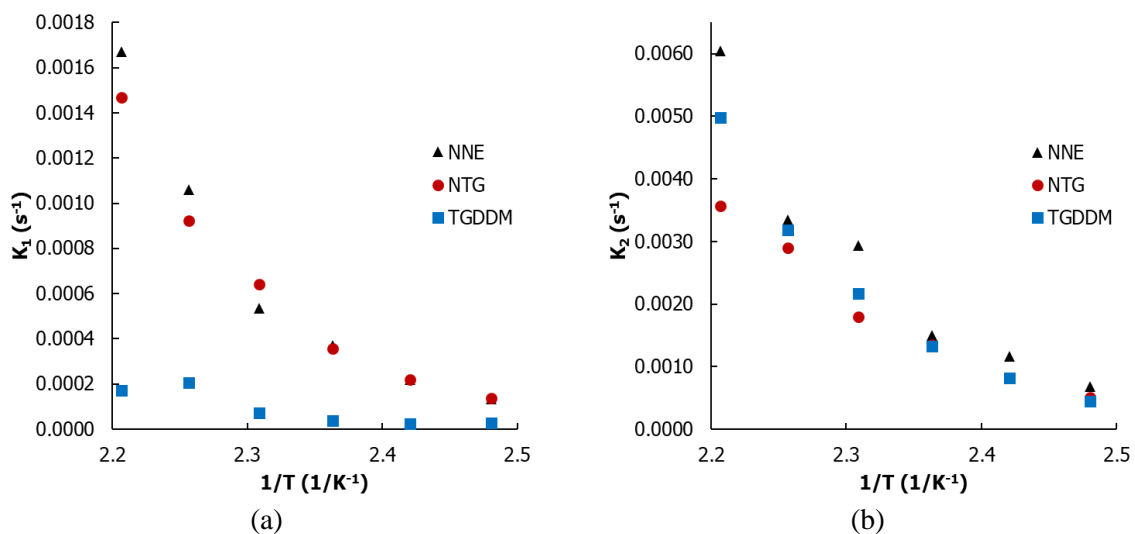


Figure 4-8 - Kinetic rate constant (a) k_1 and (b) k_2 of the three resins

It is supported, then, that the reaction rates of NNE and NTG are significantly higher during the initial stages of cure which still results in a similar T_g at lower conversion. Chemically, these resins differ in the fact that NNE is a dimeric glycidyl ether and the four oxirane rings are separate while TGDDM contains a tertiary amine where the two oxirane rings are bound on either side of the backbone. St. John & George investigated the reaction of TGDDM-DDS systems via a kinetic study and noted that the secondary amine reactivity was susceptible to influences of cure time and temperature after gelation [70]. Here there is a clear difference for primary amine addition so it is probable that the network formation for NNE and NTG slows considerably faster than TGDDM in the initial stages due to the higher reactivity of primary amine. An explanation may lie with steric effects and difference in chemical structure that could influence the overall rate of reaction and the difference in fractional conversion. Liu et al. investigated differences between a glycidyl ether (DGEBA) and a glycidyl amine (TGDDM) as well as TGPAP which contains both [64]. Their work showed that DGEBA was slower to react than TGDDM and TGPAP, in contrast to the behaviour seen with NNE. Therefore, it is likely the separate arrangement of the oxirane groups about the naphthalene backbone decreases steric effects and thus increasing reactivity. However, the subsequent rapid onset of diffusion-controlled kinetics is also likely to result in lower overall conversion due to steric effects. Oyanguren & Williams investigated a series of epoxies through gelation and vitrification and suggested the constraint of the network up to vitrification could reduce overall conversion when the cure is accelerated, in effect constraining the network [209]. The critical conversion, U_c , is modelled from the work of Chern & Poehlen [210]. This parameter represents the transition from the chemically controlled to diffusion-controlled regimes at the earliest onset. There is a marked difference, irrespective of cure temperature between the three resins. As already shown from the kinetic parameters and fractional conversion, the U_c of NNE < NTG < TGDDM. In addition, it is notable that the difference between U_c and U tends to be higher for the naphthalene resins. That would imply that the diffusion-controlled stage occurs earlier than TGDDM thus constraining the network at a lower conversion.

Table 4-4 – Fractional conversion, glass transition temperature, kinetics rate constants, and the critical conversion determined from isothermal DSC

Epoxy Resin	Cure Temp. (°C)	U	T _g (°C)	k ₁ x10 ⁻⁴ (s ⁻¹)	k ₂ x10 ⁻⁴ (s ⁻¹)	c
NNE	130	0.58	171.3	1.33	6.82	0.52
	140	0.65	184.7	2.19	11.6	0.57
	150	0.72	195.9	3.71	15.0	0.62
	160	0.82	209.4	5.36	29.4	0.67
	170	0.85	222.9	10.6	33.5	0.71
	180	0.86	237.1	16.7	60.5	0.76
NTG	130	0.61	168.3	1.36	5.12	0.58
	140	0.67	183.7	2.2	8.15	0.61
	150	0.71	199.5	3.57	13.5	0.66
	160	0.77	215.2	6.41	18.0	0.72
	170	0.80	234.0	9.24	29.0	0.74
	180	0.85	-	14.7	35.7	0.81
TGDDM	130	0.61	156.4	0.26	4.43	0.61
	140	0.72	177.2	0.23	8.20	0.66
	150	0.74	194.1	0.36	13.3	0.71
	160	0.80	210.4	0.72	21.7	0.76
	170	0.86	226.3	2.04	31.9	0.81
	180	0.91	239.7	1.71	49.8	0.85

4.3.5 Near-Infrared (NIR) Spectroscopy of the Isothermally Cured Resins

Fourier transform infrared spectroscopy was used to study the consumption and production of functional groups throughout the cure. The epoxide, primary amine, complex primary/secondary amine, and hydroxyl peaks are well resolved in the near IR (4000-8000 cm⁻¹) range and can be used to quantitatively determine a conversion of cure but also of the competing mechanisms during cure. The thermal methods (DSC, DMTA) are unable to relate the exothermic or mechanical relaxations to any one functional group. Therefore, NIR is a useful method to understand the differences in network development during various stages of the thermal history of the cure. The three resins were cured in glass slides and contained using a 1 mm thick silicon gasket with a 10x10 mm square window so that they could be removed from the heated oven intermittently. Isothermal curing was performed at temperatures of 130, 150, and 180°C. Samples were removed from heating and quickly measured in the NIR regime at 15 minute intervals for the first hour, 60 minute intervals up to 4 hours, then at 8 and 16 hours, respectively. While not performed in situ, care was taken to minimise the out-time and so as to minimise the disruption of the cure. A plot of the spectra of NNE for different stages of the isothermal cure at 150°C and after a 220°C post-cure is shown in Figure 4-9.

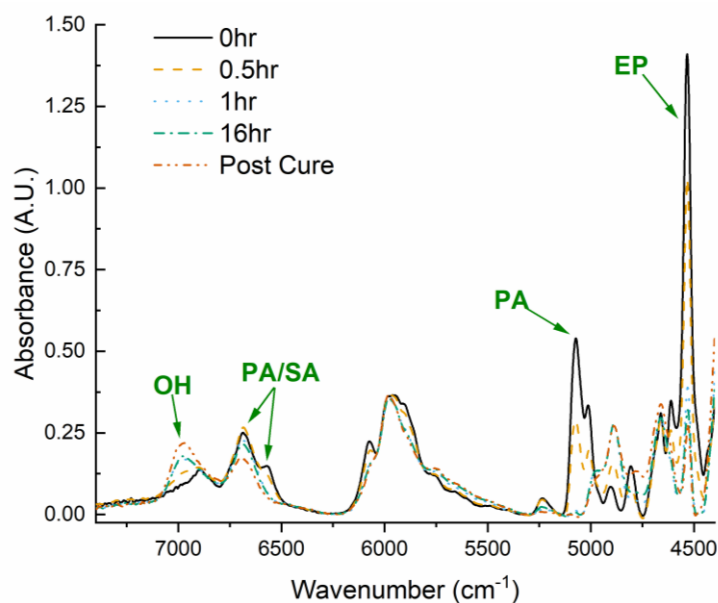


Figure 4-9 - NIR spectra of the NNE resin from the uncured and cured states after 150°C isothermal cure and a 220°C post-cure

During the initial stages of cure, the primary amine peak at 5090 cm^{-1} is progressively reduced until it disappears and the small shoulder of the broad PA/SA peak from 6300-6800 cm^{-1} eventually disappears. The reduction in PA corresponds with a reduction in the epoxide peak at 4521 cm^{-1} and an increase to the SA and OH peaks. A fractional conversion from NIR can be produced for EP and PA peaks by determining a baseline area of the uncured (A_0) and partially cured sample (A_t). The conversion of primary amine and epoxy and the changes that occur for the secondary amine and hydroxyl peaks are shown in Figure 4-10. A marked difference to the primary amine peak conversion is immediately apparent between the naphthalene resins and TGDDM. Within the first hour of cure, there is complete reduction to the primary amine peak which does not occur until two hours for TGDDM. The relation between gelation and the primary amine peak suggests a more rapid transition for the naphthalene resins. Also of note is the higher conversion of epoxy within the early stage of the isothermal cure but relatively low change between 16hr and post-cure where TGDDM epoxide conversion essentially reaches 100% but the NNE and NTG resins are still at 87% and 92%, respectively. The change to the secondary amine and hydroxyl groups are also much different. For NNE, there is a net decrease between cure and post-cure in the SA peak while a large increase to the OH peak is observed. That correlates with continued epoxy-amine addition and is also reflected in the lower conversion of epoxy (presence of a residual epoxy peak) after post-cure which is not observed in the TGDDM spectra. In fact, the TGDDM resin shows a stagnation to the hydroxyl peak after 4 hours of cure and an insignificant shift between cure

and post-cure, yet near complete conversion. When secondary amine launches a nucleophilic attack with the available unreacted epoxy functional groups then the epoxy peak should decrease, secondary amine decrease, and hydroxyl increase.

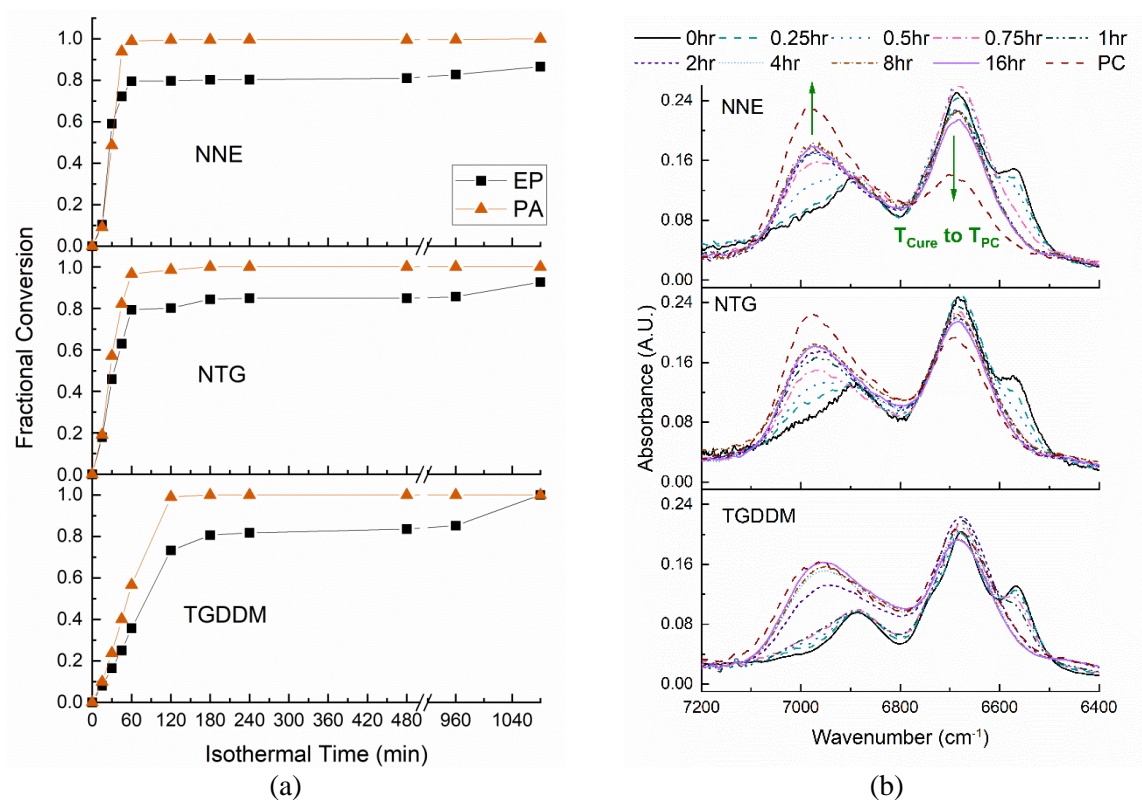


Figure 4-10 – Plots of (a) Fractional conversion from NIR for the epoxy and primary amine functional groups and (b) changes to SA and OH peaks for 150°C isothermal cure

To understand the effect of the post-cure on potential side reactions, the fraction of the secondary amine area to the hydroxyl area, A_{SA}/A_{OH} , was determined relative to the epoxy conversion, α_{ep} . For the range of isothermal temperatures up to post-cure, the ratio of areas is plotted from 55-90% conversion in Figure 4-11. Irrespective of the difference in epoxide conversion and cure temperature, the three resins show similar behaviour between the change to the SA and OH peaks across this range. In effect, that demonstrates the predominant epoxy-amine addition reaction occurs during isothermal cure.

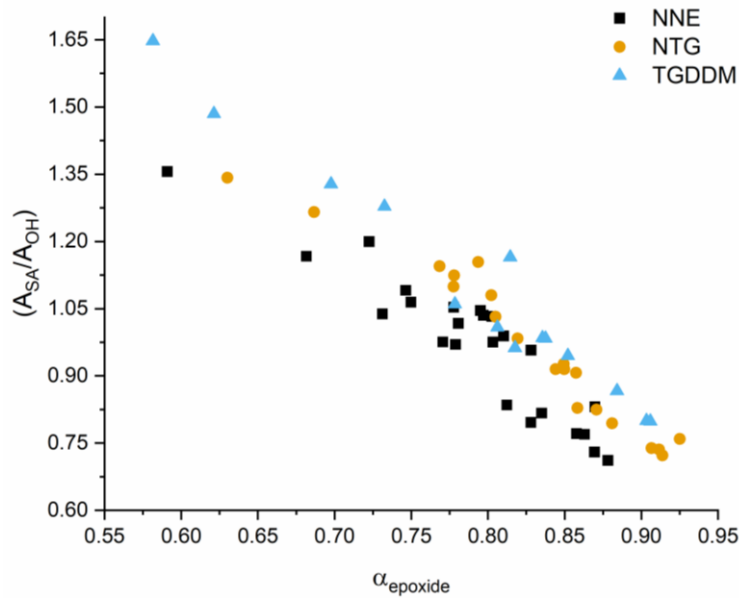


Figure 4-11 - Ratio of the SA and OH areas relative to epoxy conversion

A plot of the change in the $A_{\text{SA}}/A_{\text{OH}}$ ratio and the change in epoxy conversion at the end of cure for 180°C and subsequent post-cure at 200°C and 220°C is shown in Figure 4-12 and a summary of the conversion time and fractional conversion determined by NIR is provided in Table 4-5. From 180°C isothermal cure to 200°C post-cure, the change in the ratio for TGDDM is negligible while epoxy conversion increases significantly. In contrast, the NNE ratio decreases whilst the epoxy conversion only slightly increases. Further post-cure at 220°C shows a net decrease for NNE and increase to conversion while TGDDM undergoes a net decrease to the ratio and marginal increase to epoxy conversion. Unsurprisingly, the blend sits between the two monomeric formulations but mirrors the behaviour of NNE. Ultimately, the inverse trends between the naphthalene resins and TGDDM describe the difference in reaction at post-cure. The naphthalene resins appear to undergo continued epoxy-amine addition while the TGDDM resin may experience a side-reaction such as etherification.

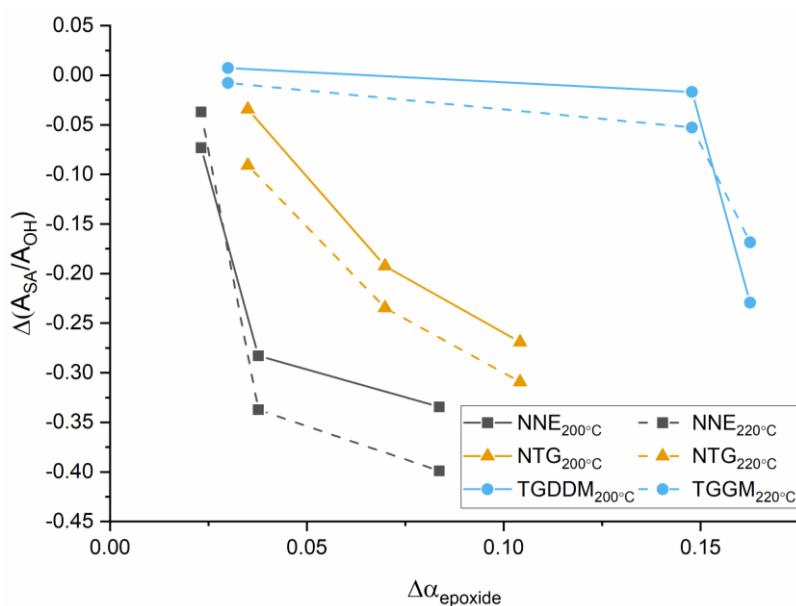


Figure 4-12 - Change to the secondary amine and hydroxyl area ratio relative to the conversion after cure and post-cure

Table 4-5 - Summary of epoxy conversion time and fractional conversion from NIR

Epoxy Resin	T _{cure} (°C)	100% U _{NH2} (min)	U _{ep} (cure)	U _{ep} (PC @200 °C)	U _{ep} (PC @220 °C)
NNE	130	120	0.78	0.86	0.88
	150	60	0.83	0.86	0.88
	180	15	0.88	0.88	0.90
NTG	130	120	0.82	0.92	0.94
	150	60	0.86	0.93	0.94
	180	30	0.93	0.95	0.96
TGDDM	130	240	0.84	0.98	1.00
	150	120	0.85	0.98	1.00
	180	45	0.96	0.99	0.99

It is important to note again the structural differences between NNE and TGDDM. The glycidyl amine characteristic of the former is shown to behave differently to glycidyl ethers in that the tertiary amine can catalyse etherification [70], [200] at elevated temperatures as well as undergoing the phenomenon of internal cyclisation [199], [211]. Therefore, despite the lower reactivity of the NNE after vitrification, when the reaction proceeds, it is more likely to proceed via epoxy-amine addition. That is in agreement with the investigation by Min et al. They utilised NIR to study a DGEBA/DDS blend and observed that the glycidyl ether resin showed no signs of undergoing etherification at elevated temperatures [212]. Further investigations by Min into the same resin formulation but with viscosity increasing thermoplastic modifiers, however, suggested that as much as 30% of the reaction could be consumed by side-reactions

such as etherification, but only when the viscosity significantly reduced conversion upon entering the glassy state [80]. Also of note is the proximity of adjacent epoxy groups. It has been shown that the intramolecular spacing of the epoxide relative to the catalytic centre of the tertiary amine tends to promote etherification [66], [70]. The spacing between the two epoxide groups of TGDDM is much closer to one another. In contrast, the NNE epoxide groups are well-distributed about the larger backbone structure.

4.3.6 Rheology of Neat Resin Cure

4.3.7 Dynamic Rheology

A gelation temperature and the minimum viscosity are determined by dynamic rheology. The three resins were heated at a constant rate of 2°C/min under a 10 Hz oscillation and 1% strain from 90°C (molten state) to a maximum of 200°C. The traces of the rheological curves are shown in Figure 4-13. Immediately apparent is the higher storage and loss modulus of the NNE and NTG resins prior to gelation which translates to a higher complex viscosity. Prior to gelation, primary amine groups sit at the end of chain segments and, as suggested by St. John & George and would largely remain in the sol state during gelation [70]. A narrow range of temperatures around 135-150°C occur near the minimum viscosity of NNE whereas this region is extended for NTG and TGDDM. That shows a diluting effect of the TGDDM when added to NNE. The minimum viscosity is decreased progressively between NNE, NTG, and TGDDM as well as the temperature at gelation which is 168°C for NNE but 193°C for TGDDM, again supporting the prior results that NNE is a more reactive epoxy resin. It is noted here that the very high viscosity of NNE could be prohibitive to composite manufacture by liquid moulding techniques.

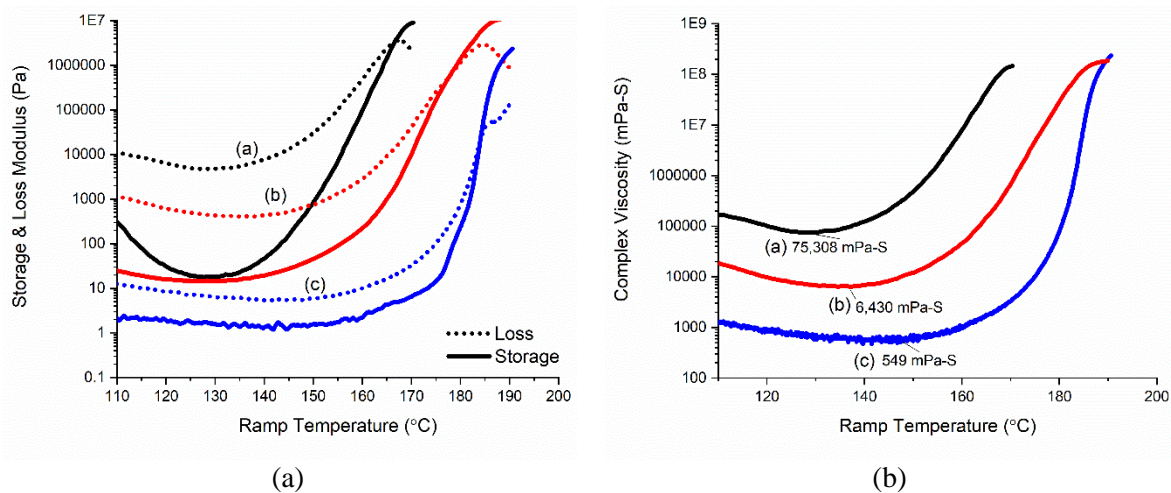


Figure 4-13 - Dynamic rheological traces of (a) NNE, (b) NTG, and (c) TGDDM resins

4.3.8 Isothermal Rheology

Under isothermal gelation from 130, 150, and 180°C, similar observations are made between the three resins. An example of the storage modulus, loss modulus, and complex viscosity for the 130°C isothermal rheological sweep are shown in Figure 4-14 and a summary of the values for the three cure temperatures are provided in Table 4-6. Again, the storage modulus (G') at gelation is higher for NNE, and decreases progressively for NTG and TGDDM both between resin formulations and as the isothermal temperature is increased. The value of storage modulus is directly related to the energy required to deform a material and at gelation would indicate the degree to which a material has become intracible. It is apparent that the gelled glass of the partially cured NNE network just after gelation is more rigid than TGDDM and NTG, which is concurrent with the slightly higher T_g at 130-150°C cure temperatures as presented earlier via DSC analysis. What is immediately apparent is the rapid onset of gelation for the naphthalene resins. At the lowest temperature regime, NNE gels within 45 minutes which is consistent with the NIR data where the primary amine peak rapidly disappears within the first hour of cure. As temperature increases, that time to gelation follows an exponential decay for TGDDM whereas it is almost linear for the naphthalene resins. That could be attributed to the magnified steric effects of the NNE resin that arise from the high reactivity, bulky naphthalene structure, and higher viscosity.

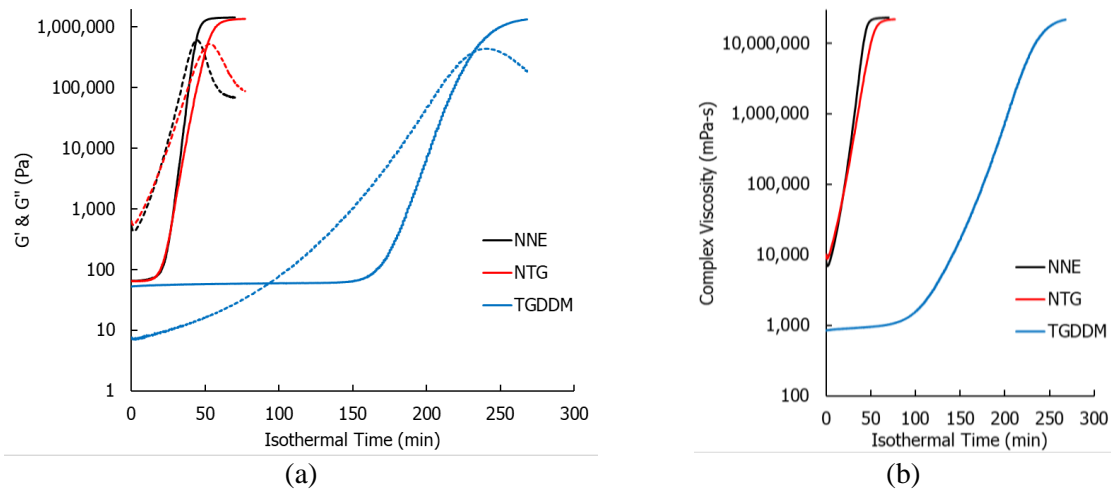


Figure 4-14 - Isothermal rheological traces of the three resins at 130°C showing (a) G' (dashed) and G'' (solid) crossover at gelation and (b) complex viscosity with respect to isothermal time

Table 4-6 - Summary of the isothermal gelation times and storage modulus at gelation

Epoxy Resin	Cure Temp. (°C)	t_{gel} (min)	G'_{gel} (MPa)
NNE	130	43.9	0.607
	150	24.1	0.488
	180	10.0	0.418
NTG	130	51.5	0.510
	150	28.1	0.310
	180	9.7	0.069
TGDDM	130	232.0	0.384
	150	106.0	0.219
	180	27.4	0.041

4.3.9 Isothermal Dynamic Mechanical Thermal Analysis of Cure

Isothermal cure of the epoxy networks was carried out by doping the unreacted epoxy onto unidirectional carbon fibre fabrics by dissolving the constituents in dichloromethane and acetone and then removing the solvent by drying at 65°C for several hours. The strips were then cut to dimensions suitable for dynamic mechanical thermal analysis in a dual cantilever bending mode. This and other methods of in situ curing whilst under oscillatory loading has been extensively used to study the evolution of the network from the uncured to the glassy state and ultimately the glass-rubber transition prior to degradation [213], [214]. The initial work by Gillham et al established via torsional braid analysis that the resin, as it cures, exhibits two peaks in the $\tan(\delta)$ spectra prior to the growth of a steady storage modulus [215]. These two peaks correspond to the gelation and vitrification points of the network, respectively. The

attainment of a constant modulus after vitrification is indicative of the formation of a glassy network.

Figures of the storage modulus and $\tan(\delta)$ spectra of the three resins cured isothermally at 160°C are shown in Figure 4-15. Similar to isothermal rheological traces, the first peak in the $\tan(\delta)$ spectra appears significantly sooner than the TGDDM resin, indicating the high reactivity and rapid onset of gelation for the naphthalene resins. The second peak, the vitrification point, occurs only tens of minutes after gelation and the transition into the glassy regime is much steeper for NNE whereas the trace of storage modulus for NTG and TGDDM gradually rise to equilibrium.

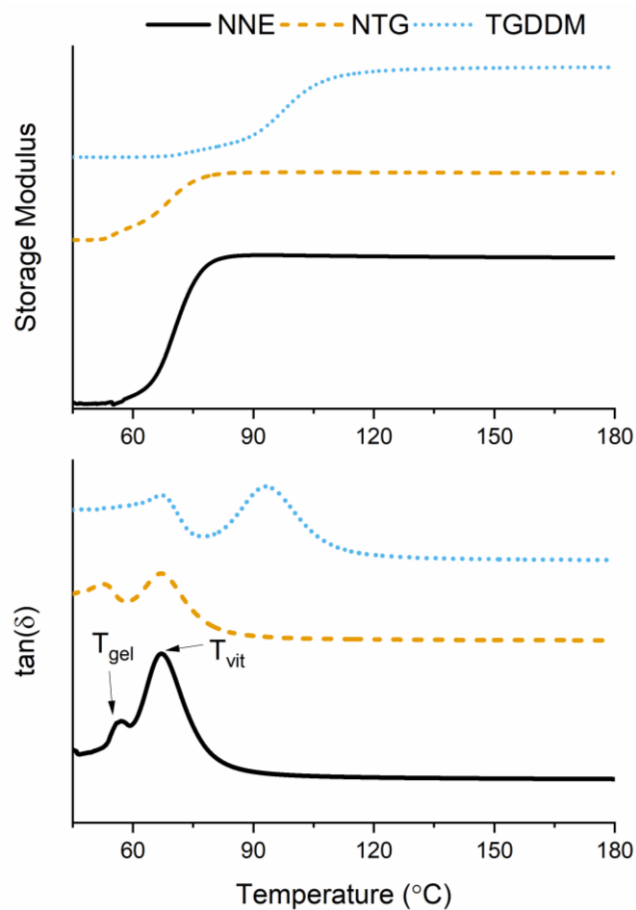


Figure 4-15 - Traces of the storage modulus and $\tan(\delta)$ of the three resins isothermally cured at 160°C

In evaluating the effect of temperature on these transitions, a behaviour is observed with NNE that is less evident in the blend and non-existent with TGDDM. In Figure 4-16 the gelation peak only emerges in the 160°C spectra and as temperature is increased, the growth of the gelation peak continues to get progressively larger. From the rheological studies, it was noted

that the viscosity of NNE below 160°C was multiples higher than NTG and TGDDM. Inherently, the $\tan(\delta)$ is representative of the reciprocal of elastic behaviour to viscous behaviour. As the viscosity of the uncured resin is already high then a damping effect to the viscous nature of NNE may affect the emergence of that peak up until the isothermal temperature is sufficiently high enough to lower the viscosity. Contrasted with TGDDM, the low melt viscosity allows for the observance of both peaks across the range of temperatures from 130-180°C, where the behaviour is similar to that observed by [216], [217]. Supplementary traces for the NTG and TGDDM resins across the cure temperatures are provides in Appendix A.

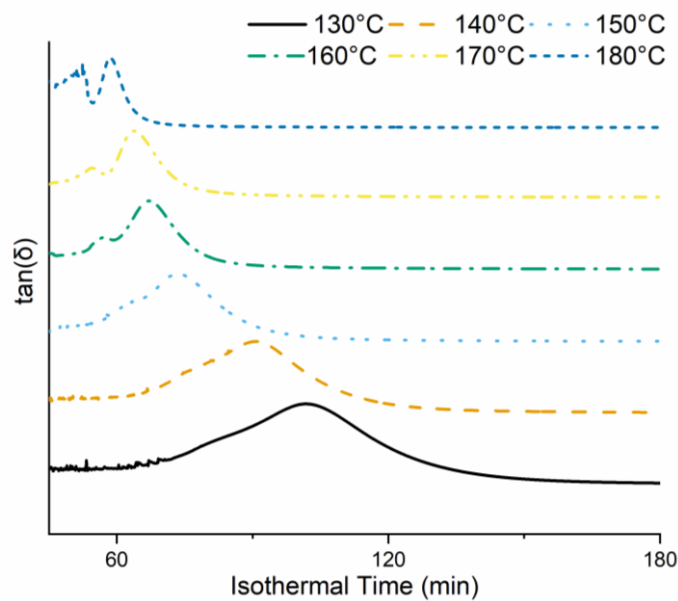


Figure 4-16 - Traces of the $\tan(\delta)$ spectra for NNE relative to the isothermal cure temperature

Gelation and vitrification differ in that the former is a chemical process and the latter is a physical phenomenon. The U_{ep} (obtained from DSC) of NNE, NTG and TGDDM at gelation and vitrification as a function of T_{cure} is shown in Figure 4-17. The U_{ep} 's at vitrification of NNE, NTG and TGDDM are observed to be relatively similar, increasing consistently with T_{cure} . Given vitrification is a physical process dependent an increase in U_{ep} with increasing T_{cure} is not unexpected. Gelation however, is a chemical process independent of T_{cure} and controlled by the functionality of the epoxide and amine group according to the Flory-Stockmeyer theory given as:

$$\alpha_c = \frac{1}{\sqrt{r(f_{EP}-1)(f_A-1)}} \quad \text{Eq. 16}$$

Assuming 1:1 epoxide amino stoichiometry and ideal reaction conditions, the model predicts gelation of these resins to occur at an U_{ep} of 0.33. Clearly the results diverge from this model considerably, with the NNE displaying the greatest degree of divergence, increasing initially from 0.41 to 0.8 over the range of cure temperatures. Serrano & Harran evaluated the rheological gelation of DGEBA and TGDDM, concluding that higher cure temperatures, and subsequently the greater potential for side reactions led to a deviation from the F-S model for both resins but more significantly for TGDDM [218]. That is similar to the behaviour seen from 170°C and 180°C isotherms in this work. A comparison of conversion via DSC is of course only indirectly related to values captured via DMTA. Labana et al. showed that not only were chemical effects such as intra-molecular reactions contributing to these deviations but also steric and topological effects as conversion increases [219]. Chemical effects have already been discussed regarding the difference in cure conversion between NNE and TGDDM. NNE appears to proceed by epoxy-amine addition and TGDDM is more susceptible to side-reactions with increasing temperature and conversion. Therefore, it is likely that steric effects contribute to the high conversion at gelation which may be compounded by the initial high reactivity and higher melt viscosity. The blend, NTG, does not appear to show the same behaviour possibly as a result of the diluting effect that TGDDM imparts on the formulation.

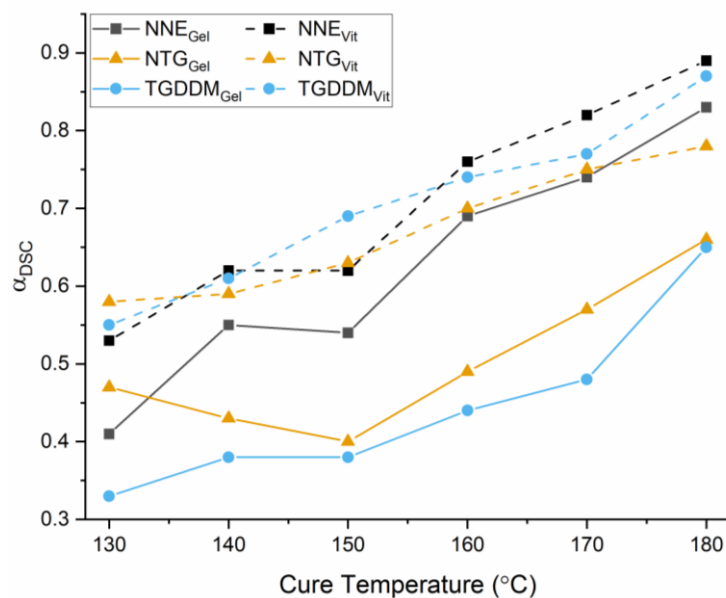


Figure 4-17 - Comparison of the DSC conversion at times for gelation and vitrification determined from DMTA

After subjecting the doped carbon fibre tapes to isothermal curing in the DMA, they were allowed to cool to ambient conditions and then re-heated under dynamic oscillatory damping

at a 5°C/min heating rate up to a maximum of 300°C, initially. From these dynamic traces, the $\tan(\delta)$ eventually grows into a distinct peak which is taken as the glass transition temperature relative to the partially cured network. Figure 4-18 shows the traces of NNE throughout the cure cycle and provides the temperature corresponding to the $\tan(\delta)$ peak. At the lower cure temperature, the peak area is maximised while the temperature of the peak is lowest. Progressively, the area is reduced and the peak shifts to higher temperatures until by 180°C there is a significant reduction in peak area and a large shift towards 300°C. For the three resins, the growth of the glass transition temperature is almost the same from 130-170°C where the blend then increases significantly to 320°C. From the previous DSC and NIR studies, it is established that NNE and NTG reach similar T_g but at lower conversion which begins to reflect in the loss tangent plot.

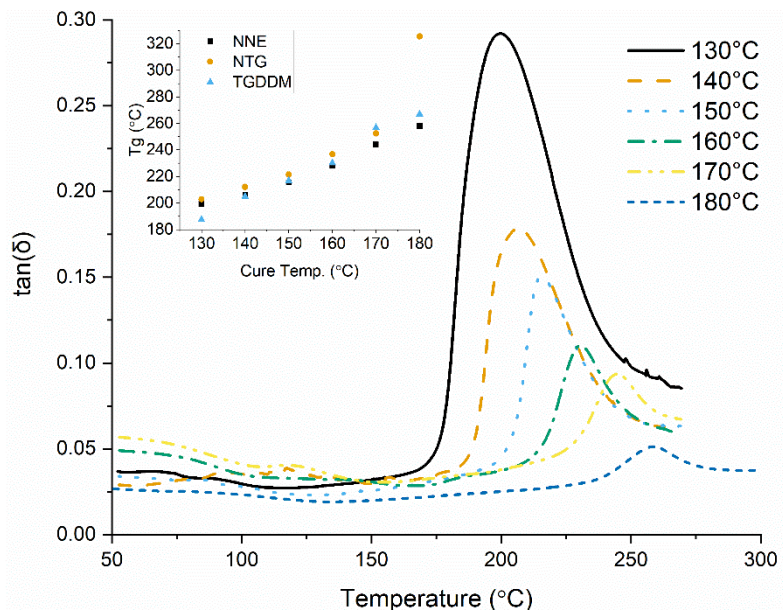


Figure 4-18 - Traces of the $\tan(\delta)$ peak under dynamic heating after the isothermal cure for NNE (inset plots T_g s of the three resins)

A general rule with epoxy resins is that cure proceeds until $T_g = T_{cure}$ and T_g will not increase until $T_{cure} < T_g$, assuming there is potential for further reaction to take place. While DSC results have already shown a deviation from this relationship here it will be discussed in the context of the cured network mobility. The transition between chemically-controlled to diffusion-controlled mechanisms is marked by a significant decrease in reactivity and subsequent increase to the activation energy barrier for etherification compared to amine-addition [220]. Guerrero et al studied the cure of TGDDM networks at varying stoichiometry and showed similar behaviour where T_g grew well above T_{cure} when the epoxide conversion was highest

[75]. Partly attributed to the effects of etherification it was also related to the limited mobility at higher conversion. The onset of the glass transition temperature is essentially a thermally activated process that allows a rigid network to relax and gain mobility. The T_g values below T_g represent the devitrification and hence more mobile network and are represented by the decrease to the $\tan(\delta)$ damping peak. The higher T_g s determined for the three resins result from a combination of the high crosslink density of multifunctional and aromatic epoxy-amine resins and their limited mobility up to the glass transition regime.

It was evident from the 180°C trace that progressive growth to the T_g above 300°C for the naphthalene resins could occur upon post-cure. Therefore, samples were cured at 180°C following the same isothermal heating regimen but then heated for an additional two hours at 200°C and 220°C before cooling and further dynamic heating. The traces of $\tan(\delta)$ after post-cure are shown in Figure 4-19 and the values of the gelation time, vitrification time, glass transitions relative to temperature, and the ultimate T_g are given in Table 4-7.

The T_g of a material as determined by a viscoelastic response is either dependent on both temperature of cure and conversion which is described by rubber elasticity theory [221]. At some partial conversion there may exist large domains where the network is less constrained due to unreacted functional groups. At 180°C cure, the T_g is a distinct secondary peak that precedes the ultimate T_g . Although less apparent in the $\tan(\delta)$ trace, a much smaller peak or shoulder is evident in the NTG spectra and disappears from 180°C to 200°C post-cure. However, no such peaks or shoulders are seen with TGDDM and ultimately, the $T_g = T_g$. The main difference between the three resin systems are that with increased post-cure there is no disappearance of the peak with NNE, rather it continues to shift to a higher temperature as conversion is increased. Nevertheless, this T_g begins to exceed the T_g of TGDDM and the value of T_g is nearly 90°C higher. This behaviour in the $\tan(\delta)$ spectra describes the topological constraint that the naphthene epoxy experiences where the unreacted functional groups are so constrained in the glassy state that T_g cannot be reached within practical cure temperatures. TGDDM reacts slowly and has a lower viscosity so that the network can reach a higher degree of conversion prior to T_g . NTG is diluted sufficiently by the amount of TGDDM so that the network is also less constrained and the apparent $T_g = T_g$ at elevated cure and post-cure conditions.

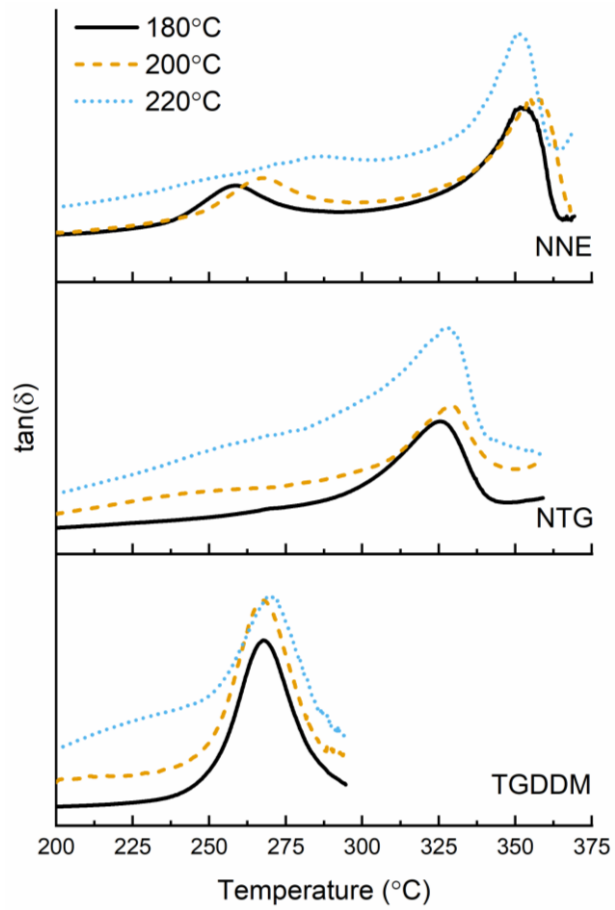


Figure 4-19 - Traces of the $\tan(\delta)$ for the three resins at post-cure

Table 4-7 – Gelation times, vitrification times, and glass transition temperatures

Epoxy Resin	T_{cure} (°C)	t_{gel} (min)	t_{vit} (min)	T_g (°C)	T_g (°C)	
NNE	130	49.5	71.6	199.3	-	
	140	44.2	60.7	206.3	-	
	150	32.6	43.6	215.5	-	
	160	27.6	37.9	227.9	-	
	170	24.1	33.7	244.0	-	
	180	20.9	29.6	258.0	351.5	
Post-cure	180+200			267.0	357.4	
Post-cure	180+220			285.6	351.3	
NTG	130	44.1	73.0	203.0	-	
	140	31.4	52.8	212.2	-	
	150	25.5	42.8	221.5	-	
	160	22.6	37.0	236.9	-	
	170	20.9	33.1	252.5	-	
	180	20.5	30.5	-	325.6	
	Post-cure	180+200			-	329.8
	Post-cure	180+220			-	328.0
	TGDDM	130	115.9	173.4	187.5	-
		140	75.0	108.5	205.0	-
150		48.3	82.5	216.9	-	
160		37.4	63.3	230.7	264.9	
170		30.2	50.2	242.2	261.9	
180		26.5	43.3	-	267.0	
Post-cure		180+200			-	267.9
Post-cure		180+220			-	267.8

4.3.10 Modified Time-Temperature-Transition Diagrams of the Neat Resins

Based on the times to gelation and vitrification as well as the glass transition temperatures determined from DMTA analysis, the time-temperature-transformation behaviour of the neat resins were established for each system. The TTT behaviour of the NNE and TGDDM resin are shown in Figure 4-20. The TTT diagram of the NTG resin is shown in the Appendix A. The devitrification behaviour is represented based on a time relative to the isothermal cure stage when no apparent growth in storage modulus occurs where it is assumed the T_g is established. While it is certain that the reaction still occurs in the glassy state, it is a useful description of the devitrification regime. Also, the fully cured T_g values are presented although for visual simplicity are only assumed with respect to time.

It is clearly illustrated that the NNE system undergoes gelation and vitrification much sooner than TGDDM, a behaviour also seen with the bi-component blend. The sigmoidal shape of the

vitrification is commonly known [213], [217], [222] and, while less evident for TGDDM compared to bi-functional epoxy resin systems, is even less apparent for NNE where the gelation and vitrification behaviour show as near parallel straight lines. The first devitrification regime for NNE (T_g) appears earlier than TGDDM. That can be attributed to the earlier onset of vitrification which correlates to the faster reaction kinetics of the resin system as well as the highly aromatic chemical structure. The second devitrification regime, T_g , appears at lower temperatures for TGDDM than NNE. It is clear that the second devitrification regime of NNE competes with degradation where at 351°C is significantly higher than TGDDM at around 267°C. Chan et al constructed the TTT diagram for a high temperature ($T_g = 324^\circ\text{C}$) resin system and assumed that T_g was unobtainable due to that competition between cure and degradation in the upper temperature regime [223]. For epoxies, this behaviour is not widely reported, largely because of the lower glass transition temperatures of most resin systems presented in the literature. However, parallels between bismaleimides and other high- T_g polymers exist which report T_g values well above the post-cure temperature and, usually as the result of different functional groups becoming activated at elevated temperatures [56], [224]. Again, it is clear that epoxies would experience clear competition between the ultimate T_g and the proceeding of degradation.

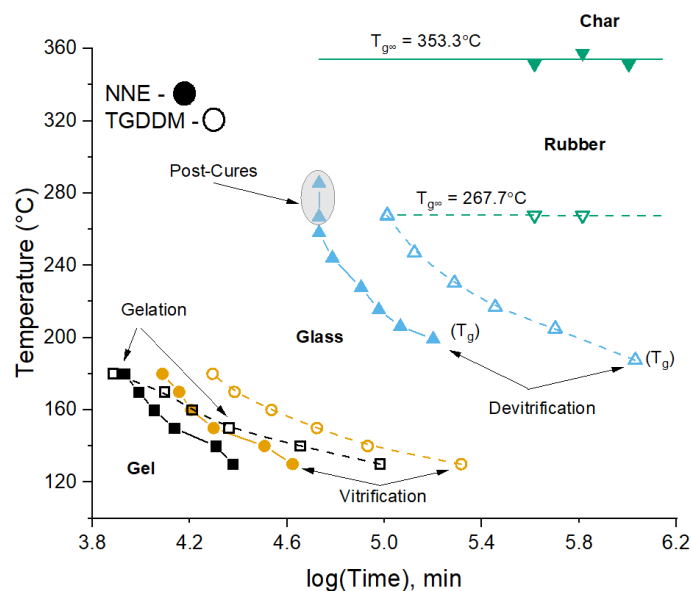


Figure 4-20 - - TTT diagrams of the NNE resin (solid) and TGDDM resin (open). Squares represent gelation, circles vitrification, triangles the sub- T_g peaks from DMTA rescans, and inverted triangles are the T_g values with horizontal lines demarking the limit of the material prior to some thermal degradation. A TTT diagram of the NTG blend is provided in Appendix A

4.4 SUMMARY

In summary, the cure reactions and network development of a high temperature glycidyl ether epoxy resin with dimeric naphthalene backbone was investigated and compared with the commercial glycidyl amine, both cured with the aromatic diamine, 4,4'-diaminodiphenylsulfone. Thermal, spectroscopic, rheological, and dynamic mechanical behaviour of the resins served to establish the cure of these highly crosslinked resins and the evolution of network properties, mainly the glass transition temperatures. Based on an autocatalytic model, it was clear that the NNE resin undergoes rapid reactivity leading to vitrification and the onset of diffusion-controlled processes earlier than TGDDM. That results in a lower final cure. The overall behaviour was attributed to the topological constraints arising from the highly aromatic structure combined with high viscosity and the inability of the resin to undergo internal cyclisation or side-reactions and homo-polymerisation. The TTT diagram was constructed to establish a framework between the gelation, vitrification, full cure, and degradation of the network.

5 PROPERTIES OF THE BULK RESINS AND THERMAL AGEING OF THE CARBON-FIBRE COMPOSITES

5.1 INTRODUCTION

The glass transition of a crosslinked network is associated with the activation of longer-range and segmental motions at the molecular level. The transition from the glassy state to a rubber-like state occurs when there is sufficient energy damping within the network to undergo thermal relaxation. It is within that knowledge that the structure of the epoxy and amino-hardener are exploited to achieve high temperature performance and stability. The conventional high temperature epoxies of TGDDM and TGAP are more thermally stable because of their tri- and tetra-functional order, highly aromatic backbones, and subsequent limited mobility when cured with aromatic diamines. However, these both contain glycidyl amine motifs within the polymer backbone which can catalyse side reactions such as internal cyclisation, creating mechanically inactive structures that can prevent the cured network from achieving ultimate mechanical properties and glass transition temperature [192], [199], [200], [225]. The desire for glycidyl ether resins as alternatives is highlighted by recent developments in epoxies derived from precursors that do not contain amine-functional groups and are therefore absent of glycidyl amine motifs within the monomer structure. [28] described the synthesis and characterisation of a tetrafunctional, nitrogen-free epoxy resin and showed that a bi-component blend of the monomer with diglycidyl ether of bisphenol A (DGEBA) had a T_g similar to TGDDM [28]. Additionally, work by Zing et al. showed similar results using a nitrogen-free tetrafunctional epoxy when blended with up to 60 wt% DGEBA [81]. Although the need to blend a DGEBA resin with the latter demonstrates the need to balance increasingly higher molecular weight and aromatic backbones with the needs for processability, particularly within the context of matrices for high-performance composites.

The synthesis and investigation of novel naphthalene-based polymers demonstrates a potential advantage over aromatic phenyl-based epoxy backbones for high temperature performance. Wang et al. synthesised trifunctional epoxies containing naphthalene structures and noted higher glass transition and thermal stability which they attributed to the three resonant structures of naphthalene versus two for phenylene [18]. Similar reports for naphthalene-containing bismaleimide and cyanate esters indicate some positive influence on thermal stability [20], [226]. Duann et al. investigated phenyl and naphthalene-based epoxies and

showed superior thermal stability of the naphthalene-containing epoxies but reported generally poor mechanical properties [42], [82]. More recently, the difunctional monomers synthesised from 2,7'-dihydroxynaphthalene and epichlorohydrin of Fila et al. showed superior glass transition and thermal degradation properties [38] for which the chemical structures were analogous to DGEBA. There is some evidence then, for the beneficial effects of naphthalene-based epoxies for high temperature performance outside of electronics and thermal insulating applications.

While the very high T_g of NNE makes this resin attractive for high temperature applications, there is a lack of fundamental knowledge regarding its structure/property relationships, particularly when compared with the much more widely studied DGEBA, TGDDM, and TGAP-based networks. Recent work by Vukovic et al. utilised large-scale molecular dynamics simulations to study the origin of the T_g for TGDDM and NNE cured with aromatic diamine and it was found that segmental motions across cross-linked domains, inhibited by the rigid dimeric naphthalene backbone of NNE, contributed to the markedly higher glass transition temperature [41].

5.1.1 Overview of the Investigation

In this section, the relation between epoxy monomer structure and subsequent thermal and mechanical properties are determined for the bulk resin and translated to the carbon fibre composite. The layout of this section is split into two key areas, the first focused on structure-property relations of the NNE resin with respect to degree of conversion and between the NNE, bi-component resin NTG, and the TGDDM resin formulation. The second section is focused on translation of resin properties to the composite and a comparative investigation of the thermal stability of the glycidyl ether resin versus glycidyl amine at an elevated temperature.

In the first section, degree of cure is investigated via differential scanning calorimetry and near-infrared spectroscopy performed on the cured resin bars. Thermal properties are studied via thermomechanical analysis (TMA), dynamic mechanical-thermal analysis (DMTA) in the sub-ambient and high temperature regimes, and via dynamic and isothermal thermo-gravimetric analysis (TGA). Moisture ingress is investigated by soaking the resins in a water bath for a long period of time and the effect is studied by moisture ingress and DMTA. Mechanical properties of the resins are studied for flexural performance and fracture toughness.

In the second section, the characterisation of the composite is performed by manufacturing carbon fibre laminates for use in flexural and dual-cantilever fracture toughness testing. Further, the thermal stability is assessed via a long-term ageing study at a single elevated temperature utilised for the three resin formulations. The retention of flexural properties is studied periodically for the composite and FTIR is utilised alongside mass loss and DMTA data to understand the performance and influence of degradation modes between the glycidyl ether and glycidyl amine resin as composite matrix systems.

5.2 MATERIALS

The epoxy resins and amino hardeners used in this study are shown in Table 5-1. Materials prepared in this study include a 1:0.95 stoichiometric formulation of NNE, a 70:30 molar ratio blend of NNE and TGDDM, and a formulation of TGDDM, all of which are cured with DDS. Analytical grade acetone and dichloromethane (DCM) were utilised as solvents in the production of the carbon fibre prepregs.

Table 5-1 - Summary of materials used in the study

Material	ID	Chemical Name	EEW/ AEHW (g/eq.)	Mfg. Supplier
Epoxy Monomer	NNE	bis(2,7 glycidyl ether naphthalenediol) methane	170.72 ±0.30	DIC Corp. (JPN)
Epoxy Monomer	TGDDM	tetraglycidyl diamine diphenyl methane	124.05 ±0.21	Huntsman Corp. (USA)
Amine Hardener	44DDS	4,4'-diaminodiphenylsulfone	62.08	TCI Chemical Inc. (JPN)

The neat resins were cured via a series of different step-wise isotherms in a convection oven following conventional cure temperatures for epoxy resins and subsequent post-curing was performed to study the effect on conversion and properties. An outline of the cure and post-cures used for the neat resins is shown in Table 5-2.

The carbon fibre laminates were constructed from a standard-modulus unidirectional carbon fibre tape of 150 g/m² areal weight. The sheets of prepregs were placed on metallic trays and 40 mL of a dichloromethane:acetone mixture containing the epoxy-amine components was evenly dispersed across the cloth. Upon saturation, the cloth was dried in a convection oven at 65°C for 15 minutes. This procedure was repeated until the desired initial resin content was

achieved. The composites were manufactured in a purely unidirectional $[0^\circ]_{15}$ configuration and nominal laminate dimensions were 100 x 150 mm rectangular panels. Based on the study of properties for the neat resins, the composite curing schedule and post-curing regime was standardised as 150°C for four hours, 180°C for four hours, and a two-hour free-standing post cure of 200°C for TGDDM and 220°C for both NNE and NTG. A standard 3°C/min ramp rate was used between each increase in cure temperature. A hydraulic heated press was used to cure the laminates under 5 bar of pressure and using applied vacuum.

Table 5-2 – Cure schedule of the neat resins studied in this chapter

Composition	Sample ID	Cure profile	Post Cure
NNE/DDS	NNE-150	8 hrs at 150°C	-
	NNE-180	4 hrs at 150 °C - 4 hrs at 180°C	-
	NNE-200	4 hrs at 150°C - 4 hrs at 180°C	200°C
	NNE-210	4 hrs at 150°C - 4 hrs at 180°C	210°C
	NNE-220	4 hrs at 150°C - 4 hrs at 180°C	220°C
	NNE-240	4 hrs at 150°C - 4 hrs at 180°C	240°C
(70 mol% NNE-30 mol%)/DDS	TGDDM	4 hrs at 150°C - 4 hrs at 180°C	200°C
TGDDM/DDS	NTG	4 hrs at 150°C - 4 hrs at 180°C	220°C

5.3 RESULTS AND DISCUSSION ó NEAT RESIN PROPERTIES

5.3.1 Differential Scanning Calorimetry

The cured NNE resins were characterised by differential scanning calorimetry by directly removing a small amount (~10mg) from the as-moulded samples. These were dynamically heated in the DSC and a comparison of the residual exothermic peaks was then used to determine a fractional degree of conversion. The average of the five dynamic runs (see Table 4-2 in Chapter 4) was utilised as the average enthalpy of cure. Traces of the rescans are shown in Figure 5-1(a-b) and a plot of the degree of conversion for varying post-cure and between the three resin formulations is provided in Figure 5-2.

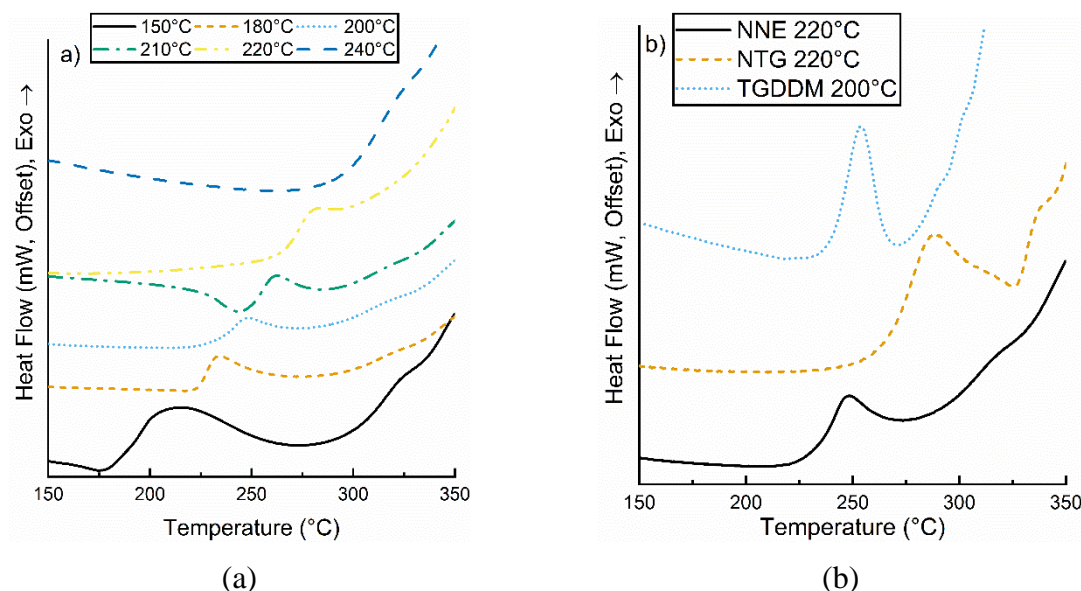


Figure 5-1 - Differential scanning calorimetry traces of the cured resins at (a) increasing cure condition of NNE and (b) between the three different epoxy formulations

The degree of cure at the lowest cure condition for NNE (150°C for 8 hours) was 88% and then plateaus for the temperatures of 200-220°C. Similarly, the TGDDM and NTG resins cured at 200 and 220°C reach a conversion 98% and 96%, respectively. Above 220°C the NNE resin shows no discernible peak exotherm however at that temperature the competition between cure and degradation cannot be ignored. The change in conversion at the lower 150°C and 180°C reflects the natural stagnation of cure that results from vitrification of the resin system as the segmental mobility of the network becomes severely limited and slower diffusion-controlled reactions consume the excess unreacted functional groups [209], [227], [228]. The extent of cure under isothermal (no post-curing) condition discussed previously (see Table 4-3 in Chapter 4) is similar to the values of 150°C and 180°C.

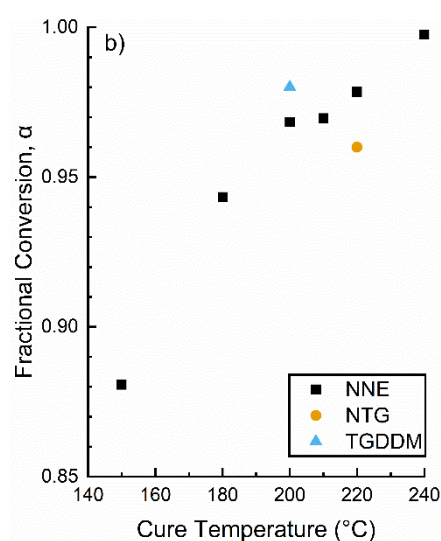


Figure 5-2 - Fractional conversion of the three resins as determined by DSC

5.3.2 Near-Infrared Spectroscopy

Near-infrared Fourier Transform Spectroscopy was utilised to determine the conversion of epoxy-functional groups after cure through varying cure temperatures for NNE and between the three resins. Cured resin bars were utilised to determine the change to the epoxy, secondary amine, and hydroxyl peaks and are shown for the NNE, NTG, and TGDDM resin in Figure 5-3a-b. The uncured resin shows a strong epoxide peak at 4520cm^{-1} and the peak is present at all cure temperatures even up to 240°C. The primary amine peak is completely consumed in the initial stages prior to vitrification and is not present in any of the spectra. As cure temperature increases, the growth of the hydroxyl peak increases, yet even from 220-240°C

the peak increases. That is concurrent with the behaviour previously reported in Chapter 4 (see Table 4-4) where no significant side-reactions or etherification occur within the cure of NNE.

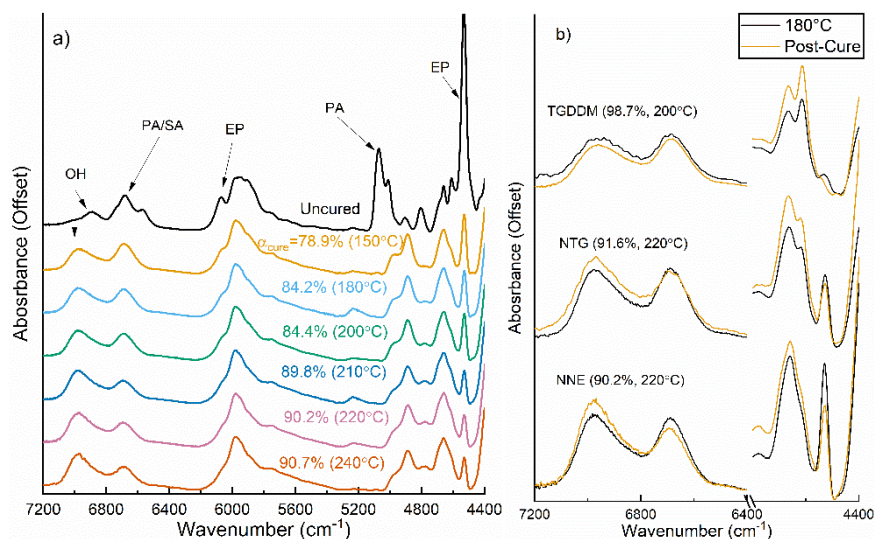


Figure 5-3 - Near-infrared spectroscopy of the NNE resin after cure and post-cure (a) and of the NNE, NTG, and TGDDM resins from cure at 180°C to post-cure

The degree of epoxide conversion was determined for the three resins at varying cure temperature and post-cure. For the NTG and TGDDM resin, the samples were measured after cure at 180°C and then again after post-cure at 220°C and 200°C, respectively. The epoxide conversion is shown for all cure temperatures and resins in Figure 5-4. Comparing the three resins at 180°C, it is apparent that the rate-limiting diffusion-controlled kinetics affect epoxide consumption for the naphthalene-based resins. The TGDDM resin shows epoxide conversion of 95% prior to post-cure, increasing to 98% during post-cure. NNE and NTG reflect epoxide conversion of just 87% and 88%, respectively and after post-cure at 220°C the NNE shows 92% and NTG just below 91% epoxide conversion. The effect of rapid gelation and vitrification clearly affects the ability of the NNE resin to undergo further epoxide conversion without either a) extreme elevated temperatures or possibly b) extensive curing times. The absence of etherification and internal cyclisation could affect the relatively higher degree of conversion achieved by TGDDM [200], [229]. However, other research on di- and tetrafunctional amine-cured glycidyl ethers have shown much higher epoxide conversion [28], [230] suggesting that, in this case, the topological constraints which arise from the rigid dimeric naphthalene structure and limited mobility in the glassy state compared to TGDDM. The effect of the lower conversion compared to TGDDM can have a significant impact on thermal and mechanical

properties as unreacted epoxide groups can act as a plasticiser to the network, lowering modulus and strength.

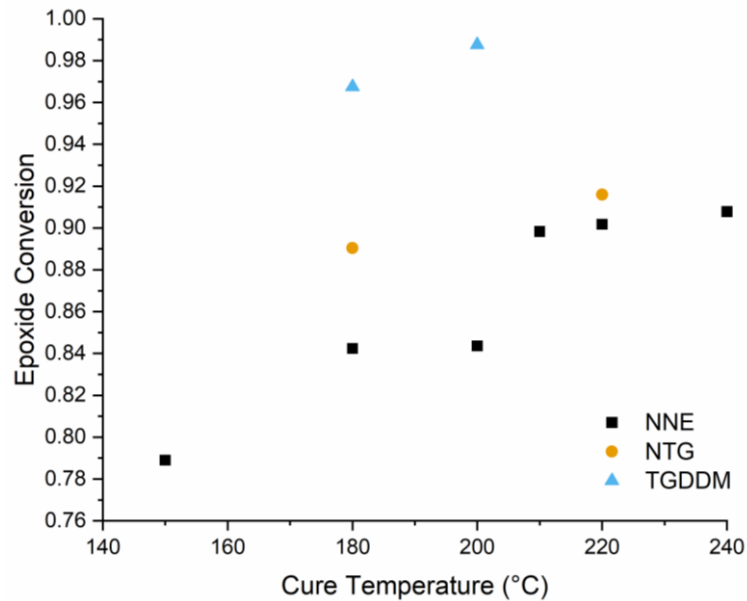


Figure 5-4 - Fractional conversion of epoxy as determined by near-infrared spectroscopy

5.3.3 Dynamic Thermal Mechanical Analysis of the Cured Resins

Dynamic thermal mechanical analysis of the three resin systems was performed in the sub-ambient and above ambient regimes to determine the glass-rubber transition onset and the peak of $\tan(\delta)$. The traces of storage modulus and loss tangent for the NNE relative to the extent of cure and post-cure are shown in Figure 5-5(a-b) and values tabulated in Table 5-3. As previously found, the lower degree of conversion results in a bi-modal behaviour in the spectrum of $\tan(\delta)$ which is related to the mobility of the partially cured network that then becomes restricted at high degree of cure as a result of the constrained network topology. The bimodal nature of the $\tan(\delta)$ peak could be attributed to heterogeneity from large domains of unreacted epoxy or variations in the crosslink density which would be active at different temperature regimes. In effect, as conversion increases, the loss tangent decreases due to reduced molecular mobility [217]. That is apparent with the post-cures where it is seen that by 220°C the peak of $\tan(\delta)$ is nearly diffused into the T_g peak and by 240°C completely disappears. It is notable, then, that the effective loss tangent maximum occurs at a significantly lower conversion than for similar resin reported in the literature, albeit at a high cure temperature. Jackson et al observed for TGDDM-based epoxies that the substitution of 33DDS and 44DDS resulted in nearly 100% and 94% conversion after elevated temperature cure [231]. Similarly, for TGAP cured with 44DDS Varley et al. found conversion reached nearly 100%

[232]. The glass transition temperatures of the three resins were evaluated using a commercial molecular dynamics (MD) software package and the results are provided in Appendix B.

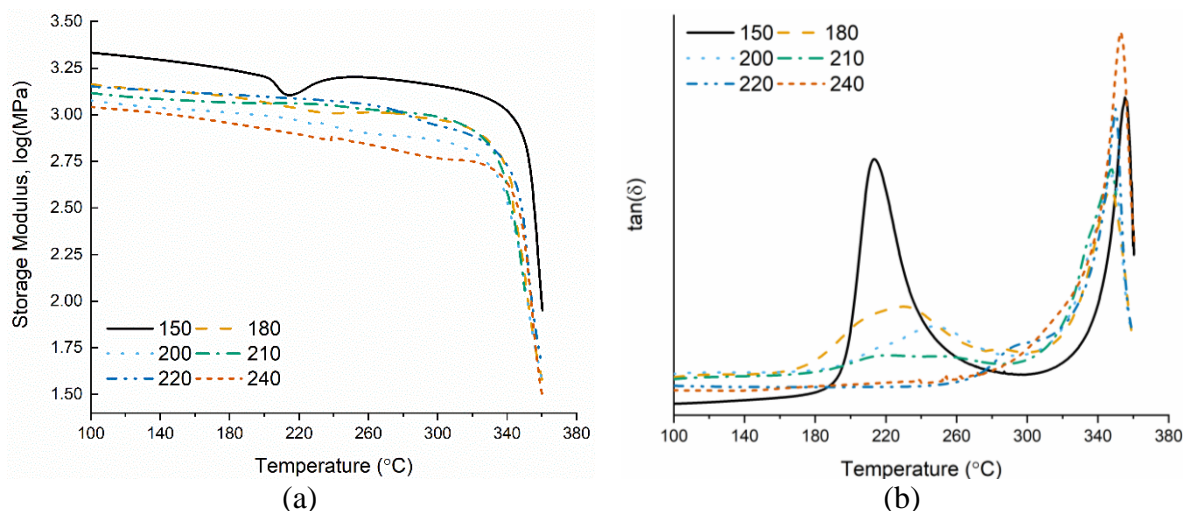


Figure 5-5 - DMTA traces for storage modulus and $\tan(\delta)$ of the different cure conditions

Between the three resin formulations, the DMTA traces provide initial context for the mechanical capabilities and how they relate to the network structure. The traces of storage modulus and $\tan(\delta)$ are shown for NNE, TGDDM, and NTG in Figure 5-6(a-b). In a similar fashion to the previous result where damping to the loss tangent was associated with reduced molecular mobility near the glass-rubber transition, the behaviour between monomer structure is also systematically different. The TGDDM resin cured with 44DDS exhibits a broad $\tan(\delta)$ peak and also a peak height nearly three times that of NNE which is also much narrower and NTG sits between the two. A broadening of the loss tangent and height is associated with increased mobility [233]. Notably, the storage modulus is highest for TGDDM and progressively decreases for NNE with respect to post-cure. That could be related, in part, to degradation of the resin as a result of elevated temperature post-cure.

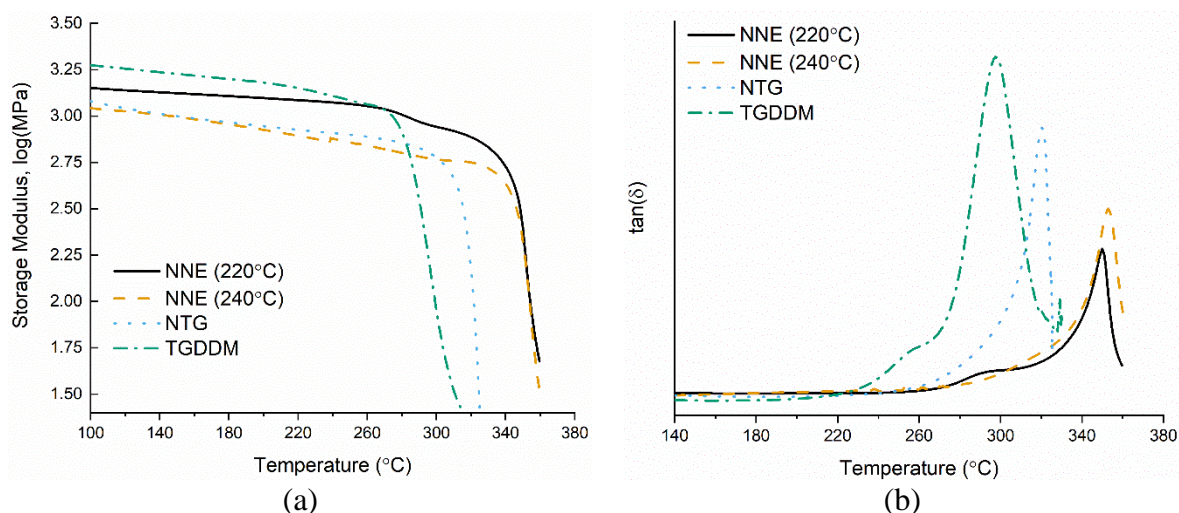


Figure 5-6 - DMTA traces for storage modulus and $\tan(\delta)$ of the different resin formulations

Table 5-3 - DMTA values for the glass transition onset from E' and peak of $\tan(\delta)$

Cure Condition	$T_{\text{onset}} (^{\circ}\text{C})$	$T_{\text{g}} \text{ d } \{ \text{ " v c } \}$	$T_{\text{g}} \text{ d } \{ \text{ " v c } \}$
NNE			
150°C Cure	201.94	213.48	355.3
180°C Cure	-	230.45	348.3
200°C PC	-	245.78	347.9
210°C PC	-	250.44	343.6
220°C PC	327.89	297.4	349.9
240°C PC	346.47	-	352.68
NTG			
220°C PC	318.03	-	320.31
TGDDM			
200°C PC	278.74	-	297.38

Sub-ambient DMTA allows for the investigation of the short-range molecular motions of polymer networks. For epoxies the peak of the loss tangent, the β -transition is ascribed to rotations of the reacted epoxide left of the peak and amino-bound groups right of the peak as well as contributions from the phenyl rings either of the epoxy or amine molecules within the network [192], [234]. Additional cooperative long-range motions are sometimes visible in the range of ~ 50 - 100°C but less well-defined as the phenyl-epoxide ring segmental motion [192] or hydrogen-bound epoxide species formed from etherification reactions [235], [236]. The plots of the loss tangent for NNE with respect to extent of cure and between the three resin formulations are shown in Figure 5-7(a-b) with peak temperatures and areas provided in Table 5-4.

Much like with the elevated temperature analysis, as extent of cure is increased, the peak height and temperature of the sub-ambient β -transition progressively shifts to a lower magnitude and

higher temperature. Again, that is associated with reduced mobility in the glassy state although as the cure reaction progresses and more epoxide is reacted, it would also result in a widening of the right-hand side of the $\tan(\delta)$ peak. Notably, as the temperature of post-cure increases to 240°C there is an emergence of a secondary peak between 50-100°C which is otherwise less apparent in the other post-cure temperatures. Assuming it were related to hydrogen-bound epoxide groups then a similar decrease to epoxide and increase to hydroxyl would show in the NIR traces (Figure 5-3) however, such a trend is not apparent. Therefore it is possible that the high cure temperature contributes to some evolution within the network more associated with degradation than etherification. Indeed, the work by Simon & Gillham highlights the need to assume no degradation occurs prior to etherification at elevated temperatures [237].

Between the three resins it is notable that the peak of NNE is both higher and narrower than either NTG or TGDDM with the latter showing a broad and diffuse right-sided half of the β -transition. As observed by Vukovic et al., the ability for TGDDM to undergo ring flips about the central axis of the backbone differentiated the molecular origin of the glass transition temperature for both NNE and TGDDM [41]. Herein, it emerges that the lack of mobility within the NNE network also constrains the segmental motion of the amino backbone. Again, a secondary peak emerges above 50°C which is narrow for NTG and broad and diffuse for TGDDM. Notably, it is previously established that a significant degree of etherification and side reactions is possible for the TGDDM-based resins.

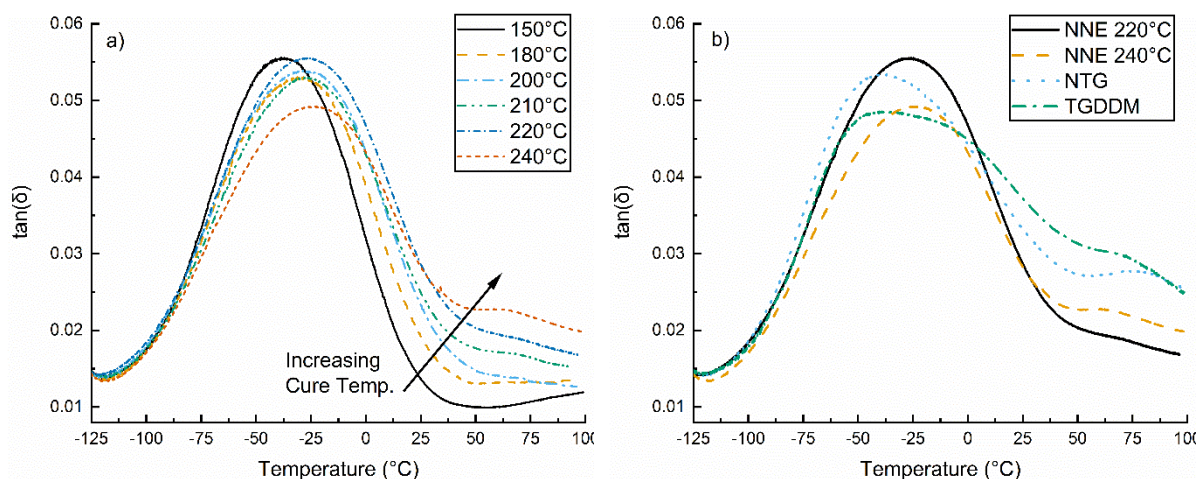


Figure 5-7 - Traces of the $\tan(\delta)$ spectra under sub ambient DMTA for (a) NNE at increasing cure and (b) the three resins

Table 5-4 - Sub-ambient DMTA values for peak temperature and partial areas of the tan(δ) traces

Cure Condition	T (°) at R g c m " v	Total Area	Area Left of Peak	Area Right of Peak
NNE				
150°C Cure	-38.5	5.25	2.65	2.60
180°C Cure	-31.9	5.5	2.87	2.63
200°C PC	-29.0	5.83	3.07	2.76
210°C PC	-26.5	5.82	3.07	2.75
220°C PC	-24.8	6.28	3.36	2.92
240°C PC	-23.8	5.85	3.02	2.83
NTG				
220°C PC	-38.4	6.59	2.70	3.89
TGDDM				
200°C PC	-35.9	6.64	2.64	4.00

5.3.4 Thermal Expansion Coefficient of the Neat Resins

The thermal expansion coefficient was determined by thermal-mechanical analysis and computed over a constant range of temperatures below non-linear behaviour that would occur near the T_g . Examples of the three resins and with respect to the extent of cure are shown in Figure 5-8(a-b). Again, it is seen that the thermal expansion behaviour follows a trend where $NNE > NTG > TGDDM$. The CTE of a material can be traced to the origin of the free volume and crosslink density within the cured polymer network. As crosslink density increases the free volume is expected to decrease, along with an increase to the physical density [238]. The behaviour is less apparent at the lower cure temperatures due to non-linear effects near the T_g . However, as conversion increases the CTE remains virtually unchanged for NNE. Between the three resins, the NNE resin being higher suggests poor equilibrium packing of the cured network due to the higher intermolecular spacing and limited mobility of the bulky NNE monomer.

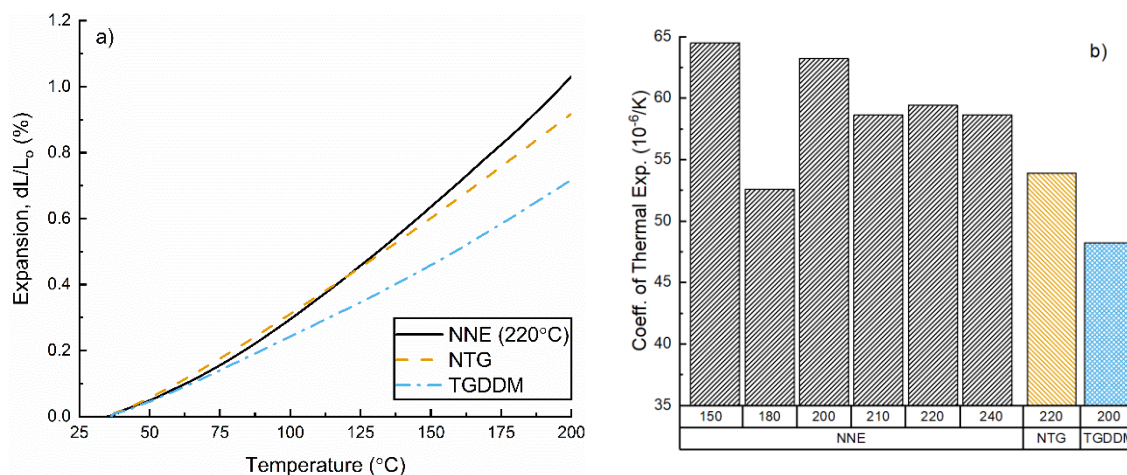


Figure 5-8 – (a) TMA traces of NNE (220 $^{\circ}\text{C}$), NTG (220 $^{\circ}\text{C}$), and TGDDM (200 $^{\circ}\text{C}$) post-cure conditions and (b) thermal coefficient of expansion relative to cure temperature and resin system

5.3.5 Thermogravimetric Analysis

Dynamic and isothermal thermogravimetric analysis was performed on the three resin systems at the 220 $^{\circ}\text{C}$ cure condition for NNE and NTG and 200 $^{\circ}\text{C}$ cure condition for TGDDM, based on the similar degree of cure as determined by DSC. All TGA was carried out in a nitrogen atmosphere. The plot of dynamic TGA curves for a 2.5 $^{\circ}\text{C}/\text{min}$ heating rate is shown in Figure 5-9 with tabulated values of the degradation onset and char yields given in Table 5-5. The activation energies were determined from a band of 50-80% weight loss, corresponding to the regime of degradation values past T_d for all three resins and are given in Figure 5-10.

The dynamic TGA trace shows distinct increase in the T_d onset for the naphthalene resins compared to TGDDM. Almost no change in mass loss is apparent until 380 $^{\circ}\text{C}$ upon which the mass loss increases sharply. TGDDM meanwhile, shows an earlier onset but gradual mass loss up to about 70 wt% of retained weight, whereby the curves intersect. That contrasting behaviour is represented in the sharp, narrow peak of the derivative of mass loss which is largely similar for both naphthalene-based formulations. The initial 5 wt% mass loss was also higher for NNE and lowest for TGDDM, irrespective of the heating rate. Final char yield is also consistently higher for NNE with NNE (~35%) > NTG (~31%) > TGDDM (~26%).

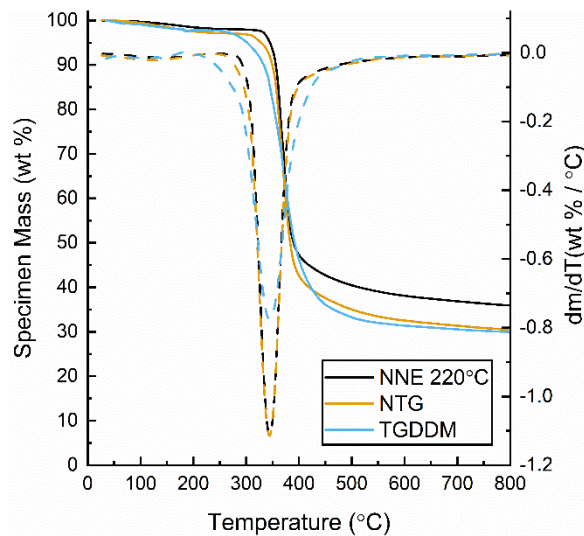


Figure 5-9 - Plot of the mass loss (solid) and derivative of mass loss (dashed) for the three resin systems heated at 10°C/min

The onset of degradation increases with respect to heating rate and allows for simple kinetic analysis by means of the Flynn-Wall-Ozawa model. From Figure 5-10(a) the constructed plot of temperature versus the logarithm of heating rate shows similar behaviour of the NNE and NTG resins and a shift for the TGDDM resin towards the lower temperature regime, reflecting the earlier onset of degradation. However, the slopes are largely the same suggesting only minor differences in the kinetics of degradation. A plot of activation energies shown in Figure 5-10(b) shows that in the earlier stages of degradation (65-80 wt% retained mass) the TGDDM resin barrier to degradation is higher, albeit at a lower temperature. As degradation progresses the activation energy of TGDDM increases while NNE and NTG remain the same. That is, as a significant char forms, the energy barrier of degradation increases. That is evident in the TGA trace where, although there is a higher char yield for NNE and NTG, the transition into the final char occurs at a lower temperature than TGDDM.

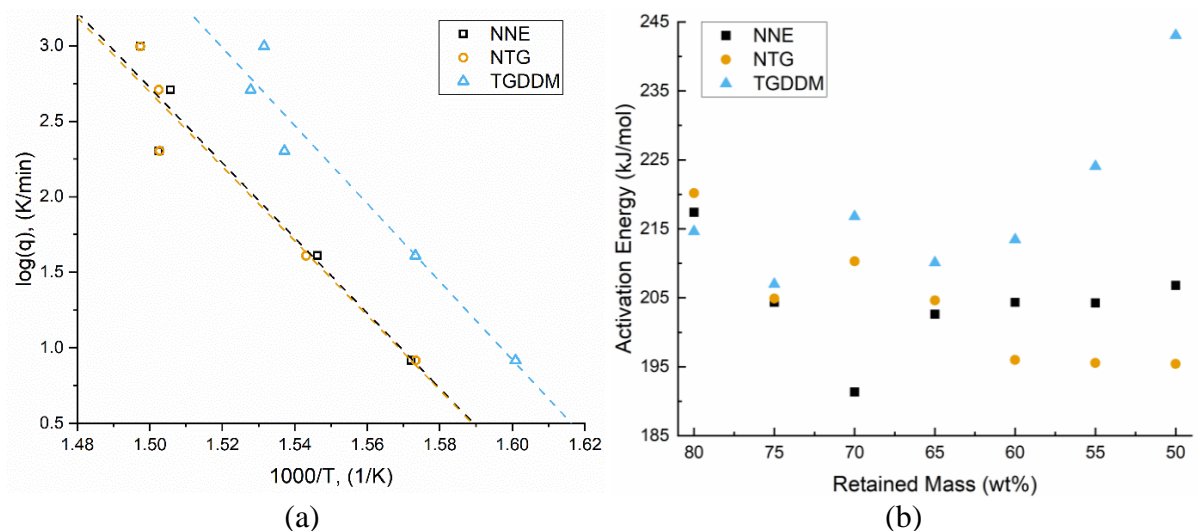


Figure 5-10 - Plot of (a) Arrhenius-like degradation model and (b) activation energies relative to retained mass (at $2.5^\circ\text{C}/\text{min}$ heating rate) of the three resins

Table 5-5 - Values of degradation temperature, char yield, and activation energies from dynamic TGA

	Heating Rates					E_a (kJ/mol)
	$2.5^\circ\text{C}/\text{min}$	$5^\circ\text{C}/\text{min}$	$10^\circ\text{C}/\text{min}$	$15^\circ\text{C}/\text{min}$	$20^\circ\text{C}/\text{min}$	
NNE						
T_d	352.2	362.5	383.8	386.7	393.1	204.45 ± 7.62 ($r=0.948$)
$T_{95\%}$	342.9	356.1	372.5	373.5	375.2	
Char Yield	35.9	34.8	34.9	34.6	33.7	
NTG						
T_d	348.0	365.2	375.9	375.5	376.6	203.85 ± 9.23 ($r=0.946$)
$T_{95\%}$	327.5	342.5	354.9	354.9	364.8	
Char Yield	30.5	31.4	30.9	31.5	30.5	
TGDDM						
T_d	342.7	350.7	359.2	361.9	365.2	218.43 ± 12.11 ($r=0.952$)
$T_{95\%}$	301.5	314.9	324.9	333.8	329.9	
Char Yield	29.9	25.1	25.4	26.8	23.9	

Only a limited understanding of the degradation kinetics for naphthalene-containing epoxies is reported, however, the higher char yields observed in naphthalene-based epoxies largely support the observations from TGA between NNE and TGDDM. Duann et al. comparatively evaluated phenyl and naphthalene-containing epoxies, all difunctional, and noted similarly high char yield for the latter although the onset was higher for the phenyl-based epoxies and activation energies varied irrespective of the type of epoxy backbone [82]. Duann et al. utilised DGEBA and naphthalene epoxy blends and showed increased char yield from 18 wt% (100 DGEBA) up to 32 wt% (50% DGEBA/ 50% naphthalene-based epoxy) with the addition of the di-functional naphthalene epoxy [42]. Wang & Hwang formulated bismaleimides with naphthalene backbones and showed similar thermal performance enhancements which was attributed, in part, to the three resonant structures afforded to a naphthalene versus phenol [20]. Fila et al evaluated six epoxy resins synthesised from the epoxidation of 2,7-dihydroxynaphthalene and noted high thermal resistance but a similarly narrow band between the degradation onset and defined a maximum temperature of degradation in the range of 380-424°C [38]. It is shown here then that the thermal degradation is influenced greatly by the difference in the backbone structure for these tetrafunctional resins.

In practical terms, degradation kinetics and the onset via dynamic TGA reflect differences in thermal resistance to degradation only in a short timeframe and do not reflect the performance in service. Therefore, isothermal TGA was performed to understand the influence of the naphthalene backbone on stability. A series of TGA isothermal runs were performed on approximately 10 mg of cured resin and heated at temperatures below the glass transition temperature of the three resins. Traces of the isothermal TGA curve at 250°C and a plot of mass loss for 225-300°C isotherms are shown in Figure 5-11. It is clear that NNE shows some short-term stability at elevated temperatures compared to TGDDM with nearly twice the retained mass after 10 hr at 250°C. Also notable is the difference in the tail-end of the isothermal TGA traces where NNE appears to reach a baseline while the slopes of NTG and TGDDM traces are negative, reflecting a continuation of thermal degradation. Above 250C, all resins show a negative slope after 10 hr but the fraction of retained mass for NNE remains consistently higher than the blend and TGDDM. It is clear that the naphthalene backbone contributes to a higher retained mass because the NTG blend is noticeably higher than TGDDM at each isothermal temperature as well.

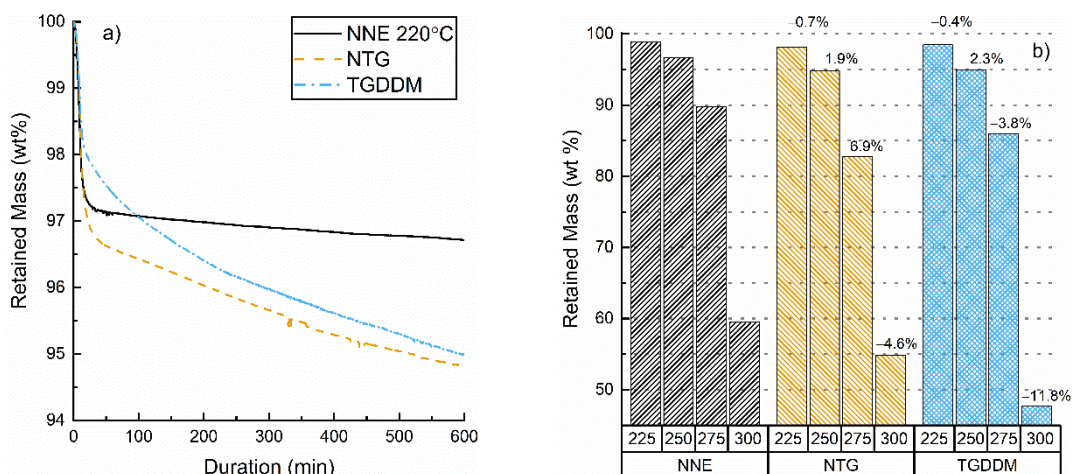


Figure 5-11 - Isothermal TGA traces for the three resins at 250°C and a comparison of mass loss for 225-300°C isothermal heating runs

5.3.6 Moisture Ingress and Physical Density

The physical density and moisture ingress relative to cure temperature and crosslink density was determined for the three systems by periodic gravimetry of the cured resins after soaking in deionised water at 80°C. The ingress of moisture was determined in triplicate for epoxy specimens over a period of 14 days. The results of moisture ingress are shown in Figure 5-12(a-b) for the increasing cure condition and between the three formulations. The physical density, diffusion coefficients, and equilibrium moisture content are provided in Table 5-6.

Fundamentally, the increase in moisture is related to the network properties and the chemistry of the network constituents. The network free volume fraction (FVF) and free volume hole size influence moisture ingress behaviour [239] while hydrophilic functionalities can form hydrogen bonds with water molecules [240]. It was observed that moisture ingress increased with respect to extent of cure while the naphthalene-based network showed a higher equilibrium moisture uptake and diffusion coefficient than TGDDM, although a clear equilibrium is not yet apparent for the latter. Previous work by Frank et al. noted that an excess of epoxy contributed to reduced moisture uptake due to more efficient packing density and a lower crosslink density [241]. Further, they demonstrated that an inverse relation exists for epoxies where, as crosslink density increases, the free volume hole size decreases and FVF increases [242]. That correlates to the behaviour with NNE where further cure would lead to an increased crosslink density but likely higher FVF. The trend in diffusion coefficient to decrease with increased cure and crosslink density also follows for decreased free volume hole

size as a result of a higher crosslink density. As seen with the DMA ramps, a rubber plateau is not readily apparent for NNE which meant crosslink density could not be quantified by rubber elasticity theory. However, the NNE, NTG and TGDDM resins at the highest degree of epoxide consumption were characterised by the Flory-Rehner equilibrium swelling theory [243], [244] and is provided in Figure A6 of Appendix B.

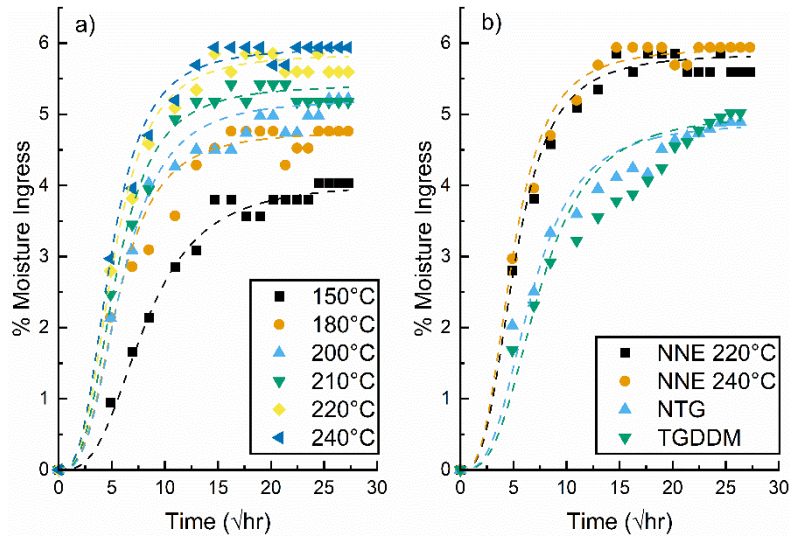


Figure 5-12 - Moisture ingress of (a) the NNE resin relative to conversion and (b) between the three resin formulations

Table 5-6 - Density, moisture ingress at equilibrium, and diffusion coefficients of the resins

	NNE						NTG	TGDDM
Cure Temp (°C)	150	180	200	210	220	240	220	200
(g/cm ³)	1.315	1.32	1.313	1.316	1.315	1.327	1.299	1.279
Eq. Wt. %	3.56	4.76	4.97	5.41	5.85	5.94	4.89	5.02
D (10 ⁻¹² m ² /s)	1.387	1.279	1.269	1.247	1.221	1.162	1.164	1.101

After moisture ageing the resins were scanned via DMTA to determine the effect on the glass transition. Figure 5-13(a-b) show the results of DMTA analysis with respect to extent of cure for NNE while Figure 5-14 shows the effect between the three resin formulations. The magnitude of storage modulus decreased for all cure conditions relative to the dry measurements (see Figure 5-5). The effect on the glass transition is highlighted in the shift of the T_g peak in tan(δ) for the 150-220°C specimens and the growth of a shoulder for 240°C. Again, between the three resins there is a decrease to the storage modulus in the glassy state compared to the dry specimens (see Figure 5-6) and a clear difference between the decrease to T_g between NNE and TGDDM. The naphthalene-containing resins showed decreased onset and T_g nominally of 20-30°C and nearly 40°C for TGDDM. The traces of tan(δ) display a large

secondary peak below 200°C for TGDDM. Previous analysis of TGDDM-DDS networks in the wet state by Musto et al. showed a similar decrease in the T_g to 180°C after saturation and for which they attributed the sub- T_g peak to plasticisation effects [35]. Moisture has the effect of plasticising epoxy networks and in the case of TGDDM appears to have induced some heterogeneity on the network that is otherwise not present for NNE or NTG at the higher cure temperatures. Indeed, only a small shift in the $\tan(\delta)$ towards lower temperatures is observed suggesting the naphthalene-based resins are less affected by moisture than TGDDM.

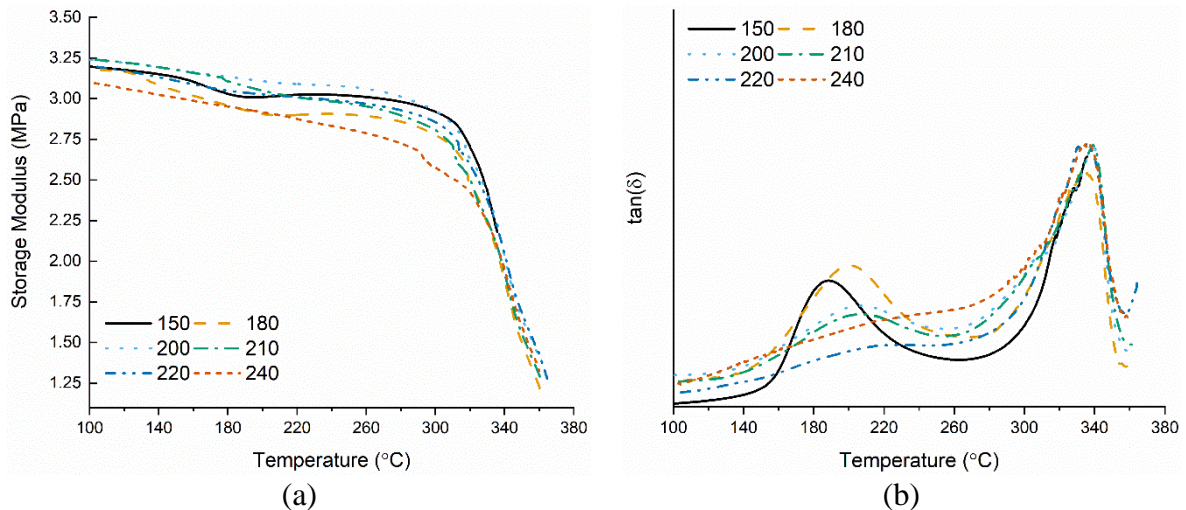


Figure 5-13 - DMTA traces relative to extent of cure for NNE of (a) storage modulus and (b) the $\tan(\delta)$ behaviour after moisture-ingress

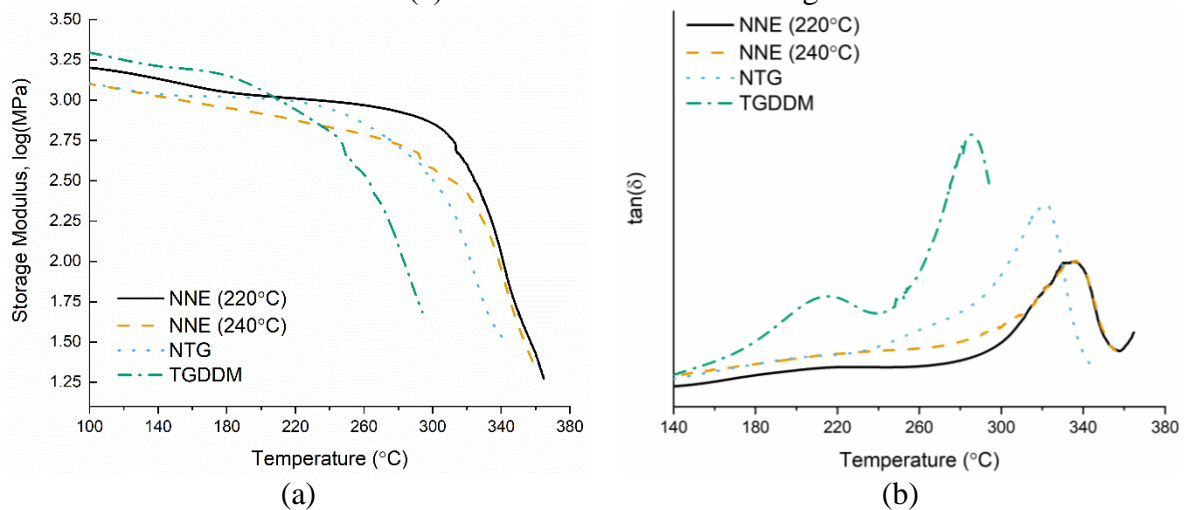


Figure 5-14 - DMTA traces of NNE, NTG, and TGDDM of (a) storage modulus, and (b) the $\tan(\delta)$ behaviour after moisture ingress

As mentioned previously, there are both physical and chemical effects to water moisture ingress. Hydrogen-bonded moisture can appear as a distinct broad peak between 5140-5240 cm^{-1} in the near-infrared regime [245]. It is clearly seen in Figure 5-15(a-b) that systematic changes

occur relative to the extent of cure and with increasing crosslink density. The NIR spectra for the different cures shows a normalised increase for the spectral intensity as a function of the cure and post-cure temperature. Likewise, the intensity is highest for NNE and lowest for TGDDM, corresponding to the differences in equilibrium saturation levels.

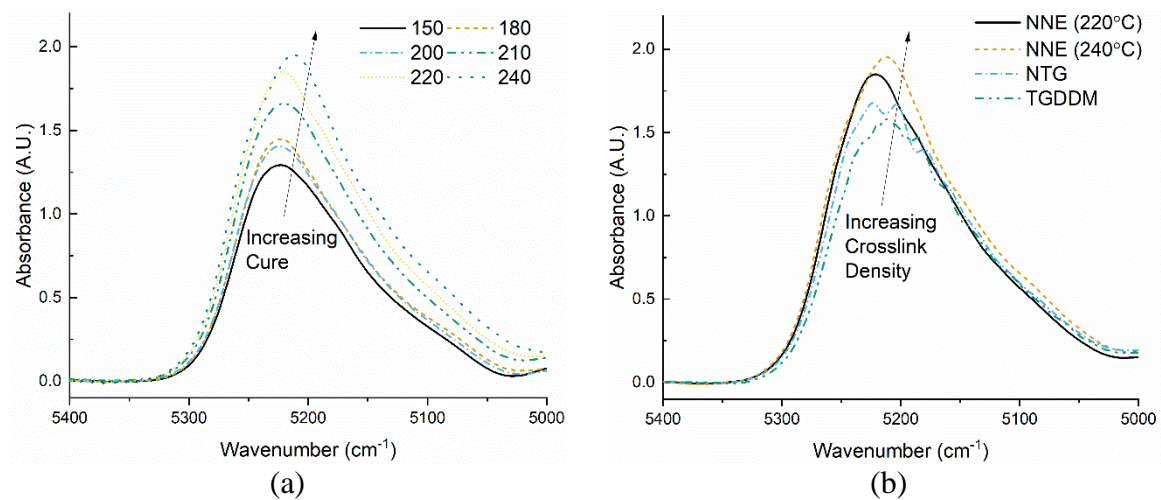


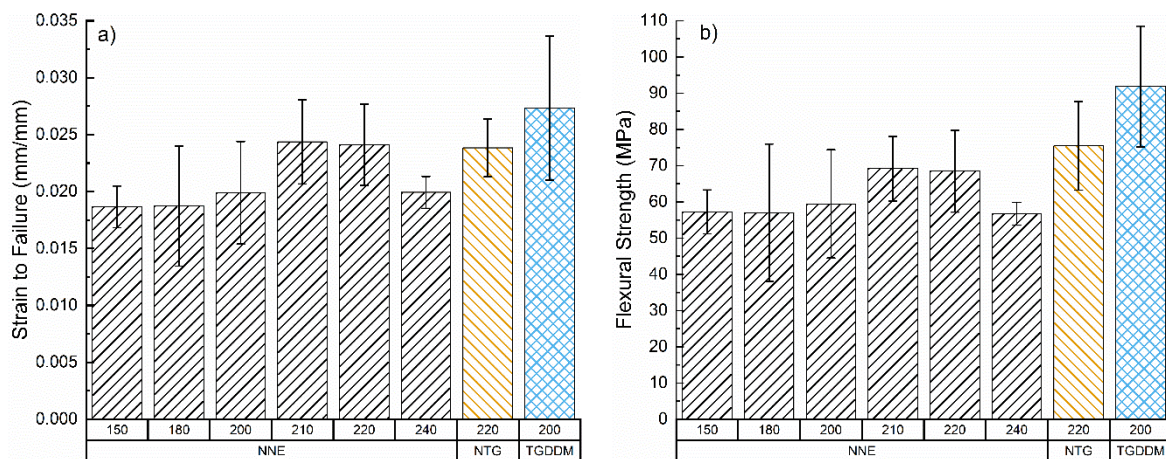
Figure 5-15 - NIR of OH peak for (a) NNE relative to extent of cure and (b) between the three resin formulations

A contrast between the higher equilibrium saturation and lower effect by plasticisation for NNE seems contradictory but can be explained by differences to the cured network properties between NNE and TGDDM. The work by Musto et al. investigated interpenetrating networks of TGDDM and a bismaleimide co-polymer (BMI), noting that with increased BMI, the moisture ingress increased and the effect on $\tan(\delta)$ decreased [35]. That behaviour was ascribed to the more rigid network formed with BMI. Here, NNE shows more rapid and a higher degree of moisture ingress but an overall lower effects to the storage modulus and T_g . The retention of thermal and mechanical properties in the glassy state could be the result of a more rigid network than TGDDM cured with DDS.

5.3.7 Mechanical Properties and Fracture Toughness of the Neat Resins

The mechanical properties of the resins were studied in flexural 3-point bending and fracture toughness was studied using single-end notch-flexural bending. Results of the mechanical properties tests are shown in Figure 5-16. With respect to degree of cure, the NNE resin shows a modest increase to flexural strength and strain to failure as well as maximal fracture toughness from 210-220°C post-cures. An effect of extended curing is to form a more dense crosslinked network hence increasing storage modulus. However, for the NNE resin, increasing cure increases the free volume fraction and reduces the ability for the network to arrange efficiently

at equilibrium. That corresponds to the decrease in elastic modulus with increased cure because of the relative high degree of cure and diminished extent of crosslinking that occurs from 150°C to 180°C and the post-cures. In contrast, post-curing of the NTG and TGDDM resins does have a significant increase to degree of cure and modulus is maximised to more efficient packing density at equilibrium. That is supported by the lower moisture ingress (related to free volume hole size and fractional free volume) for both the lower degree of cure and between the three resins. Also, the lower coefficient of thermal expansion of NTG and TGDDM suggests a lower free volume fraction and more efficiently packed network. Notably, the fracture toughness is almost unchanged between the three resins. From 220°C to 240°C, the flexural strength decreases. That can result from some factors related to thermal degradation and further chemical conversion or side reactions that change the properties of the cured network. It is noted that the flexural modulus increases and strain to failure between 220°C and 240°C which could relate to further curing and an increase to the crosslink density, thus causing embrittlement to the cured network. The elastic modulus as determined by MD simulations in compressive loading were computed for the resins, following a similar trend to the experimental flexural properties (combined tensile & compressive stress state) where TGDDM > NTG > NNE and are available in Appendix B.



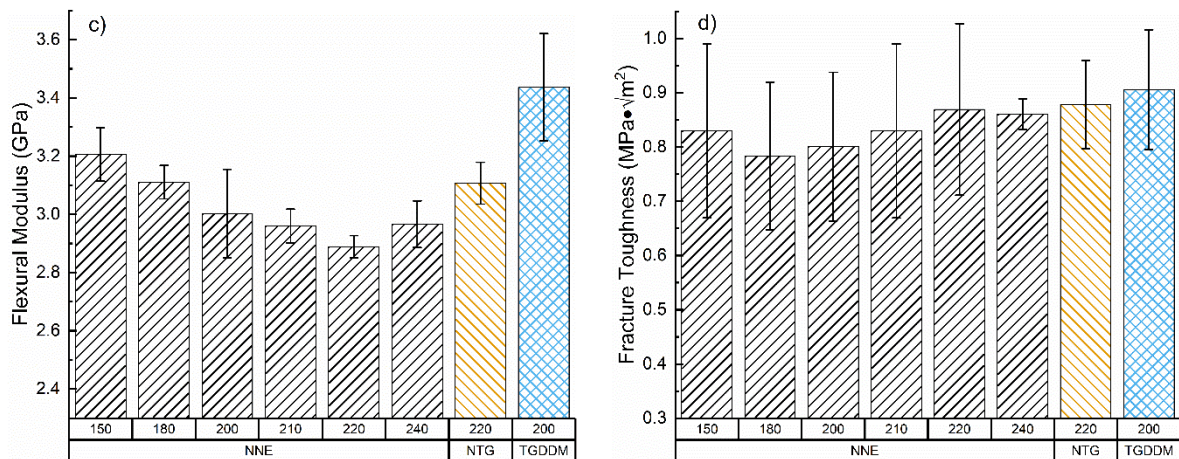


Figure 5-16 - Mechanical properties showing the flexural (a) strain at failure, b) ultimate strength, c) modulus and d) fracture toughness from SENB testing

5.4 RESULTS AND DISCUSSIONS ó THERMAL AGEING OF THE COMPOSITE

5.4.1.1 Mass Loss and Physical Changes to the Resins and Composites

The mass loss of the resin and composite were periodically measured in triplicate from the unaged and dried state up to 504 hr of exposure to an temperature 250°C. Unaged composite specimens were cut into 1 x 1 cm coupons and a resin burn-off test was performed in a muffle furnace to determine the resin content of the composite and that value was used to calculate matrix weight loss from the measured weight of the composite. Presented in Figure 5-17 is the mass loss of the matrix and the resin. Initially the three composites had similar matrix weight content (40-42 wt%) but it was apparent that initially the matrix mass loss was more rapid for TGDDM than NNE and NTG. However, by 120 hr the rate of loss for TGDDM became more gradual. By the end of the ageing trial, the matrix weight loss was highest for TGDDM and lowest for NNE by near 4%. In stark contrast was the weight loss of the neat resin coupons. Rapid weight loss was again observed for TGDDM and NTG relative to NNE but for the initial stages of measurements the NNE resin showed higher retention of resin mass loss and by 504 hr was within 1 wt% of TGDDM. The NTG resin showed very significant weight loss by 216 hr which also corresponded with a change in physical appearance. Large wrinkles on the surface of the sample were apparent by 120 hr for NTG while only appeared near the end of the ageing trials for the other two resins.

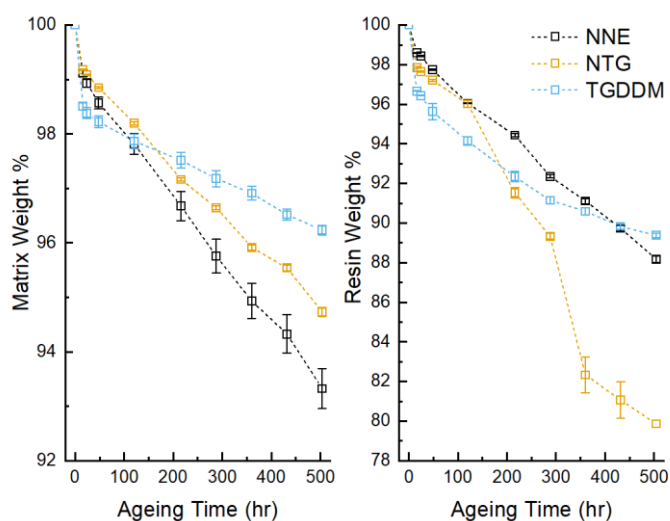


Figure 5-17 - Mass loss of the composite (left) and of the neat resins (right) under thermal ageing

The difference in behaviour of the composite and resin is likely due to the thermal-oxidative effects that can arise in the composite. That is, while the neat resin still undergoes micro-cracking and hence creates a pathway for thermal degradation, the differences in thermo-oxidative ageing via micro-cracking and pathways for the composite rely on compatibility between the matrix and reinforcement [246]. Thermally-induced stresses could create an uneven distribution of pathways for the naphthalene-based resins resulting from the higher coefficient of thermal expansion than for that of TGDDM which was determined earlier (NNE > NTG > TGDDM).

5.4.1.2 Fourier-Transform Infrared Spectroscopy of the Degraded Systems

The resins were studied by FTIR in the mid-IR and near-IR range as a way to evaluate the changes within the network as a result of long-term exposure to elevated temperatures. The primary assignments for analysis of the spectral data are provided in Table 5-7.

Table 5-7 - Peak and band assignments for mid- and near-IR analysis

Peak / Band Position (cm ⁻¹)	Assignment	Notes & Designations
821	Aromatic	
1040	C-O-C	
1215	C-O-C	
1391	δ(CH)	Fundamental Freq.
1520	Aromatic	
1583	δ(NH ₂)	Fundamental Freq.
1593	Aromatic	
1625	C=O	

1725	ν (C=O)	Fundamental Freq.
2870	CH ₃	
2925	CH ₂	
3400	-OH	Fundamental Freq.
4520	ν (CH ₃ , CH ₂ , + ν (C=O))	CH ₂ , CH ₃ , and C=O bonds
4778	ν (NH ₂ , sym.) + δ (CH)	Amine-Oxirane
4600-4900	ν + δ (NH)	Amino
5140-5240	Water Vapour	Water Vapour
5890-5990	C-H Stretching	First Overtone
6300-6800	2 ν (NH, NH ₂)	Primary/Secondary Amine
6800-7200	-OH	Hydroxyl

Thermo-oxidation involves numerous and sometimes complex changes in the polymer network. In the mid-IR regime, the formation of alcohols, the scission of bonds, and formation of oxidised char can become apparent and help describe the process by which the cured network changes as it ages. However, a limitation with mid-IR is that the depth of penetration is only on the scale of a few hundred micrometres whereas near-infrared analysis enables characterisation at a bulk level on the scale of millimetres. The difficulty with NIR is that the entire spectra only represents overtones of the fundamental frequencies within the mid-IR range and thus limits the description of chemical changes during degradation [247]. The mid-IR spectra of the NNE resin is shown in Figure 5-18(a-b). The NTG and TGDDM resins in Figure 5-19(a-b) and Figure 5-20(a-b), respectively. At the upper range of wavelength can be seen the hydroxyl band and signatures relating to CH₂ and CH₃ bonds within the cured network. From 1900-600 cm⁻¹ specific peaks show changes to C=O, C-O-C, and aromatic peaks associated with structures of the cured network. At the early stages of ageing, minor changes to the hydroxyl peak and C=O at 1725cm⁻¹ and 1215cm⁻¹ are less apparent but as ageing progresses beyond 120 hr significant changes can be seen. A significant growth to the 1725cm⁻¹ peak is seen and near the end of ageing at 432hr the hydroxyl and aromatic peaks begin to destabilise suggesting large-scale chemical changes within the cured network.

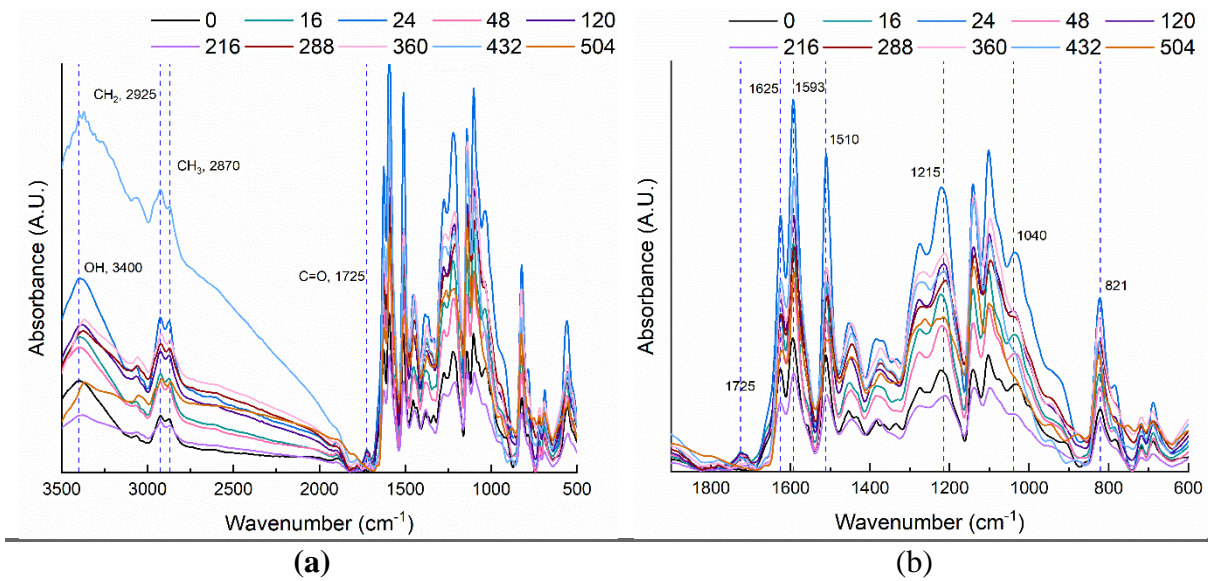


Figure 5-18 - The (a) full mid-infrared spectra and (b) narrow range spectra for the NNE resin progressively aged

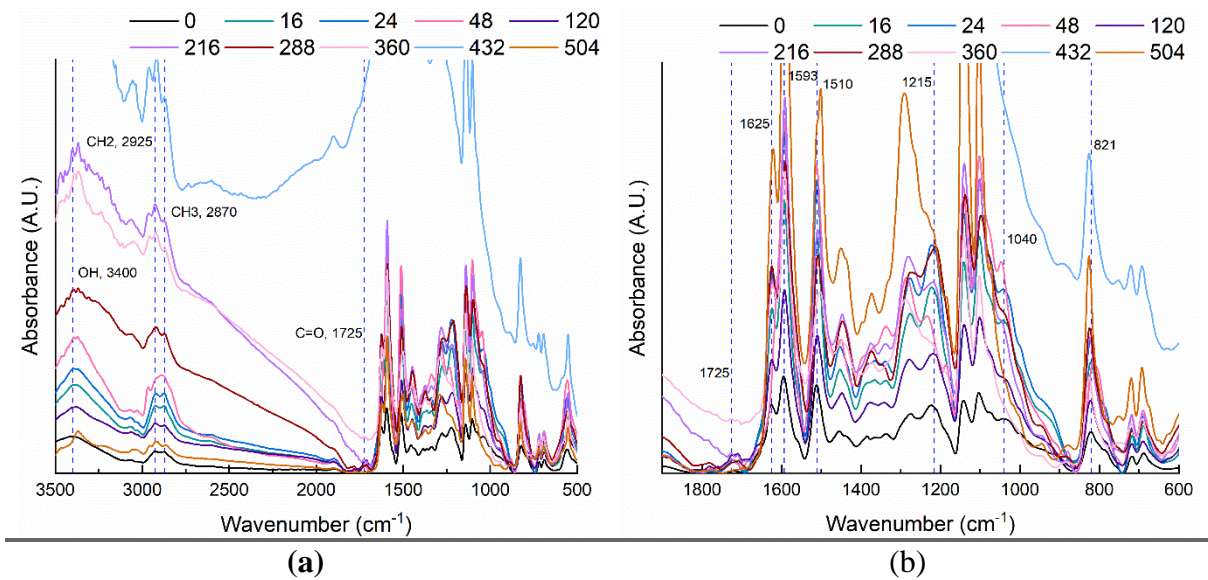


Figure 5-19 - The (a) full mid-infrared spectra and (b) narrow range spectra for the NTG resin progressively aged

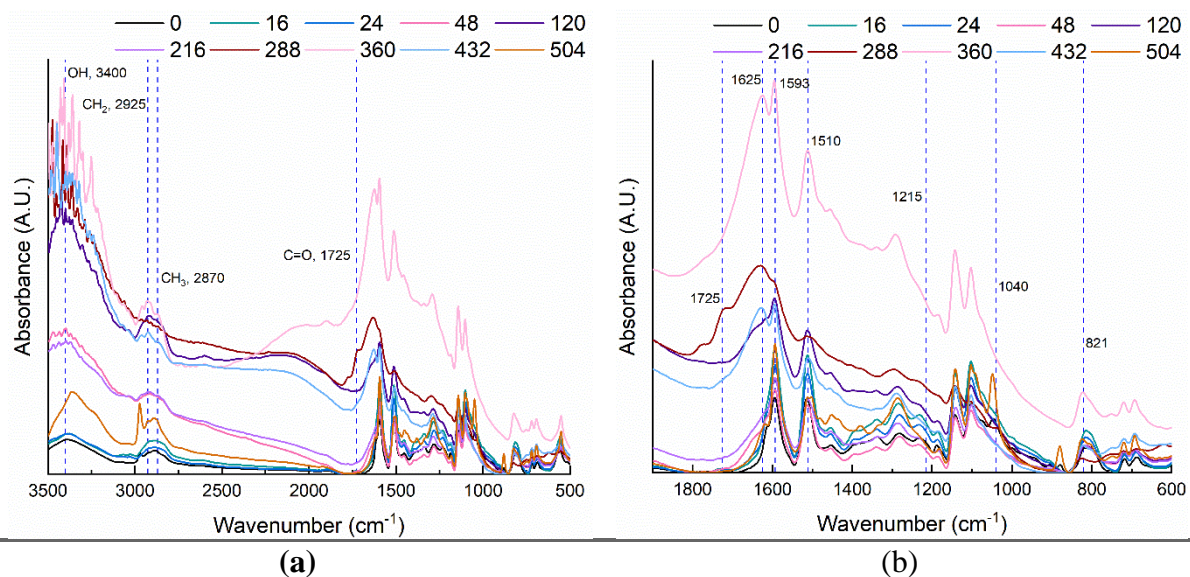
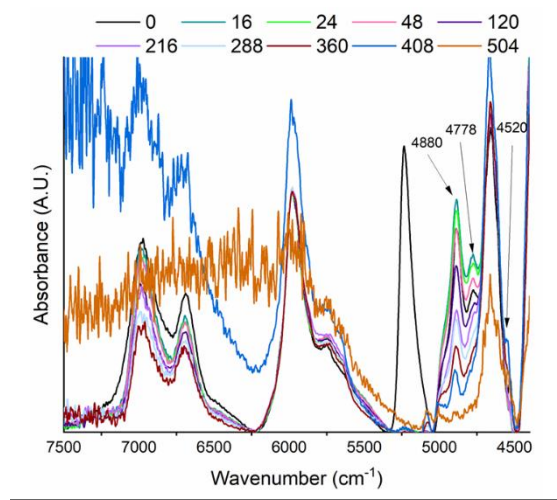


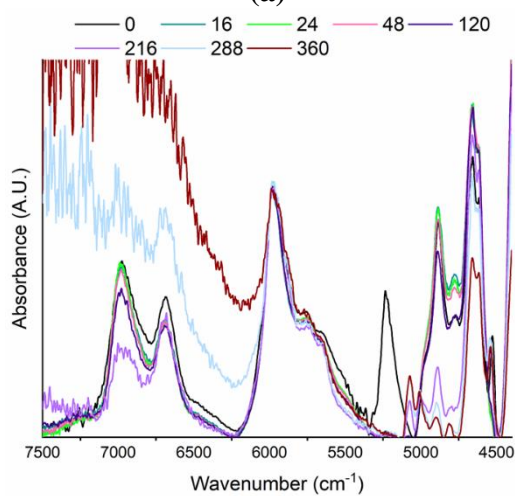
Figure 5-20 -The (a) full mid-infrared spectra and (b) narrow range spectra for the TGDDM resin progressively aged

In addition to mid-IR analysis, resins were tracked by near infrared spectroscopy. Spectral traces of the three resins are shown in Figure 5-21(a-c) from the unaged to aged conditions. While the NIR spectra are comprised of overtones for the various fundamental frequency peaks in mid-IR, some noticeable changes emerge which can correlate to structural changes in the network. Of note is the peak between $5140\text{-}5240\text{cm}^{-1}$. This peak is only present for the unaged specimens and shows some residual moisture even after drying of the specimens. The NIR results showed a rapidly diminished epoxide peak at 4520cm^{-1} within the first 16 hr of ageing, regardless of resin. This is associated with a slight increase to the secondary amine ($6300\text{-}6800\text{cm}^{-1}$) and hydroxyl ($6800\text{-}7200\text{cm}^{-1}$) bands resulting from further addition reaction of the unreacted epoxy present. In contrast to TGDDM, the hydroxyl peaks become impossible to distinguish for the latter stages of ageing for both glycidyl ether based resins (NNE and NTG). It was observed that the surfaces of all three resins show noticeable signs of physical degradation which could be more prevalent in NNE and NTG, resulting in a reduction in the transmission of light through the samples at 432hr and 504hr. It is unclear why TGDDM shows less noise in that regime and whether it relates to the differences between network chemistry or other effects from physical degradation. Notably, the peak at 4520cm^{-1} shows some additional growth at 408hr for NNE, 216hr for NTG, and 216hr for TGDDM, respectively. Normally, this peak is associated primarily with the epoxide functional group prior to reaction with the active hydrogen of the amino hardener. However, it also can show as an overtone for the C=O double bond. Therefore, its appearance can be attributed to network degradation.

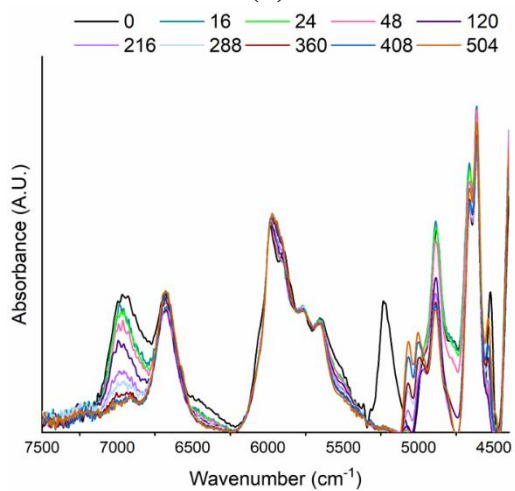
While all three resins exhibit some growth to this peak, it is noted that the emergence is delayed for NNE to 306hr ageing time. The assignment at 4778cm^{-1} is related to the bond between the oxirane ring and primary amine. This bond progressively disappears for the three resins which is suggestive of bond cleavage. That is in corollary with the reduction to the peak at 4880cm^{-1} , associated with amino-functional species.



(a)



(b)



(c)

Figure 5-21 - Near infrared spectra of (a) NNE, (b) NTG, and (c) the TGDDM resins progressively aged

5.4.1.3 Thermal Analysis of the Degraded Resins

A combination of dynamic thermal mechanical analysis and thermomechanical analysis was utilised to understand the change in chemistry as it affected the glass transition as well as the degradation at the interface of fibre and matrix. Shown in Figure 5-22 is the effect of ageing on the NNE composite at zero, 24, 216, and 504hr of thermal ageing. An increase to the storage modulus occurred between zero to 24 hours which largely held to 216hr before finally decreasing by 504hr. The peak of $\tan(\delta)$ decreased with increased ageing as well as the initial onset of degradation. Figure 5-23 displays the change in T_g based on the storage modulus onset and the peak of $\tan(\delta)$ between the three resins. It is notable that the NNE and NTG resins showed a significantly higher storage modulus onset ($\sim 250^\circ\text{C}$ and $\sim 225^\circ\text{C}$, respectively) at 504hr. In contrast, the TGDDM composites showed rapid decrease in the onset to just 225°C by 24hr and dropped below 200°C by 504hr.

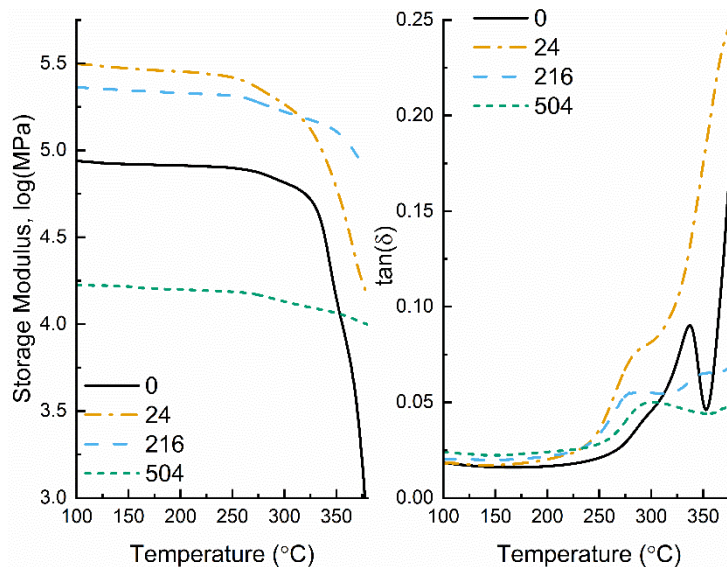


Figure 5-22 - DMTA traces of storage modulus (left) and $\tan(\delta)$ spectra (right) for the aged NNE composite

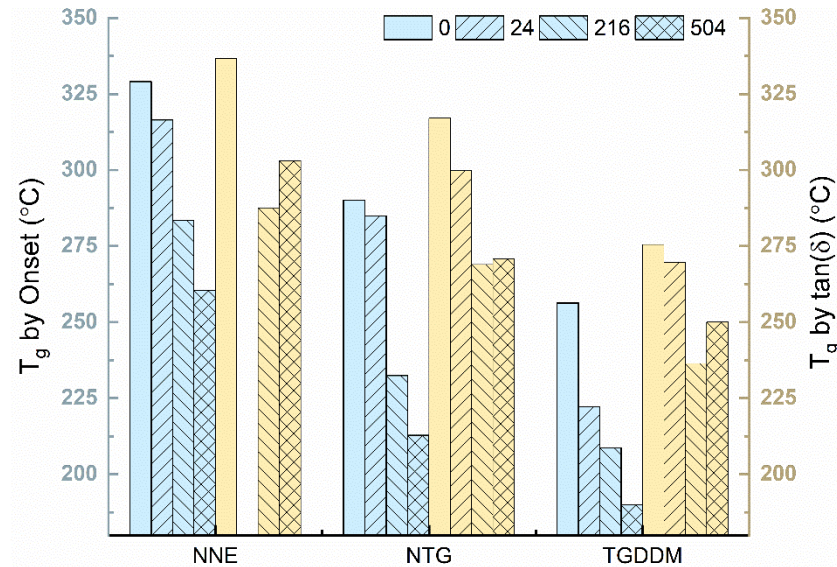


Figure 5-23 - Change in glass transition of the three composites with respect to ageing duration

5.4.1.4 Mechanical Properties of the Aged Specimens

The flexural and interlaminar shear (ILSS) properties of the composites were studied with respect to thermal ageing time. Shown in Figure 5-24 are the effects of ageing on mechanical properties. For the initial stages of ageing ($t > 100$ hr), the NNE resin shows superior retention of strength and modulus compared to TGDDM and NTG. Virtually no change to ILSS performance is seen for NNE which is in line with the 10hr TGA ageing and minimal initial mass loss. As $t < 200$ hr the three resins show significant mass loss and that is reflected in deterioration of mechanical performance by nearly 50% of the unaged specimens. However, NNE shows superior flexural strength up till 504hr when the resins show significant decrease to all mechanical properties.

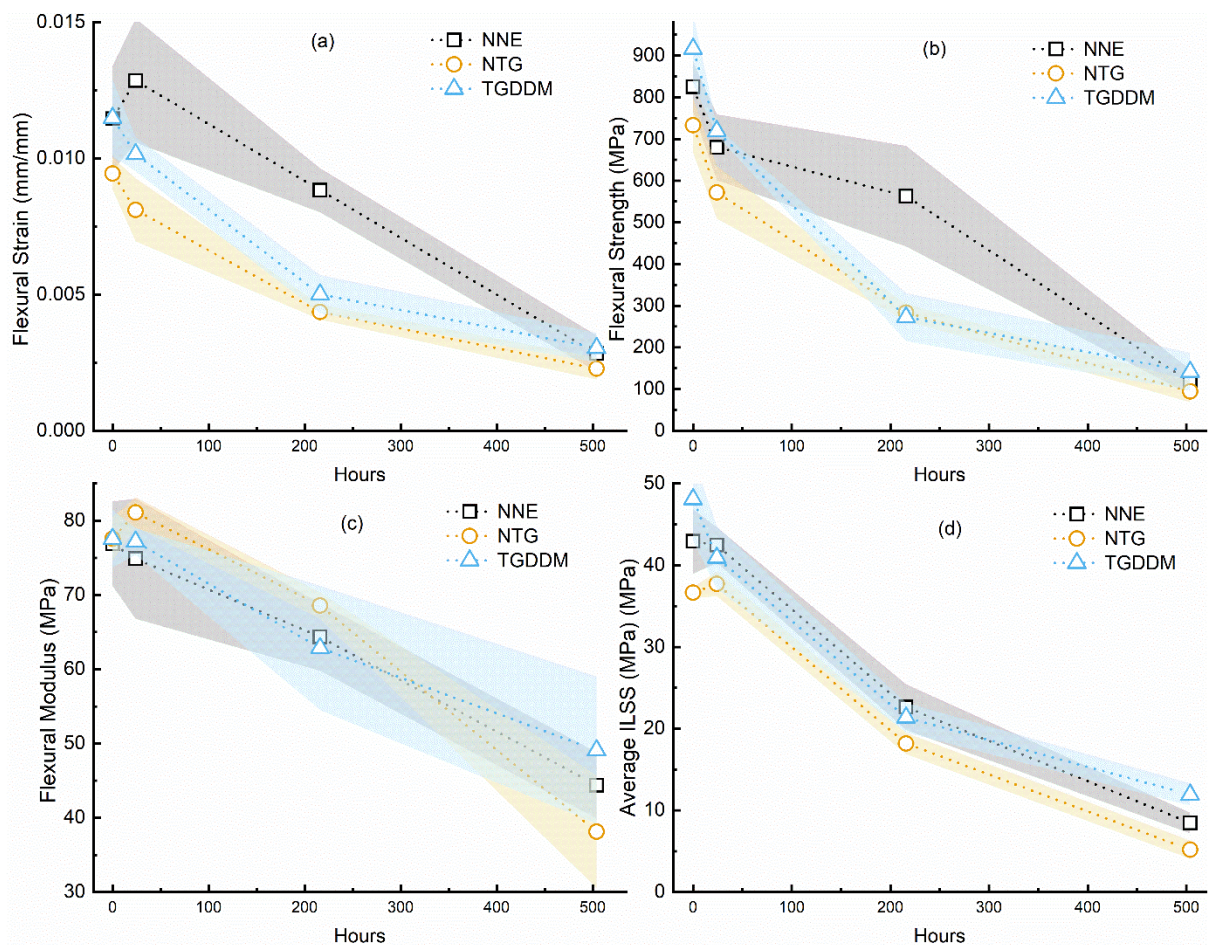


Figure 5-24 - Mechanical properties of the aged composites with respect to duration of exposure

5.5 SUMMARY OF WORK

This work presents a comprehensive study of the structure-property relationships of the DDS cured bis(2,7-glycidyl ether naphthalenediol) methane (NNE) epoxy resin. The effects of the rigid dimeric naphthalene structure and the differences between networks of glycidyl ether and glycidyl amine epoxy networks are studied. While the NNE resin shows high thermal stability and glass transition temperatures, it is inhibited by lower degree of cure, higher thermal expansion coefficient, moisture uptake at equilibrium is higher, and lower strength and modulus in flexure. These properties are related to the higher free volume fraction and plasticising effects at lower degree of epoxide conversion which is evidenced by the greater short range molecular mobility and poor equilibrium packing. The increased T_g and T_g corresponds to a higher crosslink density at increased cure temperature and subsequently reduced thermal expansion and increased fracture toughness. The lower modulus arises from higher free volume with extended cure which accounts for the higher moisture ingress. The naphthalene units contribute to a higher char yield and the rigid network also offsets the

degradation to higher temperatures. Thermal ageing of the composite showed benefits in the earlier stages of degradation with minimal loss of mechanical properties and retention of the T_g . This resin shows promise for structural composite applications where short, high-temperature exposure may occur and is one of an emerging class of glycidyl ether epoxy monomers with good thermal and mechanical properties.

6 MOLECULAR ADDITIVES AS MODIFIERS OF THE TETRAFUNCTIONAL EPOXY-AMINE RESIN SYSTEM

6.1 INTRODUCTION

There is a growing body of research taking alternative approaches to the more traditional routes of modifying epoxy resins (e.g. micro- and nanoscale addition of rubbers, thermoplastics and inorganic particulate) to enhance specific mechanical properties of highly crosslinked networks. The first, is to alter the inherent chemical structure using mono-functional reactive diluents, the second is to control the topology of the network using bulky constituents pendant to the network, while the third is to use structurally similar additives that are not covalently attached to the network but reside within the free volume. In this chapter, these strategies are used to modify the highly crosslinked tetrafunctional NNE epoxy-amine system and explore the effects upon the chemical, thermal, mechanical, and physical properties of the modified resin. Finally, translation of the mechanical and thermal properties from the modified resin to the composite are presented.

6.1.1 Reactive Diluents

Low molecular weight reactive diluents incorporated into an epoxy network to induce a lower viscosity resin, improve processability but can also enhance toughness. These functional additives often include aliphatic mono- and di-functional epoxy resins to increase molecular mobility, flexibility and toughness. [248]. This approach applies both to epoxy and amine functional groups with flexible chain segments and has been shown to significantly enhance toughness of the resulting network [249]–[251]. Halary studied a series of controlled networks comprising aliphatic and aromatic epoxies and amines, and showed that cross-link density, impacted strength, stiffness, and moisture uptake more systematically than altering the flexibility of segmental chains [252]. However, that contrasts with more recent conclusions by Espuche et al. which found that incorporating flexible aliphatic compounds had a greater role in determining strength and stiffness [253]. Ijima et al. added elastomeric acrylic monomers containing a mono-epoxide pendant to the network and demonstrated that the combination of a flexible backbone and compatibility through the pendant epoxide with the DGEBA matrix could enhance toughness whilst imparting only a modest deterioration of other mechanical properties [254]. In contrast, Marks et al created a series of mono-epoxide terminated resins by adding stoichiometrically-balanced amounts of phenylglycidylether (PGE) to a catalysed DGEBA network [9]. They showed that increasing PGE content actually led to a decrease in

storage modulus, glass transition temperature, and fracture toughness after an initial plateau. The lack of contribution of these pendant groups on the elasticity of the network was attributed to the observed decrease in mechanical and thermal properties.

Aside from toughness, mono-functional reactive diluents are associated with an increase in modulus and strength but also a corresponding decrease in failure strain and fracture toughness due to anti-plasticisation effects [255]. Reyes et al. demonstrated that monofunctional epoxide addition significantly increased modulus while decreasing strain to failure due to an anti-plasticisation effect caused by large siloxane cages hanging pendant to the network. They drew correlations to the reduced molecular mobility increasing modulus, despite no relation to yield strength [256]. Due to the large-scale intermolecular nature of yielding, it is also likely that any relation between mono-functional addition and strength is more related to inter-molecular motions beyond the length-scale that contributes to the increase in glassy modulus. Work by Li et al. investigated the addition of a mono-functional epoxy-functionalised anthracene monomer as a pendant group in an aliphatic epoxy resin and found the combination of the highly-aromatic polycyclic molecule increased T_g which they also attributed to a lower chain mobility [257]. Interestingly, they were also able to demonstrate shape-memory capability by reversing the anthracene dimer by heating and vitrifying under UV light.

6.1.2 Partially-reacted substructures

Recently, molecular modelling and experimental research into the yield of epoxy-amine resins have pointed to the influence of nano-scale void formation on increasing both strength and strain to failure. Sharifi et al. cured an epoxy amine resin in the presence of dichloromethane to create nano-scale voids within the material by the expansion of the solvent via thermal annealing [258]. While chemically the same, their work showed that the growth of ordered, nano-scale proto-voids could create a topology that exhibited strain hardening under tension with no change to the T_g and minimal effect on crosslink density. In contrast, molecular dynamics simulations by Mukherji & Abrams surmised that ductility in the crosslinked polymer arose from a combination of void formation under strain and lower crosslink density of the polymer network [259], [260]. That suggests a competition between the chemistry of the modified systems and the so-called proto-void formation as it concerns the mechanism of plastic yielding and toughening. The concept here is that the introduction of localised concentrations of non-covalently bound molecular surfaces will induce favourable void growth under strain.

Naturally, the presence of solvents within the unreacted polymer is not ideal and a solvent-free approach to achieve a similar proto-void development in the network is desirable. That is largely due to the volatility of solvents under heat and pressure which can lead to physical defects such as voids and porosity. Sharif & Palmese utilised a partially reacted substructures (PRS) approach, whereby a monoamine and TGDDM were pre-reacted at 60%, and 80% conversion prior to addition to the uncured primarily epoxy resin network [261]. A higher elongation to break, attributed to the formation of micro-voids caused by these partially reacted substructures was observed, despite a significant reduction in T_g . Gao et al. demonstrated that the degree of polymerisation directly affected the ability of this strain-hardening behaviour, by comparing unreacted and 75% converted PRS structures to a difunctional and tetrafunctional epoxy-amine system [262]. They also studied the effect of loading on the network and showed that improvement to ductility was apparent from 5 wt% up to 20 wt%. More recently, Eaton et al. utilised a cycloaliphatic diamine and a low molecular weight monoamine, to exhibit nano-scale domains that greatly enhanced the toughness of epoxies [263].

6.1.3 Molecular Additives as Antiplasticisers

Alternative techniques to modify the resin network architecture also includes the inclusion of non-reactive or non-covalently bound species to the network. Daly et al. studied an antiplasticiser formed from the reaction of PGE end-capped with 2-(acetylamino)phenol and showed that the inclusion within the network architecture enhanced modulus and strength by suppression of the β -transition. Further work by Heux et al. studied the origin of the suppressed β -transition and associated enhancement of modulus, noting that lower crosslink density corresponded to weaker effects and that the segmental motions across multiple units appeared to be hindered. This was in contrast to the ring-flip of the monomer backbones [123]. Sauvant & Halary studied three antiplasticisers that varied by molecular weight and flexibility all of which successfully enhanced modulus whilst also suppressing the β -transition and showed a beneficial decrease to equilibrium moisture uptake [126]. They also noted nano-phase separation for two of the additives which showed higher antiplasticisation although a large reduction in the glass transition temperature was observed.

6.1.4 Overview of the Study

In this study, the effect of molecular level modification is studied on the tetrafunctional dimeric naphthalene epoxy-amine resin at different levels. The first is to directly incorporate the mono-functional epoxy resin, o-cresyl glycidyl ether (CGE), into the epoxy resin to create pendant

groups reducing the crosslink density of the overall network. Following this, CGE is reacted with 3,3'-diaminodiphenylsulfone (33DDS) and 4,4'-diaminodiphenylsulfone (44DDS) to create low-molecular weight yet highly aromatic mono-amines denoted individually as 33CGE and 44CGE, respectively. These oligomers are similar to the partially reacted substructures (PRS) mentioned above, and were then introduced into the epoxy network, again as pendant groups after cure. In this scenario, these partially reacted substructures are larger and bulkier than the more simple addition of monofunctional epoxide CGE. Non-covalent molecular level modification uses naphthalene and a naphthalene based oligomer endcapped with CGE via pre-reaction (denoted as MFN, "molecular fortifier using 2,7'-dihydroxynaphthalene and CGE), to determine the influence of non-reactive molecular surfaces on the network properties. The concept here is that these modifiers reside within the free volume of the network suppressing molecular mobility and enhancing molecular level reinforcement. The naphthalene would be unreactive, while the endcapped naphthalene (MNF) is expected to be much less reactive and primarily attached to the network via non-covalent hydrogen bonding. Finally, for selected resins, the corresponding composites have been prepared to explore the translation of resin properties to the composite. A diagram representation of the toughening approaches is shown in Figure 6-1 below.

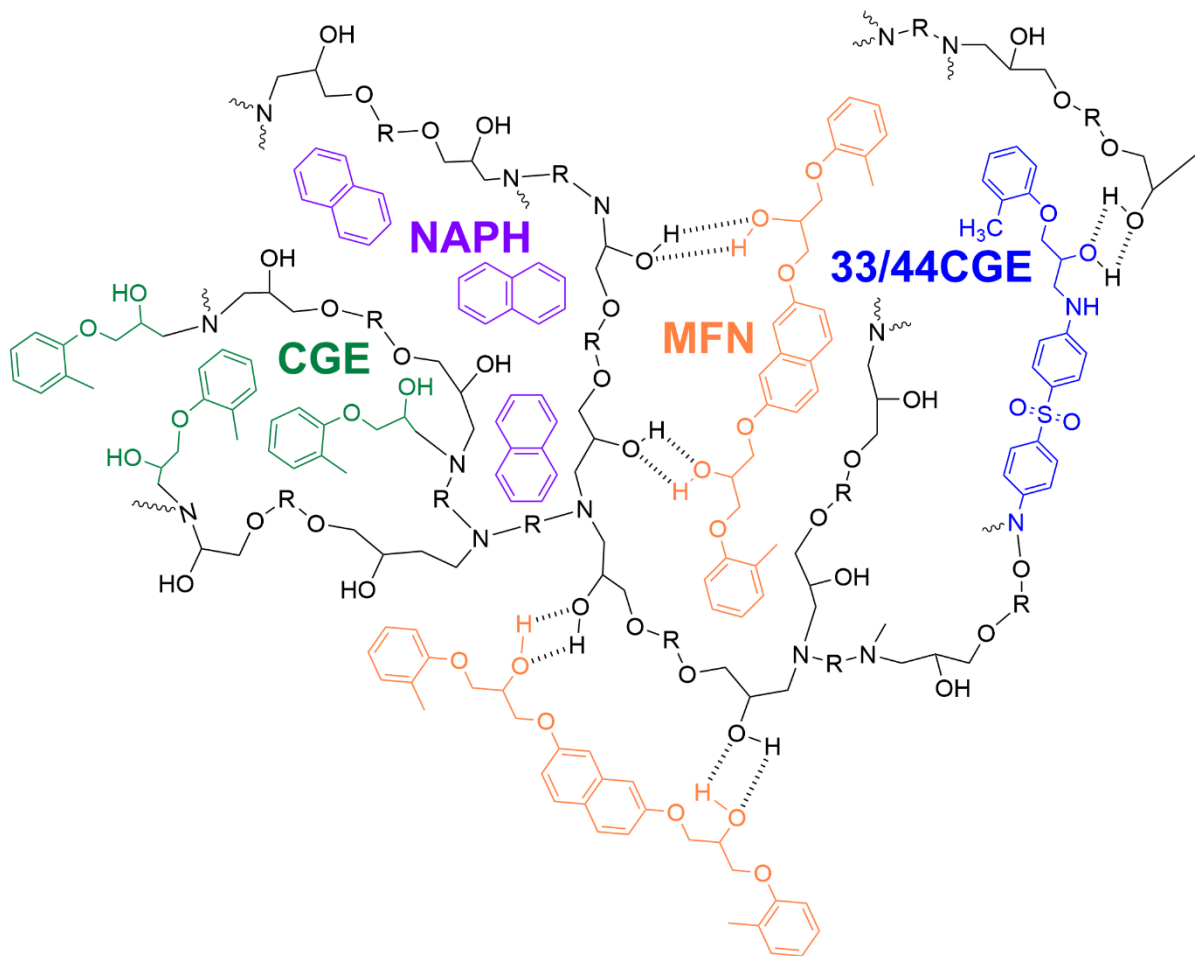


Figure 6-1 – Diagram representation depicting the reactive (CGE), reactive and hydrogen-bonded (33CGE and 44CGE), hydrogen-bonded (MFN), and non-reactive (NAPH) modification approaches within the cured epoxy network

6.2 MATERIALS AND EXPERIMENTAL DETAILS

6.2.1 Materials

The materials used in this chapter are outlined in Table 6-1. The reaction of the 27DHN and CGE was aided by 1 wt% addition of triethylamine (MW=101.19g/mol, TEA, SigmaAldrich Corp., USA). Solvents of dichloromethane (DCM), ethanol, and methyl ethyl ketone (MEK) were of analytical grade purity and used without further purification.

Table 6-1 - Summary of materials used in this chapter

Material	Acronym	Chemical Name	EEW (g/mol)	Mfg. Supplier
Epoxy Monomer	NNE	1,1- bis(2,7 glycidyl ether naphthalenediol) methane	170	DIC Corp. (JPN)
Epoxy Monomer	CGE	o-cresyl glycidyl ether	164.2	Hexion Corp. (USA)
Amine Hardener	33DDS	3,3'-diaminodiphenylsulfone	248.30	Glentham Life Sciences (UK)
Amine Hardener	44DDS	4,4'-diaminodiphenylsulfone	238.30	TCI Chemical Inc. (JPN)
Alcohol	27DHN	2,7-dihydroxynaphthalene	160.17	Acros Organics (USA)
Additive	NAPH	Naphthalene	128.17	SigmaAldrich (USA)

6.2.2 Preparation of Partially Reacted Substructures (PRS); (33CGE, 44 CGE)

The partially reacted substructures were created by adding a 0.5:1 epoxide to amino stoichiometric amount of CGE to either 33DDS or 44DDS into a round bottom flask. Then, the flask was transferred to a roto-evaporator and heated to 120°C. The mixture was stirred until the DDS isomer was dissolved into CGE and a transparent liquid emerged, occurring in approximately 30 minutes. Then, the flask was transferred to a convection oven where the mixture was allowed to cure for 36 hr at an isothermal temperature of 150°C. The resulting adducts were termed either 33CGE or 44CGE and were cast onto a Teflon sheet and frozen. Both adducts were semi-solid at room temperature and free-flowing liquids at elevated temperatures.

Critically, the stoichiometry of these PRS into epoxy resin was maintained so that a direct comparison could be made from the PRS and the NNE/CGE/44DDS epoxy blend cured without any pre-reaction. The adducts were added based on a 1:1 stoichiometry utilised for the neat resin. The reaction sequence to prepare 44CGE is shown in Figure 6-2. From this point onwards the discussion of the PRS shall denote either the 33CGE or 44CGE variants independently. Near-infrared spectroscopy traces of the adducts are provided in Appendix C and display the conversion of epoxide after pre-reaction.

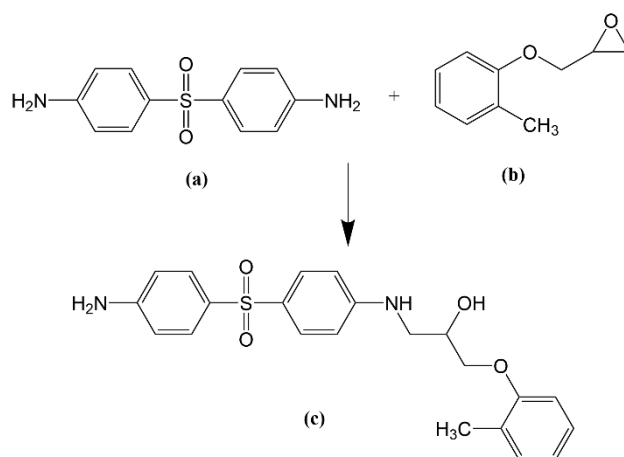


Figure 6-2 - Structures of (a) 4,4'-diaminodiphenylsulfone reacted with (b) 0.5 molar ratio of o-cresyl glycidyl ether to form (c) the partially reacted substructure where a free primary amine group remains to further react with the bulk epoxy network

6.2.3 Preparation of End-capped Naphthalene Additive (MFN)

The end-capped naphthalene additive was formed by adding 2:1 molar epoxy to hydroxyl amounts of the CGE and 27DHN. The mixture was placed in a two-neck round bottom flask to which 100mL of ethanol and 1 wt% of TEA was added and heated under mechanical mixing at 80°C for 24hr. Then, the concentrate was transferred to a round bottom flask and mixed at 120°C for 1 hour until the ethanol was removed. The resulting adduct is a transparent dark green liquid under normal processing temperatures for NNE (<90°C) and solid at room temperature. This was further heated at 150°C for 36hr in a convection oven. The structure of the resulting molecular fortifier, MFN, is shown in Figure 6-3. From this point onwards this system is referred to as MFN. FT-IR traces of the MFN are provided in Appendix C and display the decrease in epoxide after reaction in the presence of the tertiary amine highlighting the end-capping reaction.

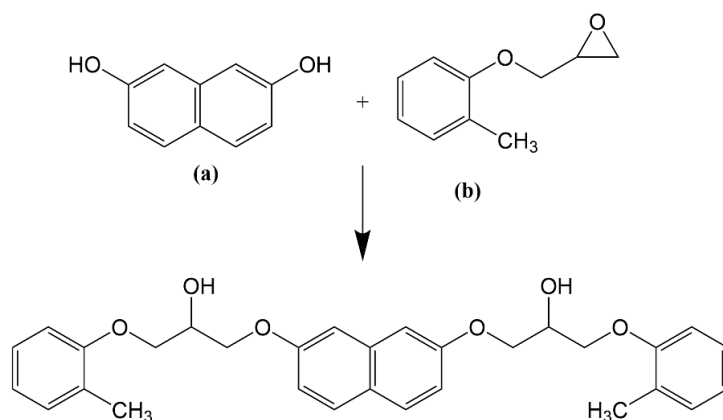


Figure 6-3 - Constituents of (a) 2,7-dihydroxynaphthalene and (b) o-cresyl glycidyl ether reacted in the presence of a tertiary amine to (c) induce ring-opening polymerisation of the

oxirane ring and hydrogen bonding with the hydroxyl of 27DHN and form the molecular fortifier

6.2.4 Preparation of Resins and Composites

The modified resins were prepared following the general procedure of the unmodified NNE/44DDS resin established in the general experimental section. Where the preparation differed however, was in how the modifiers were added during preparation. The CGE, 33CGE, 44CGE, MFN and NAPH modifiers were added, blended or dissolved into the NNE prior addition of the DDS. At all times, the formulations were prepared such that the overall stoichiometry of epoxide to amino was 1:0.95. The CGE, 33CGE and 44CGE modifiers resins contained 5, 10, 15, and 20 mol% of the modifier, while the NAPH and MFN fortifiers were added at 5, 10, 15, and 20 wt% to the NNE/DDS resin. The neat resins and carbon fibre composites were prepared in accordance with the methods outlined in the experimental section. The cure schedule for all resins and composites consisted of 150°C for four hours, 180°C for four hours, and a 220°C post-cure for two hours. The CGE, 33CGE, and 44CGE composite matrix systems were modified at 10 mol% of additive while the NAPH and MFN additives were kept at 10 wt% in the matrix.

6.3 RESULTS AND DISCUSSIONS

6.3.1 Differential Scanning Calorimetry

Dynamic differential scanning calorimetry at 2.5, 5, 10 15, and 20°C/min heating rates were performed on the uncured resins. Results comparing the 10 mol% CGE, 33CGE, and 44CGE and 10wt% NAPH and MFN modifiers under dynamic conditions at 10 °C/min heating rates are shown in Figure 6-4 with peak exothermic temperatures, enthalpy, and activation energies provided in Table 6-2. From the traces of heating, the enthalpy of cure for the CGE, NAPH, and MFN resins increases as does the breadth of the exothermic peak. For the partially reacted substructures, 33CGE and 44CGE, a sharp decrease to the exothermic peak is notable. Due to the relatively high conversion of the adducts (~45-55 %), the decrease in exothermic behaviour can be attributed to the reduced concentration unreacted epoxide available to undergo reaction with primary and secondary amine.

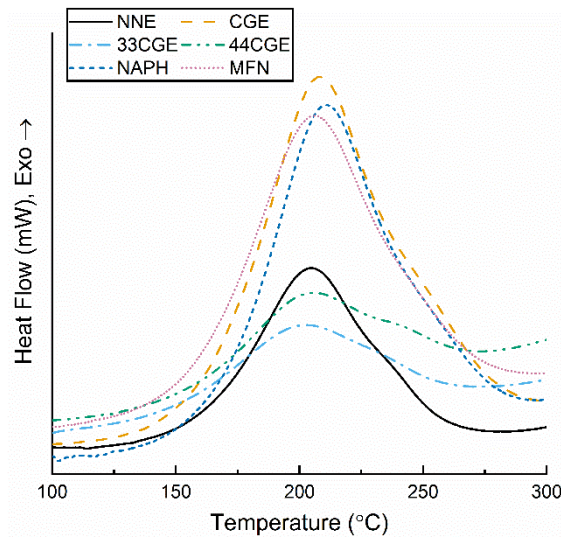


Figure 6-4 - Dynamic DSC thermograms of the resins at 10 % modifier addition

For the unmodified NNE resin the average enthalpy from 2.5-20°C/min heating rates is 311.5J/g and increases to between 321.7 - 371.5 (3.2 - 19.3 %) with increasing addition of the mono-functional CGE epoxy. The 33CGE addition decreased between 216.5 – 249.5 J/g (19.9 - 30.5 % decrease) and 44CGE a similar decrease in the range of 2147-262.1 (15.8-31.0 % decrease). The NAPH and MFN systems deviated slightly from the unmodified NNE resin. Activation energies changed less than 7% regardless of modifier suggesting limited effect to the reaction mechanisms during cure. Peak exothermic temperatures showed a slight increase with increased addition of CGE, NAPH, and less so for MFN. That indicates some decrease to the rate of cure for the resins and the difference increased from 10-20 % loading. In contrast, the 33CGE and 44CGE modified resins showed a slight decrease to the peak exothermic temperature irrespective of loading, which suggests more rapid cure.

Table 6-2 - Values of peak exothermic temperature, average enthalpy, and activation energies for dynamic DSC

Mol % / wt %	T _p (@ 2.5 ó 20°C/min (°C)	C x g t c i g (J/g)	E _a (kJ/mol)
NNE			
0	224.4	311.45	65.84
CGE			
5	225.2	321.4	65.82
10	227.9	347.2	67.54
15	230.3	371.5	67.73
20	231.5	370.0	67.51
33CGE			
5	221.6	227.1	66.81
10	221.8	216.5	65.90
15	221.8	232.6	65.30
20	222.7	249.5	65.30
44CGE			
5	224.1	220.2	65.59
10	224.6	214.7	70.96
15	224.5	225.4	65.07
20	223.4	262.1	66.93
NAPH			
5	227.4	315.3	68.44
10	229.9	317.0	66.68
15	232.2	258.7	66.06
20	235.7	296.7	66.90
MFN			
5	223.3	320.3	66.55
10	225.5	296.9	66.54
15	225.4	261.3	67.42
20	226.5	318.9	65.36

*E_a calculated from heating rates at 2.5, 5, 10, 15, and 20°C/min

6.3.2 Near Infra-red Spectroscopy

Near-infrared spectroscopy of the cured resin bars was performed to evaluate the effect of additive addition on the conversion of functional groups. Spectra of the unmodified resin and the modified resins at 10% loading are shown in Figure 6-5. The first difference between the unmodified NNE resin and the modified ones is the intensity of the epoxide peak. While direct comparison is made difficult due to the inclusion of additives, there is a large reduction to the epoxide peak at 4521cm⁻¹ for CGE, 33CGE and MFN and slightly less so for 44CGE and NAPH. That may suggest the inclusion of these additives may contribute to higher epoxide conversion during cure and after post-cure. Less apparent are differences to the secondary amine and hydroxyl peaks (~6600-6800cm⁻¹ and ~6800-7200cm⁻¹, respectively). Another clear

difference emerges in the peak at $5220\text{-}5240\text{cm}^{-1}$. This peak relates to the stretching and bending overtone of hydroxyl [264]. Both CGE and MFN show a growth to the peak and NAPH shows a complete absence. There is no discernible change between NNE, 33CGE, and 44CGE at this peak. This peak is normally associated with hydrogen-bonded molecules of H_2O [265]–[267] although previously published spectra of as-cured resins show discrepancies in the vicinity of this peak for the same epoxy cured with different amino hardeners but are not commented on [268]. This provides some evidence for the proposition that the MFN, in particular, is associated with a greater degree of hydrogen bonding.

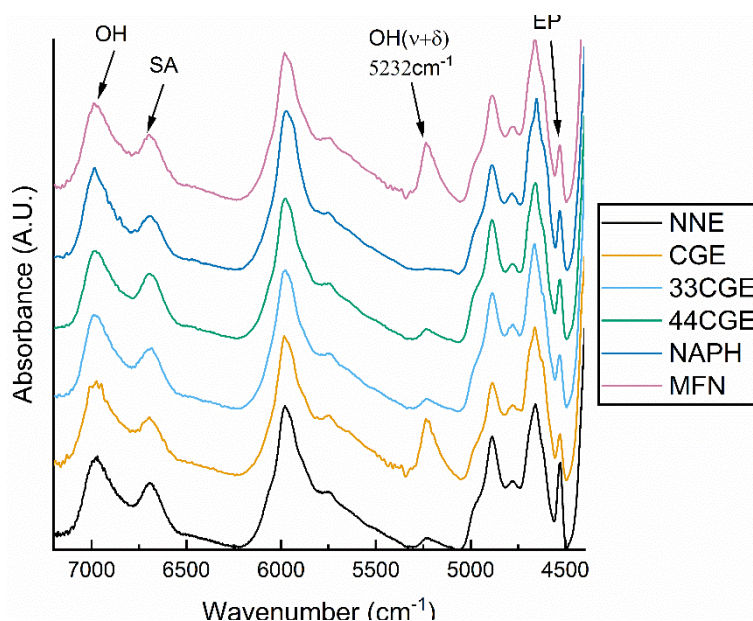


Figure 6-5 - Near infrared spectra of the unmodified and modified resins at 10% loading

6.3.3 Rheological performance of modified resins

The modified resins were studied by dynamic oscillating rheology from $25\text{-}200^\circ\text{C}$ at a heating rate of $2^\circ\text{C}/\text{min}$. Effects of the CGE, NAPH, and MFN additives are shown in Figure 6-6 for a 10% concentration and further data of the modified resins in Table 6-3. Adding 10% showed a diluting quality for CGE and NAPH where minimum viscosity is lowered and gelation temperature increased to a higher temperature. However, the higher molecular weight of the MFN showed no diluting effect and in some cases greatly increased the complex viscosity but with no apparent effect on the gelation temperature. In contrast the CGE and NAPH offset the gelation temperature to higher values with increasing concentration. The partially reacted adducts, 33CGE and 44CGE, were difficult to process due to higher melting temperatures than NNE and only the smallest amount of 5 mol% could be characterised. No diluting effect was noted and a major increase in the complex viscosity was apparent. The CGE and NAPH showed

a slower reaction, signified by the higher T_{gel} , yet also improve processability by lowering the viscosity and expanding the range between T_{melt} and T_{gel} .

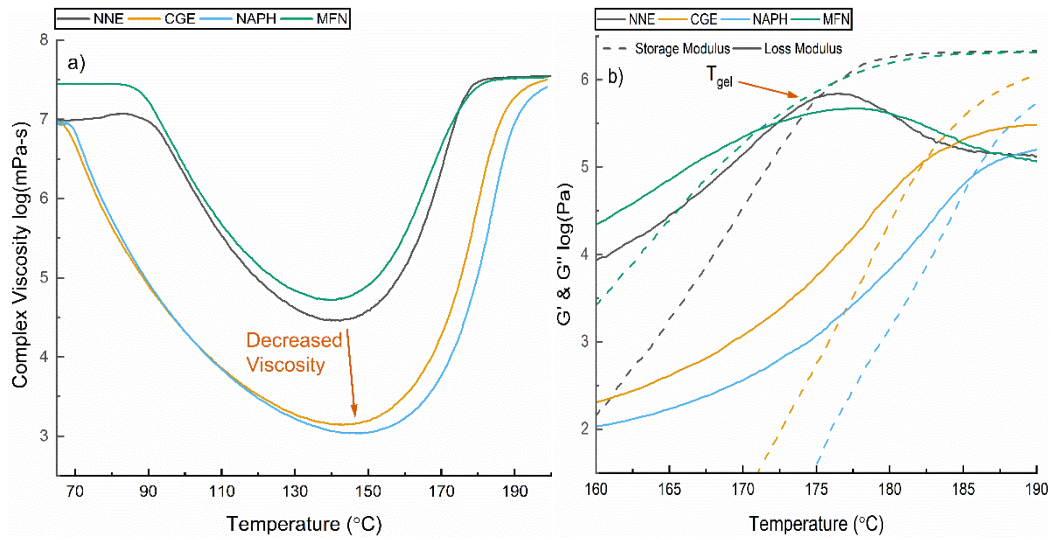


Figure 6-6 - Dynamic rheological trace of the NNE resin and modified NCGE, NAPH, and MFN resins at 10% concentration showing (a) the change to complex viscosity, and (b) the gelation point crossover of G' and G''

Table 6-3 - Dynamic rheological behaviour of the modified resins

% Additive	T_{gel} (°C)	Minimum Viscosity (Pa-s)
NNE	175.25	28.6
CGE (mol %)		
5	176.19	12.87
10	182.1	1.39
15	183.4	0.73
20	184.65	0.51
33CGE (mol %)		
5	177.47	30.95
10	167.82	N/A
15	174.20	N/A
44CGE (mol %)		
5	177.67	67.60
10	176.54	75.16
15	179.23	N/A
NAPH (wt%)		
5	182.52	3.28
10	185.79	1.09
15	188.6	1.04
20	191.03	0.375
MFN (wt%)		
5	173.74	25.46
10	171.20	52.18
15	175.74	13.71
20	171.21	24.40

6.3.4 Dynamic Thermomechanical Analysis

The thermal properties of the modified resins were studied by DMTA both in dynamic heating and sub-ambient means. The results of dynamic heating DMTA for the 10 % modifier addition are shown in Figure 6-7 and a comparison of the change in peak $\tan(\delta)$ for T_g and T_{gw} are presented in Figure 6-8. As with the unmodified NNE resin, a secondary peak around 297°C is apparent which was previously attributed to the evidence of unreacted functional groups. Notably, for all the resins, this sub- T_{gw} peak shifts towards a lower temperature and the intensity increases. Also of interest is the apparent peak that consistently shows around 80-100°C for the naphthalene-doped formulations. Similar behaviour is reported for thermoplastic-modified resins. Hameed et al noted that the addition of 10 phr of a poly(styrene-

co-acrylonitrile) thermoplastic to a DGEBA-DDS formulation causes a secondary relation in the sub- T_{gW} regime which they attributed to the higher mobility of the thermoplastic phase present [269]. It is noted that the melting point of 80.2°C [270] for pure naphthalene aligns perfectly with the relaxation seen in the $\tan(\delta)$ traces.

The effect of modifier loading on the change in thermal mechanical properties showed minimal effect at 5-10 % addition. The CGE, NAPH, and MFN modified systems showed minimal effect to T_g and the 33CGE and 44CGE systems exhibited sharp decreases to below 250°C by 20 mol% modifier addition. In terms of the T_{gW} peak, there was a consistent decrease from upwards of 340°C to 320°C regardless of system which is suggestive of a decreased crosslink density of the bulk system as a result of modifier addition.

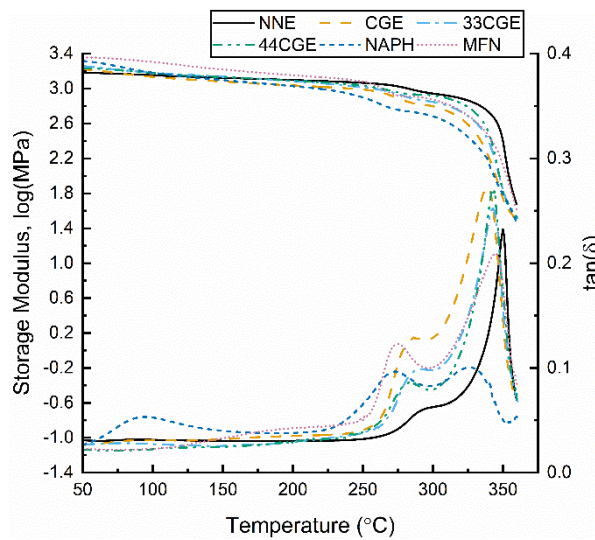


Figure 6-7 - DMA ramp traces of storage modulus and $\tan(\delta)$ for the modified resins at 10% modifier addition

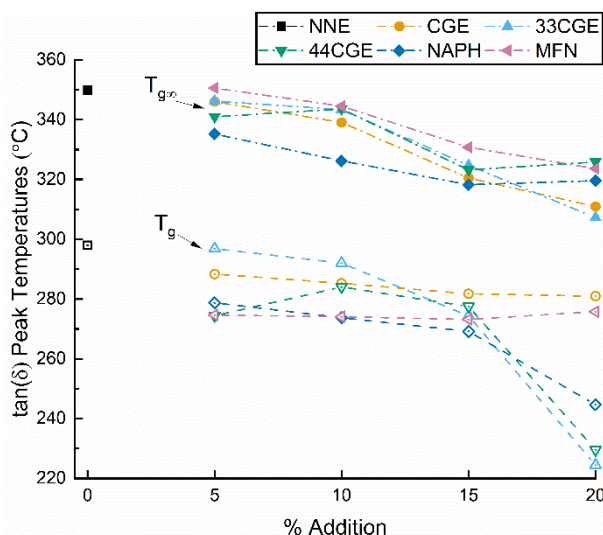


Figure 6-8 - Comparison of peak temperatures from $\tan(\delta)$ spectra respective to % modifier addition

The sub-ambient traces of the 10 % modified specimens were determined by DMTA initially cooling to -125°C followed by a slow $3^\circ\text{C}/\text{min}$ heating rate up to 100°C . Traces of the storage modulus and $\tan(\delta)$ for these systems is shown in Figure 6-9. Addition of the modifiers shifts the peak of the β -transition to a lower temperature whilst also diminishing the intensity and widening the half-width. The decrease can be associated with a decrease in the mobility of a reacted oxirane ring, suggesting the modifiers have an effect on constraining mobility in the glassy state. A notable transition occurs between 60 - 100°C for CGE, MFN, 33CGE, and the NAPH system from 30 - 100°C . This transition was previously noted for the 240°C post-cured NNE resin and was also present in the NTG and TGDDM resins cured with DDS.

The intensity and breadth of the peaks reflect influences on the mobility in the glassy state. As the lower peak temperature suggests, the effect of modifier addition has a benefit of increased molecular mobility in the glassy state as peak temperature shifts to the left. A comparison of the T_Ω , a secondary transition that occurs between 50 - 100°C and is associated with intermolecular motions of whole segments of the network. transitions shows conflicting behaviour. On one hand, this peak has been associated with a greater degree of hydrogen bonding [235], [236]. The MFN modifier is prepared in part by catalysing etherification between the cresyl glycidyl ether with the available hydroxyl of the 2,7'-dihydroxynaphthalene utilising a tertiary amine. The appearance of the T_Ω peak could arise from motions of large domains of the modifier incorporated into or interstitial to the network. For CGE, it is less apparent as no tertiary amine is utilised in the preparation nor does the monomer contain a

tertiary amine. Between the 3,3'- and 4,4'-CGE based adducts, a small diffuse peak is shown for the meta-substituted modifier which is similar to the sub-ambient behaviour of a para-substituted TGAP-33DDS where a distinct transition was not apparent for the 44DDS-cured resin as reported by Ramsdale-Capper & Foreman [192]. Previously, the dynamic traces showed a distinct peak emerging in the naphthalene resin around 80°C and the high intensity peak here appears to correlate to the melting point of naphthalene. The antiplasticising phenomenon has been studied extensively by sub-ambient DMTA techniques and a frequent observation is the suppression of the β -transition [121]–[123], [126]. Regardless of modifier, there is a decrease in the peak to a lower temperature and the breadth of the peak narrows for all but the 44CGE additive which appears the largest and most diffuse peak.

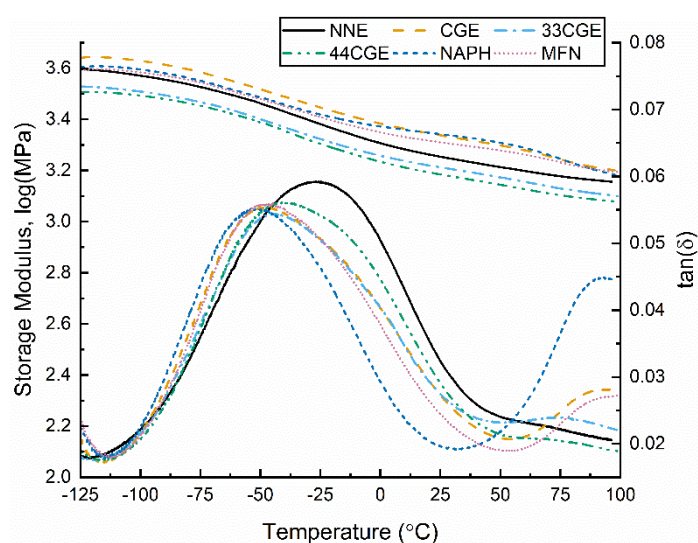


Figure 6-9 – Sub-ambient DMA traces of storage modulus and $\tan(\delta)$ for the modified resins at 10% modifier addition

6.3.5 Thermogravimetric Analysis

Dynamic thermogravimetry was used to assess the effect of modifiers on thermal degradation and stability. A comparison of the modifiers at 10% loading is shown in Figure 6-10 and temperatures at the tangential onset and at steps in mass loss of 95, 90, and 70 wt% as well as final char yield for all concentrations of additives are shown in Table 6-4. From the TGA traces at 10% modifier addition it is apparent that a slight decrease to the T_d is visible compared to the neat NNE resin. That trend is consistent for all concentrations of additives, lowering the onset by 7-11°C. The char yield also decreases with between 3-4% decrease in char yield apparent. In general, a slight but minor decrease with increasing additive is shown for all modifiers except CGE where a sharp decline is exhibited for 15-20 wt%, reaching a minimum

char yield of 27.9-26.8%, respectively. For the MFN modified resin, a final char yield of 28.9 wt% represents the second highest decrease at 20 wt% of additive. The NAPH, 33CGE, and 44CGE resins all remain around 20 wt% irrespective of additive loading. It is apparent that the combination of pre-reaction to create a large molecular weight and subsequent capability of the primary amine to react with the NNE resin improves the thermal stability whereas the absence of pre-reaction progressively diminishes with additional loading. The highly aromatic nature of the pure naphthalene shows superior thermal stability when incorporated as a non-reactive fortifier. The decrease to char yield largely represents the lower stability of the modifiers. Naphthalene has vaporisation temperature in the pure state below 300°C and is not bound to the network. The CGE, 33CGE, 44CGE, and MFN are bound to the network, covalently or non-covalently, but are less thermally stable than the dimeric naphthalene backbone with a more rigid network structure.

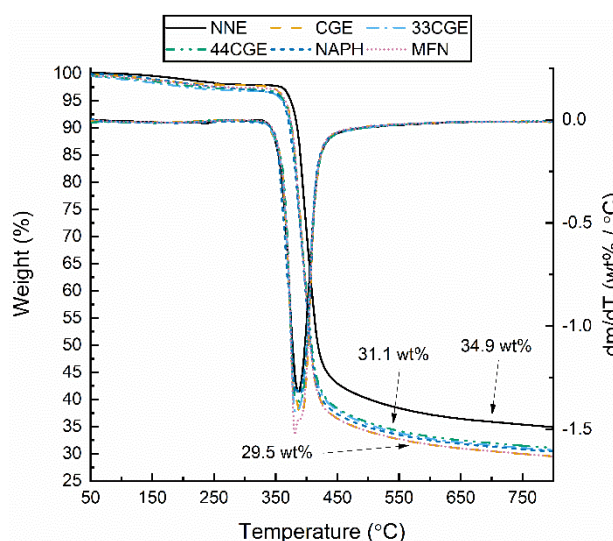


Figure 6-10 - Dynamic TGA (10°C/min heating rate) comparison at 10% modifier addition showing wt % (left axis) and derivative of mass loss (right axis)

Table 6-4 - Results of dynamic TGA analysis for degradation onsets and char yield

% Modifier	T_d (°C)	T_{95wt%} (°C)	T_{90wt%} (°C)	T_{70wt%} (°C)	Char Yield (wt%)
NNE					
0	383.6	363.3	373.8	390.8	34.9
CGE (mol%)					
5	375.9	366.9	376.5	391.5	29.9
10	373.6	365.7	375.5	391.6	29.5
15	369.1	358.6	372.6	390.7	27.9
20	370.9	359.5	371.5	390.7	26.8
33CGE (mol%)					
5	373.4	362.6	375.6	390.5	31.7
10	374.3	359.6	374.6	390.6	30.7
15	375.4	359.3	373.3	389.5	31.6
20	370.9	363.6	375.7	390.6	30.9
44CGE (mol%)					
5	376.4	364.5	377.6	393.4	31.6
10	374.4	362.3	375.5	391.4	31.1
15	373.4	362.5	376.4	392.3	29.0
20	373.7	367.6	376.4	391.7	30.1
NAPH (wt%)					
5	376.3	362.8	375.6	393.3	31.5
10	369.0	361.6	371.5	390.6	30.4
15	370.0	345.8	369.6	389.5	29.4
20	370.3	345.5	368.6	388.3	28.5
MFN (wt%)					
5	369.3	351.9	371.9	390.9	29.5
10	373.0	364.8	375.9	390.6	29.5
15	375.9	365.9	376.8	393.3	29.6
20	376.8	365.9	377.5	393.6	28.9

6.3.6 Effect of Moisture and Physical Properties

The effects of moisture on the cured networks were studied by long-term submersion in a deionised water bath. Results of the moisture ingress for the unmodified NNE and the modified CGE, NAPH, and MFN resins are shown in Figure 6-11 for 10% modifier concentration. A summary of physical densities and equilibrium moisture ingress relative to % loading of additive is provided in Table 6-5. An effect of filling the interstitial voids of the resin is that free volume previously unoccupied is filled, hence a reduction to the moisture ingress at equilibrium. For the NNE resin it has been established that a higher free volume fraction contributes to the high (~6 wt%) equilibrium moisture uptake. The higher molecular weight MFN shows a small reduction to the uptake whereas the lower molecular weight NAPH and CGE modifiers significantly reduce the moisture uptake to below 5 wt%. The effect of modifier

concentration systematically reduces equilibrium moisture uptake with increasing concentration and a minimum is established for CGE at 3.67 wt% (20 mol% loading), NAPH at 3.96 wt% (15 wt% loading), and MFN at 3.83 wt% (15 wt% loading). The resins show decrease in physical density subject to incorporating the modifiers which may result from the inclusion of lower molecular weight species and non-covalently bound nature of NAPH and MFN, porosity, and swelling of the network.

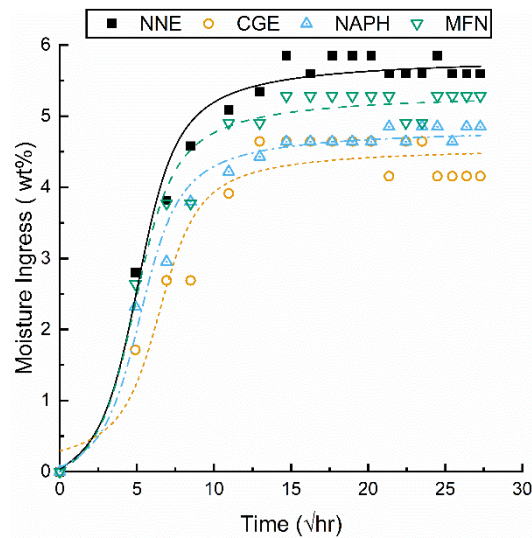


Figure 6-11 - Moisture ingress of the unmodified NNE and the 10% modified CGE, NAPH, and MFN formulations

Table 6-5 - Physical density and equilibrium moisture uptake for the NNE, CGE, NAPH, and MFN resins

% Modifier	Cured Resin Density (g/cm ³)	Equilibrium Moisture Uptake (wt%)
NNE		
0	1.315	5.66
CGE (mol %)		
5	1.305	4.96
10	1.304	4.15
15	1.298	4.47
20	1.295	3.67
NAPH (wt%)		
5	1.313	4.97
10	1.309	4.85
15	1.304	3.96
20	1.305	4.28
MFN (wt%)		
5	1.315	5.37
10	1.312	5.28
15	1.310	3.83
20	1.307	3.96

6.3.7 Mechanical Properties of the Neat Resin

The effect of modifier addition on mechanical properties were studied via flexural testing on neat resin bars. The flexural modulus of the resin modifiers is shown in Figure 6-12. The CGE, MFN, and NAPH modifiers show immediate increase to the stiffness of the network even at low (5%) additions. For 33CGE, the partially reacted substructure shows little benefit below 10 mol% and a maximum effect at 20 mol%. Again, an exception to that behaviour arises with the 44CGE where flexural modulus progressively decreases, regardless of percentage addition. The reduction in modulus of the 44CGE parallels with the broad and diffuse peak seen in sub-ambient DMTA analysis which suggests a weak ability to antiplasticise the network.

These results clearly indicate an anti-plasticising effect where the stiffness of the resin increases and strength decreases. It is noted that Morel et al, when studying glycidyl ether and glycidyl amine partially reacted with aniline, they noted an independence of network structure and T_g on glassy state behaviour whereas a significant enhancement is apparent with increased hydrogen bonding [271]. Here, the high temperature post-cure and relative mobility of CGE and the higher concentration of hydroxyl possible from the 33CGE, 44CGE, and MFN could influence the extent of hydrogen bonding thereby increasing modulus. Marks et al studied mono-functional epoxides incorporated into a DGEBA-based network and noted that a critical value of mono-epoxide behaved as a mild anti-plasticiser which were termed as non-elastically active pendant chains which also increased the effective crosslink density [33]. Herein, the unreacted parts of the CGE, 33CGE, and MFN can form such pendant structures within the network. The NAPH system showed the largest increase in glassy modulus at low (5-10 wt%) concentrations. Unlike the previous works reported on fortifier addition, the use of naphthalene is relatively unique because of the lower molecular weight and because it is assumed to have very little potential to bond with the bulk polymer network via covalent or non-covalent mechanisms. It can be inferred that the mechanism by which modulus is increased could relate to the extended processing window during cure (lower viscosity, increased gelation) and the hypothesis that some domains of the bulk network are filled by the free naphthalene, thereby occupying free volume and reinforcing the network. It is notable that the modulus shown for CGE, NAPH, and MFN now approaches the value of the TGDDM formulation examined earlier (see Fig. 5-16 in Ch. 5)

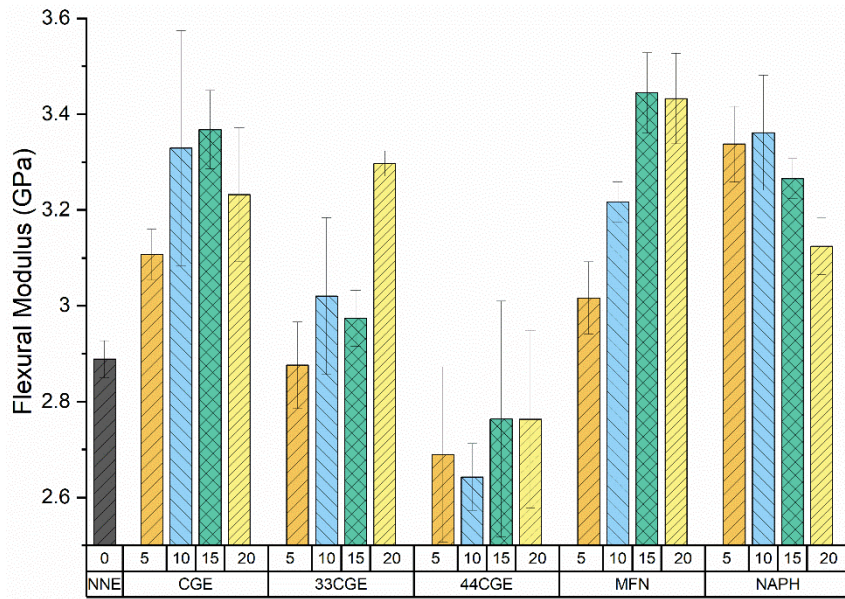


Figure 6-12 - Flexural modulus with respect to % modifier addition

In Figure 6-13 the flexural strength relative to modifier addition is shown for the different resin systems. While the results only correlate loosely to the increased modifier addition, some differences are readily apparent between the reactive, partially-reacted, and non-reactive modifiers. Generally, lower amounts of addition below 10% have a negative effect on flexural strength whereas above 10%, most of the resins show a recovery of flexural strength. The exception to that is the 44CGE modifier which shows progressively decreased strength.

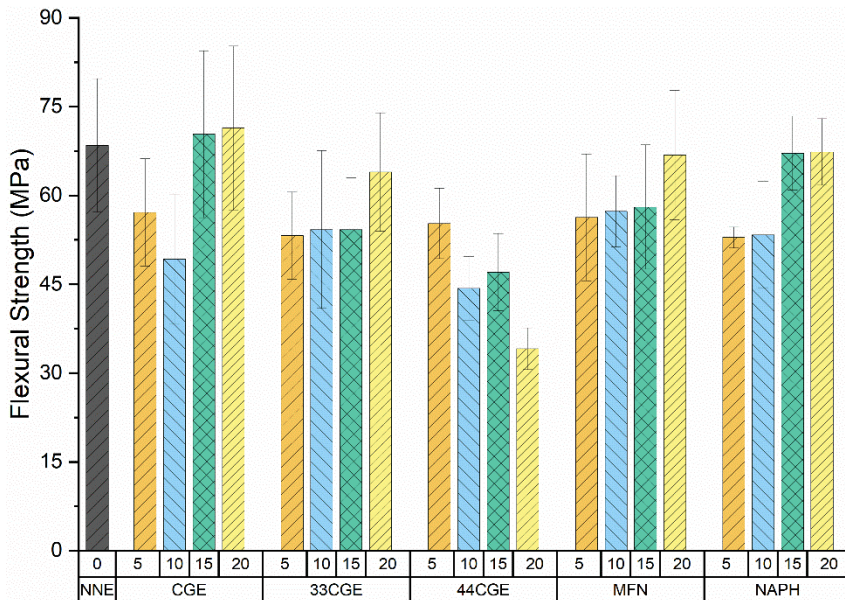


Figure 6-13 - Flexural strength relative to % modifier addition

Fracture toughness of the neat resins was studied via single-edge notch flexural testing and the results are shown in Figure 6-14. The CGE, 33CGE, and 44CGE showed no improvement to fracture toughness and virtually no correlation between diminished toughness and percentage of the modifier. Additionally, the 44CGE mirrored the behaviour of flexural strength and modulus showing a decrease in all respects. In contrast, the MFN and NAPH resins showed improved fracture toughness up to 10 wt% that, while modest shows benefits over previous works in this field of study. It has previously been reported that anti-plasticisation decreases the fracture toughness as the network is less able to absorb and dissipate energy partly due to the increased modulus [252].

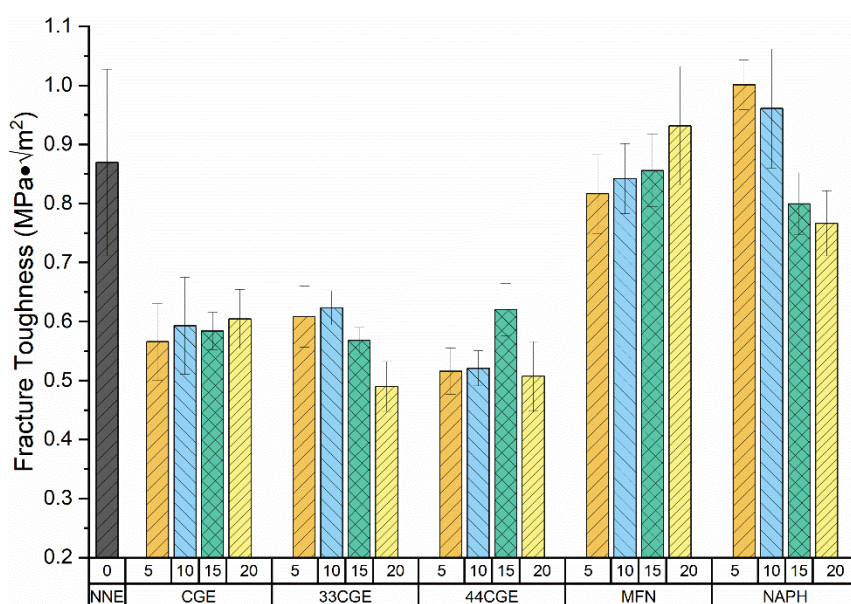


Figure 6-14 - Effect of % modifier addition on fracture toughness of the resins

From the mechanical properties, it is shown that low molecular weight additives have an anti-plasticising effect on the highly rigid NNE resin and subsequently reduced strength and toughness. The 33CGE and 44CGE partially reacted substructures incorporated into the network did not improve mechanical strength or toughness. Notably, these structures are largely aromatic whereas the partially-reacted work by Sharif & Palmese [261] and Gao et al. [272] amongst others utilised aliphatic amines to increase flexibility but subsequently decreased T_g below 200°C for the tetrafunctional epoxy formulation. Those PRS' incorporate inherent flexibility into an otherwise rigid network. The lack of an improvement to fracture toughness from CGE, 33CGE, and 44CGE more closely mirrors the results of Grishchuc et al. where increased modulus by a reactive diluent decreased fracture toughness [125].

It is interesting, then, that the non-reactive NAPH and MFN modifiers show some retention to the fracture toughness and increased modulus. That could partially be explained by contrasting the bulk network with the particular modifiers. Ngai et al. studied chlorinated biphenyl on DGEBA and PMMA polymers, noting a plasticising effect for the former but the opposite effect on the latter [273]. While their explanation relies on corollary observations in other areas polymer physics theory, they attribute increase to damping (and subsequent increase to modulus) of the DGEBA-based polymer network to enhancement of the dynamic constraints arising from the presence of the plasticiser in the vicinity of the network but as molecular weight or concentration increases, the constraints are diminished.

6.3.8 Mechanical Properties of the Composite

Composite panels were manufactured from unidirectional fibre tape that was pre-impregnated with the resin matrix systems to a target 45 vol% resin content. A minimum of 8 samples were then prepared for flexural and interlaminar shear strength testing. The results of flexural 3-point bend testing are shown in Figure 6-15 for the unmodified and modified matrix systems. In general, the translation of the composite properties from neat resin is diminished due in part to the heterogeneity of the composite (i.e. high modulus reinforcing fibre, low strain to failure) and also the interaction of fibre with matrix.

The addition of CGE resulted in a reduction to flexural strength and strain, consistent with the resin properties while a modest increase to flexural modulus of the composite also appeared. The addition of 33CGE and 44CGE showed modest decrease in strain at failure whilst an increase, maximised for 33CGE, was apparent in the flexural strength. That also corresponded with a significant increase to the modulus from 74GPa to 92GPa. Notably, between CGE, 33CGE, and 44CGE the possible network formation differs significantly. While the CGE forms a small molecular weight pendant, the pre-reaction of *o*-cresyl glycidyl ether consumed only one of the available primary amines of the DDS isomers and allows for a further reaction of primary amine and secondary amine with the bulk network. It is likely that the network formed has higher crosslink density directly contributing to mechanical stiffness than CGE resulting in the increased flexural modulus. The NAPH matrix showed similar performance with a modest increase to strength and flexural modulus increasing to nearly 89GPa. The MFN matrix showed the highest strain at failure whilst exhibiting the largest decline in flexural strength and modulus, showing poor translation of resin performance to the composite.

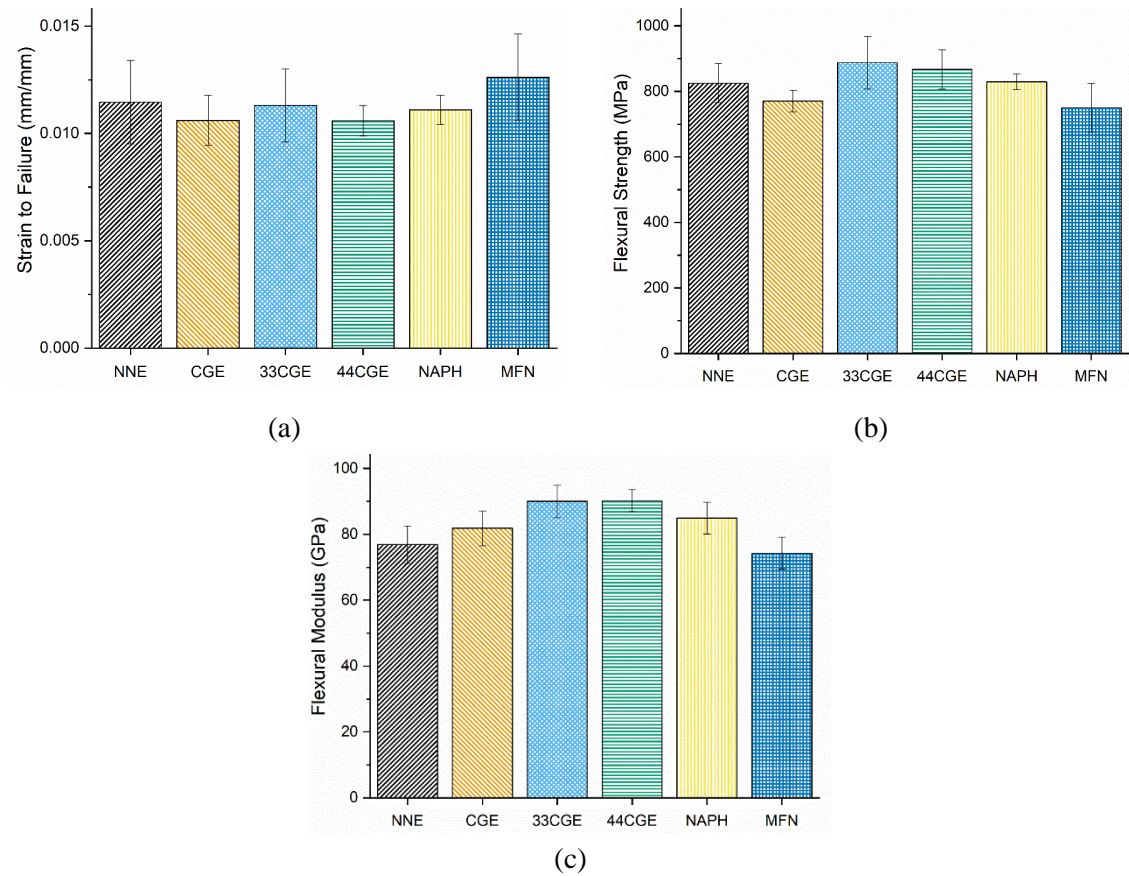


Figure 6-15 - Mechanical properties of the composites in flexural 3-point bending showing (a) strain-to-failure, (b) flexural strength at failure, and (c) the flexural modulus of the composites

Interlaminar shear strength tests were conducted to understand the relation between fibre-matrix interaction and the effect of the different additives on performance. A number of factors influence ILSS performance some of which include resin mechanical properties, presence of voids and porosity, fibre content, and the level of impregnation. Hernandez et al. studied the ILSS performance as it related to cure temperature and viscosity noting that improved ILSS correlated to a cure profile where minimum viscosity was achieved the longest [274]. Work by Wu et al. explored matrix modifiers and showed additives that reduced viscosity and expanded the working life of the matrix correlated to improved ILSS performance over an unmodified epoxy matrix [275]. ILSS values are shown in Figure 6-16. The maximum ILSS values were achieved for CGE. Improvements to ILSS for CGE can be related to the longer processing window at lower viscosity making for improved wet-out and consolidation of the laminate preform during cure. A modest increase for 33CGE, 44CGE, and MFN is shown suggesting

the changes to matrix properties drove improved ILSS. The NAPH matrix showed reduced ILSS, 39MPa compared to 42MPa for the unmodified NNE matrix. Naphthalene undergoes sublimation at 80°C, well below the initial cure temperature of the composite so it is possible that defects can occur within the heating and cooling cycles, thus resulting in reduced ILSS performance.

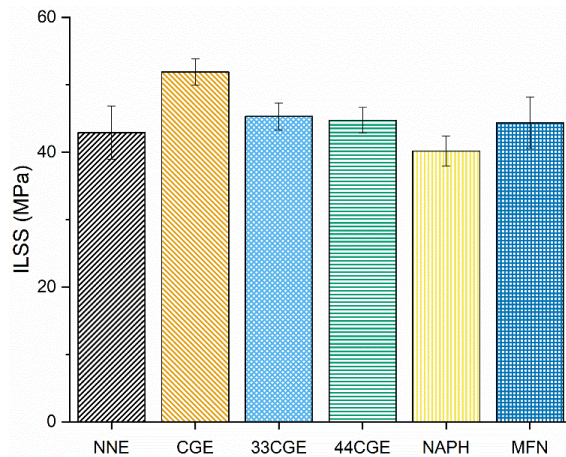


Figure 6-16 – Interlaminar shear strength of the 10% modifier addition composites

6.4 SUMMARY

In this chapter a survey of four molecular-level additives and different functionality with the bulk epoxy-amine resin were synthesised and studied for the effect on thermal and mechanical properties of the resin and translation to the carbon fibre composite. Monofunctional o-cresyl glycidyl ether epoxy addition forms a pendant to the bulk network generally reduced mechanical performance but antiplasticised the resin resulting in higher modulus. Composite flexural modulus was improved as was the wet-out and consolidation of the preform during cure which was attributed to the diluting effects of CGE. Partially reacted structures of 33CGE and 44CGE did not exhibit a diluting effect but resulted in improved strength and stiffness for 33CGE in part due to the linkage between the available primary amine of the partially-reacted 33DDS. Improvement of the modulus translated to the composite for both 33CGE and 44CGE due to the higher molecular weight of the pendant group and ability to form a denser crosslinked system than by CGE alone. The molecular fortifier MFN showed a high degree of antiplasticising capabilities with minimal impact to fracture toughness but ultimately poor translation to the composite. The addition of naphthalene showed good antiplasticisation performance and even improved resin fracture toughness but ultimately poor interlaminar shear strength. Nevertheless, the CGE and NAPH additives, when incorporated into the resin,

imparted beneficial reductions to viscosity and slowed the reaction to increase the processing window. Enhancements to the modulus led to similar values obtained for a TGDDM-44DDS resin formulation previously studied. While not an exhaustive survey of molecular-level additives, these routes show the potential as multi-functional modifiers for epoxy matrix formulation through simultaneously improved mechanical and rheological characteristics which can be exploited to create readily processable high-performance composites.

AUTHORSHIP STATEMENT

1. Details of publication and executive author

Title of Publication		Publication details
Study of the acoustic emission response of a shell-rubber-toughened, high-temperature composite		Published, Journal of Materials Science, 56 5605-5623 (2021)
Name of executive author	School/Institute/Division if based Deakin; Organisation and address non-Deakin	Email or phone
Russell J. Varley	Carbon Nexus at the Institute of Frontier Materials	(03) 5247 9577

2. Inclusion of publication in a thesis

Is it intended to include this publication in a higher degree by research (HDR) thesis?	Yes	If Yes, please complete Section 3 If No, go straight to Section 4.
---	-----	---

Name of HDR thesis author different from above. (If the same as above, leave blank)	School/Institute/Division if based Deakin	Thesis title
Samuel R. Swan	Carbon Nexus at the Institute of Frontier Materials	Investigating the structure-property relations of a high temperature epoxy matrix for structural and thermal applications

For each publication (for example, how much did you contribute to the conception of the project, the design of method, experimental protocol, data collection, analysis, drafting the manuscript, revising it critically for intellectual content, etc)

<i>I declare that the above is an accurate description of my contribution to this paper, and the contribution of other authors are as described below.</i>	Signature and date	
--	--------------------	--

4. Description of all author contributions

Name and affiliation of author	Contribution(s) (for example, conception of the project, design methodology or experimental protocol, data collection, analysis, drafting manuscript, revising it critically for important intellectual content, etc)
Samuel R. Swan	Conception, sample preparation, thermal and mechanical testing, analysis, writing, editing
Timothy Devenport	Mechanical testing, data analysis, writing, editing
Seyed M. Seraji	Scanning electron microscopy, writing, editing
James M. Griffin	Review, some idea generations and overseeing experiments
Bekim V. Gashi	Reviewing the papers, technical aspects, methodologies, data presentation and experiments.
Claudia Creighton	Conception, data analysis, writing, editing

Russell J. Varley	Conception, data analysis, writing, editing
-------------------	---

5. Author Declarations

I agree to be named as one of the authors of this work, and confirm:

- i. that I have met the authorship criteria set out in the Deakin University Research Policy,*
- ii. that there are no other authors according to these criteria,*
- iii. that the description in Section 4 of my contribution(s) to this publication is accurate,*
- iv. that the data on which these findings are based are stored as set out in Section 7 below.*

If this work is to form part of an HDR thesis as described in Sections 2 and 3, I further

v.

Deakin University and, if the higher degree is awarded, the submission of the thesis by the university (subject to relevant Copyright provisions).

6. Other contributor declarations

I agree to be named as a non-author contributor to this work.

Name and affiliation of contributor	Contribution	Signature* and date

* If an author or contributor is unavailable or otherwise unable to sign the statement of authorship, the Head of Academic Unit may sign on their behalf, noting the reason for their unavailability, provided there is no evidence to suggest that the person would not be named as author

7. Data storage

The original data for this project are stored in the following locations. (The locations must be within an appropriate institutional setting. If the executive author is a Deakin staff member and data is stored outside Deakin University, permission for this must be given by the Head of Academic Unit within which the executive author is based.)

Data format	Storage Location	Date lodged	Name of custodian if other than the executive author
Electronic	S: Drive	288-21	

Physical	Carbon Nexus	288-21	
----------	--------------	--------	--

This form must be retained by the executive author, within the school or institute in which they are based. If the publication is to be included as part of an HDR thesis, a copy of this form must be included in the thesis with the publication.

7 TOUGHENING OF A HIGHLY CROSSLINKED EPOXY MATRIX VIA CORE SHELL RUBBERS

7.1 INTRODUCTION

As has been previously highlighted, high temperature epoxy resins combine highly aromatic structures, chemical multi-functionality, and when cured have a high crosslink density. However, the consequence of such chemical networks is lower mechanical strength and fracture toughness due to restricted mobility of the higher crosslink density [19], [39]. An increased thermal stability generally results in deleterious effect on fracture toughness due to the brittle nature of highly crosslinked epoxies [17].

A significant area of interest for such epoxies is the enhancement of toughness. That has led to a large body of research on thermoplastic modification, reactive and phase-separated rubbers, and inorganic particles [28], [35], [92], [93], [96], [108], [276]–[279]. Resins of lower functionality such as DGEBA comprise most of the literature although some reports on TGDDM and other multifunctional epoxies do exist. The evidence of toughness enhancement or “toughenability” of TGDDM and highly cross-linked networks point to a generally lower degree of improvement due in part to the higher crosslink density of the bulk resins which can restrict the formation of shear bands and yielding [280]–[282]. Even when a toughening response is achieved, the effect of such tougheners tends to decrease strength, stiffness, the glass transition temperature, and processability.

Pre-formed core shell rubber particles (CSR) are a non-reactive additive comprised of a hard outer shell containing a soft elastomeric core material. For DGEBA-based and resins of lower crosslink density, these particles have shown ready toughenability with almost no effect to the T_g and minimal effect on other mechanical properties [30], [104], [105], [109], [112], [113]. These particles are usually 50-100nm in diameter with shell thickness in the range of 10-20nm. Often dispersed into an epoxy masterbatch, these can be incorporated into formulations to tailor toughness, processability, and mechanical properties. As a crack tip propagates through the resin, the toughening effect is induced when an isostatic tensile load causes the CSR particle to cavitate. Upon dilation of the core material and subsequent cavitation, shear bands can form which can absorb some of the energy from the crack tip thereby enhancing the yield response and toughness of the bulk resin [104], [107], [163], [283]–[285].

Few studies explore toughening of a highly-crosslinked material such as TGDDM. Bradley et al studied some higher- T_g (189-225°C) materials and noted an absence of toughening with increased T_g [164]. Other work notes an inverse correlation between effective toughening and the bulk resin thickness [161]–[163] lending support to enhanced toughness for thin matrix layers in a composite as opposed to the bulk resin. As of writing, only one previous work outside of the study presented here investigates highly crosslinked epoxies with CSR addition. Riew et al. showed that a TGDDM/DGEBA blend cured with 44DDS increased energy (G_{IC}) of the composite 45 %, from 500 J/m² to 890 J/m² [117].

7.1.1 Overview of the Study

In this study the effect of core shell rubber addition is studied for how it relates to processing the resin, the effect on resin properties and toughenability, and finally the translation to the composite fracture toughness. The resin utilised is commercial TGDDM cured with 3,3'-diaminodiphenylsulfone, the meta-substituted isomer of para-substituted 4,4'-diaminodiphenylsulfone. A masterbatch of commercial CSR particles in TGDDM is diluted into the resin from 2.5-20 wt% and cured. Combinations of dynamic differential scanning calorimetry, near-infrared spectroscopy, and rheology is performed to determine the effects of CSR on processing. Mechanical and thermal properties are studied via dynamic mechanical analysis, thermogravimetric analysis, moisture ingress, flexural loading and fracture toughness testing on the neat resins. A comparison of the fracture toughness of an unmodified TGDDM-33DDS carbon fibre composite laminate and one containing 20 wt% CSR is performed for mode I fracture and studied by in situ acoustic emission sensing.

7.2 EXPERIMENTAL

7.2.1 Materials and Manufacturing of Laminates

Neat epoxy resins were prepared from tetraglycidyl-diaminodiphenyl methane ((124 g-eq⁻¹) Araldite MY720, Huntsman Corp., USA) and cured with a 1:0.95 stoichiometric amount of 3,3'-diaminodiphenylsulfone (DDS) ((62 g-eq⁻¹) Tokyo Chemical Industries, JPN). The core shell rubbers were provided by Kaneka Corporation of Japan and are pre-dispersed by the proprietary MXTM process into an epoxy master batch marketed under the Kane-Ace brand. Kane-Ace MX416 consists of CSR particles with a 50-70 nm diameter. These particles consist of a polybutadiene rubber and a PMMA core which is dispersed in a TGDDM (148 g-eq⁻¹, Araldite MY721) resin at a concentration of 25 wt% (± 1 %). The unmodified TGDDM was

then used to dilute the master batch and achieve a particle concentration of 2.5, 5, 10, 15, and 20 wt% CSR in epoxy.

Composite laminates were fabricated from pre-impregnated carbon fibre tape. The epoxy-amine resin (75 g) was dissolved in dichloromethane (200 mL) and acetone (100 mL) by rigorous stirring until the mixture was a transparent yellow in the case of the unmodified resins, or a slightly opaque light pink for the core-shell modified variant. The carbon fibre was a standard modulus, 300 g.sqm^{-1} unidirectional tape. The dissolved resin was wound through a manual infusion device onto a spool which was then placed in a ventilated drying oven at $45 \text{ }^\circ\text{C}$ for one hour followed by $75 \text{ }^\circ\text{C}$ for 30 minutes to remove the solvent. A total of 16 plies were used for each panel. A thin PTFE release film was inserted into the panels between the mid-ply at both ends of the laminates to act as a pre-crack. The lay-ups were vacuum-bagged, debulked, and cured on a hydraulic press pre-heated to $120 \text{ }^\circ\text{C}$ and applied pressure of 6.5 bar. The cure schedule for the neat resins and composites were the same with the exception that the composite laminates were debagged and post-cured in a convection oven. The laminates were 3.8 mm nominal thickness after cure and eight specimens were cut to nominal dimensions of $21 \times 150 \text{ mm}$ from each of the laminates.

7.2.2 Mode I Fracture Toughness Testing and Acoustic Emission Sensing

The mode I strain energy release rate (G_{IC}) of the composites was measured by the double cantilever beam method according to ASTM Standard D5528 [286]. The loading rate was 10 mm/min. A high definition digital camera was used to track the crack tip front. The compliance calibration method was utilized to determine the value of fracture energy based on the load and displacement recorded at the servo-electromechanical load frame relative to the crack propagation in the sample.

The acoustic emission apparatus consisted of a Micro-II data acquisition unit, two voltage pre-amplifiers, two 20 mm diameter ceramic wide-band acoustic emission sensors and associated waveform extraction software (Mistras Group Inc., USA). The amplification to each sensor was maintained at 20 dB with a 35 dB threshold. The AE sensors have an operational range between 70 kHz to 1 MHz and were placed along the centerline of the top face of the DCB specimens. Sensors were coupled to the surface by use of a polypropylene double-sided tape of 220 μm nominal thickness (tesa 51970 SE, Germany). The arrangement of DCB samples with AE sensors is shown in Figure 7-1.

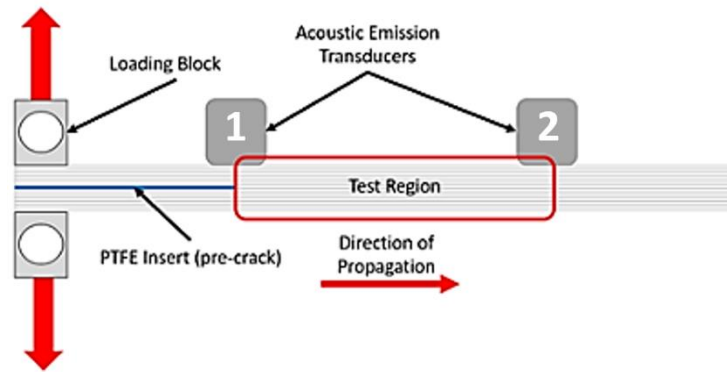


Figure 7-1 - Diagram of AE sensors onto DCB specimens for fracture toughness characterization

The attenuation of the sample material affects the propagation of soundwaves as the density of the material changes. That includes changes to material thickness and distance between the source and the sensor. The leading sensor (#1) was kept centered over the pre-crack tip and the lagging sensor (#2) placed 55mm from the crack tip. Each was aligned down the lengthwise centre of the beam.

Prior to each test, an automatic sensor test (AST) was carried out to assess the contact between sensor and sample and compare the sensitivity of sensor 1 to sensor 2 before and after testing. The AST sends a prescribed pulse from one sensor that is received by the other sensor. The output of this test displays the amplitude and hits of the sending and receiving sensors and the contact is considered good if at least 50% of the sent signal is received. Between sensors 1 and 2, the average received signal from a 96 dB nominal pulse amplitude was 58.33 dB (± 6.62) and 59 dB (± 5.87), respectively. Post-test, the average was 52 dB (± 3.21) and 52 dB (± 4.00), respectively. The cumulative drop in received signal from both sensors corresponded to a 10.1% decrease at the end-of-test state which is attributed to the reduction in laminate thickness after crack propagation.

7.3 RESULTS AND DISCUSSIONS

7.3.1 Differential Scanning Calorimetry

The thermograms for the modified and 20wt% modified resin systems shown in Figure 7-2 display a typical exothermic response during epoxy amine cure where peak exothermic temperature increases with increasing heating rates while the magnitude of the heat flux remains independent. A summary of the kinetic analysis are shown in Table 7-1 which highlight that CSR addition reduces the peak exothermic temperature, T_p , yet increases the enthalpy of reaction. The activation energy barriers to reaction were determined to be 61.2

kJ/mol (Kissinger) and 69.4 kJ/mol (FWO) for the unmodified resins and 66.8 kJ/mol (Kissinger) and 75.0 kJ/mol (FWO) for the 20 wt% CSR modified, indicating an increase of about 5.5 kJ/mol regardless of model [287], [288]. The modest acceleration of the reaction as evidenced by the lower T_p and consistently higher enthalpies (after normalization) suggests some promotion of the cure reaction by the CSR particles. Despite this acceleration, higher activation energy for the 20wt% CSR modified system likely reflects a comparatively restricted mobility or steric hindrance caused by the sub-micron scale particles in the glassy state. An accelerated effect has previously been reported for CSR modified epoxy resins [116], [289].

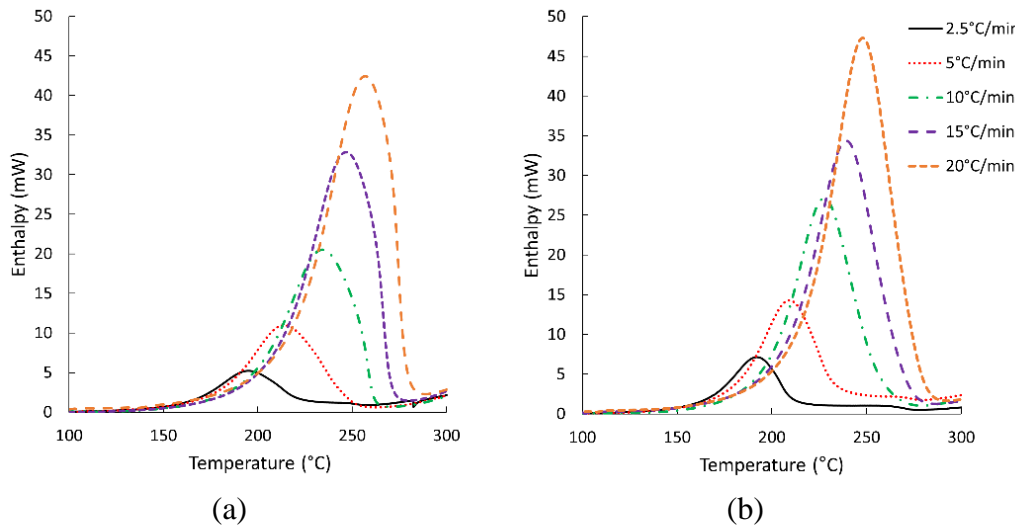


Figure 7-2 - DSC thermograms of uncured resins for (a) the unmodified 0 wt% CSR and (b) the 20 wt% CSR formulations

Table 7-1 - Summary of peak temperature, enthalpies, and activation energies for neat resins studied by differential scanning calorimetry

	Heating Rate (°C/min)					Kissinger	FWO
	2.5	5	10	15	20	E_a (kJ/mol)	E_a (kJ/mol)
Unmodified							
T_p (°C)	194.79	213.99	234.23	246.81	256.83	61.2	69.4
$J'' * I$	474.12	571.90	477.00	540.4	481.8		
20 wt% CSR Modified							
T_p (°C)	191.82	209.66	227.63	239.26	247.94	66.8 (5.6%)	75.0 (5.5%)
$J'' * L$	587.63	634.63	654.25	585.38	591.25		

7.3.2 Rheological Characteristics of the Resins

Dynamic rheology was performed on the resins to evaluate the effect of CSR loading on the gelation and minimum viscosity. Results of the analysis are shown in Figure 7-3 and Table 7-2. The comparison of minimum and maximum loading shows that CSR have almost no effect to gelation temperature and the minimum viscosity largely remains unchanged from 2.5-20 wt% CSR. There is a slight and systematic increase to the E' value after gelation which can be attributed to synergistic effects of high particle loading and agglomeration.

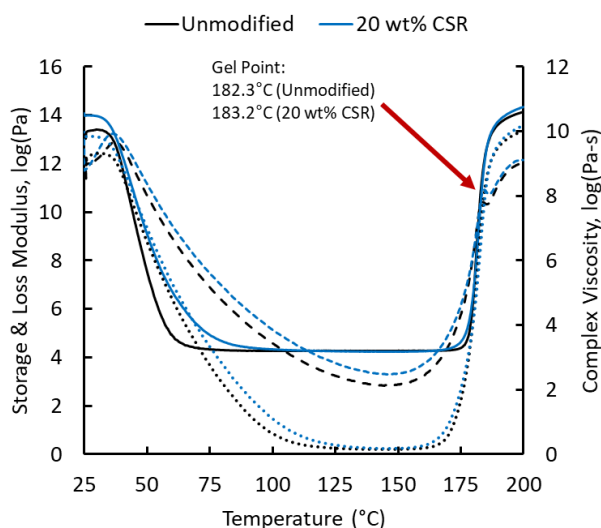


Figure 7-3 - Dynamic rheological traces of the unmodified and 20 wt% CSR resins

Table 7-2 - Dynamic rheology of the compositions from 0-20 wt%

CSR Addition (wt%)	T _{gel} (°C)	Minimum Viscosity(Pa-s)	Crossover G ₀ " I (MPa)
0	182.3	1.174	.027
2.5	183.6	0.952	.034
5	184.9	1.071	.038
10	183.6	0.934	.035
15	182.3	1.177	.034
20	183.2	1.185	.038

7.3.3 Near-infrared Spectroscopy of Cured Resins

Near infrared spectroscopy (NIR) was used to gain insight into the cure mechanism of the epoxy amine reaction, particularly during later stages of cure and to explore the impact of CSR on cure conversion. The NIR spectra of all the modified resins are shown in Figure 7-4(a) which show similar behavior, suggesting that the mechanism is relatively unaffected by the addition of the CSRs. The regions of interest, namely the epoxide (just under 4500 cm⁻¹), secondary amine (about 6600-6800 cm⁻¹) and hydroxyl peaks (7200-6800 cm⁻¹) are more

closely examined in Figure 7-4(b) and 4(c) for the unmodified and 20 wt% CSR modified systems only. Figure 7-4(b) shows qualitatively that CSR addition produces a very small reduction in the extent of cure which can be attributed to the increased steric hindrance effects of the CSRs. The secondary amine and hydroxyl region, again, whilst mostly very similar for different CSR concentration, does possibly show some effect with increasing CSR addition. Figure 7-4(c) whilst comparing the unmodified and 20 wt% CSR system, shows that there is a modest increase in the secondary amine peak and decrease in the hydroxyl peak. Again, whilst being very minor, this suggests to a greater degree of etherification at higher CSR concentrations.

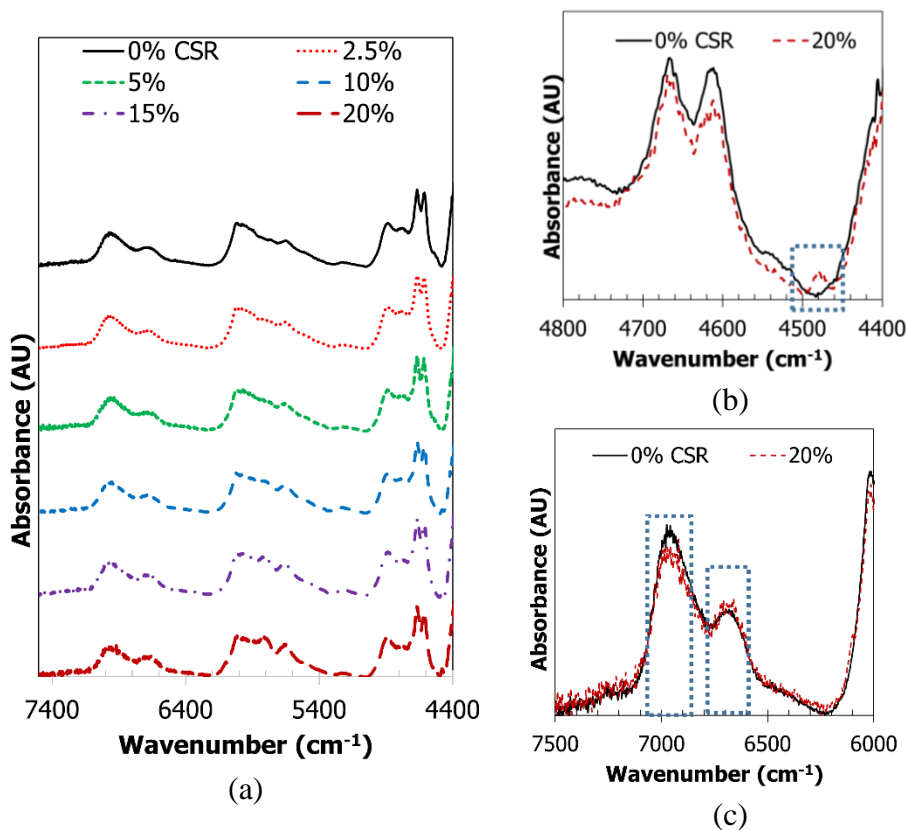


Figure 7-4 - NIR of (a) fully cured TGDDM-DDS from 0-20 wt% CSR loading and (b-c) the unmodified and 20 wt% for epoxide, hydroxyl, and primary/secondary amine peaks

7.3.4 Thermal Analysis of the Cured Resins

The T_g , as determined by DMA shown in Figure 7-5 and Table 7-3, exhibited a modest but consistent increase with increasing concentration of CSR as measured by the extrapolated onset of E' and the peak in the $\tan \delta$ spectra, likely due to increased chemical interactions between the CSR and polymer matrix, as previously suggested. In addition to this modest

increase in T_g , the magnitude of the $\tan \delta$ peak also decreased somewhat with increasing CSR concentration, albeit erratically, reflecting restricted mobility around the CSR dispersed particles. Another observation from the traces is that, the storage modulus, again despite being somewhat erratic shows an overall decrease with increasing CSR concentration due to their inherently lower modulus. Concurrent with a decreased storage modulus is a decrease in the physical density. Previously, investigations into DGEBA-based resin systems have reported similar reductions in storage modulus and minor increases to the T_g with CSR addition [114], [290] which has been associated with good dispersion of the particles in the cured resin [109], [112], [291]. Whilst the $\tan \delta$ spectra was incomplete, from as much as could be determined, it appeared mostly symmetrical or unimodal suggesting a homogeneous network, at least on the microstructural level.

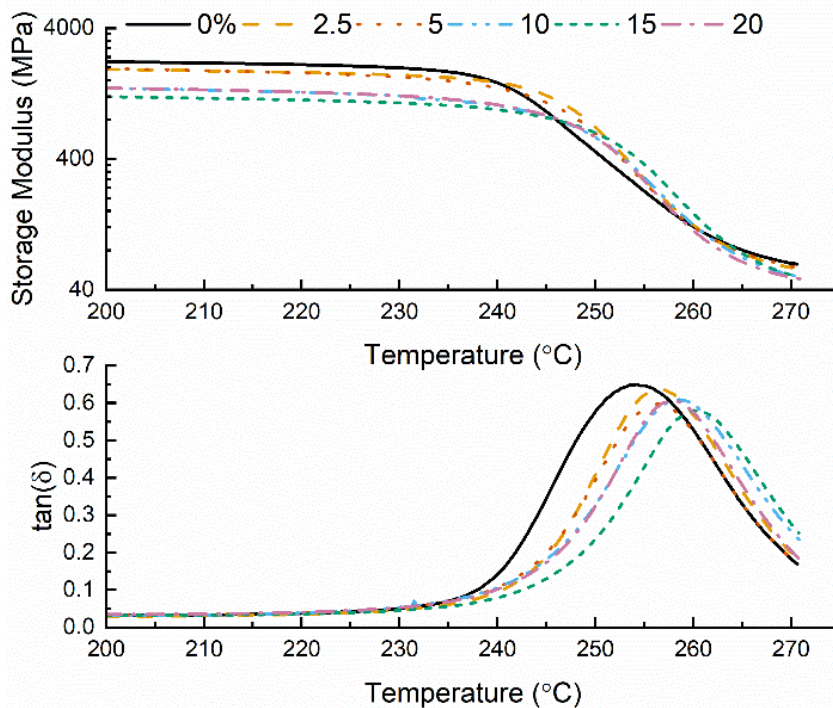


Figure 7-5 - Scans from dynamic mechanical analysis showing (a) storage modulus and (b) $\tan(\delta)$ relative to ramp temperature

The thermal stability of the cured networks was also investigated using TGA, as measured by the onset of degradation (T_d) and the char yield (%) as shown in Table 7-3. Despite somewhat scattered and modest trends, it is still clear that the T_d increased while the char yield decreased with increasing CSR concentration. The increase can be attributed to an increase in cohesive strength arising from the epoxy CSR interactions, while the reduced char yield reflects the

reduced thermal stability of the CSRs themselves.

Table 7-3 - Summary of glass transition, degradation temperatures, and char yield for the neat resins

	CSR WT%					
	0	2.5	5	10	15	20
T_g (°C)	238 [254]	244 [256]	246 [258]	244 [256]	249 [260]	246 [258]
T_d (ext. onset) (°C)	334	351	346	336	355	360
Char yield (wt%)	25.5	20.4	23.6	26.3	20.4	18.9
Cured resin density (g/cm ³)	1.283	1.251	1.229	1.219	1.212	1.198

7.3.5 Flexural Properties and Fracture Toughness of the Neat Resins

The mechanical and fracture properties of the neat resins shown in Figure 7-6 indicate a consistent decrease in flexural strength and modulus but an increase in fracture toughness with increasing CSR concentration. Despite the hard outer shell of the CSR, the core material is a polybutadiene rubber, so a reduction in stiffness is consistent with inclusions of more compliant additives [292]. No discernible trend is observed for the strain to failure, likely due to the brittle nature of the epoxies and so less related to the presence of CSR regardless of concentration. In contrast, the fracture toughness while not showing any improvement in toughness at low levels of addition, did show a modest increase in K_{IC} from 15 wt% to 20 wt% CSR addition. The improvement to average fracture toughness was 11.4% for 15 wt% of CSR and 45.0% for the 20wt% CSR samples. It is important to note that the high level of CSR required to achieve significant improvements in fracture toughness is not typical. As discussed earlier, CSRs have been shown to impart very large improvements to toughness in epoxy networks either at much lower concentrations [109], [113], [290] or toughened to orders of magnitude higher than the pure epoxy [112], [291], [293]. Importantly however these results were not for very high crosslink density networks as discussed here, where the crosslink density restricts complementary toughening mechanisms such as matrix shear yielding [30], [104] from occurring in conjunction with the CSR particle cavitation and crack bridging.

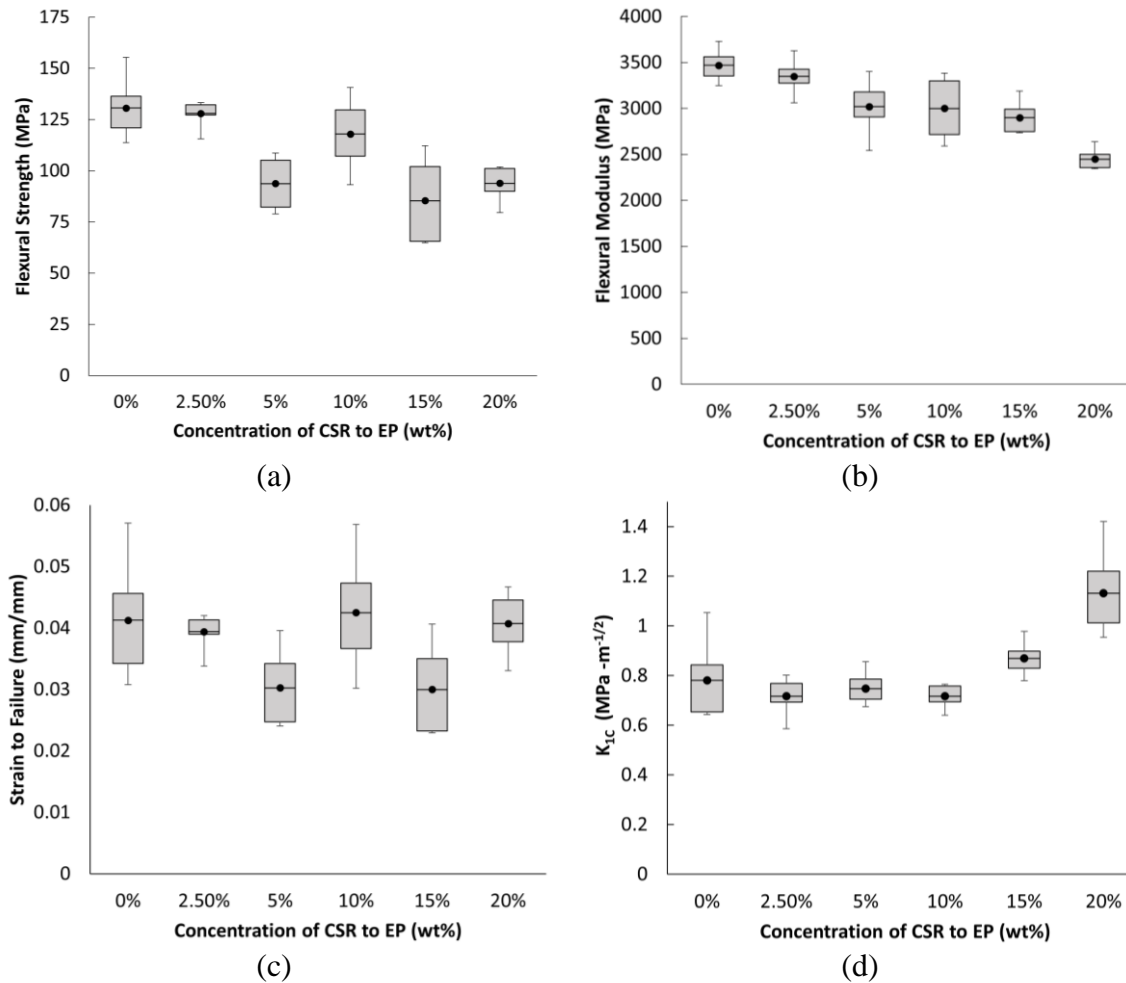


Figure 7-6 - Summary of flexural strength, modulus, and SENB fracture toughness for 0-20 wt% CSR modified neat resins

7.3.6 Comparative Assessment of the Carbon Fibre Composites in Mode I Fracture

Given the very good improvement in fracture toughness (K_{IC}) for the 20 wt% CSR modified epoxy network, the corresponding composite was fabricated and compared to the unmodified TGDDM/DDS composite to further understand the failure mechanism and explore the AE response.

AE sensors measure the voltage response from failure events that excite the sensor at a given frequency and above a threshold amplitude. In addition, the dataset for an event includes both a hit and a count. One event produces one hit and within that hit are one or many counts that represent the cumulative number of pulses above a certain amplitude. These hits and counts provide a partial description about the amount of AE activity that occurs and the relative shape of the acoustic waveform. Examples of how the experimental load during crack propagation relates to the hit and count data measured from AE spectroscopy for an unmodified and CSR toughened composites therefore, are shown below in Figure 7-7.

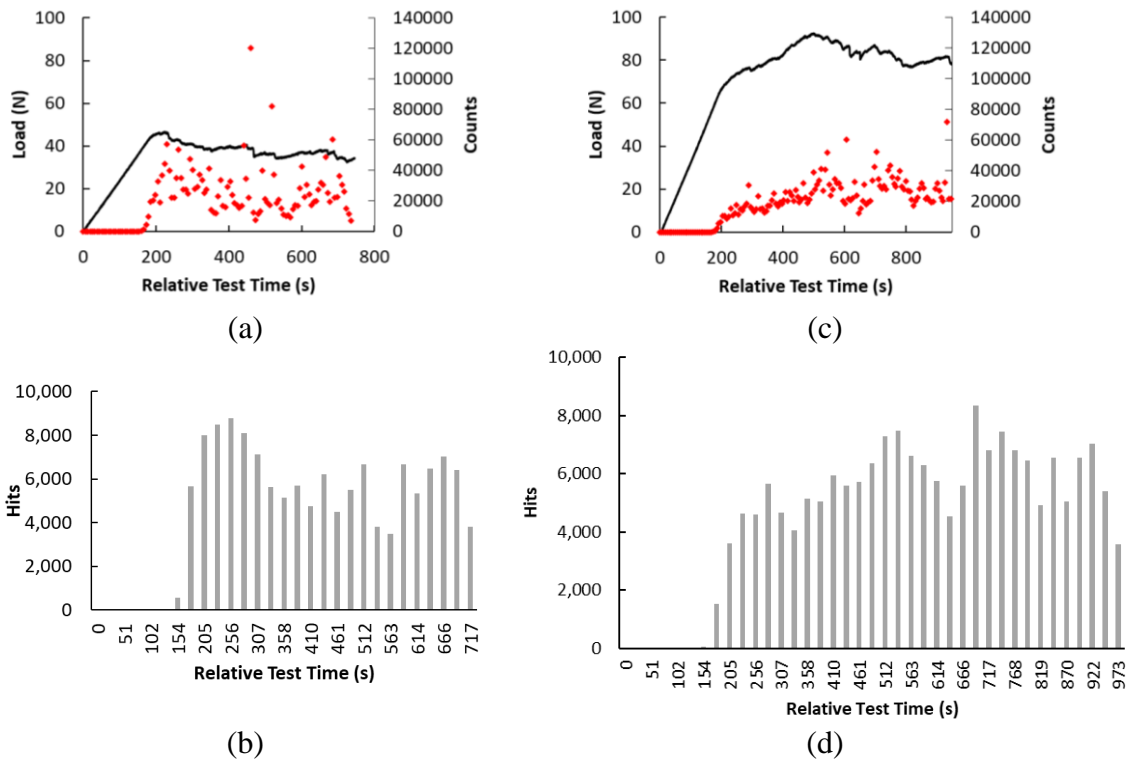


Figure 7-7 – Summary load profile (black), counts (red), and hits versus relative test time for (a-b), TGDDM-DDS Sample 1 and (c-d) TGDDM-DDS 20 wt% CSR Sample 5

The load versus time curves of the unmodified and 20 wt% CSR modified systems show quite different behaviour clearly reflected by their respective counts and hits. The unmodified resin shows a decaying load with increasing crack length which corresponds to a high number of hits at the start of the test but also decreases with crack length, indicating reduced acoustic activity during propagation. In contrast, the loading curve of the 20 wt% CSR system shows a series of events where the load exhibits stick-slip behaviour and a gradual increase during the later stages of crack propagation. This behaviour is consistent with a stick-slip phenomena where the crack front is continually arrested along the length of the DCB test regime. Similarly, the hits tend to peak near the peak load and diminish after the intermittent drop in load and the counts tend to remain constant suggesting an accumulation of damage prior to unloading. These instances were often observed to occur in conjunction with a visually apparent bridging at the crack tip or a jump in crack tip location along the edge of the sample specimens.

The mean and peak frequencies of AE signals were determined for all AE-DCB tests relative to the lead and lag sensors and are shown in Figure 7-8. Here, the peak events tended to occur at slightly higher magnitudes for sensor 1 versus sensor 2 and are attributed to the initial distance of 55 mm between the lag sensor 2 and the crack tip. As the crack propagates a slight

reduction in the difference between the signals is observed as the crack tip approaches sensor 2. For both the unmodified and CSR toughened laminates, the lower frequency (mean and peak) events (70-250 kHz) are the most common events throughout the test compared to the higher frequencies (250-550 kHz). Observation of the peak frequencies, highlight more clearly the differences in the AE response of the unmodified and toughened laminates. As can be seen in Figure 7-8(b) and (d), in the 250-550 kHz range, a two-fold increase in the peak frequency events occurring for the toughened laminates illustrates the greater number of energy dissipation events as would be expected for a toughened network. Typically, the test time of an unmodified laminate was 750 s while the toughened laminates were carried out to completion around 1000 s, further highlighting the enhanced resistance to crack propagation.

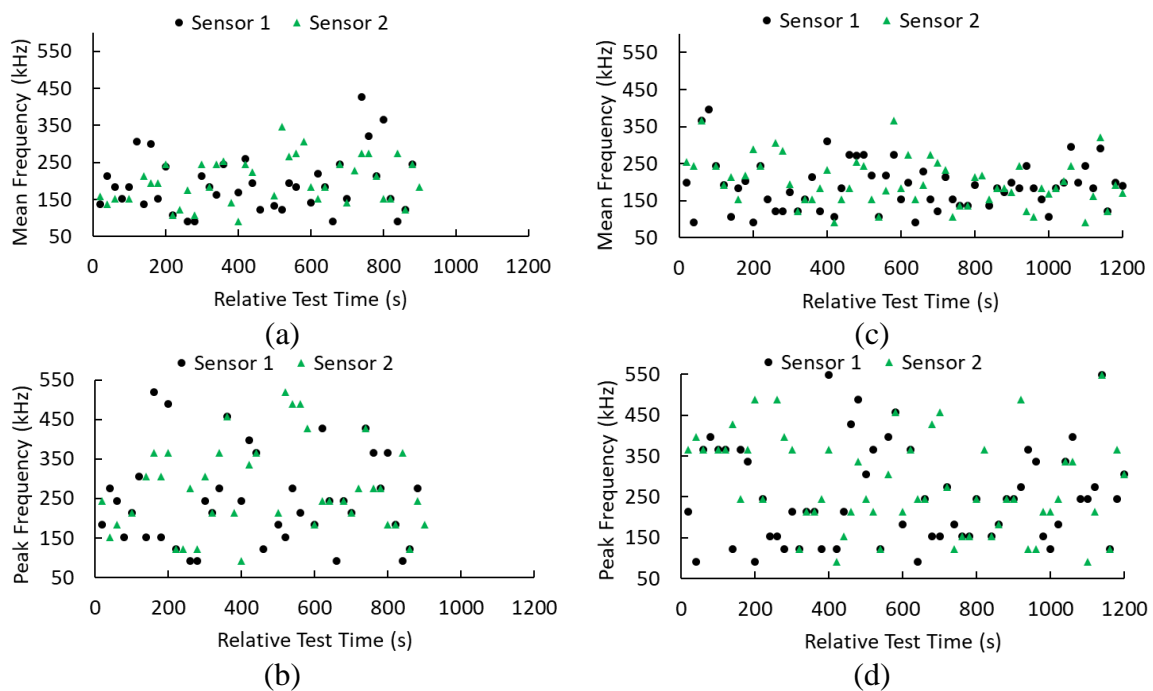


Figure 7-8 - Summary of mean and peak frequencies relative to test time for (a-b), TGDDM-DDS Sample 1 and (c-d) TGDDM-DDS 20 wt% CSR Sample 5

Previous work into the AE response of resins and composites emphasises the dependence of failure mechanisms on excitation frequency. While its not possible to specify the cut off frequencies exactly, lower frequency events are associated primarily with matrix failure while higher frequencies are associated with fibre-matrix interactions and interply failures. Figure 7-9(a) and (b) plots the number of events measured by the mean and peak frequencies respectively, measured by AE for bands of 70-150 kHz, and in 100 kHz increments up to a maximum 550 kHz. The peaks occurred above a threshold voltage of 10mV. For both mean

and peak frequencies, the most number of events occur in the 150-250 kHz range, still associated primarily with matrix failure. For the lower lower-frequency band (70-150 kHz), also likely to be matrix failure, the number of events between the unmodified and modified laminates are similar to each other. As the frequency bands increase from 150 to 550 kHz a higher number of peak events for the CSR toughened composites is observed. Clearly, increased matrix toughness is evident from the higher number of events at higher frequencies and reflects the importance of additional dissipation mechanisms related to fibre matrix and interply failure. Indeed peak frequencies above 250 kHz are associated with interply and fibre-dominated failure and correlate with the stick-slip behaviour observed during loading.

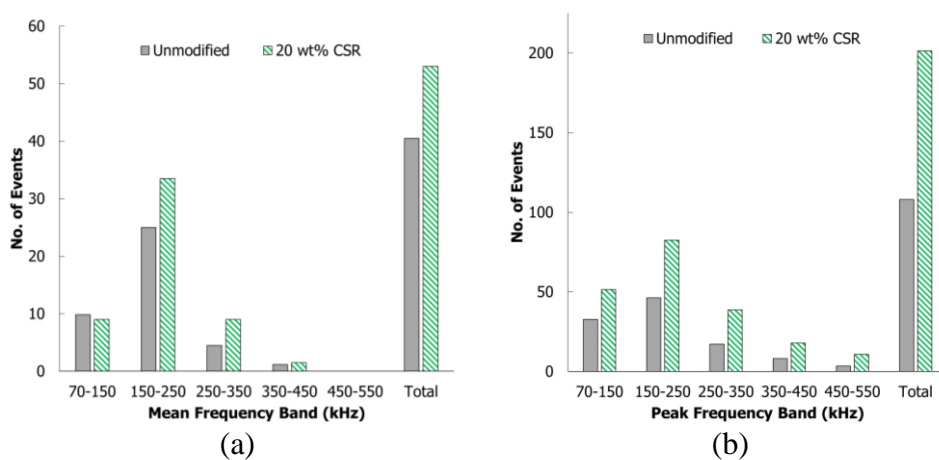


Figure 7-9 – Count of (a) mean frequencies and (b) peak frequency events per band for unmodified and 20 wt% CSR samples averaged across all AE tests

The R-curves of the unmodified and 20 wt% CSR modified epoxy composites are shown in Figure 7-10 and illustrate the large improvement in fracture toughness. The results are presented in Table 7-4 for the mode I strain energy release rate and the cumulative AE energy. Fracture toughness of the unmodified composite was 211.8 J/m² but increased to 454.1 J/m² an increase of 114.7%, significantly higher than the 45% improvement at the same concentration for the neat resin. This compares well with other studies which have ranged from improvements of 53-197% (K_{IC} and G_{IC}) using core shell rubber to toughen epoxy networks [30], [104], [105], [109], [112], [113]. For example, Riew et al. observed a 78% improvement to G_{IC} in a formulation containing diglycidyl ether of bisphenol A (DGEBA) and TGDDM cured with DDS [117].

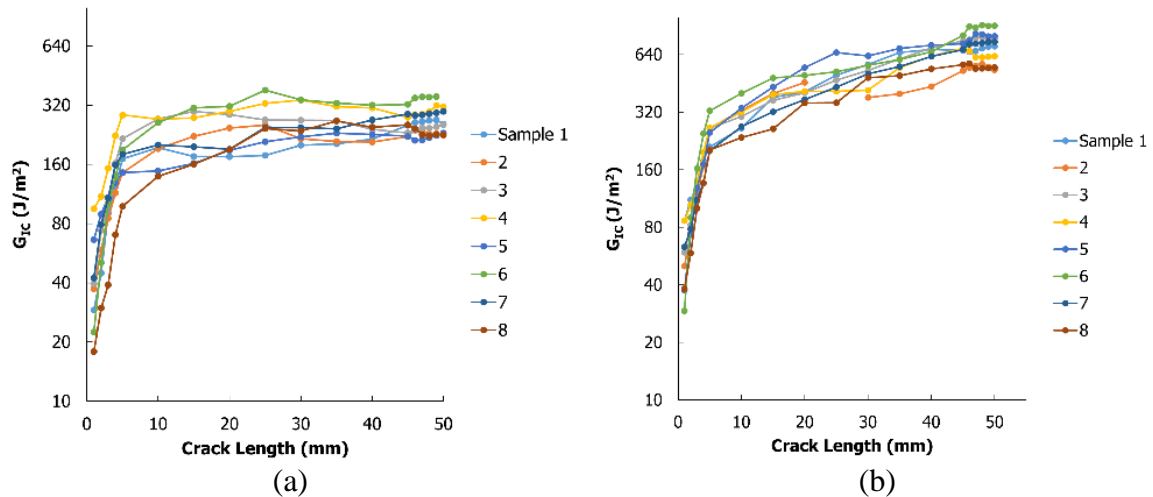


Figure 7-10 - Fracture toughness R-curves of (a) unmodified and (b) 20 wt% CSR laminates

Table 7-4 – Fracture toughness and cumulative AE energy

	G_{1c} Fracture Toughness (J/m²)	Cumulative AE Energy (J)
Unmodified	211.8 (\pm 36.5)	1.59 (\pm .71)
20 wt% CSR	454.1 (\pm 64.6)	2.06 (\pm .86)
% Diff.	114.7	29.56

7.4 SEM INVESTIGATION OF FAILURE MECHANISMS

Scanning electron microscopy (SEM) was carried out on segments of the composite in the region of 5, 25, and 50 mm lengths from the initial pre-crack. Images of the fracture surface of a resin-rich region from a segment cut from the 25 mm region are shown in Figure 7-11(a) and (b) for the unmodified and modified composites respectively. The fracture surfaces of the neat resin (Figure 7-11(a)) display brittle behaviour consisting of smooth surfaces and sharp ordered striations. Further evidence of brittle failure of the resin is shown on the surface of the matrix and fibre. The CSR modified laminate in Figure 7-11(b) shows markedly different behaviour, consistent with more ductile failure. Extensive cavitation of sub-micron sized particles is evident and the striations observed in Figure 7-11(a) are more abundant and ragged, similar in appearance to a rubber toughened composite and consistent with crazing and cavitation behavior [294].

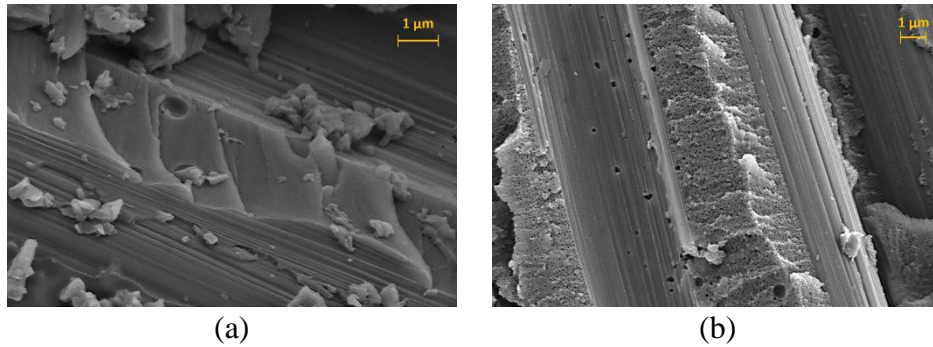


Figure 7-11 - SEM fractograms of the (a) unmodified and (b) 20 wt% CSR toughened composites taken from a segment of the laminate at the 25mm region of the crack length

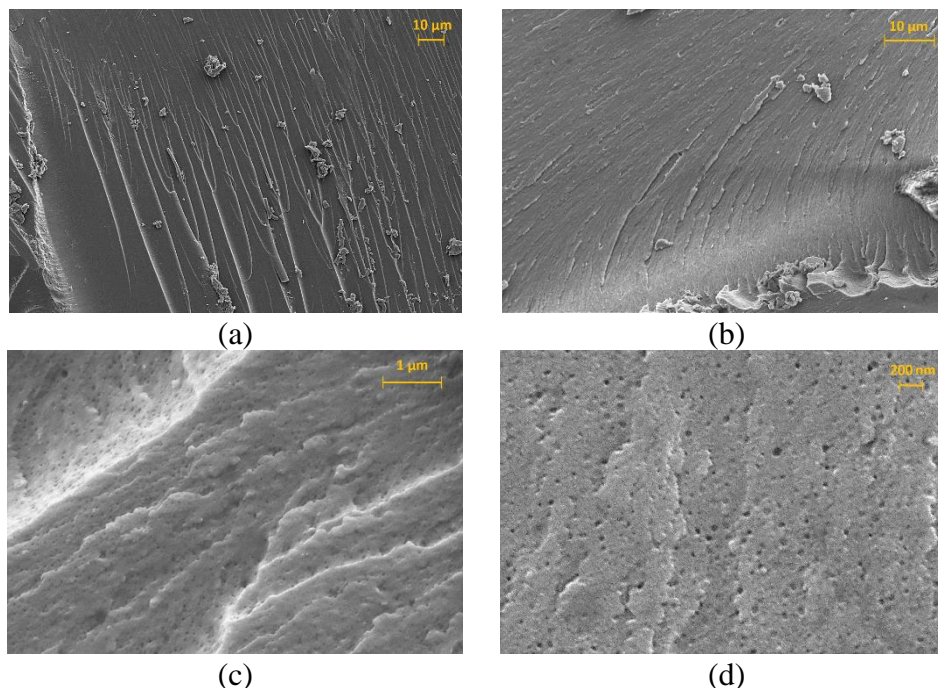


Figure 7-12 - SEM fractograms of the (a) unmodified and (b-d) 20 wt% CSR modified neat resins at different magnifications

With respect to the polymer network toughening, the effect of CSR addition is modest compared with other reported studies. The fracture surfaces of the unmodified network and selected images of the 20 wt% CSR modified network are shown Figure 7-12. The fracture surface of unmodified network shown in Figure 7-12(a) exhibits very brittle behavior and shows multiple parallel striations. Several images of the fracture surfaces of the 20 wt % CSR at various magnifications are shown in Figure 7-12(b)-(d) to illustrate the significant transformation from brittle to increasingly ductile behaviour. Extensive cavitation of sub-micron particles, stress whitening and shear band formation is evident. Importantly, and particularly evident in Figure 7-12(d) is the excellent dispersion of the CSR with no evidence

of large-scale agglomeration being apparent.

The large difference between the improvements in fracture of the neat resin and the composite may be attributed to a size effect described by Bagheri & Pearson [162], where they observed that thinner samples (1 mm) had higher toughness than thicker samples (max of 6 mm). The increase to toughness was also shown to follow a power law. Matrix-rich regions of the laminate have a much smaller aspect ratio. Also, CSR particles reduce the strength and stiffness of epoxy network. A combination of these two factors may contribute to the excellent improvement to the composite fracture toughness by CSR addition.

7.5 CONCLUSIONS

In summary, this study presents a CSR toughening study of a high T_g TGDDM/DDS network in neat polymer and composite form. Some key findings from this investigation are as follows:

1. CSR particles of a polybutadiene core and poly methyl methacrylate shell produce a modest increase in T_g and T_d of the cured network while decreasing the char yield and physical density.
2. CSR addition increases the cure reaction modestly while not affecting the chemistry to any significant degree, although the activation energy barrier increases with CSR addition.
3. Flexural modulus and strength all decrease with increasing CSR concentration while the strain to failure is unaffected.
4. Toughening (K_{IC}) of the neat resin was not observed for lower concentrations of CSR but achieved 11.4% and 45% improvement in fracture toughness at 15 wt% and 20 wt% CSR, respectively. The strain energy release rate (G_{IC}) displayed a 115% improvement for the 20 wt% CSR modified carbon fibre composite. Toughening mechanisms of the polymer and composite included cavitation and shear band formation.
5. Acoustic emission spectroscopy showed that the toughened matrix displayed significantly more AE events across a wide range of frequencies. This was particularly evident at higher frequencies and was attributed to the presence of additional fibre dominated toughening mechanisms operating.

8 CONCLUSIONS AND FUTURE WORK

The work presented in this thesis investigates the network development, thermal and mechanical performance, modification to the network, and toughening strategies for some high temperature epoxy resins. A summary of the findings and concluding remarks are provided as follows:

The network development of tetrafunctional glycidyl ether epoxy resins containing a dimeric naphthalene backbone (NNE) was investigated. Conversion of functional groups, kinetic rate constants, and the gelation and vitrification behaviour of the glycidyl ether resin is compared to a tetrafunctional glycidyl amine (TGDDM) to understand the effects of etherification and side reactions on the glass transition temperature. Network development of the glycidyl ether is characterised by rapid gelation and vitrification at a lower degree of epoxide conversion than TGDDM. The NNE network establishes a similar T_g under conventional isothermal curing and exceeds the T_g of TGDDM after post-curing above 200°C but exhibits a T_g of 350°C, albeit experimentally unattainable. The autocatalytic model agreed with the thermal mechanical analysis, showing rapid cure but ultimately lower conversion of functional groups. This behaviour was attributed to a combination of the high viscosity, rigid aromatic structure of the backbone, and inability of the glycidyl ether groups to undergo significant etherification and side reactions, in part due to the topologically-constrained network structure. The time-temperature-transformation behaviour of the resins were constructed to provide a framework for understanding the relation between gelation, vitrification, full cure, and degradation.

Properties of the cured networks of NNE, TGDDM, and a bi-component blend of the two resins were separately cured with an aromatic diamine and the bulk properties of the resins were studied. The rigid nature of the dimeric naphthalene backbone imparts high thermal stability as characterised by dynamic and isothermal gravimetric analysis at elevated temperatures. Consequently, the limited mobility and lower degree of conversion for the NNE network also exhibits higher moisture ingress, coefficient of thermal expansion, and a decrease to flexural properties. These are attributed to a higher free volume fraction in the cured network which was determined by the greater short range mobility shown in sub-ambient dynamic mechanical analysis. The rapid vitrification and low conversion result in a poor equilibrium packing density and even at elevated temperature post cure (240°C) little evidence of homopolymerisation or side reactions are evident, in contrast to the glycidyl amine, TGDDM. Nevertheless, the thermal stability of NNE was demonstrated for the neat resin at 250°C to be far superior to TGDDM

and the blend. Further long-term ageing of the carbon fibre composites demonstrated initially superior retention of mechanical properties and glass transition temperature even as weight loss of NNE exceeded TGDDM. Spectral analysis in the near infrared showed rapid growth of the overtone associated with C=O double bond for TGDDM and NTG but a delayed response for NNE, suggesting better resistance to network degradation. Eventually, however, all three matrix systems catastrophically degrade. It is shown then, that NNE cured with an aromatic diamine can serve as a structural matrix for applications where extended periods of elevated temperatures are frequent.

A series of approaches are taken to alter characteristics and properties of the NNE resin at the network level. Both reactive and non-reactive diluents (CGE, NAPH), partially-reacted substructures (33CGE, 44CGE), and a molecular fortifier were added to the uncured network. It was shown that the CGE, NAPH, MFN, and 33CGE exhibited the phenomenon of antiplasticisation as characterised by an increase to the glassy modulus. The 44CGE showed signs of plasticisation, a reduction to modulus and strength. Sub-ambient dynamic mechanical analysis confirmed a reduction to the β -transition and suppression of molecular mobility, a signature attributed to antiplasticised resins. While fracture toughness was significantly reduced for CGE, 33CGE, and 44CGE, there was a retention and slight benefits for the NAPH and MFN resins. Further study of the rheological performance showed a significant reduction to the complex viscosity and an expansion between melt and gelation for CGE and NAPH, which demonstrates their efficacy as diluents for ease of processing. Further, the CGE, NAPH, and MFN resins reduced equilibrium moisture uptake. The combination of increased stiffness and reduced moisture uptake is taken as a sign that the free volume fraction of the unmodified NNE resins is partly occupied. Translation of the neat resin properties after the addition of the fortifiers showed enhanced stiffness across the range of modifiers although the NAPH diluent exhibited poor interlaminar qualities. These modifiers can successfully enhance processability and stiffness of the topologically constrained NNE network with some tertiary benefits to material performance.

Core shell rubber particles at the sub-micron scale are used to investigate the toughenability of a high-temperature, highly aromatic epoxy-amine resin. The commercial TGDDM resin is cured with 3,3'-diaminodiphenylsulfone. A combination of thermal, spectral, and rheological analysis showed minimal effect of the CSR particles on the cure and processability of the resins, even at 20 wt% CSR loading. Further, the glass transition temperature remained virtually

unaffected. Mechanical testing of the neat resins demonstrated signs of improved notched fracture toughness at concentrations of 15-20 wt% while flexural strength and stiffness tended to decrease with increased CSR loading. The maximum improvement to the resin fracture toughness was shown for 20 wt% CSR and increased over the unmodified fracture toughness by 45%. The mode I strain energy release rate (G_{IC}) of carbon fibre composites manufactured with 20 wt% CSR were compared using a multispectral testing approach using advanced acoustic emission (AE) sensing in situ with mechanical tests. It was shown that the G_{IC} increased 115% over the unmodified laminate. Spectral analysis by AE was correlated to higher rates of interply and fibre-dominant failure modes of the CSR toughened laminate where mostly lower-energy matrix failure events were detected in the unmodified laminate. The study indicates that CSR particles can successfully toughen highly cross-linked network and are translatable to the composite.

8.1 SUMMARY AND FUTURE WORKS

Aspects of this work demonstrate the effectiveness of a unique tetrafunctional glycidyl ether epoxy resin as a thermally-stable and high temperature matrix for composites. The NNE resin can exhibit properties, when cured with an aromatic diamine, that have similar mechanical performance and superior thermal stability to conventional TGDDM-based resins which offers promise either as a resin for or a component of matrix systems for structural applications that demand high heat performance and stability. Future works in continuation with the study presented here could include:

- ◁ Exploration of stoichiometry on cure conversion and network development of NNE to achieve higher epoxide conversion
- ◁ Use of other hydrocarbon molecules such as anthracene as network fortifiers for high temperature polymers
- ◁ Partially-reacted structures as network modifiers using monofunctional amines pendant to the network
- ◁ Exploration of toughenability for the NNE resin via core shell particles and effect of high thermal loads on efficacy of CSR tougheners

9 REFERENCES

- [1] “A350 XWB Family.” <http://www.airbus.com/aircraft/passenger-aircraft/a350xwb-family.html> (accessed Feb. 02, 2018).
- [2] “The markets: Civil infrastructure (2017) : CompositesWorld.” <https://www.compositesworld.com/articles/the-markets-civil-infrastructure-2016> (accessed Jun. 14, 2018).
- [3] “The markets: Boatbuilding and marine (2015) : CompositesWorld.” <https://www.compositesworld.com/articles/the-markets-boatbuilding-and-marine-2015> (accessed Jun. 14, 2018).
- [4] “The markets: Sports and recreation (2017) : CompositesWorld.” <https://www.compositesworld.com/articles/the-markets-sports-and-recreation-2016> (accessed Jun. 14, 2018).
- [5] “Aviation Outlook: Composites in General Aviation 2011-2020 : CompositesWorld.” <https://www.compositesworld.com/articles/aviation-outlook-composites-in-general-aviation-2011-2020> (accessed Jun. 14, 2018).
- [6] M. McClure, “The rising need for plastics in aerospace,” *Upstate Business Journal*, 2018.
- [7] M. Sauer and M. Kühnel, “Composites Market Report 2017 The global CF-and CC-Market –,” 2017.
- [8] S. Ebnesajjad, “Introduction to Plastics,” in *Chemical Resistance of Commodity Thermoplastics*, Elsevier, 2016, pp. xiii–xxv.
- [9] E. A. Campo, “Thermal Properties of Polymeric Materials,” in *Selection of Polymeric Materials*, Elsevier, 2008, pp. 103–140.
- [10] S. Ray and R. P. Cooney, “Thermal degradation of polymer and polymer composites,” in *Handbook of Environmental Degradation Of Materials: Third Edition*, Elsevier Inc., 2018, pp. 185–206.
- [11] W. Fan, J. L. Li, Y. Y. Zheng, T. J. Liu, X. Tian, and R. J. Sun, “Influence of thermo-oxidative aging on the thermal conductivity of carbon fiber fabric reinforced epoxy composites,” *Polym. Degrad. Stab.*, vol. 123, pp. 162–169, Jan. 2016, doi: 10.1016/j.polymdegradstab.2015.11.016.

- [12] F. Rezaei, R. Yunus, and N. A. Ibrahim, "Effect of fiber length on thermomechanical properties of short carbon fiber reinforced polypropylene composites," *Mater. Des.*, vol. 30, no. 2, pp. 260–263, Feb. 2009, doi: 10.1016/j.matdes.2008.05.005.
- [13] H. Stutz, "Lifetime assessment of epoxies by the kinetics of thermal degradation," *J. Appl. Polym. Sci.*, vol. 91, no. 3, pp. 1881–1886, Feb. 2004, doi: 10.1002/app.13240.
- [14] M. R. Tant, H. L. N. Mcmanus, and M. E. Rogers, "High-Temperature Properties and Applications of Polymeric Materials An Overview," 2018.
- [15] Pure, Appl, and Chern, "Composites for high temperatures," vol. 60, no. 3, pp. 287–302, 1988.
- [16] G. Henson, "Materials for Launch Vehicle Structures."
- [17] P. M. Hergenrother, "The Use, Design, Synthesis, and Properties of High Performance/High Temperature Polymers: An Overview," *High Perform. Polym.*, vol. 15, no. 1, pp. 3–45, Mar. 2003, doi: 10.1177/095400830301500101.
- [18] C.-S. Wang and M.-C. Lee, "Synthesis and modification of a naphthalene-containing trifunctional epoxy resin for electronic applications," *J. Appl. Polym. Sci.*, vol. 70, no. 10, pp. 1907–1921, Dec. 1998, doi: 10.1002/(SICI)1097-4628(19981205)70:10<1907::AID-APP5>3.0.CO;2-Y.
- [19] S. P. Rwei, C. Y. Cheng, G. S. Liou, and K. C. Cheng, "Curing and pyrolysis of cresol novolac epoxy resins containing BABODOPN," *Polym. Eng. Sci.*, vol. 45, no. 4, pp. 478–486, Apr. 2005, doi: 10.1002/pen.20305.
- [20] C.-S. Wang and H.-J. Hwang, "Investigation of bismaleimide containing naphthalene unit. II. Thermal behavior and properties of polymer," *J. Polym. Sci. Part A Polym. Chem.*, vol. 34, no. 8, pp. 1493–1500, Jun. 1996, doi: 10.1002/(SICI)1099-0518(199606)34:8<1493::AID-POLA13>3.0.CO;2-3.
- [21] C.-S. Wang and M.-C. Lee, "Synthesis, characterization, and properties of multifunctional naphthalene-containing epoxy resins cured with cyanate ester," *J. Appl. Polym. Sci.*, vol. 73, no. 9, pp. 1611–1622, Aug. 1999, doi: 10.1002/(SICI)1097-4628(19990829)73:9<1611::AID-APP2>3.0.CO;2-8.
- [22] A. Matsumoto, K. Hasegawa, and A. Fukuda, "Studies on modified phenolic resin. Iv: Properties of phenolic resin modified with 4-hydroxyphenyl- maleimide/n-

- butylacrylate copolymers,” *Polym. Int.*, vol. 30, no. 1, pp. 65–72, 1993, doi: 10.1002/pi.4990300110.
- [23] J.-P. Pascault and R. J. J. Williams, “General Concepts about Epoxy Polymers,” in *Epoxy Polymers*, Weinheim, Germany: Wiley-VCH Verlag GmbH & Co. KGaA, 2010, pp. 1–12.
- [24] L. Xu and J. R. Schlup, “Etherification versus amine addition during epoxy resin/amine cure: An in situ study using near-infrared spectroscopy,” *J. Appl. Polym. Sci.*, vol. 67, no. 5, pp. 895–901, Jan. 1998, doi: 10.1002/(SICI)1097-4628(19980131)67:5<895::AID-APP15>3.0.CO;2-N.
- [25] L. Matějka, “Amine cured epoxide networks: Formation, structure, and properties,” *Macromolecules*, vol. 33, no. 10, pp. 3611–3619, 2000, doi: 10.1021/ma991831w.
- [26] R. J. Iredale, C. Ward, and I. Hamerton, *Modern advances in bismaleimide resin technology: A 21st century perspective on the chemistry of addition polyimides*, vol. 69. 2017, pp. 1–21.
- [27] T. Takeichi and N. Furukawa, “Epoxy Resins and Phenol-Formaldehyde Resins,” in *Polymer Science: A Comprehensive Reference, 10 Volume Set*, vol. 5, Elsevier, 2012, pp. 723–751.
- [28] T. Liu *et al.*, “Nitrogen-Free Tetrafunctional Epoxy and Its DDS-Cured High-Performance Matrix for Aerospace Applications,” *Ind. Eng. Chem. Res.*, vol. 56, no. 27, pp. 7708–7719, Jul. 2017, doi: 10.1021/acs.iecr.7b00096.
- [29] T. H. Hsieh, M. Y. Shen, Y. S. Huang, Q. Q. He, and H. C. Chen, “Mechanical properties of glass bead-modified polymer composite,” *Polym. Polym. Compos.*, vol. 26, no. 1, pp. 35–43, 2018, doi: 10.1177/096739111802600105.
- [30] K. T. Gam, M. Miyamoto, R. Nishimura, and H. J. Sue, “Fracture behavior of core-shell rubber-modified clay-epoxy nanocomposites,” *Polym. Eng. Sci.*, vol. 43, no. 10, pp. 1635–1645, Oct. 2003, doi: 10.1002/pen.10137.
- [31] R. J. Varley, J. H. Hodgkin, D. G. Hawthorne, G. P. Simon, and D. McCulloch, “Toughening of a trifunctional epoxy system: Part III. Kinetic and morphological study of the thermoplastic modified cure process,” *Polymer (Guildf.)*, vol. 41, no. 9, pp. 3425–3436, 2000, doi: 10.1016/S0032-3861(99)00503-0.

- [32] A. J. Kinloch, M. L. Yuen, and S. D. Jenkins, “Thermoplastic-toughened epoxy polymers,” 1994.
- [33] M. J. Marks, N. E. Verghese, C. L. O’Connell, and A. S. Mansour, “The effects of monoepoxide chain termination and their derived soluble fractions on the structure-property relationships of controlled epoxy networks,” *J. Polym. Sci. Part B Polym. Phys.*, vol. 47, no. 1, pp. 72–79, Jan. 2009, doi: 10.1002/polb.21614.
- [34] J. Daly, A. Britten, A. Garton, and P. D. McLean, “An additive for increasing the strength and modulus of amine-cured epoxy resins,” *J. Appl. Polym. Sci.*, vol. 29, no. 4, pp. 1403–1414, Apr. 1984, doi: 10.1002/app.1984.070290433.
- [35] P. Musto, E. Martuscelli, G. Ragosta, P. Russo, and G. Scarinzi, “An interpenetrated system based on a tetrafunctional epoxy resin and a thermosetting bismaleimide: Structure-properties correlation,” *J. Appl. Polym. Sci.*, vol. 69, no. 5, pp. 1029–1042, Aug. 1998, doi: 10.1002/(SICI)1097-4628(19980801)69:5<1029::AID-APP23>3.0.CO;2-V.
- [36] E. Barjasteh, S. Gouni, C. Sutanto, and P. Narongdej, “Bisphenol-A benzoxazine and cycloaliphatic epoxy copolymer for composite processing by resin infusion,” *J. Compos. Mater.*, vol. 53, no. 13, pp. 1777–1790, Jun. 2019, doi: 10.1177/0021998318810841.
- [37] I. Ogura and Y. Takahashi, “Multi-functional epoxy resins performing high thermal resistance with good flow-ability based on dimeric Naphthols,” *High Perform. Polym.*, vol. 22, no. 7, pp. 834–847, Nov. 2010, doi: 10.1177/0954008309347638.
- [38] K. Fila, M. Gargol, M. Goliszek, and B. Podkościelna, “Synthesis of epoxy resins derivatives of naphthalene-2,7-diol and their cross-linked products,” *J. Therm. Anal. Calorim.*, vol. 138, no. 6, pp. 4349–4358, Dec. 2019, doi: 10.1007/s10973-019-08852-y.
- [39] C.-S. Wang, T.-S. Leu, and K.-R. Hsu, “Novel bismaleimide with naphthalene side group. 1. From 1-naphthaldehyde and 2,6-dimethylaniline,” *Polymer (Guildf)*, vol. 39, no. 13, pp. 2921–2927, Jun. 1998, doi: 10.1016/S0032-3861(97)10008-8.
- [40] G. Pan, Z. Du, C. Zhang, C. Li, X. Yang, and H. Li, “Synthesis, characterization, and properties of novel novolac epoxy resin containing naphthalene moiety,” *Polymer (Guildf)*, vol. 48, no. 13, pp. 3686–3693, Jun. 2007, doi:

- 10.1016/J.POLYMER.2007.04.032.
- [41] F. Vuković, S. R. Swan, L. Q. Reyes, R. J. Varley, and T. R. Walsh, “Beyond the ring flip: A molecular signature of the glass–rubber transition in tetrafunctional epoxy resins,” *Polymer (Guildf)*., vol. 206, p. 122893, Oct. 2020, doi: 10.1016/j.polymer.2020.122893.
- [42] Y.-F. Duann, B.-L. Chen, and T.-H. Tsai, “Mechanical properties of copper-clad laminate using composite naphthalene-phenyl-based epoxy as prepreg,” *J. Appl. Polym. Sci.*, vol. 95, no. 6, pp. 1485–1492, Mar. 2005, doi: 10.1002/app.21399.
- [43] C.-S. Wang and T.-S. Leu, “Novel bismaleimide with naphthalene and aryl ether linkages,” *J. Appl. Polym. Sci.*, vol. 73, no. 5, pp. 833–839, Aug. 1999, doi: 10.1002/(SICI)1097-4628(19990801)73:5<833::AID-APP24>3.0.CO;2-1.
- [44] C.-S. Wang and T.-S. Leu, “Synthesis and characterization of polyimides containing naphthalene pendant group and flexible ether linkages,” *Polymer (Guildf)*., vol. 41, no. 10, pp. 3581–3591, May 2000, doi: 10.1016/S0032-3861(99)00613-8.
- [45] H. Yan, H. Wang, and J. Cheng, “Interpenetrating polymer networks from the novel bismaleimide and cyanate containing naphthalene: Cure and thermal characteristics,” *Eur. Polym. J.*, vol. 45, no. 8, pp. 2383–2390, Aug. 2009, doi: 10.1016/J.EURPOLYMJ.2009.04.031.
- [46] A. Hodzic, J. K. Kim, A. E. Lowe, and Z. H. Stachurski, “The effects of water aging on the interphase region and interlaminar fracture toughness in polymer–glass composites,” *Compos. Sci. Technol.*, vol. 64, no. 13–14, pp. 2185–2195, Oct. 2004, doi: 10.1016/J.COMPSCITECH.2004.03.011.
- [47] T. Agag, S. Geiger, S. M. Alhassan, S. Qutubuddin, and H. Ishida, “Low-Viscosity Polyether-Based Main-Chain Benzoxazine Polymers: Precursors for Flexible Thermosetting Polymers,” *Macromolecules*, vol. 43, no. 17, pp. 7122–7127, Sep. 2010, doi: 10.1021/ma1014337.
- [48] N. N. Ghosh, B. Kiskan, and Y. Yagci, “Polybenzoxazines—New high performance thermosetting resins: Synthesis and properties,” *Prog. Polym. Sci.*, vol. 32, no. 11, pp. 1344–1391, Nov. 2007, doi: 10.1016/J.PROGPOLYMSCI.2007.07.002.
- [49] A. Hariharan, K. Srinivasan, C. Murthy, and M. Alagar, “A Novel Imidazole-Core-

- Based Benzoxazine and Its Blends for High-Performance Applications,” *Ind. Eng. Chem. Res.*, vol. 56, no. 33, pp. 9347–9354, Aug. 2017, doi: 10.1021/acs.iecr.7b01816.
- [50] B.-Y. Ryu and T. Emrick, “Bisphenol-1,2,3-triazole (BPT) Epoxies and Cyanate Esters: Synthesis and Self-Catalyzed Curing,” *Macromolecules*, vol. 44, no. 14, pp. 5693–5700, Jul. 2011, doi: 10.1021/ma200767j.
- [51] N. J. Suman, S. K. Pathak, and S. Tammishetti, “Assessment of Bismaleimide-modified Cyanate Ester as Matrix Resin for Elevated Service Temperature Carbon Composite Applications,” *J. Reinf. Plast. Compos.*, vol. 24, no. 10, pp. 1105–1114, Jul. 2005, doi: 10.1177/0731684405048835.
- [52] C. A. Corley *et al.*, “Di(cyanate Ester) Networks Based on Alternative Fluorinated Bisphenols with Extremely Low Water Uptake,” *ACS Macro Lett.*, vol. 3, no. 1, pp. 105–109, Jan. 2014, doi: 10.1021/mz400520s.
- [53] Z. Ren, Y. Cheng, L. Kong, and F. Xiao, “Preparation and characterization of a high Tg cyanate ester/epoxy composite resin,” in *2014 15th International Conference on Electronic Packaging Technology*, May 2014, pp. 288–291, doi: 10.1109/ICEPT.2014.6922656.
- [54] L. Li Huang, C. Chen Wang, and Y. Yafei Lu, “Thermal and Moisture Adsorption Properties of Cyanate Ester Modified Epoxy Resin and Fiber-Glass Composites,” *J. Reinf. Plast. Compos.*, vol. 27, no. 7, pp. 725–738, May 2008, doi: 10.1177/0731684407084251.
- [55] Z. Liu, L. Yuan, G. Liang, and A. Gu, “Tough epoxy/cyanate ester resins with improved thermal stability, lower dielectric constant and loss based on unique hyperbranched polysiloxane liquid crystalline,” *Polym. Adv. Technol.*, vol. 26, no. 12, pp. 1608–1618, Dec. 2015, doi: 10.1002/pat.3590.
- [56] R. J. Morgan, R. J. Jurek, A. Yen, and T. Donnellan, “Toughening procedures, processing and performance of bismaleimide-carbon fibre composites,” *Polymer (Guildf)*, vol. 34, no. 4, pp. 835–842, Feb. 1993, doi: 10.1016/0032-3861(93)90371-G.
- [57] Z. Karami, M. J. Zohuriaan-Mehr, and A. Rostami, “Biobased Diels-Alder Engineered Network from Furfuryl Alcohol and Epoxy Resin: Preparation and Mechano-Physical Characteristics,” *ChemistrySelect*, vol. 3, no. 1, pp. 40–46, Jan. 2018, doi: 10.1002/slct.201702387.

- [58] P. Musto, G. Ragosta, P. Russo, and L. Mascia, "Thermal-Oxidative Degradation of Epoxy and Epoxy-Bismaleimide Networks: Kinetics and Mechanism," *Macromol. Chem. Phys.*, vol. 202, no. 18, pp. 3445–3458, Dec. 2001, doi: 10.1002/1521-3935(20011201)202:18<3445::AID-MACP3445>3.0.CO;2-N.
- [59] R. K. Jena, C. Y. Yue, M. M. Sk, and K. Ghosh, "A novel high performance bismaleimide/diallyl bisphenol A (BMI/DBA)–epoxy interpenetrating network resin for rigid riser application," *RSC Adv.*, vol. 5, no. 97, pp. 79888–79897, Sep. 2015, doi: 10.1039/C5RA14474D.
- [60] D. S. Kim, M. J. Han, and J. R. Lee, "Cure behavior and properties of an epoxy resin modified with a bismaleimide resin," *Polym. Eng. Sci.*, vol. 35, no. 17, pp. 1353–1358, Sep. 1995, doi: 10.1002/pen.760351705.
- [61] J. L. MASSINGILL and R. S. BAUER, "EPOXY RESINS," in *Applied Polymer Science: 21st Century*, Elsevier, 2000, pp. 393–424.
- [62] I. Hamerton, *Chemistry and Technology of Cyanate Ester Resins*. Springer Netherlands, 1994.
- [63] G. Gibson, "Epoxy Resins," in *Brydson's Plastics Materials: Eighth Edition*, Elsevier Inc., 2017, pp. 773–797.
- [64] H. Liu, A. Uhlherr, R. J. Varley, and M. K. Bannister, "Influence of substituents on the kinetics of epoxy/aromatic diamine resin systems," *J. Polym. Sci. Part A Polym. Chem.*, vol. 42, no. 13, pp. 3143–3156, Jul. 2004, doi: 10.1002/pola.20169.
- [65] S. Beck and R. Narain, "Polymer synthesis," in *Polymer Science and Nanotechnology*, Elsevier, 2020, pp. 21–85.
- [66] C. C. Riccardi and R. J. J. Williams, "A kinetic scheme for an amine-epoxy reaction with simultaneous etherification," *J. Appl. Polym. Sci.*, vol. 32, no. 2, pp. 3445–3456, Aug. 1986, doi: 10.1002/app.1986.070320208.
- [67] L. Xu and J. R. Schlup, "Etherification Versus Amine Addition During Epoxy Resin/ Amine Cure: An In Situ Study Using Near-Infrared Spectroscopy," 1998. doi: 10.1002/(SICI)1097-4628(19980131)67:5.
- [68] W. H. Stockmayer, "Theory of molecular size distribution and gel formation in branched-chain polymers," *J. Chem. Phys.*, vol. 11, no. 2, pp. 45–55, 1943, doi:

10.1063/1.1723803.

- [69] L. Matějka, K. Dušek, and I. Dobáš, “Curing of epoxy resins with amines - Gelation of polyepoxides derived from diglycidylaniline,” *Polym. Bull.*, vol. 14, no. 3–4, pp. 309–315, Oct. 1985, doi: 10.1007/BF00254954.
- [70] N. A. St John and G. A. George, “Cure kinetics and mechanisms of a tetraglycidyl-4,4'-diaminodiphenylmethane/diaminodiphenylsulphone epoxy resin using near i.r. spectroscopy,” *Polymer (Guildf.)*, vol. 33, no. 13, pp. 2679–2688, Jan. 1992, doi: 10.1016/0032-3861(92)90438-3.
- [71] Y. Tanaka, J. L. Stanford, and R. Stepto, “Interpretation of gel points of an epoxy-amine system including ring formation and unequal reactivity: Measurements of gel points and analyses on ring structures,” *Macromolecules*, vol. 45, no. 17, pp. 7197–7205, Sep. 2012, doi: 10.1021/ma3009838.
- [72] M. T. Demeuse, “Introduction to high temperature polymer blends,” in *High Temperature Polymer Blends*, Cambridge, United Kingdom: Woodhead Publishing, 2014, pp. 1–13.
- [73] L. Barral, J. Cano, J. López, P. Nogueira, C. Ramírez, and M. J. Abad, “Isothermal Cure of an Epoxy System Containing Tetraglycidyl-4,4'-diaminodiphenylmethane (TGDDM), a Multifunctional Novolac Glycidyl Ether and 4,4'-Diaminodiphenylsulphone (DDS): Vitrification and Gelation,” *Polym. Int.*, vol. 42, no. 3, pp. 301–306, Mar. 1997, doi: 10.1002/(SICI)1097-0126(199703)42:3<301::AID-PI714>3.0.CO;2-F.
- [74] Y. Zhang, C. Shang, X. Yang, @bullet Xiaojuan, Z. @bullet, and W. Huang, “Morphology and properties of TGDDM/DDS epoxy systems toughened by amino-bearing phenyl silicone resins,” doi: 10.1007/s10853-012-6298-1.
- [75] P. Guerrero, K. De La Caba, A. Valea, M. A. Corcuera, and I. Mondragon, “Influence of cure schedule and stoichiometry on the dynamic mechanical behaviour of tetrafunctional epoxy resins cured with anhydrides,” *Polymer (Guildf.)*, vol. 37, no. 11, pp. 2195–2200, May 1996, doi: 10.1016/0032-3861(96)85865-4.
- [76] O. Becker, G. P. Simon, R. J. Varley, and P. J. Hal, “Layered Silicate Nanocomposites Based on Various High-Functionality Epoxy Resins: The Influence of an Organoclay on Resin Cure.”

- [77] Š. Podzimek, I. Dobáš, Š. Švestka, M. Tkaczyk, M. Kubín, and V. Štěřba, "Epoxy resins based on aromatic glycidylamines. IV. Preparation of N,N,N',N'-tetraglycidyl-4,4'-diaminodiphenylmethane from aniline and analysis of the product by GPC and HPLC," *J. Appl. Polym. Sci.*, vol. 42, no. 3, pp. 795–800, Feb. 1991, doi: 10.1002/app.1991.070420323.
- [78] S. V. Levchik *et al.*, "Mechanistic study of thermal behaviour and combustion performance of epoxy resins. II. TGDDM/DDS system," *Polym. Degrad. Stab.*, vol. 48, no. 3, pp. 359–370, Jan. 1995, doi: 10.1016/0141-3910(95)00084-Y.
- [79] L. Matějka, S. Podzimek, and K. Dušek, "Differences in structure growth in amine curing of diglycidyl ether of bisphenol a and N,N-diglycidylaniline epoxy resins: Bifunctional models," *J. Polym. Sci. Part A Polym. Chem.*, vol. 33, no. 3, pp. 473–480, Feb. 1995, doi: 10.1002/pola.1995.080330314.
- [80] B.-G. Min, J. H. Hodgkin, and Z. H. Stachurski, "Reaction mechanisms, microstructure, and fracture properties of thermoplastic polysulfone-modified epoxy resin," *J. Appl. Polym. Sci.*, vol. 50, no. 6, pp. 1065–1073, Nov. 1993, doi: 10.1002/app.1993.070500615.
- [81] A. Xing *et al.*, "Tertiary-amine-free, non-planar, fluorine-containing tetrafunctional epoxy and its application as high performance matrix," *Polym. Test.*, vol. 71, pp. 38–48, Oct. 2018, doi: 10.1016/j.polymertesting.2018.08.022.
- [82] Y.-F. Duann, T.-M. Liu, K.-C. Cheng, and W.-F. Su, "Thermal stability of some naphthalene- and phenyl-based epoxy resins," *Polym. Degrad. Stab.*, vol. 84, no. 2, pp. 305–310, May 2004, doi: 10.1016/J.POLYMDEGRADSTAB.2004.01.016.
- [83] P. Gradin, P. G. Howgate, R. Seldén, and R. A. Brown, "Dynamic-mechanical Properties," in *Comprehensive Polymer Science and Supplements*, Elsevier, 1989, pp. 533–569.
- [84] C. U. Pittman, "Polymer Supported Catalysts," in *Comprehensive Organometallic Chemistry*, vol. 8, Elsevier Inc., 1982, pp. 553–611.
- [85] J. M. Stuart and D. A. Smith, "Some aspects of the degradation of epoxide resins," *J. Appl. Polym. Sci.*, vol. 9, no. 9, pp. 3195–3214, Sep. 1965, doi: 10.1002/APP.1965.070090923.

- [86] M. A. Keenan and D. A. Smith, "Further aspects of the thermal degradation of epoxide resins," *J. Appl. Polym. Sci.*, vol. 11, no. 7, pp. 1009–1026, Jul. 1967, doi: 10.1002/app.1967.070110701.
- [87] D. P. Bishop and D. A. Smith, "Combined pyrolysis and radiochemical gas chromatography for studying the thermal degradation of epoxy resins and polyimides. I. The degradation of epoxy resins in nitrogen between 400°C and 700°C," *J. Appl. Polym. Sci.*, vol. 14, no. 1, pp. 205–223, Jan. 1970, doi: 10.1002/app.1970.070140120.
- [88] N. Grassie, M. I. Guy, and N. H. Tennent, "Degradation of epoxy polymers: Part 1—Products of thermal degradation of bisphenol-A diglycidyl ether," *Polym. Degrad. Stab.*, vol. 12, no. 1, pp. 65–91, Jan. 1985, doi: 10.1016/0141-3910(85)90057-6.
- [89] S. V. Levchik *et al.*, "Mechanistic study of thermal behavior and combustion performance of epoxy resins: I homopolymerized TGDDM," *Polym. Adv. Technol.*, vol. 6, no. 2, pp. 53–62, Feb. 1995, doi: 10.1002/pat.1995.220060201.
- [90] S. V. Levchik *et al.*, "Mechanistic study of thermal behaviour and combustion performance of epoxy resins. II. TGDDM/DDS system," *Polym. Degrad. Stab.*, vol. 48, no. 3, pp. 359–370, Jan. 1995, doi: 10.1016/0141-3910(95)00084-Y.
- [91] A. Al-Yami, V. Wagle, W. C. Jimenez, and P. Jones, "Evaluation of Epoxy Resin Thermal Degradation and its Effect on Preventing Sustained Casing Pressure in Oil and Gas Wells," *Arab. J. Sci. Eng.*, vol. 44, no. 6, pp. 6109–6118, Jun. 2019, doi: 10.1007/s13369-018-3651-y.
- [92] Y. F. Yu, J. Cui, W. J. Chen, and S. J. Li, "Studies on the Phase Separation of Polyetherimide Modified Tetrafunctional Epoxy Resin. II. Effects of the Molecular Weight," vol. 35, no. 1, pp. 121–135, 1998.
- [93] X. Cheng, Q. Wu, S. E. Morgan, and J. S. Wiggins, "Morphologies and mechanical properties of polyethersulfone modified epoxy blends through multifunctional epoxy composition," *J. Appl. Polym. Sci.*, vol. 134, 2017, doi: 10.1002/app.44775.
- [94] J. N. Suman, J. Kathi, and S. Tammishetti, "Thermoplastic modification of monomeric and partially polymerized Bisphenol A dicyanate ester," *Eur. Polym. J.*, vol. 41, no.

- 12, pp. 2963–2972, Dec. 2005, doi: 10.1016/J.EURPOLYMJ.2005.06.006.
- [95] C. B. Bucknall and A. H. Gilbert, “Toughening tetrafunctional epoxy resins using polyetherimide,” *Polymer (Guildf)*., vol. 30, no. 2, pp. 213–217, Feb. 1989, doi: 10.1016/0032-3861(89)90107-9.
- [96] D. . Hourston and J. . Lane, “The toughening of epoxy resins with thermoplastics: 1. Trifunctional epoxy resin-polyetherimide blends,” *Polymer (Guildf)*., vol. 33, no. 7, pp. 1379–1383, Jan. 1992, doi: 10.1016/0032-3861(92)90110-I.
- [97] W. D. Bascom, R. Y. Ting, R. J. Moulton, C. K. Riew, and A. R. Siebert, “The fracture of an epoxy polymer containing elastomeric modifiers,” *J. Mater. Sci.*, vol. 16, no. 10, pp. 2657–2664, Oct. 1981, doi: 10.1007/BF00552947.
- [98] A. J. Kinloch, M. L. Yuen, and S. D. Jenkins, “Thermoplastic-toughened epoxy polymers,” *J. Mater. Sci.*, vol. 29, no. 14, pp. 3781–3790, 1994, doi: 10.1007/BF00357349.
- [99] R. D. Brooker, A. J. Kinloch, and A. C. Taylor, “The Morphology and Fracture Properties of Thermoplastic-Toughened Epoxy Polymers,” *J. Adhes.*, vol. 86, no. 7, pp. 726–741, Jul. 2010, doi: 10.1080/00218464.2010.482415.
- [100] L. M. Johnson and N. D. Huffman, “Rheology of Epoxy/Thermoplastic Blends,” in *Handbook of Epoxy Blends*, Cham: Springer International Publishing, 2017, pp. 613–648.
- [101] F. J. Guild and A. J. Kinloch, “Predictive modelling of the mechanical properties of rubber-toughened epoxy,” *J. Mater. Sci.*, vol. 13, pp. 629–632, 1994.
- [102] M. I. Giannotti, M. L. Foresti, I. Mondragon, M. J. Galante, and P. A. Oyanguren, “Reaction-induced phase separation in epoxy/polysulfone/poly(ether imide) systems. I. Phase diagrams,” *J. Polym. Sci. Part B Polym. Phys.*, vol. 42, no. 21, pp. 3953–3963, Nov. 2004, doi: 10.1002/polb.20192.
- [103] M. I. Giannotti, I. Mondragon, M. J. Galante, and P. A. Oyanguren, “Reaction-induced phase separation in epoxy/polysulfone/poly(ether imide) systems. II. Generated morphologies,” *J. Polym. Sci. Part B Polym. Phys.*, vol. 42, no. 21, pp. 3964–3975, Nov. 2004, doi: 10.1002/polb.20193.
- [104] E. R. Mafi and M. Ebrahimi, “Role of core-shell rubber particle cavitation resistance

- on toughenability of epoxy resins,” *Polym. Eng. Sci.*, vol. 48, no. 7, pp. 1376–1380, Jul. 2008, doi: 10.1002/pen.21104.
- [105] L. Becu, A. Maazouz, H. Sautereau, and J. F. Gerard, “Fracture behavior of epoxy polymers modified with core-shell rubber particles,” *J. Appl. Polym. Sci.*, vol. 65, no. 12, pp. 2419–2431, Sep. 1997, doi: 10.1002/(SICI)1097-4628(19970919)65:12<2419::AID-APP14>3.0.CO;2-W.
- [106] “Kaneka Belgium - Structure and range.” <http://www.kaneka.be/products/liquid-polymers/kane-ace-mx/structure-and-range> (accessed Jun. 12, 2018).
- [107] D. S. Parker, H.-J. Suet, J. Huang, and A. F. Yee~, “Toughening mechanisms in core-shell rubber modified polycarbonate.”
- [108] C. B. Bucknall, P. S. Heather, and A. Lazzeri, “Rubber toughening of plastics,” *J. Mater. Sci.*, vol. 24, no. 6, pp. 2255–2261, Jun. 1989, doi: 10.1007/BF02385450.
- [109] J. Chen, A. J. Kinloch, S. Sprenger, and A. C. Taylor, “The mechanical properties and toughening mechanisms of an epoxy polymer modified with polysiloxane-based core-shell particles,” *Polymer (Guildf)*., vol. 54, no. 16, pp. 4276–4289, Jul. 2013, doi: 10.1016/J.POLYMER.2013.06.009.
- [110] S. Li, Q. Wu, H. Zhu, Q. Lin, and C. Wang, “Impact Resistance Enhancement by Adding Core-Shell Particle to Epoxy Resin Modified with Hyperbranched Polymer,” *Polymers (Basel)*., vol. 9, no. 12, p. 684, Dec. 2017, doi: 10.3390/polym9120684.
- [111] H.-J. Sue, “Craze-like damage in a core-shell rubber-modified epoxy system,” *J. Mater. Sci.*, vol. 27, no. 11, pp. 3098–3107, 1992, doi: 10.1007/BF01154125.
- [112] D. Quan and A. Ivankovic, “Effect of core-shell rubber (CSR) nano-particles on mechanical properties and fracture toughness of an epoxy polymer,” *Polymer (Guildf)*., vol. 66, pp. 16–28, Jun. 2015, doi: 10.1016/J.POLYMER.2015.04.002.
- [113] W. Wan, D. Yu, J. He, Y. Xie, L. Huang, and X. Guo, “Simultaneously improved toughness and dielectric properties of epoxy/core-shell particle blends,” *J. Appl. Polym. Sci.*, vol. 107, no. 2, pp. 1020–1028, Jan. 2008, doi: 10.1002/app.26102.
- [114] A. Maazouz, H. Sautereau, and J. F. Gerard, “Toughening of epoxy networks using pre-formed core-shell particles or reactive rubbers,” *Polym. Bull.*, vol. 33, no. 1, pp. 67–74, Jun. 1994, doi: 10.1007/BF00313475.

- [115] U. Szeluga and P. Moryc, "Curing of dicyanate ester/epoxy copolymers modified with polysiloxane and butadiene-acrylonitrile rubbers," *J. Therm. Anal. Calorim.*, vol. 109, no. 1, pp. 73–80, Jul. 2012, doi: 10.1007/s10973-011-1717-0.
- [116] L. Yang, C. Zhang, S. Pilla, and S. Gong, "Polybenzoxazine-core shell rubber-carbon nanotube nanocomposites," *Compos. Part A Appl. Sci. Manuf.*, vol. 39, no. 10, pp. 1653–1659, Oct. 2008, doi: 10.1016/J.COMPOSITESA.2008.07.004.
- [117] C. K. Riew, A. R. Siebert, R. W. Smith, M. Fernando, and A. J. Kinloch, "Toughened Epoxy Resins: Preformed Particles as Tougheners for Adhesives and Matrices," 1996, pp. 33–44.
- [118] C. K. Riew, A. J. Kinloch, American Chemical Society. Division of Polymeric Materials: Science and Engineering., and C. . American Chemical Society. Meeting (207th : 1994 : San Diego, *Toughened plastics II : novel approaches in science and engineering*, vol. 252. Washington, DC: American Chemical Society, 1996.
- [119] L. Mascia, Y. Kouparitsas, D. Nocita, and X. Bao, "Antiplasticization of polymer materials: Structural aspects and effects on mechanical and diffusion-controlled properties," *Polymers*, vol. 12, no. 4. MDPI AG, Apr. 01, 2020, doi: 10.3390/POLYM12040769.
- [120] R. A. Venditti, J. K. Gillham, Y. C. Jean, and Y. Lou, "Free volume after cure vs. fractional conversion for a high-Tg epoxy/amine thermosetting system," *J. Appl. Polym. Sci.*, vol. 56, no. 10, pp. 1207–1220, 1995, doi: 10.1002/app.1995.070561003.
- [121] N. Hata, R. Yamauchi, and J. Kumanotani, "Viscoelastic properties of epoxy resins. II. Antiplasticization in highly crosslinked epoxy system," *J. Appl. Polym. Sci.*, vol. 17, no. 7, pp. 2173–2181, 1973, doi: 10.1002/APP.1973.070170716.
- [122] N. Hata and J. Kumanotani, "Viscoelastic properties of epoxy resins. III. Effect of molecular weight of antiplasticizers in highly crosslinked antiplasticization system," *J. Appl. Polym. Sci.*, vol. 21, no. 5, pp. 1257–1266, 1977, doi: 10.1002/APP.1977.070210508.
- [123] L. Heux, F. Lauprêtre, J. L. Halary, and L. Monnerie, "Dynamic mechanical and ¹³C n.m.r. analyses of the effects of antiplasticization on the β secondary relaxation of aryl-aliphatic epoxy resins," *Polymer (Guildf.)*, vol. 39, no. 6–7, pp. 1269–1278, Jan. 1998, doi: 10.1016/S0032-3861(97)00423-0.

- [124] V. A. Bershtein, N. N. Peschanskaya, J. L. Halary, and L. Monnerie, “The sub-T g relaxations in pure and antiplasticized model epoxy networks as studied by high resolution creep rate spectroscopy.”
- [125] S. Grishchuk, S. Schmitt, O. C. Vorster, and J. Karger-Kocsis, “Structure and properties of amine-hardened epoxy/benzoxazine hybrids: Effect of epoxy resin functionality,” *J. Appl. Polym. Sci.*, vol. 124, no. 4, pp. 2824–2837, May 2012, doi: 10.1002/app.35302.
- [126] V. Sauvant and J. L. Halary, “Improvement of the performance of epoxy-amine thermosets by antiplasticizer-induced nano-scale phase separation during cure,” *Compos. Sci. Technol.*, vol. 62, no. 4, pp. 481–486, Mar. 2002, doi: 10.1016/S0266-3538(01)00137-3.
- [127] H. S. Kaufman, “Handbook of epoxy resins. Henry Lee and Kris Neville,” *J. Appl. Polym. Sci.*, vol. 14, no. 1, pp. 253–253, Jan. 1970, doi: 10.1002/APP.1970.070140126.
- [128] C. M. Manjunatha, A. C. Taylor, A. J. Kinloch, and S. Sprenger, “The tensile fatigue behaviour of a silica nanoparticle-modified glass fibre reinforced epoxy composite,” *Compos. Sci. Technol.*, vol. 70, no. 1, pp. 193–199, Jan. 2010, doi: 10.1016/J.COMPSCITECH.2009.10.012.
- [129] A. Sinha, N. Islam Khan, S. Das, J. Zhang, and S. Halder, “Effect of reactive and non-reactive diluents on thermal and mechanical properties of epoxy resin,” *High Perform. Polym.*, vol. 30, no. 10, pp. 1159–1168, Dec. 2018, doi: 10.1177/0954008317743307.
- [130] G. Slayter, “STRENGTH AND PHYSICAL PROPERTIES OF FINE GLASS FIBERS AND YARNS,” *J. Am. Ceram. Soc.*, vol. 19, no. 1–12, pp. 335–337, Jan. 1936, doi: 10.1111/j.1151-2916.1936.tb19847.x.
- [131] W. H. Carothers and J. W. Hill, “Studies of polymerization and ring formation. XII. Linear superpolyesters,” *J. Am. Chem. Soc.*, vol. 54, no. 4, pp. 1559–1566, Apr. 1932, doi: 10.1021/ja01343a048.
- [132] W. H. Carothers and J. W. Hill, “Studies of polymerization and ring formation. XIII. Polyamides and mixed polyester-polyamides,” *J. Am. Chem. Soc.*, vol. 54, no. 4, pp. 1566–1569, Apr. 1932, doi: 10.1021/ja01343a049.

- [133] J. W. Hill and W. H. Carothers, “Studies of polymerization and ring formation. Xiv. A linear superpolyanhydride and a cyclic dimeric anhydride from sebacic acid,” *J. Am. Chem. Soc.*, vol. 54, no. 4, pp. 1569–1579, Apr. 1932, doi: 10.1021/ja01343a050.
- [134] “Dec. 18, 1878: Let There Be Light — Electric Light | WIRED.” <https://www.wired.com/2009/12/1218joseph-swan-electric-bulb/> (accessed Apr. 08, 2020).
- [135] R. Bacon, “Growth, structure, and properties of graphite whiskers,” *J. Appl. Phys.*, vol. 31, no. 2, pp. 283–290, Feb. 1960, doi: 10.1063/1.1735559.
- [136] M. . Tang and R. Bacon, “Carbonization of cellulose fibers—I. Low temperature pyrolysis,” *Carbon N. Y.*, vol. 2, no. 3, pp. 211–220, Dec. 1964, doi: 10.1016/0008-6223(64)90035-1.
- [137] R. Bacon and M. M. Tang, “Carbonization of cellulose fibers—II. Physical property study,” *Carbon N. Y.*, vol. 2, no. 3, pp. 221–225, Dec. 1964, doi: 10.1016/0008-6223(64)90036-3.
- [138] S. Otani, “On the Carbon Fiber from the Molten Pyrolysis Products,” *Carbon N. Y.*, vol. 3, pp. 31–38, 1965.
- [139] W. Watt, L. N. Phillips, and W. Johnson, “High Strength, High Modulus Carbon Fibers,” *Eng.*, vol. 221, pp. 815–816, 1966.
- [140] R. Moreton, W. Watt, and W. Johnson, “Carbon fibres of high strength and high breaking strain [6],” *Nature*, vol. 213, no. 5077. Nature Publishing Group, pp. 690–691, 1967, doi: 10.1038/213690a0.
- [141] W. Johnson and W. Watt, “Structure of high modulus carbon fibres [8],” *Nature*, vol. 215, no. 5099. Nature Publishing Group, pp. 384–386, 1967, doi: 10.1038/215384a0.
- [142] M. Crump, “Composite Frac Plugs Optimize Costs in Plug-and-Perf Completions,” *American Oil & Gas Reporter*, Derby, KS, Aug. 2015.
- [143] A. Siriruk and D. Penumadu, “Hygrothermal Effects on Polymeric Composite Materials and Sandwich Structures,” in *Encyclopedia of Thermal Stresses*, Dordrecht: Springer Netherlands, 2014, pp. 2306–2318.
- [144] “Composite Parts for Automotive Internal Combustion Engines,” *JEC Composites e-Newsletter*, 2015. <http://www.jeccomposites.com/knowledge/international-composites->

- news/composites-parts-automotive-internal-combustion-engines (accessed Jul. 17, 2018).
- [145] S. Black, “Composite Engine Valves?,” *Composites World*, 2009.
- [146] J. C. Williams and E. A. Starke, “Progress in structural materials for aerospace systems,” *Acta Mater.*, vol. 51, pp. 5775–5799, 2003, doi: 10.1016/j.actamat.2003.08.023.
- [147] H.-J. Sue, R. E. Jones, and E. I. Garcia-Meitin, “Fracture behaviour of model toughened composites under Model and Mode II delaminations,” *J. Mater. Sci.*, vol. 28, pp. 6381–6391, 1993.
- [148] S. Laurenzi, S. Botti, A. Ruffoloni, and M. G. Santonicola, “Fracture Mechanisms in Epoxy Composites Reinforced with Carbon Nanotubes,” *Procedia Eng.*, vol. 88, pp. 157–164, Jan. 2014, doi: 10.1016/J.PROENG.2014.11.139.
- [149] M. H. Woldemariam *et al.*, “Effects of nanomaterials and particles on mechanical properties and fracture toughness of composite materials: a short review,” *AIMS Mater. Sci.* 2019 61191, vol. 6, no. 6, pp. 1191–1212, 2019, doi: 10.3934/MATERSCI.2019.6.1191.
- [150] H. Zhang, A. Bharti, Z. Li, S. Du, E. Bilotti, and T. Peijs, “Localized toughening of carbon/epoxy laminates using dissolvable thermoplastic interleaves and electrospun fibres,” *Compos. Part A Appl. Sci. Manuf.*, vol. 79, pp. 116–126, Dec. 2015, doi: 10.1016/j.compositesa.2015.09.024.
- [151] T. K. Tsotsis, “Interlayer toughening of composite materials,” *Polym. Compos.*, vol. 30, no. 1, pp. 70–86, Jan. 2009, doi: 10.1002/pc.20535.
- [152] D. Quan, R. Alderliesten, C. Dransfeld, N. Murphy, A. Ivanković, and R. Benedictus, “Enhancing the fracture toughness of carbon fibre/epoxy composites by interleaving hybrid meltable/non-meltable thermoplastic veils,” *Compos. Struct.*, p. 112699, 2020, doi: 10.1016/j.compstruct.2020.112699.
- [153] P. Chang, A. P. Mouritz, and B. N. Cox, “Properties and failure mechanisms of z-pinned laminates in monotonic and cyclic tension,” *Compos. Part A Appl. Sci. Manuf.*, vol. 37, no. 10, pp. 1501–1513, Oct. 2006, doi: 10.1016/J.COMPOSITESA.2005.11.013.

- [154] A. H. I. Mourad, A. M. Beckry Mohamed, and T. El-Maaddawy, "Effect of seawater and warm environment on glass/epoxy and glass/polyurethane composites," *Appl. Compos. Mater.*, vol. 17, no. 5, pp. 557–573, Oct. 2010, doi: 10.1007/S10443-010-9143-1.
- [155] N. Rasoldier *et al.*, "Model systems for thermo-oxidised epoxy composite matrices," *Compos. Part A Appl. Sci. Manuf.*, vol. 39, no. 9, pp. 1522–1529, Sep. 2008, doi: 10.1016/J.COMPOSITESA.2008.05.016.
- [156] E. Vassileva and K. Friedrich, "Epoxy/alumina nanoparticle composites. I. Dynamic mechanical behavior," *J. Appl. Polym. Sci.*, vol. 89, no. 14, pp. 3774–3785, Sep. 2003, doi: 10.1002/APP.12463.
- [157] A. K. Subramaniyan and C. T. Sun, "Toughening polymeric composites using nanoclay: Crack tip scale effects on fracture toughness," *Compos. Part A Appl. Sci. Manuf.*, vol. 38, no. 1, pp. 34–43, Jan. 2007, doi: 10.1016/J.COMPOSITESA.2006.01.021.
- [158] C. Keith Kiew, A. R. Siebert, R. W. Smith, M. Fernando, and A. J. Kinloch, "Toughened epoxy resins: Preformed particles as tougheners for adhesives and matrices," *Adv. Chem. Ser.*, vol. 252, pp. 33–44, 1996, doi: 10.1021/BA-1996-0252.CH003.
- [159] D. M. Scott and D. C. Phillips, "Carbon fibre composites with rubber toughened matrices," 1975.
- [160] H. M. Chong and A. C. Taylor, "The microstructure and fracture performance of styrene-butadiene- methylmethacrylate block copolymer-modified epoxy polymers," *J. Mater. Sci.*, vol. 48, no. 19, pp. 6762–6777, Oct. 2013, doi: 10.1007/s10853-013-7481-8.
- [161] R. Bagheri and R. A. Pearson, "Role of particle cavitation in rubber-toughened epoxies: I. Microvoid toughening," *Polymer (Guildf)*, vol. 37, no. 20, pp. 4529–4538, Sep. 1996, doi: 10.1016/0032-3861(96)00295-9.
- [162] R. Bagheri and R. A. Pearson, "Role of particle cavitation in rubber-toughened epoxies: II. Inter-particle distance," *Polymer (Guildf)*, vol. 41, no. 1, pp. 269–276, Jan. 2000, doi: 10.1016/S0032-3861(99)00126-3.

- [163] C. B. Bucknall, A. Karpodinis, and X. C. Zhang, "A model for particle cavitation in rubber-toughened plastics," *J. Mater. Sci.*, vol. 29, no. 13, pp. 3377–3383, 1994, doi: 10.1007/BF00352036.
- [164] W. L. Bradley, W. Schultz, C. Corleto, and S. Komatsu, "The Synergistic Effect of Cross-Link Density and Rubber Additions on the Fracture Toughness of Polymers," 1993, pp. 317–334.
- [165] T. K. Tsotsis, "Thermo-Oxidative Aging of Composite Materials," *J. Compos. Mater.*, vol. 29, no. 3, pp. 410–422, Feb. 1995, doi: 10.1177/002199839502900307.
- [166] T. K. Tsotsis, "Long-Term Thermo-Oxidative Aging in Composite Materials: Experimental Methods," *J. Compos. Mater.*, vol. 32, no. 11, pp. 1115–1135, Jun. 1998, doi: 10.1177/002199839803201104.
- [167] K. Arita and T. Oyama, "Selective preparation of oligomeric naphthylene ether and its applications to epoxy resin for silicon carbide power semiconductor device materials," *J. Appl. Polym. Sci.*, vol. 133, no. 17, May 2016, doi: 10.1002/app.43339.
- [168] R. E. Zacharia and S. L. Simon, "Dynamic and Isothermal Thermogravimetric Analysis of a Polycyanurate Thermosetting System."
- [169] G. M. Odegard and A. Bandyopadhyay, "Physical aging of epoxy polymers and their composites," *J. Polym. Sci. Part B Polym. Phys.*, vol. 49, no. 24, pp. 1695–1716, Dec. 2011, doi: 10.1002/polb.22384.
- [170] N. Rose, M. Le Bras, and R. Delobel, "Thermal oxidative degradation of an epoxy resin," 1993.
- [171] R. Martin, "Ageing of Composites," *Ageing Compos.*, pp. 1–517, 2008.
- [172] G. A. Schoepner, G. P. Tandon, and E. R. Ripberger, "Anisotropic oxidation and weight loss in PMR-15 composites," *Compos. Part A Appl. Sci. Manuf.*, vol. 38, no. 3, pp. 890–904, Mar. 2007, doi: 10.1016/J.COMPOSITESA.2006.07.006.
- [173] B. Dao, J. Hodgkin, J. Krstina, J. Mardel, and W. Tian, "Accelerated aging versus realistic aging in aerospace composite materials. I. The chemistry of thermal aging in a low-temperature-cure epoxy composite," *J. Appl. Polym. Sci.*, vol. 102, no. 5, pp. 4291–4303, Dec. 2006, doi: 10.1002/app.24862.
- [174] A. Kubit, T. Trzepiecinski, M. Kłonica, M. Hebda, and M. Pytel, "The influence of

- temperature gradient thermal shock cycles on the interlaminar shear strength of fibre metal laminate composite determined by the short beam test,” *Compos. Part B Eng.*, vol. 176, p. 107217, Nov. 2019, doi: 10.1016/j.compositesb.2019.107217.
- [175] B. C. Ray, “Effect of thermal shock on interlaminar strength of thermally aged glass fiber-reinforced epoxy composites,” *J. Appl. Polym. Sci.*, vol. 100, no. 3, pp. 2062–2066, May 2006, doi: 10.1002/app.23019.
- [176] K. K. Mahato, K. Dutta, and B. C. Ray, “Effect of Thermal Spike Conditioning on the Tensile Behavior of Glass/Epoxy Composites,” in *Materials Today: Proceedings*, Jan. 2018, vol. 5, no. 5, pp. 12109–12114, doi: 10.1016/j.matpr.2018.02.188.
- [177] J. Delozanne, N. Desgardin, N. Cuvillier, and E. Richaud, “Thermal oxidation of aromatic epoxy-diamine networks,” doi: 10.1016/j.polymdegradstab.2019.05.030i.
- [178] S. V Levchik *et al.*, “Mechanistic study of thermal behavior and combustion performance of epoxy resins. II. TGDDM/DDS system,” 1995.
- [179] S. Bondzic, J. Hodgkin, J. Krstina, and J. Mardel, “Chemistry of thermal ageing in aerospace epoxy composites,” *J. Appl. Polym. Sci.*, vol. 100, no. 3, pp. 2210–2219, May 2006, doi: 10.1002/app.23692.
- [180] C. J. de Bakker, N. A. St John, and G. A. George, “Simultaneous differential scanning calorimetry and near-infra-red analysis of the curing of tetraglycidyl-diaminodiphenylmethane with diaminodiphenylsulphone,” *Polymer (Guildf)*, vol. 34, no. 4, pp. 716–725, Feb. 1993, doi: 10.1016/0032-3861(93)90353-C.
- [181] C. L. Sherman, R. C. Zeigler, N. E. Verghese, and M. J. Marks, “Structure-property relationships of controlled epoxy networks with quantified levels of excess epoxy etherification,” *Polymer (Guildf)*, vol. 49, no. 5, pp. 1164–1172, Mar. 2008, doi: 10.1016/j.polymer.2008.01.037.
- [182] S. Podzimek, I. Dobás, S. Svestka, J. Horálek, M. Tkaczyk, and M. Kubín, “Epoxy resins based on aromatic glycidylamines. I. Analysis of N,N-diglycidylaniline by GPC and HPLC,” *J. Appl. Polym. Sci.*, vol. 41, no. 56, pp. 1151–1160, Jan. 1990, doi: 10.1002/app.1990.070410524.
- [183] S. Podzimek, I. Dobás, S. Svestka, J. Horálek, M. Tkaczyk, and M. Kubín, “Epoxy resins based on aromatic glycidylamines. II. Preparation of N,N,N,N-tetraglycidyl-

- 4,4'-diaminodiphenylmethane from 4,4'-diaminodiphenylmethane: Analysis of product by GPC and HPLC," *J. Appl. Polym. Sci.*, vol. 41, no. 56, pp. 1161–1170, Jan. 1990, doi: 10.1002/app.1990.070410525.
- [184] S. Podzimek and A. K. Ta'nek, "Characterization of Bisphenol A-Based Epoxy Resins by HPLC, GPC, GPC-MALLS, VPO, Viscometry, and End Group Analysis: On the Identification of 2,3-Dihydroxypropyl-Containing Compounds, Determination of Molar Mass Distribution, and Branching," 1999.
- [185] H. Li, S. Niu, and C. Lu, "Thermal Characteristics and Kinetic Calculation of Castor Oil Pyrolysis," in *Procedia Engineering*, Jan. 2017, vol. 205, pp. 3711–3716, doi: 10.1016/j.proeng.2017.10.297.
- [186] A. W. Coats and J. P. Redfern, "Kinetic parameters from thermogravimetric data [12]," *Nature*, vol. 201, no. 4914. Nature Publishing Group, pp. 68–69, 1964, doi: 10.1038/201068a0.
- [187] E. Duemichen *et al.*, "Analyzing the network formation and curing kinetics of epoxy resins by in situ near-infrared measurements with variable heating rates," *Thermochim. Acta*, vol. 616, pp. 49–60, Sep. 2015, doi: 10.1016/j.tca.2015.08.008.
- [188] S. Cholake *et al.*, "Quantitative Analysis of Curing Mechanisms of Epoxy Resin by Mid- and Near- Fourier Transform Infra Red Spectroscopy," *Def. Sci. J.*, vol. 64, no. 3, pp. 314–321, May 2014, doi: 10.14429/dsj.64.7326.
- [189] N. Poisson, G. Lachenal, and H. Sautereau, "Near- and mid-infrared spectroscopy studies of an epoxy reactive system," *Vib. Spectrosc.*, vol. 12, no. 2, pp. 237–247, Oct. 1996, doi: 10.1016/0924-2031(96)00027-6.
- [190] J. Mijovic, S. Andjelic, C. F. W. Yee, F. Bellucci, and L. Nicolais, "A Study of Reaction Kinetics by Near-Infrared Spectroscopy. 2. Comparison with Dielectric Spectroscopy of Model and Multifunctional Epoxy/Amine Systems," *Macromolecules*, vol. 28, no. 8, pp. 2797–2806, Apr. 1995, doi: 10.1021/ma00112a027.
- [191] R. J. Varley, G. R. Heath, D. G. Hawthorne, J. H. Hodgkin, and G. P. Simon, "Toughening of a trifunctional epoxy system: 1. Near infra-red spectroscopy study of homopolymer cure," *Polymer (Guildf.)*, vol. 36, no. 7, pp. 1347–1355, Mar. 1995, doi: 10.1016/0032-3861(95)95911-J.

- [192] R. Ramsdale-Capper and J. P. Foreman, "Internal antiplasticisation in highly crosslinked amine cured multifunctional epoxy resins," *Polymer (Guildf)*., vol. 146, pp. 321–330, Jun. 2018.
- [193] A. C. Grillet, J. Galy, J. F. Gérard, and J. P. Pascault, "Mechanical and viscoelastic properties of epoxy networks cured with aromatic diamines," *Polymer (Guildf)*., vol. 32, no. 10, pp. 1885–1891, 1991, doi: 10.1016/0032-3861(91)90380-2.
- [194] H. Zhou, A. Badashah, Z. Luo, F. Liu, and T. Zhao, "Preparation and property comparison of ortho, meta, and para autocatalytic phthalonitrile compounds with amino group," *Polym. Adv. Technol.*, vol. 22, no. 10, pp. 1459–1465, Oct. 2011, doi: 10.1002/pat.2018.
- [195] O. Becker, R. Varley, and G. Simon, "Morphology, thermal relaxations and mechanical properties of layered silicate nanocomposites based upon high-functionality epoxy resins," *Polymer (Guildf)*., vol. 43, no. 16, pp. 4365–4373, Jun. 2002, doi: 10.1016/S0032-3861(02)00269-0.
- [196] C.-P. Wong and S.-H. Shi, "No-flow underfill of epoxy resin, anhydride, fluxing agent and surfactant," US6180696B1, 1998.
- [197] K. Kawai and S. Nakamura, "Resin composition for insulating layer for multi-layered printed board," US8956702B2, 2013.
- [198] S. Osada, Y. Kimura, E. Asano, and T. Shiobara, "Semiconductor encapsulating epoxy resin composition and semiconductor device," 11/408,955, 2006.
- [199] R. J. Varley, W. Liu, and G. P. Simon, "Investigation of the reaction mechanism of different epoxy resins using a phosphorus-based hardener," *J. Appl. Polym. Sci.*, vol. 99, no. 6, pp. 3288–3299, Mar. 2006, doi: 10.1002/app.23016.
- [200] L. Matějka, M. Tkaczyk, S. Pokorný, and K. Dušek, "Cyclization in the reaction between diglycidylaniline and amine," *Polym. Bull.*, vol. 15, no. 5, pp. 389–396, May 1986, doi: 10.1007/BF00265719.
- [201] A. J. Attias, B. Bloch, and F. Laupretre, "Chemical structure of networks resulting from curing of N,N-diglycidylaniline-type resins with aromatic amines. IV. Characterization of TGDDM/DDS and TGDDM/DDM networks by high-resolution solid-state ¹³C-NMR," *J. Polym. Sci. Part A Polym. Chem.*, vol. 28, no. 12, pp. 3445–

- 3466, Nov. 1990, doi: 10.1002/pola.1990.080281221.
- [202] J. Wan, C. Li, Z. Y. Bu, C. J. Xu, B. G. Li, and H. Fan, "A comparative study of epoxy resin cured with a linear diamine and a branched polyamine," *Chem. Eng. J.*, vol. 188, pp. 160–172, Apr. 2012, doi: 10.1016/j.cej.2012.01.134.
- [203] F. Meyer, G. Sanz, A. Eceiza, I. Mondragon, and J. Mijović, "The effect of stoichiometry and thermal history during cure on structure and properties of epoxy networks," *Polymer (Guildf)*., vol. 36, no. 7, pp. 1407–1414, 1995, doi: 10.1016/0032-3861(95)95918-Q.
- [204] R. J. Varley, B. Dao, T. Nguyen, S. Lee, and T. Nishino, "Effect of aromatic substitution on the cure reaction and network properties of anhydride cured triphenyl ether tetraglycidyl epoxy resins," *Polym. Adv. Technol.*, vol. 30, no. 6, pp. 1525–1537, Jun. 2019, doi: 10.1002/pat.4584.
- [205] J. Charlesworth, "Analysis of the Substitution Effects Involved in Diepoxide-Diamine-Copolymerization Reactions," *J. Polym. Sci. A1.*, vol. 18, no. 2, pp. 621–628, Feb. 1980, doi: 10.1002/pol.1980.170180221.
- [206] R. M. R. Wellen and E. L. Canedo, "On the Kissinger equation and the estimate of activation energies for non-isothermal cold crystallization of PET," *Polym. Test.*, vol. 40, pp. 33–38, Dec. 2014, doi: 10.1016/j.polymertesting.2014.08.008.
- [207] M. G. Lu, M. J. Shim, and S. W. Kim, "DYNAMIC DSC CHARACTERIZATION OF EPOXY RESIN BY MEANS OF THE AVRAMI EQUATION," 1999.
- [208] K. Leena, P. B. Soumyamol, M. Baby, S. Suraj, R. Rajeev, and D. S. Mohan, "Non-isothermal cure and decomposition kinetics of epoxy–imidazole systems," *J. Therm. Anal. Calorim.*, vol. 130, no. 2, pp. 1053–1061, Nov. 2017, doi: 10.1007/s10973-017-6410-5.
- [209] P. A. Oyanguren and R. J. J. Williams, "Cure of epoxy novolacs with aromatic diamines. I. Vitrification, gelation, and reaction kinetics," *J. Appl. Polym. Sci.*, vol. 47, no. 8, pp. 1361–1371, Feb. 1993, doi: 10.1002/app.1993.070470806.
- [210] C.-S. Chern and G. W. Poehlein, "A kinetic model for curing reactions of epoxides with amines," *Polym. Eng. Sci.*, vol. 27, no. 11, pp. 788–795, Jun. 1987, doi: 10.1002/pen.760271104.

- [211] N. A. St John, G. A. George, P. A. Cole-Clarke, M. E. Mackay, and P. J. Halley, "The effect of impurities on gel times for TGDDM epoxy resins cured with DDS," *High Perform. Polym.*, vol. 5, no. 1, pp. 21–36, Feb. 1993, doi: 10.1088/0954-0083/5/1/003.
- [212] B.-G. Min, J. H. Hodgkin, and Z. H. Stachurski, "The dependence of fracture properties on cure temperature in a DGEBA/DDS epoxy system," *J. Appl. Polym. Sci.*, vol. 48, no. 7, pp. 1303–1312, May 1993, doi: 10.1002/app.1993.070480719.
- [213] R. J. Varley, J. H. Hodgkin, D. G. Hawthorne, and G. P. Simon, "Toughening of a trifunctional epoxy system. II. Thermal characterization of epoxy/amine cure," *J. Appl. Polym. Sci.*, vol. 60, no. 12, pp. 2251–2263, Jun. 1996, doi: 10.1002/(SICI)1097-4628(19960620)60:12<2251::AID-APP24>3.0.CO;2-8.
- [214] J. López *et al.*, "Isothermal curing by dynamic mechanical analysis of three epoxy resin systems: Gelation and vitrification," *J. Appl. Polym. Sci.*, vol. 83, no. 1, pp. 78–85, Jan. 2002, doi: 10.1002/app.10023.
- [215] J. K. Gillham, J. A. Benci, and A. Noshay, "Isothermal transitions of a thermosetting system," *J. Appl. Polym. Sci.*, vol. 18, no. 4, pp. 951–961, Apr. 1974, doi: 10.1002/app.1974.070180401.
- [216] K. P. Pang and J. K. Gillham, "Competition between cure and thermal degradation in a high T_g epoxy system: Effect of time and temperature of isothermal cure on the glass transition temperature," *J. Appl. Polym. Sci.*, vol. 39, no. 4, pp. 909–933, Feb. 1990, doi: 10.1002/app.1990.070390411.
- [217] G. Jiawu, S. Kui, and G. Zong Mong, "The cure behavior of tetraglycidyl diaminodiphenyl methane with diaminodiphenyl sulfone," *Thermochim. Acta*, vol. 352, no. 353, pp. 153–158, Jul. 2000, doi: 10.1016/S0040-6031(99)00460-8.
- [218] D. Serrano and D. Harran, "On the increase of viscoelastic modulus with advancement of reaction of an epoxy resin," *Polym. Eng. Sci.*, vol. 29, no. 8, pp. 531–537, Apr. 1989, doi: 10.1002/pen.760290807.
- [219] S. S. Labana, S. Newman, and A. J. Chomppff, "Chemical Effects on the Ultimate Properties of Polymer Networks in the Glassy State," in *Polymer Networks*, Springer US, 1971, pp. 453–477.
- [220] M. Opalički, J. M. Kenny, and L. Nicolais, "Cure kinetics of neat and carbon-fiber-

- reinforced TGDDM/DDS epoxy systems,” *J. Appl. Polym. Sci.*, vol. 61, no. 6, pp. 1025–1037, Aug. 1996, doi: 10.1002/(SICI)1097-4628(19960808)61:6<1025::AID-APP17>3.0.CO;2-V.
- [221] S. L. Simon, G. B. Mckenna, and O. Sindt, “Modeling the evolution of the dynamic mechanical properties of a commercial epoxy during cure after gelation,” *J. Appl. Polym. Sci.*, vol. 76, no. 4, pp. 495–508, 2000, doi: 10.1002/(SICI)1097-4628(20000425)76:4<495::AID-APP7>3.0.CO;2-B.
- [222] P. G. Babayevsky and J. K. Gillham, “Epoxy thermosetting systems: Dynamic mechanical analysis of the reactions of aromatic diamines with the diglycidyl ether of bisphenol A,” *J. Appl. Polym. Sci.*, vol. 17, no. 7, pp. 2067–2088, Jul. 1973, doi: 10.1002/app.1973.070170709.
- [223] L. C. Chan, H. N. Naé, and J. K. Gillham, “Time-temperature–transformation (TTT) diagrams of high T_g epoxy systems: Competition between cure and thermal degradation,” *J. Appl. Polym. Sci.*, vol. 29, no. 11, pp. 3307–3327, Nov. 1984, doi: 10.1002/app.1984.070291109.
- [224] E. Drukker, A. K. Green, and G. Marom, “Mechanical and chemical consequences of through thickness thermal gradients in polyimide matrix composite materials,” *Compos. Part A Appl. Sci. Manuf.*, vol. 34, no. 2, pp. 125–133, Feb. 2003, doi: 10.1016/S1359-835X(02)00261-0.
- [225] R. J. Morgan and E. T. Mones, “The cure reactions, network structure, and mechanical response of diaminodiphenyl sulfone-cured tetraglycidyl 4,4’diaminodiphenyl methane epoxies,” *J. Appl. Polym. Sci.*, vol. 33, no. 4, pp. 999–1020, Mar. 1987, doi: 10.1002/app.1987.070330401.
- [226] H. qiang Yan, H. qiang Wang, and G. qong Qi, “Curing, thermal stability and composite properties for blends of the novel bismaleimide and cyanate containing naphthalene,” *Int. J. Mater. Prod. Technol.*, vol. 37, no. 3/4, p. 369, 2010, doi: 10.1504/IJMPT.2010.031436.
- [227] V. Antonucci, M. Giordano, and L. Nicolais, “Effect of the segmental mobility restriction on the thermoset chemical kinetics,” *J. Polym. Sci. Part A Polym. Chem.*, vol. 40, no. 21, pp. 3757–3770, Nov. 2002, doi: 10.1002/pola.10471.
- [228] D. H. Kim and S. C. Kim, “Vitrification effect on the curing reaction of epoxy resin,”

- Polym. Bull.*, vol. 18, no. 6, pp. 533–539, Dec. 1987, doi: 10.1007/BF00255338.
- [229] L. Xu and J. R. Schlup, “Etherification versus amine addition during epoxy resin/amine cure: An in situ study using near-infrared spectroscopy,” *J. Appl. Polym. Sci.*, vol. 67, no. 5, pp. 895–901, Jan. 1998, doi: 10.1002/(SICI)1097-4628(19980131)67:5<895::AID-APP15>3.0.CO;2-N.
- [230] B. G. Min, Z. H. Stachurski, J. H. Hodgkin, and G. R. Heath, “Quantitative analysis of the cure reaction of DGEBA/DDS epoxy resins without and with thermoplastic polysulfone modifier using near infra-red spectroscopy,” *Polymer (Guildf.)*, vol. 34, no. 17, pp. 3620–3627, Sep. 1993, doi: 10.1016/0032-3861(93)90046-D.
- [231] M. Jackson, M. Kaushik, S. Nazarenko, S. Ward, R. Maskell, and J. Wiggins, “Effect of free volume hole-size on fluid ingress of glassy epoxy networks,” *Polymer (Guildf.)*, vol. 52, no. 20, pp. 4528–4535, Sep. 2011, doi: 10.1016/j.polymer.2011.07.042.
- [232] R. Varley, J. H. Hodgkin, and G. P. Simon, “Toughening of trifunctional epoxy system. V. Structure-property relationships of neat resin,” *J. Appl. Polym. Sci.*, pp. 237–248, 2000.
- [233] X. Wang, H. Liu, and S. Ouyang, “Damping properties of flexible epoxy resin,” *J. Wuhan Univ. Technol. Mater. Sci. Ed.*, vol. 23, no. 3, pp. 411–414, Jun. 2008, doi: 10.1007/s11595-007-3411-4.
- [234] J. Tu, S. J. Tucker, S. Christensen, A. R. Sayed, W. L. Jarrett, and J. S. Wiggins, “Phenylene ring motions in isomeric glassy epoxy networks and their contributions to thermal and mechanical properties,” *Macromolecules*, vol. 48, no. 6, pp. 1748–1758, Mar. 2015, doi: 10.1021/ma5022506.
- [235] M. Ochi, M. Yoshizumi, and M. Shimbo, “Mechanical and dielectric relaxations of epoxide resins containing the spiro-ring structure. II. Effect of the introduction of methoxy branches on low-temperature relaxations of epoxide resins,” *J. Polym. Sci. Part B Polym. Phys.*, vol. 25, no. 9, pp. 1817–1827, Sep. 1987, doi: 10.1002/polb.1987.090250903.
- [236] M. Ochi, T. Shiba, H. Takeuchi, M. Yoshizumi, and M. Shimbo, “Effect of the introduction of methoxy branches on low-temperature relaxations and fracture toughness of epoxide resins,” in *Polymer*, Jun. 1989, vol. 30, no. 6, pp. 1079–1084,

- doi: 10.1016/0032-3861(89)90084-0.
- [237] S. L. Simon and J. K. Gillham, "Thermosetting cure diagrams: Calculation and application," *J. Appl. Polym. Sci.*, vol. 53, no. 6, pp. 709–727, Aug. 1994, doi: 10.1002/app.1994.070530601.
- [238] J. S. Nakka, K. M. B. Jansen, and L. J. Ernst, "Effect of chain flexibility in the network structure on the viscoelasticity of epoxy thermosets," *J. Polym. Res.*, vol. 18, no. 6, pp. 1879–1888, Nov. 2011, doi: 10.1007/s10965-011-9595-5.
- [239] J. Wang *et al.*, "Effect of curing agent polarity on water absorption and free volume in epoxy resin studied by PALS," *Nucl. Instruments Methods Phys. Res. Sect. B Beam Interact. with Mater. Atoms*, vol. 268, no. 14, pp. 2355–2361, Jul. 2010, doi: 10.1016/j.nimb.2010.04.010.
- [240] J. Zhou and J. P. Lucas, "Hygrothermal effects of epoxy resin. Part I: The nature of water in epoxy," *Polymer (Guildf.)*, vol. 40, no. 20, pp. 5505–5512, Sep. 1999, doi: 10.1016/S0032-3861(98)00790-3.
- [241] K. Frank and J. Wiggins, "Effect of stoichiometry and cure prescription on fluid ingress in epoxy networks," *J. Appl. Polym. Sci.*, vol. 130, no. 1, pp. 264–276, Oct. 2013, doi: 10.1002/app.39140.
- [242] K. Frank *et al.*, "Fluid uptake behavior of multifunctional epoxy blends," *Polymer (Guildf.)*, vol. 54, no. 1, pp. 403–410, Jan. 2013.
- [243] P. J. Flory and J. Rehner, "Statistical Mechanics of Cross-Linked Polymer Networks II. Swelling," *J. Chem. Phys.*, vol. 11, no. 11, pp. 521–526, Nov. 1943, doi: 10.1063/1.1723792.
- [244] Y.-H. Zang, R. Muller, and D. Froelich, "Determination of crosslinking density of polymer networks by mechanical data in simple extension and by swelling degree at equilibrium," *Polymer (Guildf.)*, vol. 30, no. 11, pp. 2060–2062, Nov. 1989, doi: 10.1016/0032-3861(89)90294-2.
- [245] P. Musto, L. Mascia, G. Ragosta, G. Scarinzi, and P. Villano, "The transport of water in a tetrafunctional epoxy resin by near-infrared Fourier transform spectroscopy," *Polymer (Guildf.)*, vol. 41, no. 2, pp. 565–574, Jan. 2000, doi: 10.1016/S0032-3861(99)00210-4.

- [246] T. K. Tsotsis, S. Keller, J. Bardis, and J. Bish, "Preliminary evaluation of the use of elevated pressure to accelerate thermo-oxidative aging in composites," *Polym. Degrad. Stab.*, vol. 64, pp. 207–212, 1999.
- [247] A. Doblies, B. Boll, and B. Fiedler, "Prediction of thermal exposure and mechanical behavior of epoxy resin using artificial neural networks and Fourier transform infrared spectroscopy," *Polymers (Basel)*, vol. 11, no. 2, 2019, doi: 10.3390/POLYM11020363.
- [248] M. Bakar, J. Szymanska, J. Rudecka, and J. Fitas, "Effect of reactive diluents and kaolin on the mechanical properties of epoxy resin," *Polym. Polym. Compos.*, vol. 18, no. 9, pp. 503–511, Sep. 2010.
- [249] K. P. Unnikrishnan and E. T. Thachil, "Toughening of epoxy resins," *Designed Monomers and Polymers*, vol. 9, no. 2. Taylor & Francis Group, pp. 129–152, 2006, doi: 10.1163/156855506776382664.
- [250] Y. Yang, G. Chen, and K. M. Liew, "Preparation and analysis of a flexible curing agent for epoxy resin," *J. Appl. Polym. Sci.*, vol. 114, no. 5, pp. 2706–2710, Dec. 2009, doi: 10.1002/app.30893.
- [251] X.-H. Jing, Y.-X. Liu, R. Liao, H.-J. Kang, H.-F. Tan, and Y.-Y. Liu, "Synthesis, characterization, and shape-memory performances of monoamine-toughened epoxy resin," doi: 10.1177/0954008315616467.
- [252] J. L. Halary, *Structure-property relationships in epoxy-amine networks of well-controlled architecture †*, vol. 12. 2000, pp. 141–153.
- [253] E. Urbaczewski-Espuche, J. Galy, J.-F. Gerard, J.-P. Pascault, and H. Sautereau, "Influence of chain flexibility and crosslink density on mechanical properties of epoxy/amine networks," *Polym. Eng. Sci.*, vol. 31, no. 22, pp. 1572–1580, Nov. 1991, doi: 10.1002/pen.760312204.
- [254] T. Iijima, M. Tomoi, J. Yamasaki, and H. Kakiuchi, "Toughening of epoxy resins by modification with acrylic elastomers containing pendant epoxy groups," *Eur. Polym. J.*, vol. 26, no. 2, pp. 145–151, Jan. 1990, doi: 10.1016/0014-3057(90)90179-8.
- [255] E. Espuche, J. Galy, J.-F. Gérard, J.-P. Pascault, and H. Sautereau, "Influence of crosslink density and chain flexibility on mechanical properties of model epoxy

- networks,” *Macromol. Symp.*, vol. 93, no. 1, pp. 107–115, Apr. 1995, doi: 10.1002/masy.19950930115.
- [256] L. Q. Reyes, S. R. Swan, H. Gan, S. M. Seraji, J. Zhang, and R. J. Varley, “The role of β relaxations in determining the compressive properties of an epoxy amine network modified with POSS and mono-functional epoxy resins,” *Polym. Test.*, vol. 93, 2021, doi: 10.1016/j.polymertesting.2020.106873.
- [257] Y. Li *et al.*, “Combined light- and heat-induced shape memory behavior of anthracene-based epoxy elastomers,” *Sci. Rep.*, vol. 10, no. 1, pp. 1–12, Dec. 2020, doi: 10.1038/s41598-020-77246-0.
- [258] M. Sharifi, C. W. Jang, C. F. Abrams, and G. R. Palmese, “Toughened epoxy polymers via rearrangement of network topology,” *J. Mater. Chem. A*, vol. 2, no. 38, pp. 16071–16082, Oct. 2014, doi: 10.1039/c4ta03051f.
- [259] D. Mukherji and C. F. Abrams, “Microvoid formation and strain hardening in highly cross-linked polymer networks,” *Phys. Rev. E - Stat. Nonlinear, Soft Matter Phys.*, vol. 78, no. 5, p. 050801, Nov. 2008, doi: 10.1103/PhysRevE.78.050801.
- [260] D. Mukherji and C. F. Abrams, “Anomalous ductility in thermoset/thermoplastic polymer alloys,” *Phys. Chem. Chem. Phys.*, vol. 11, no. 12, pp. 2113–2115, Mar. 2009, doi: 10.1039/b818039c.
- [261] M. Sharifi and G. R. Palmese, “Ductile high-Tg epoxy systems via incorporation of partially reacted substructures,” *J. Mater. Chem. A*, vol. 9, no. 2, pp. 1014–1024, Jan. 2021, doi: 10.1039/d0ta08158b.
- [262] N. Li, Y. Li, X. Hao, and J. Gao, “A comparative experiment for the analysis of microwave and thermal process induced strains of carbon fiber/bismaleimide composite materials,” *Compos. Sci. Technol.*, vol. 106, pp. 15–19, Jan. 2015, doi: 10.1016/J.COMPSCITECH.2014.10.008.
- [263] M. D. Eaton, L. C. Brinson, and K. R. Shull, “Temperature Dependent Fracture Behavior in Model Epoxy Networks with Nanoscale Heterogeneity,” *Polymer (Guildf.)*, p. 123560, Feb. 2021, doi: 10.1016/j.polymer.2021.123560.
- [264] M. Gonzalez, J. Cabanelas, and J. Baselga, “Applications of FTIR on Epoxy Resins - Identification, Monitoring the Curing Process, Phase Separation and Water Uptake,”

- 2012.
- [265] P. Musto, E. Martuscelli, G. Ragosta, and P. Russo, “The Curing Process and Moisture Transport in a Tetrafunctional Epoxy Resin as Investigated by FT-NIR Spectroscopy:,” <http://dx.doi.org/10.1088/0954-0083/12/1/312>, vol. 12, no. 1, pp. 155–168, Nov. 2016, doi: 10.1088/0954-0083/12/1/312.
- [266] R. Sales, G. Thim, and D. Brunelli, “Understanding the water uptake in F-161 glass-epoxy composites using the techniques of luminescence spectroscopy and FT-NIR,” *Polímeros*, vol. 27, no. 2, pp. 171–182, Jun. 2017, doi: 10.1590/0104-1428.05516.
- [267] A. E. Krauklis, A. I. Gagani, and A. T. Echtermeyer, “Near-infrared spectroscopic method for monitoring water content in epoxy resins and fiber-reinforced composites,” *Materials (Basel)*., vol. 11, no. 4, Apr. 2018, doi: 10.3390/ma11040586.
- [268] B. Chabert, G. Lachenal, and C. V. Tung, “Epoxy resins and epoxy blends studied by near infra-red spectroscopy,” *Macromol. Symp.*, vol. 94, no. 1, pp. 145–158, May 1995, doi: 10.1002/MASY.19950940113.
- [269] N. Hameed, P. A. Sreekumar, B. Francis, W. Yang, and S. Thomas, “Morphology, dynamic mechanical and thermal studies on poly(styrene-co-acrylonitrile) modified epoxy resin/glass fibre composites,” *Compos. Part A Appl. Sci. Manuf.*, vol. 38, no. 12, pp. 2422–2432, Dec. 2007, doi: 10.1016/j.compositesa.2007.08.009.
- [270] “Naphthalene | C₁₀H₈ - PubChem.”
<https://pubchem.ncbi.nlm.nih.gov/compound/Naphthalene> (accessed Jul. 03, 2021).
- [271] E. Morel, V. Bellenger, M. Bocquet, and J. Verdu, “Structure-properties relationships for densely cross-linked epoxide-amine systems based on epoxide or amine mixtures - Part 3 Elastic properties,” *J. Mater. Sci.*, vol. 24, no. 1, pp. 69–75, Jan. 1989, doi: 10.1007/BF00660934.
- [272] J. Gao, X. Chu, C. K. Henry, S. C. Santos, and G. R. Palmese, “Highly ductile glassy epoxy systems obtained by network topology modification using partially reacted substructures,” *Polymer (Guildf)*., vol. 212, p. 123260, Jan. 2021, doi: 10.1016/J.POLYMER.2020.123260.
- [273] K. L. Ngai, R. W. Rendell, A. F. Yee, and D. J. Plazek, “Antiplasticization effects on a secondary relaxation in plasticized glassy polycarbonates,” *Macromolecules*, vol. 24,

- no. 1, pp. 61–67, Jan. 2002, doi: 10.1021/MA00001A010.
- [274] S. Hernández, F. Sket, J. M. Molina-Aldareguí a, C. González, and J. LLorca, “Effect of curing cycle on void distribution and interlaminar shear strength in polymer-matrix composites,” *Compos. Sci. Technol.*, vol. 71, no. 10, pp. 1331–1341, Jul. 2011, doi: 10.1016/J.COMPSCITECH.2011.05.002.
- [275] Z. Wu, J. Li, C. Huang, and L. Li, “Effect of Matrix Modification on Interlaminar Shear Strength of Glass Fibre Reinforced Epoxy Composites at Cryogenic Temperature,” *Phys. Procedia*, vol. 67, pp. 1068–1073, Jan. 2015, doi: 10.1016/J.PHPRO.2015.06.202.
- [276] A. Chandramohan and M. Alagar, “Synthesis and characterization of 1, 1-bis (3-methyl-4-epoxyphenyl) cyclohexane-toughened DGEBA and TGDDM organo clay hybrid nanocomposites,” *High Perform. Polym.*, 2011, doi: 10.1177/0954008310397634.
- [277] D. S. Kim, M. J. Han, and J. R. Lee, “Cure behavior and properties of an epoxy resin modified with a bismaleimide resin,” *Polym. Eng. Sci.*, vol. 35, no. 17, pp. 1353–1358, 1995, doi: 10.1002/pen.760351705.
- [278] J. Zhang, Q. Guo, and B. Fox, “Thermal and mechanical properties of a dendritic hydroxyl-functional hyperbranched polymer and tetrafunctional epoxy resin blends,” *J. Polym. Sci. Part B Polym. Phys.*, 2010, doi: 10.1002/polb.21902.
- [279] E. Martuscelli, P. Musto, G. Ragosta, F. Riva, and L. Mascia, “Toughening of tetrafunctional (TGDDM) epoxy resins with telechelic extended perfluoroligomers,” *J. Mater. Sci.*, vol. 35, no. 15, pp. 3719–3726, 2000, doi: 10.1023/A:1004852624444.
- [280] C. B. Bucknall and I. K. Partridge, “Phase separation in epoxy resins containing polyethersulphone,” *Polymer (Guildf.)*, 1983, doi: 10.1016/0032-3861(83)90120-9.
- [281] R. S. Raghava, “Role of matrix-particle interface adhesion on fracture toughness of dual phase epoxy-polyethersulfone blend,” *J. Polym. Sci. Part B Polym. Phys.*, 1987, doi: 10.1002/polb.1987.090250504.
- [282] R. S. Raghava, “Development and characterization of thermosetting-thermoplastic polymer blends for applications in damage-tolerant composites,” *J. Polym. Sci. Part B Polym. Phys.*, 1988, doi: 10.1002/polb.1988.090260103.

- [283] J. U. Starke, R. Godehardt, G. H. Michler, and C. B. Bucknall, "Mechanisms of cavitation over a range of temperatures in rubber-toughened PSAN modified with three-stage core-shell particles," *J. Mater. Sci.*, 1997, doi: 10.1023/A:1018556923774.
- [284] D. S. Ayre and C. B. Bucknall, "Particle cavitation in rubber-toughened PMMA: Experimental testing of the energy-balance criterion," *Polymer (Guildf.)*, 1998, doi: 10.1016/S0032-3861(97)10253-1.
- [285] C. B. Bucknall, "Applications of microscopy to the deformation and fracture of rubber-toughened polymers," *J. Microsc.*, 2001, doi: 10.1046/j.1365-2818.2001.00838.x.
- [286] "Standard Test Method for Mode I Interlaminar Fracture Toughness of Unidirectional Fiber-Reinforced Polymer Matrix Composites 1," doi: 10.1520/D5528-13.
- [287] J. M. Barton and D. C. L. Greenfield, "Differential Scanning Calorimetry Cure Studies of Tetra-N-glycidyl-diaminodiphenylmethane Epoxy Resins 3 - Reaction with Dicyandiamide," *Br. Polym. J.*, vol. 18, no. 3, pp. 196–200, May 1986, doi: 10.1002/pi.4980180311.
- [288] J. Gonis, G. P. Simon, and W. D. Cook, "Cure properties of epoxies with varying chain length as studied by DSC," *J. Appl. Polym. Sci.*, vol. 72, no. 11, pp. 1479–1488, Jun. 1999, doi: 10.1002/(SICI)1097-4628(19990613)72:11<1479::AID-APP9>3.0.CO;2-E.
- [289] S. R. Mousavi and I. Amiri Amraei, "Influence of nanosilica and methyl methacrylate-butadiene-styrene core-shell rubber particles on the physical-mechanical properties and cure kinetics of diglycidyl ether of bisphenol-A-based epoxy resin," *High Perform. Polym.*, vol. 28, no. 7, pp. 809–819, Sep. 2016, doi: 10.1177/0954008315600228.
- [290] H. J. Sue, J. L. Bertram, E. I. Garcia-Meitin, J. W. Wilchester, and L. L. Walker, "Fracture behavior of core-shell rubber-modified crosslinkable epoxy thermoplastics," *Colloid Polym. Sci.*, 1994, doi: 10.1007/BF00659459.
- [291] G. Giannakopoulos, K. Masania, and A. C. Taylor, "Toughening of epoxy using core-shell particles," *J. Mater. Sci.*, 2011, doi: 10.1007/s10853-010-4816-6.
- [292] B. J. Cardwell and A. F. Yee, "Rate and temperature effects on the fracture toughness

of a rubber-modified epoxy.”

- [293] D. R. Long, L. Conca, and P. Sotta, “Dynamics in glassy polymers: The Eyring model revisited,” *Phys. Rev. Mater.*, vol. 2, no. 10, p. 105601, Oct. 2018, doi: 10.1103/PhysRevMaterials.2.105601.
- [294] J. Y. Lee, I.-J. Chin, and J. Choi, “Effect of particle size and crosslinking on the toughening of core-shell-type rubber-modified poly(lactic acid) composites,” 2018, doi: 10.1016/j.polymertesting.2017.12.028.

APPENDIX A 6 NETWORK DEVELOPMENT OF THE TETRAFUNCTIONAL EPOXY RESINS

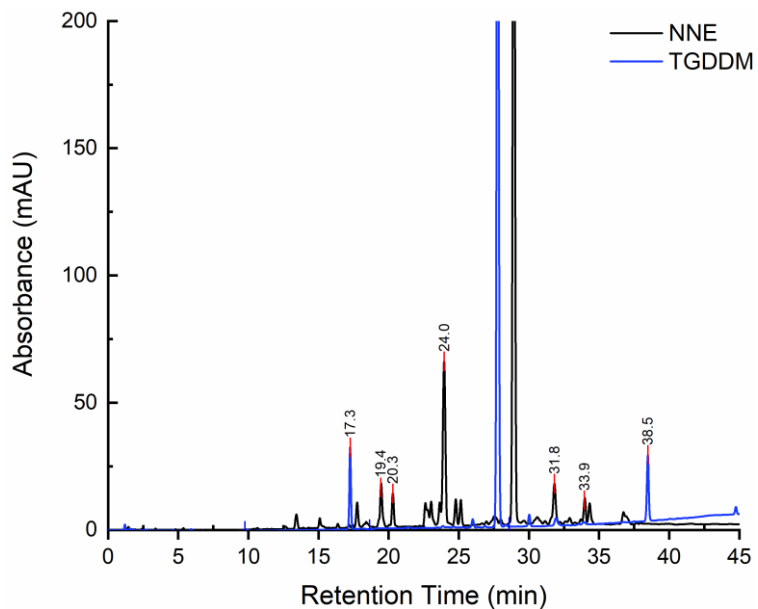


Figure A 1 – HPLC gradient elution absorbance plot of NNE and TGDDM monomers at 230nm intensity

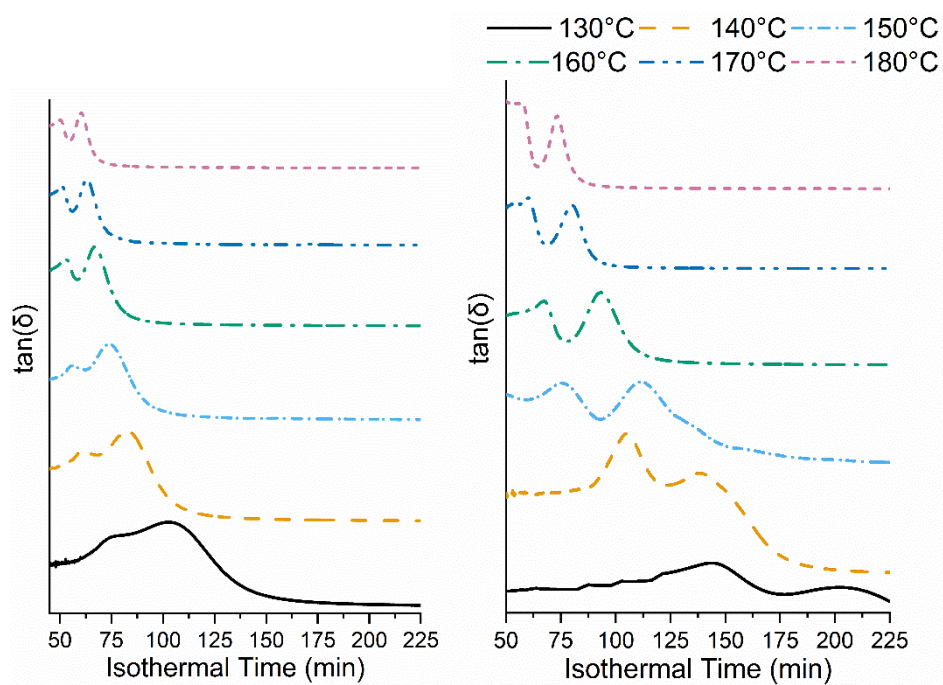


Figure A 2 - Isothermal $\tan(\delta)$ traces for the NTG (left) and TGDDM (right) resin at 130-180°C cures (offset)

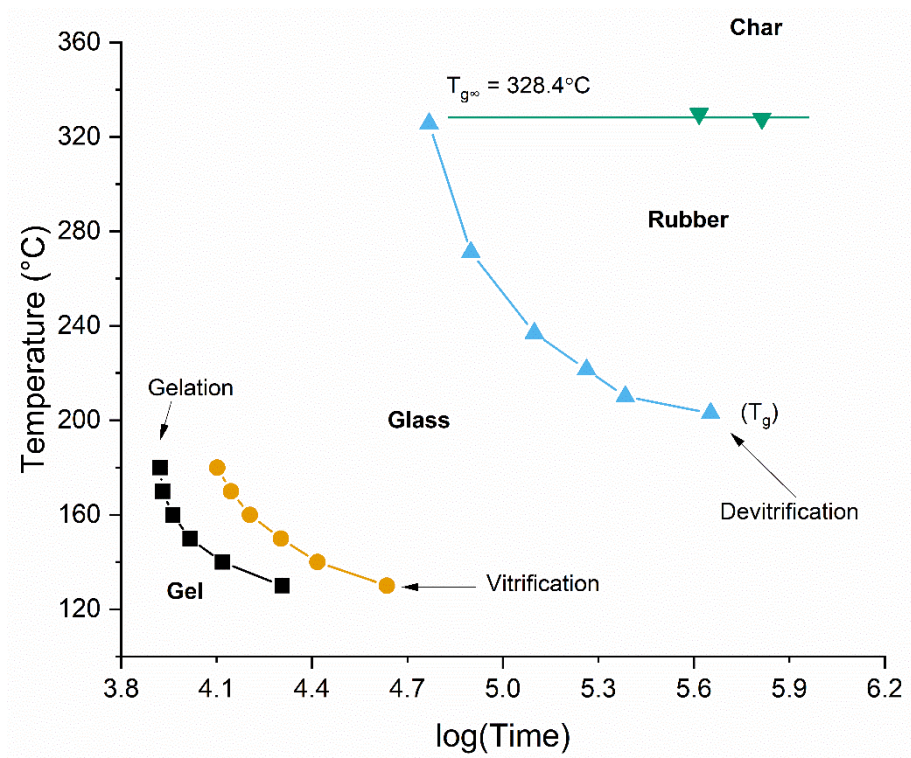


Figure A 3 - TTT diagram of the NTG resin blend

APPENDIX B ó PROPERTIES OF THE BULK RESINS AND THERMAL AGEING OF THE CARBON-FIBRE COMPOSITES

Commercial molecular dynamics simulations were performed using the Schrodinger Materials Science suite to characterise some of the experimentally determined properties and determine a relation between simulated network properties and the effect of the monomer backbone. Simulations were conducted for unit cells consisting of nominally 20,000 atoms or 500 molecules at 1:1 stoichiometry of the epoxy to amino.

Upon assignment of the cross-linking protocol between the epoxide and nucleophile from the amino, the crosslink iterations are performed iteratively until 20 final iterations fail to find suitable reactive sites that satisfy a maximum atomic spacing of 7Å , at which point the crosslink simulation is terminated. The system is equilibrated using a MD compressive relaxation protocol and values of the first largest molecular weight and crosslink saturation are determined for the crosslinked network. Figure A3 presents the plot of the change in molecular weight and free volume percentage relative to crosslink saturation of the simulation for NNE and Table A 1 shows the results for the three resins. The molecular weight between crosslinks is highest for NNE and lowest for TGDDM which follows from the structure of the epoxy monomers, respectively. Crosslink saturation is identical showing similar degrees of

crosslinking between simulations while the free volume percentage is highest for NTG. That could result from a reduced orientation arising from the blend of monomers in the simulation.

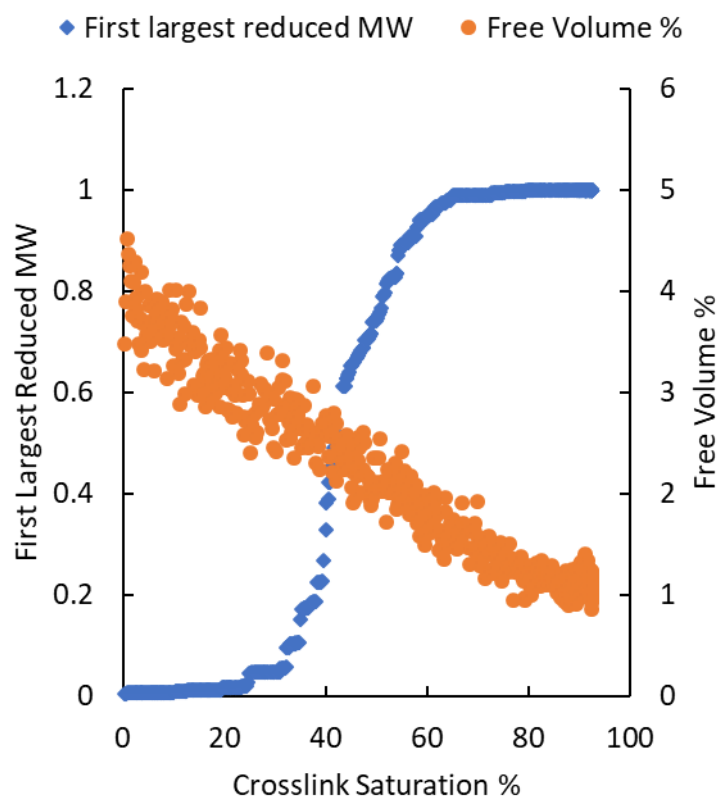


Figure A 4 – First largest MW decrease and free volume of NNE crosslinking simulation

Table A 1 – Summary of Simulation Parameters for Crosslinking Calculations

	MW between Crosslinks (g/mol)	Final Free Volume %	Crosslink Saturation %
NNE	217.82	1.13	92.38
NTG	207.22	1.16	92.69
TGDDM	182.11	1.26	92.08

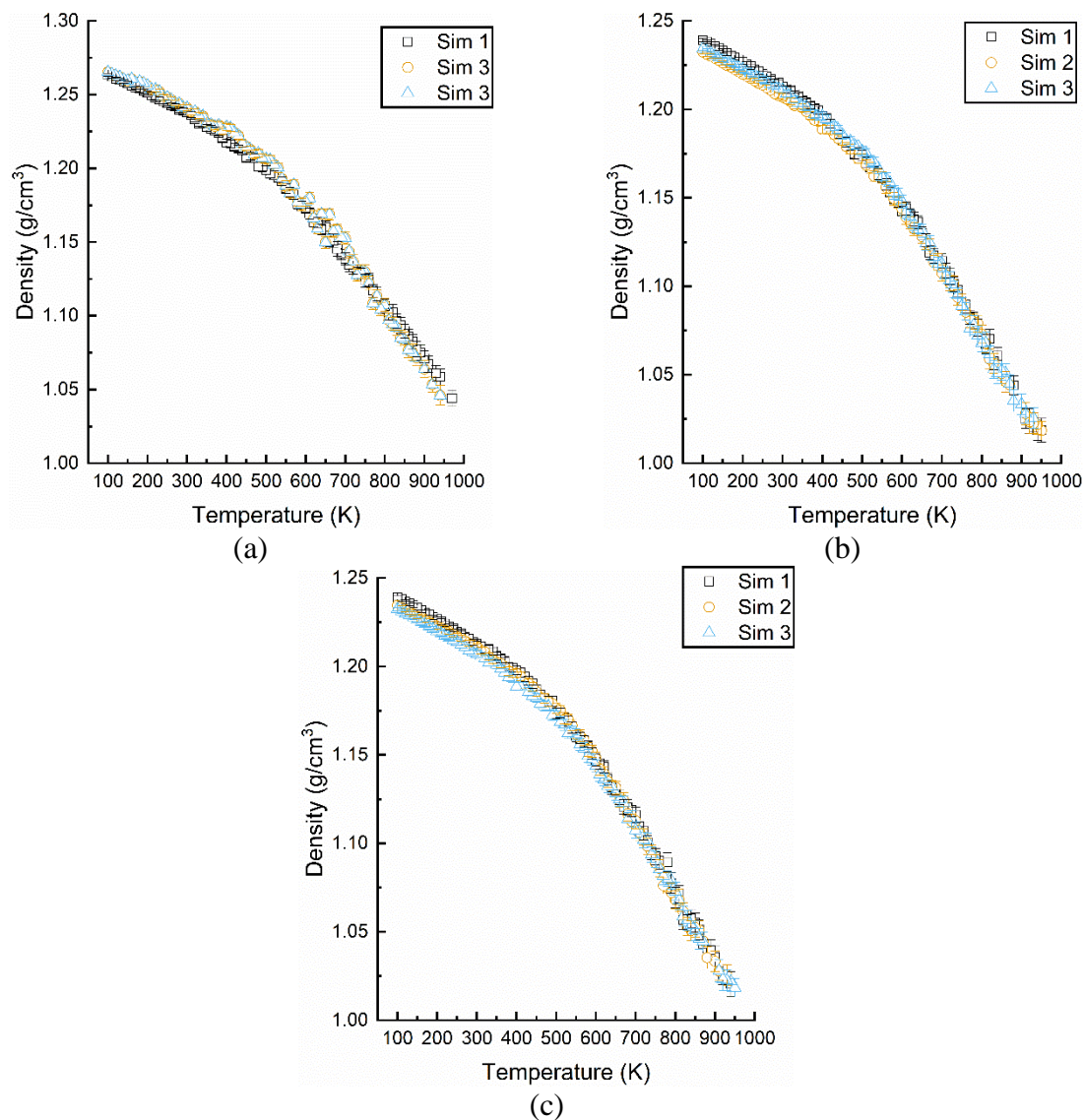


Figure A 5 – Thermal simulation results for (a) NNE, (b) NTG, and (c) TGDDM resins

Table A 2 – Summary of glass transition temperatures (given in °C) from simulations and difference between simulation and experimental T_g (via DMTA)

Simulation #	Glass Transition Temperature (°C)		
	NNE	NTG	TGDDM
1	331	298	264
2	316	285	253
3	326	291	264
Average	324	290	260
* U-Exp)	(27)	(27)	(14)

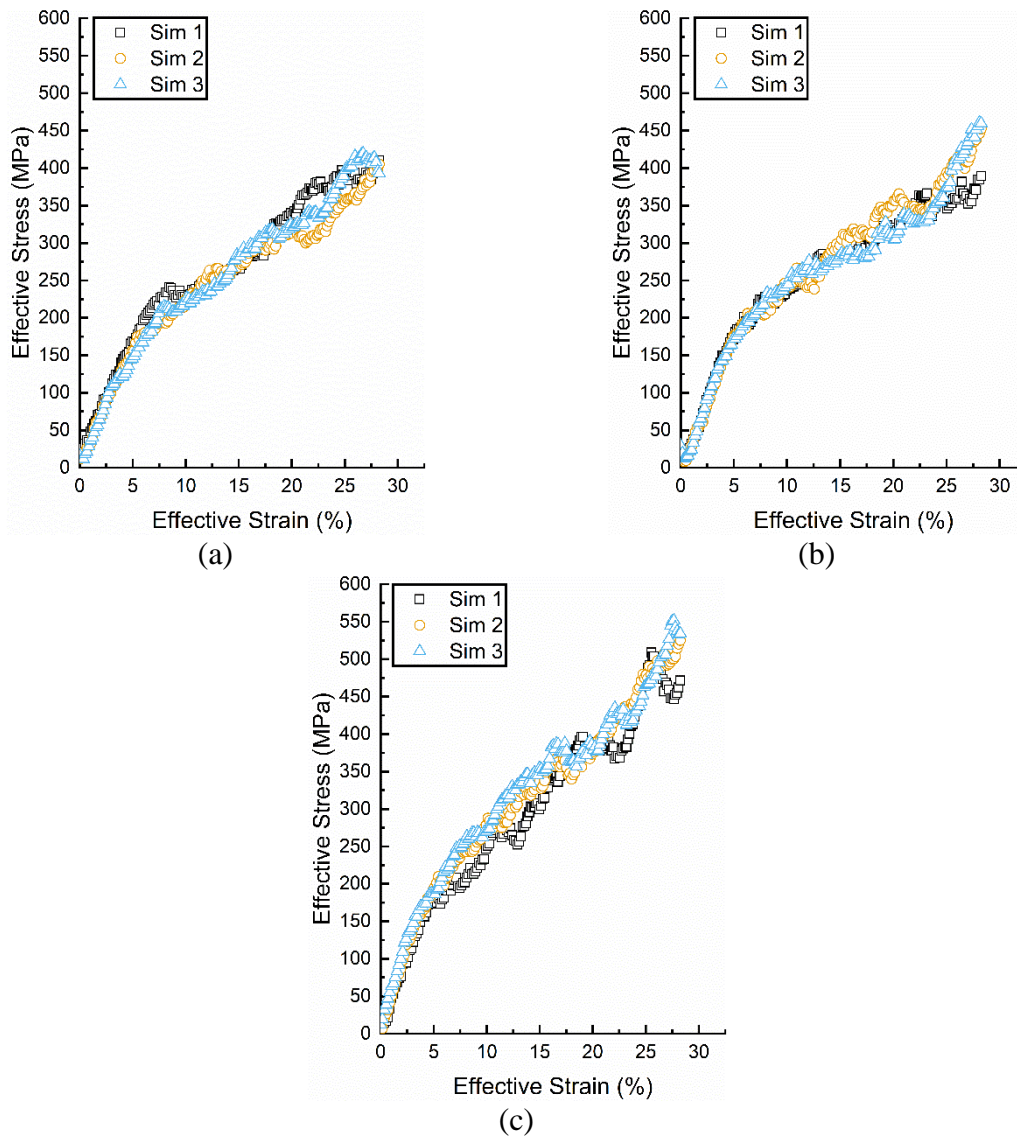


Figure A 6 – Tri-axial tensile effective stress versus effective strain results for (a) NNE, (b) NTG, and (c) TGDDM resin simulations

Table A 3 – Summary of the elastic modulus determined from mechanical simulations

Simulation #	Elastic Modulus (MPa)		
	NNE	NTG	TGDDM
1	3090	3648	3735
2	3128	3555	3897
3	3078	3545	3760
Average	3098	3583	3797

The moisture ingress experimental data were utilised to determine a relative quantification of the crosslink density for the NNE, NTG, and TGDDM resins for the highest cure degree. The relation between free volume and crosslink density is shown in Figure A 6.

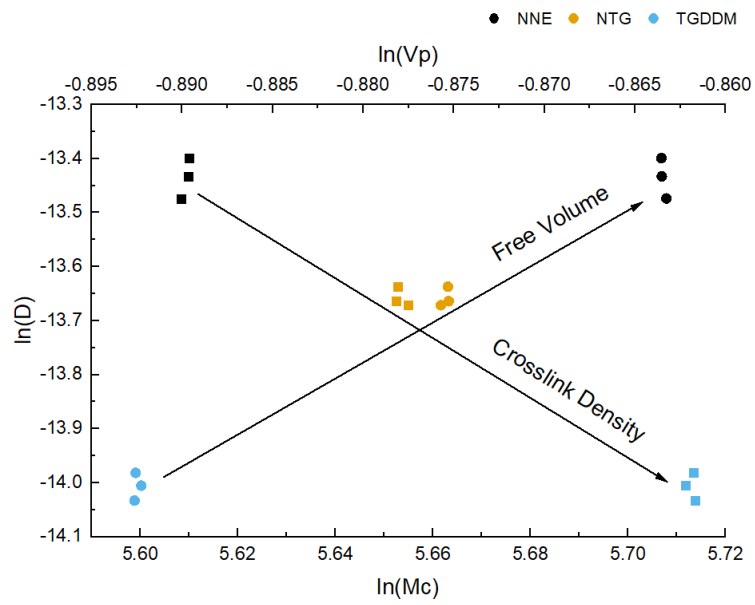


Figure A 7 – Results of crosslink density for NNE, NTG, and TGDDM as determined from solvent (deionised water) swelling experiments

APPENDIX C 6 MOLECULAR ADDITIVES AS MODIFIERS OF THE TETRAFUNCTIONAL EPOXY-AMINE RESIN SYSTEM

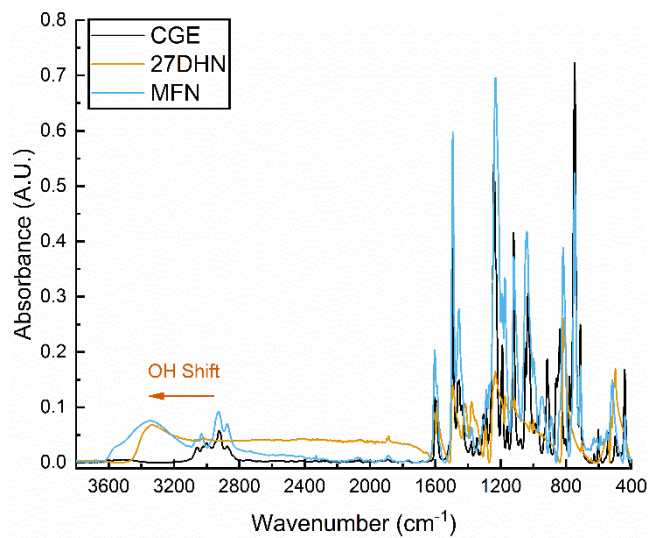


Figure A 8 – FT-IR spectra of the individual constituents and synthesised MFN fortifier

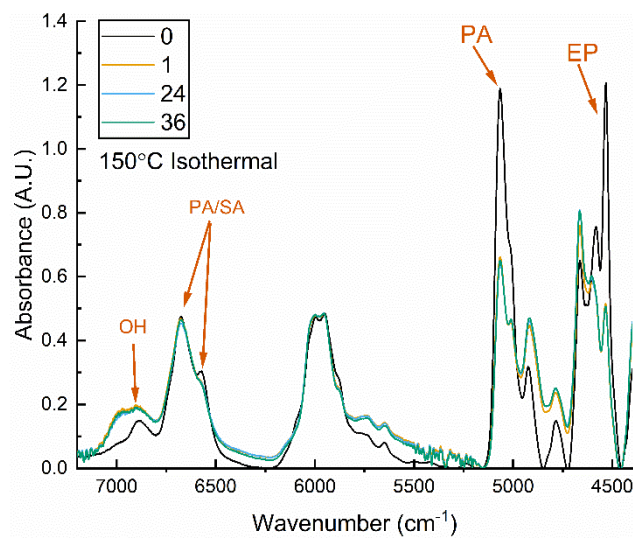


Figure A 9 – NIR spectra of the 33CGE adduct from the uncured state through to end of cure

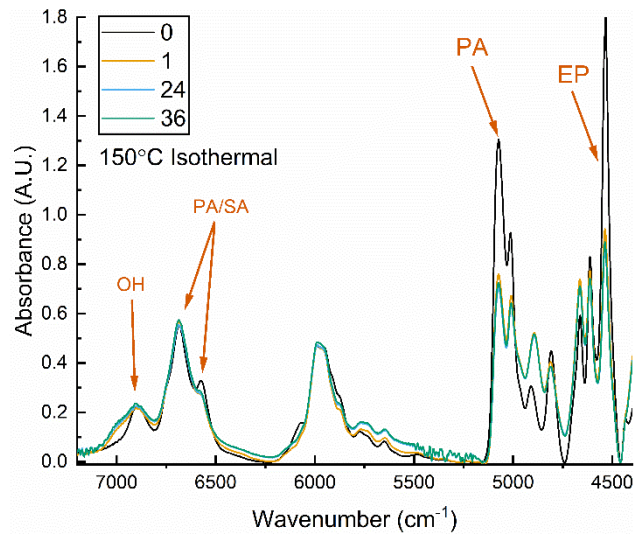


Figure A 10 - NIR spectra of the 44CGE adduct from the uncured state through to end of cure

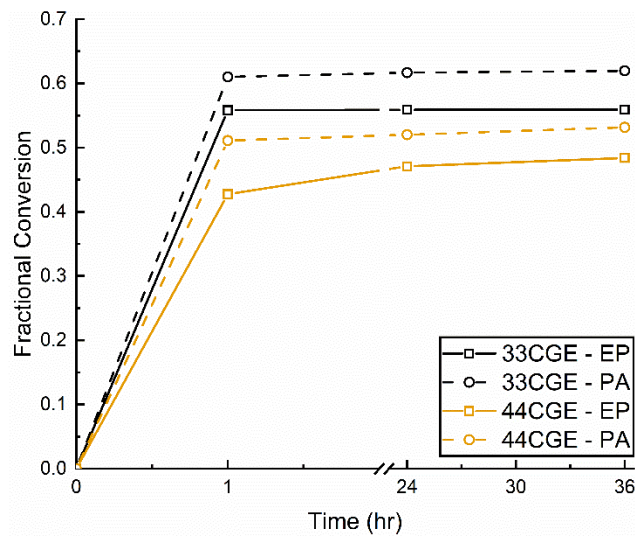


Figure A 11 – Conversion of the epoxide and primary amine peak areas from NIR analysis for the 33CGE and 44CGE adducts